Development of an agricultural drought assessment system

Integration of agrohydrological modelling, remote sensing and geographical information

Majid Vazifedoust

Development of an agricultural drought assessment system

Integration of agrohydrological modelling, remote sensing and geographical information

Promotor: Prof. dr. ir. R. A. Feddes
Hoogleraar in de Bodemnatuurkunde, agrohydrologie en grondwaterbeheer, Wageningen Universiteit

Co-promotoren: Dr. ir. J.C. Van Dam
Universitair hoofddocent, leerstoelgroep Bodemnatuurkunde, ecohydrologie en grondwaterbeheer, Wageningen Universiteit

Prof. dr. W.G.M. Bastiaanssen
Hoogleraar Remote Sensing, Technische Universiteit Delft

Samenstelling Promotiecommissie:
Prof. dr. P. Struik (Wageningen Universiteit)
Prof. dr. A. Alizadeh (Ferdowsi University, Mashhad)
Dr. ir. P. Droogers (Future Water, Wageningen)
Dr. ir. A. Sharifi (ITC, Enschede)

Dit onderzoek is uitgevoerd binnen de onderzoekschool WIMEK-SENSE

Development of an agricultural drought assessment system

Integration of agrohydrological modelling, remote sensing and geographical information

Majid Vazifedoust

Proefschrift
ter verkrijging van de graad van doctor
op gezag van de rector magnificus
van Wageningen Universiteit
Prof. dr. M.J. Kropff
in het openbaar te verdedigen
op woensdag 28 november 2007
des morgens te 11.00 uur in de Aula

Development of an agricultural drought assessment system: Integration of agrohydrological modelling, remote sensing and geographical information

Key words: Agricultural drought, distributed modelling, remote sensing, inverse modelling, data assimilation, Borkhar irrigation district.

This book is dedicated to:
my lovely wife, Zahra and
my son, Amirreza

Abstract

Vazifedoust, M. 2007. *Development of an agricultural drought assessment system: Integration of agrohydrological modelling, remote sensing and geographical information*. Doctoral thesis, Wageningen University, Wageningen, The Netherlands.

Iran faces widespread droughts regularly, causing large economical and social damages. The agricultural sector is with 80-90 % by far the largest user of water in Iran and is often the first sector to be affected by drought. Unfortunately, water management in agriculture is also rather poor and hence water productivity of crops *WP* is far below potential. The growing water scarcity due to drought and the increasing water demands of industries, households and environment, are major threats to sustainable agricultural development in Iran. Therefore, *the development of a reliable agricultural drought assessment system* would be very beneficial for proper operational decision making on farms, for early warning, for identification of potential vulnerability of areas and for mitigation of drought impacts.

Given the current water scarcity, the limited available amount of water should be used as efficient as possible. To explore on-farm strategies which result in higher *WP*-values and thus economic gains, the physically based agrohydrological model Soil Water Atmosphere Plant (SWAP), was calibrated and validated using measured data at 8 selected farmer's fields (wheat, fodder maize, sunflower and sugar beet) in the Borkhar irrigation district in Iran during the agricultural year 2004-05. Using the calibrated SWAP model, on-farm strategies i.e. deficit irrigation scheduling, optimal irrigation intervals and extent of cultivated area, were analyzed based on relations between *WP*- indicators and water consumption. The results showed *a large potential of the improvement of water productivity under limited water supply in the Borkhar irrigation district.*

Although agrohydrological models like SWAP offer the possibilities for predicting crop yield, such models may become inaccurate because of uncertainty of input parameters like irrigation scheduling, soil hydraulic parameters and planting dates. This holds especially true when applying distributed modelling at regional scale. Hence to reduce the uncertainty in application of SWAP at regional scales, remotely sensed data of leaf area index and evapotranspiration were used in combination with a geographical information system. The remotely sensed data were inserted into the distributed SWAP model using data assimilation techniques i.e. sequential updating.

Data of *LAI* were derived from Visible and Near Infrared (VNIR) spectral bands of remote sensing data with moderate to high spatial resolution. However, due to resolution limitations of existing remotely sensed data i.e. thermal bands, these data could not be used directly for routine *ET* estimation of individual fields. Therefore, a new disaggregation method based on linear disaggregation of *ET* components within each MODIS pixel, was developed and applied to the simulated MODIS data. The results of the proposed approach were further compared with two other disaggregation approaches being based on weighted ratios, as derived from dividing *ET* maps of high and low spatial resolution data.

The biggest advantage of the proposed linear disaggregation approach was that *the number of high spatial resolution images needed in this method is low,* i.e. the approach can even be applied using one land cover map only. As in many regions access to high spatial resolution thermal images is currently not possible, the linear disaggregation method can still be used to assess drought impacts far in advance.

Water balance components as computed by SWAP are quite sensitive to the upper boundary conditions, and hence to irrigation times and application depths. In order to know how much water has been applied, the cumulative actual *ET* data were therefore used in an automatic calibration mode, i.e. inverse modelling of irrigation scheduling. The ability of inverse modelling to reproduce the initial irrigation times and depth, was first investigated using forward cumulative *SWAP simulated **ET*** data based on 5, 15 and 30 days. Thereafter, the cumulative disaggregated remotely sensed **ET** data based on 5 days were used in the inverse modelling process.

The results showed that *the performance of inverse modelling is promising in identifying the irrigation time and depth of irrigation using 5 days based cumulative ET data.* However, irrigation amounts, which rewet the soil profile beyond field capacity and thus cause excessive percolation, could not be detected by the applied inverse modelling approach. Also, assimilation of remotely sensed data into a distributed SWAP by automatic calibration needed a large amount of computation time, especially at regional scale.

Hence, to insert the valuable information from remotely sensed land surface data into the SWAP model at regional scale, a simple updating assimilation technique was used. The SWAP model was implemented in a distributed way using the spatial distributed information of soil types, land use and water supply on a raster basis with a grid size of 250 m. In order to link spatial information data with SWAP, *a coupling program was written by the author in MATLAB.* This program took care of the transfer of in- and output data from one system to the other, as well as to run the model for each pixel.

To have a prediction of crop yield far in advance, the sequential updating process of remotely sensed based data (LAI and/or relative evapotranspiration ET/ET_p) was halted at one respectively two months before the end of the wheat growing season. During the sequential updating process known weather data were used, while for the remaining part of the growing season different scenarios were considered based on weather data of a dry, wet and normal year. A value for the optimum gain factor K_g, that performed best with respect to the observations, was selected

*S*imulation with assimilation of both LAI and ET/ET_p *data at both the regional and field scale* (bias about $\pm 10\%$) *was very promising in forecasting crop production one month in advance.* However, longer term predictions i.e. two months in advance, resulted in a higher bias between the simulated and statistical data. It appeared that *in the assimilation process LAI data have a dominant influence.* Because of this dominant influence, it is suggested to repeat the assimilation process using the *LAI data of the most advanced satellite i.e. IRS-P6 (ResourceSAT1&2)* with higher spatial and temporal resolution.

The surface water in the Borkhar irrigation canal network is provided by diversion of the water from the Zayande Rud river. Since this river is mainly fed by the snow melt from January to April, a comprehensive drought assessment system *on seasonal basis* can be developed by integration of the developed agricultural drought assessment system with the estimates of available surface water being derived from snow pack and snow cover.

Acknowledgement

I would like to express my profound gratitude to the Almighty Allah for all good graces and mercies he granted me in my life. I am also grateful to the Ministry of Science, Research, and Technology (MSRT) of Iran for granting me a fulltime scholarship to follow my PhD study abroad. The work presented in this thesis was made possible with the support and contribution of many individuals whom I like to acknowledge sincerely.

With deep gratitude, I wish to express my sincere thanks to my promotor, Prof. R.A. Feddes. Dear Reinder, I thank you for your invaluable comments, suggestions, support and encouragement throughout my PhD research. I learnt a lot from you and I am honoured to have had the opportunity to do my PhD under your supervision. I will never forget the four years of my life that I was involved in the learning and working environment that you managed and provided. Your comprehensive guidelines and support in all steps of my research enabled me to follow and finally get the job done. I am not sure if I am able to put my gratitude into words so please let me just simply say " Thank you for everything".

I would like to extend my sincere appreciation to the person most involved with this dissertation, my daily supervisor Dr. J.C van Dam, for his excellent guidance and invaluable support. Dear Jos, when I look at my thesis I see your precious ideas throughout all chapters of the book and your emotional support in all stages of the study. I must admit that without your guidance the study would have been far more difficult and perhaps even impossible. I enjoyed all your constructive and helpful comments during our meetings and discussions. I deeply thank you and wish to keep in touch with you in the future.

Special thanks are extended to my co-promotor, Prof. W.G.M. Bastiaanssen, for his help, intellectual ideas, and valuable guidance. Dear Wim, you reviewed carefully my drafts, and kept me up to date with the art of RS applications in water management.

A major part of this study includes the data collection and field work. The practical work of this study would never have been accomplished without Dr. Ali Sharifi's support from ITC, Enschede and the facilities and logistics provided by the Research Institute of Soil and Water (SWRI) in Esfahan, and Agriculture Planning and Economic (APERI) in Tehran. I sincerely thank Dr. Ali Sharifi for his continuous support, time, advice, and comments. I would like also to express my sincere gratitude to the former director of APERI, Mr. S.H. Kazemi for his strong support and sharing available data in this Institute. I would like to extend my special gratitude to Mr. Nasiri and Mr. Azimi for their technical support and all the staff members of the APERI. My special gratitude goes to the director of management and planning, Mr. Shams, and his deputy, Mr. Sadeghi, at the Esfahan Jihad-e- Agriculture for providing the facilities and logistics. I would like to extend my special gratitude to the director and all staff of the Esfahan meteorological organization for providing the meteorological data from weather stations in the Borkhar district.

I would like to extend my sincere gratitude to the former director of SWRI, Mr. Shahabifar for his strong support, providing laboratory facilities and sharing available data in this Institute. I would like to extend my deepest appreciation to the person most involved with my field work in Esfahan, Mr. M. Feizi. He is a highly valuable researcher at SWRI. He arranged all preliminary and logistic affairs before and after my arrival to Esfahan. Dear Mohammad, I enjoyed very much your hospitality and readiness to help me settling down at Esfahan and setting up my field work in the Borkhar irrigation district. Your hospitality and generosity made the difficult task of field visits as comfortable as possible. I deeply thank you and wish to keep in touch with you in the future.

My special thanks go to Mr. M. Fathi, a young researcher at the SWRI, who helped me with field work and data collection at the beginning of my field campaigns. He also assisted me in the tough tasks of equipment installation and maintenance, data collection, and laboratory tests.

The directors of Ghiam and Gorgab companies in Esfahan are sincerely acknowledged for their permission to conduct my field works on their properties. I would also like to acknowledge all staff in Jihad-e-Agriculture of Borkhar, especially Mr. Shafi, Mr. Hajhashemi, Mr. Abbasi and Mr. Hamidzadeh for providing the basic information about the Borkhar irrigation district.

I would like to take the opportunity to express my gratitude to all the members of the Iranian student community here in Wageningen. Our occasional gatherings and your emotional support prevented me and my family to get homesick. Thanks all. My special thanks go to Ali, Hossein, Kaka, Mohammad Kazem, Mohammad Ali and Vahedberdi. We shared pleasant moments during our meeting and parties. I would like also to extend my sincere gratitude to my friends in Enschede especially Bahman, Farhang and Dr. Abkar for sharing data and information from the Borkhar irrigation district.

I enjoyed the friendly atmosphere of the chair group of Soil Physics, Ecohydrology and Groundwater Management. I experienced very pleasant times during parties, drinks and dinners organized by people in the group. My special thanks go to Henny van Werven and Annemarie Hofs who were always ready to translate so many letters and forms which I was receiving in Dutch language and to handle all the bureaucratic administration affairs which I was facing. I also would like to thank all my friends and colleagues in the chair group of SEG: Quirijn, Klaas, Louise, Esther; Franck; Sara, Tineke, Ranvir, Harm, Heriberto, Ger, Tessa, Willemijn, Marieke, Ype and Anton. My dear colleagues and friends, I enjoyed very much working with you. I benefited from your thoughts and ideas during our formal and informal meeting and parties. You showed me how rich the culture of the Netherlands is. I take this opportunity to express my sincere thanks to all of you.

I wish to express my deepest appreciation to my parents, my brother, my sister, my father-in-law, my mother-in-law and other family members especially my two uncles, Mr. T. Sabbaghi and Mr. M. Sabbaghi. Although I was living far from them, their continuous emotional support and encouraging words helped me to accomplish my academic study successfully.

Most important of all, I am extremely grateful of my wife Zahra and my little baby Amirreza. I am quite sure that it would not have been possible to accomplish my PhD without benefiting their patience, tolerance, good willing, and emotional support. Dear Zahra, you left your job, relatives and friends to support me and to stay with and beside me. My dears you always accompanied me and provided a source of happiness throughout the period of our common life. THANK YOU for every thing.

Majid Vazifedoust
Wageningen
28-11-2007

Contents

Part	Title	Page

1. Agricultural drought

1.1 Definition of droughts

Drought is an inevitable part of Earth's climate that occurs regularly with no clear warning and without recognizable borders, causing billions of dollars in loss annually for the farming community (*Kagon*, 2000). Although deviation from the normal amount of precipitation over an extended period of time is broadly accepted as the cause for drought, there is no universally accepted definition for drought. One of the main reasons is that drought, unlike floods, is not a distinct event. Drought is often the result of many complex factors which act and interact within the environment without no distinct start or end. This complicates a clear definition of drought. Furthermore, the impacts of drought vary by the sector affected, making different definitions of drought relevant for specific groups (*Chimpanshi*, 1995). Droughts are commonly classified in four different forms (Fig 1.1):

Weather variability

Meteorological drought

Low precipitation

High potential evapotranspiration

Soil moisture drought

Low soil moisture

Hydrological drought

Low stream flow and low surface water levels

Low groundwater levels and discharge

Socio-economical drought

Damage
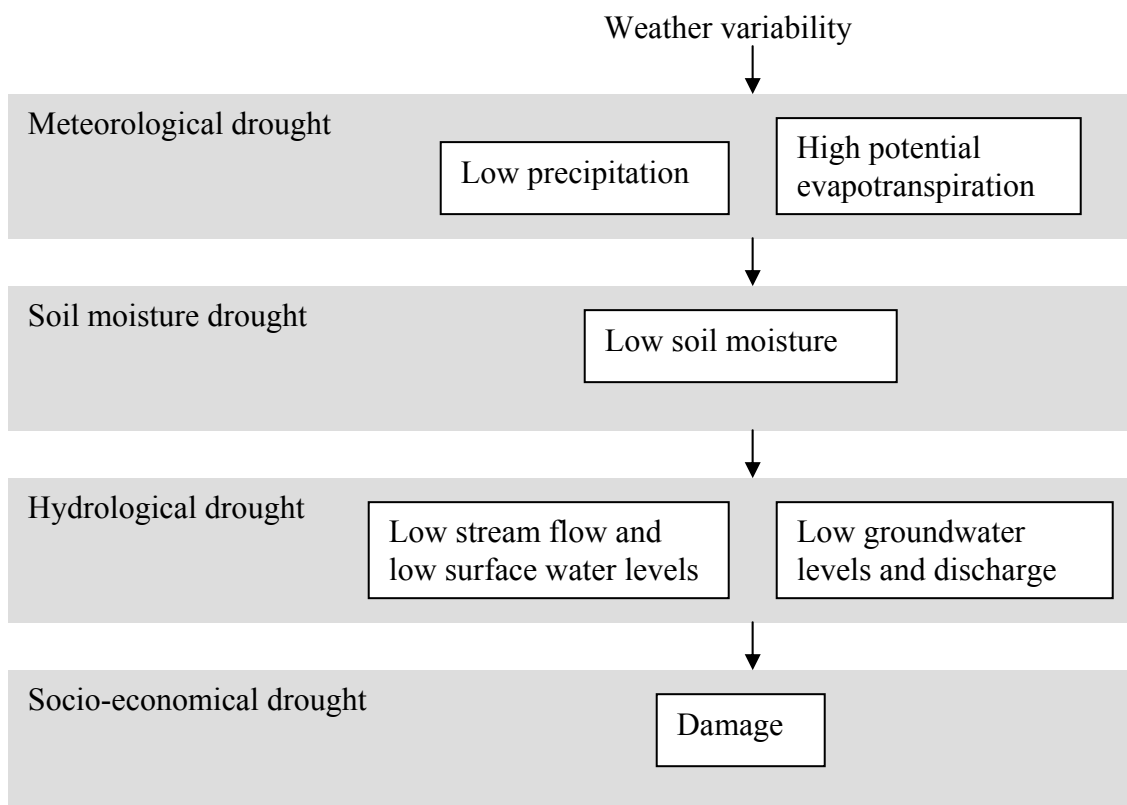
Figure 1.1 Classification of droughts (after *Peters*, 2003)

- Meteorological droughts, which starts by the lack of rainfall, possibly in combination with high evapotranspiration, result from the natural variability of the weather.
- Soil moisture drought, which is caused by meteorological drought, directly affects agricultural crops and /or natural vegetations. Hence in this thesis we classify this drought further as _Agricultural Drought_.
- Hydrological droughts, are caused by meteorological and soil moisture droughts through a decrease in the amount of recharge and precipitation, which in turn causes lower groundwater levels and stream flows. Stream flow or groundwater deficit directly affects urban and human water supply.
- Socio-economical drought, which is an extreme form of agricultural drought, addresses the damage caused by all the above mentioned types of drought.

Naturally these droughts can be connected and often one type of drought results in another. In comparison to other natural hazards like floods that develop quickly and last for a short time, drought is a creeping hazard and its impact is accumulative over a period of time across a vast area (*Kagon*, 2000). It is more difficult to detect the emergence of droughts compared to other natural hazards because of drought's unique characteristics: its slow-onset, absence of a universally accepted definition for drought, and its non-structural impacts. In addition it is more difficult to assess drought impacts in various sectors because the impacts can spread over a large geographical area (*Wu and Wilhite*, 2004). Three areas where drought research shows gaps are the relationship between crop yield and soil moisture, the regional aspect of drought and the forecasting of start and end of droughts (*Panu and Sharma*, 2002).

Agriculture is the primary economic sector affected by drought and a short-term drought at the critical crop stages has severe impacts on agriculture (*Wu and Wilhite*, 2004). In absence of a drought forecast system, drought management and preparedness planning have become widely accepted tools for reducing the agricultural drought risks. Monitoring, assessment and mitigation of drought impacts are the most important elements of drought preparedness plans (*Wilhite and Svoboda*, 2000). Understanding of the interactions between soil, atmosphere, plant and water are key factors in assessment of drought impacts.

1.2 The agricultural drought problem in Iran

Agricultural drought in Iran is one of the natural disasters, which cause large economic and social damages. Iran is located in an arid to semi-arid region and is facing widespread drought regularly. The drought during the 1990's had devastating impacts on Iran's agriculture and livestock. According to United Nations reports, also the cumulative effect of droughts from 1999 to 2001 has seriously affected Iran's agriculture and livestock production (*UNDP*, 2003; *Foltz*, 2002). Almost all of Iran's 32 provinces suffered from significant shortage of water and roughly 2.6 million hectares of irrigated farms and 4 million hectares of rain-fed agriculture were affected by widespread drought. Farmers had reductions of 35-75 percent in wheat and barley production and the government had to import a record seven million tons of wheat. Furthermore, livestock was hard hit by the drought, with about 1 million animals dying during those years. The economic damage of agricultural drought over the three years was estimated at about $ 7.0 billion (*UNDP*, 2003; *Foltz*, 2002).

The total cultivated land in Iran is about 18.5 million ha of which only 8 million hectares are irrigated annual crops, 6 million hectares are rain-fed annual crops, and 4.5 million hectare remain in the form of fallow land. From the total of 8.1 million ha of irrigated lands in Iran, 7.6 million ha (95%) are under surface irrigation and 0.4 million ha (5%) under the pressurized irrigation (*IRNCID*, 2007). The agricultural sector is also with 80-90 % by far the largest user of water in Iran and is often the first sector to be affected by drought. Unfortunately, water management in agriculture is also very poor and hence water productivity *WP* is far below potential.

For wheat, *WP* is estimated to be 0.5 kg dry matter m^{-3} of evapotranspiration, compared to a world average of 1.1 kg m^{-3} (*Bastiaanssen*, 2003). Wheat is the core commodity of the food and agriculture system, providing 40 percent of the energy and 45 percent of the total protein supply in Iran. Iran's domestic wheat consumption now stands at about 14 million ton a year. Until recently, Iran relied on large wheat imports to meet its growing domestic demand. This made Iran rank among the world's leading wheat importers, with an annual intake ranging from 2.5 to 7.5 million tone over the past two decades (Fig. 2.1).

4
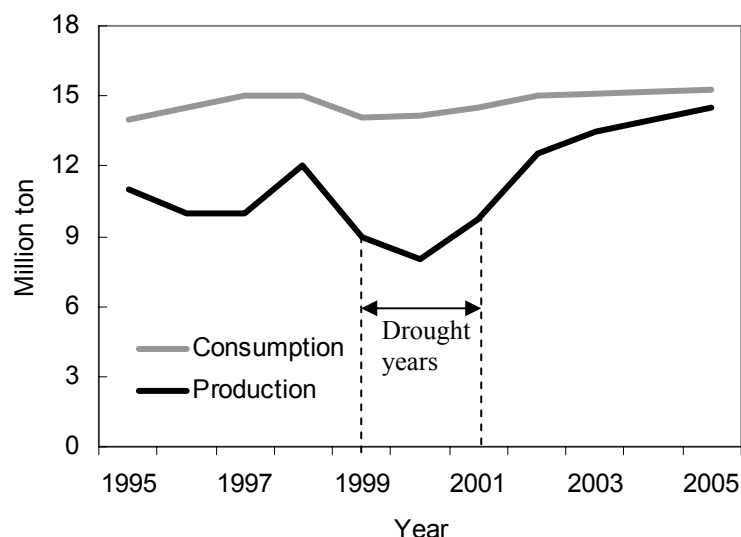
Figure 2.1 Wheat production and consumption in Iran from 1995 to 2005 (*FAO*, 2005)

In recent years, the Government has made wheat self-sufficiency a very high priority and stepped up efforts to increase wheat productivity. In the years 2004 and 2005, strong government support i.e. supplying higher yielding seeds, improving machinery services, augmenting fertilizer usage, enhancing water systems and pest management practices resulted in wheat self-sufficiency. Favourable weather in these two years had also a significant contribution in raising wheat production.

About 40 percent of Iran's wheat is rain-fed with an average yield of only 0.8 ton/ha. The average wheat yield of irrigated land in Iran rarely exceeds 3.0 ton/ha. Good and timely precipitation in the years 2004 and 2005, lifted the average wheat yield (irrigated and rain-fed) to 2.3 ton ha^{-1}, slightly below the world average of around 2.6 ton ha^{-1} (*FAO*, 2005). This shows that sustaining production at self sufficient levels to meet the growing domestic consumption requirements is a difficult and challenging task. The growing water scarcity due to drought and the increasing water demands of industries, households and environment, is the major threat to sustainable agricultural production in Iran (*APERI*, 2001).

These threats emphasize the vulnerability of the agricultural sector to drought and the need for more research to understand and develop tools that would help to mitigate the impacts of drought. In the absence of a drought forecast, alternative means of preparing for drought and mitigation actions must be sought so that the benefits of crop production are acceptable. An agricultural drought assessment is necessary for food security, operational decision making on the farm, early warning for disaster preparedness, identification of potential vulnerability of the area and mitigation of drought impact. Decisions that can be taken on the basis of reported drought conditions include rationing water for irrigation, stockpiling produce for resale during a drought year and delaying farm operations (*Chimpanshi*, 1995). Adequate status reports and estimates of future trends in crop yields may result in prompt provisions of relief and payments to farmers instead of having to wait to the end of the growing season for compensation.

1.3 Assessment of agricultural drought

Hence to be better prepared and to limit the effects of drought a tool for drought assessment is essential. During the last decades different approaches have been used for drought detection and characterization of the effect of environmental and climatologically variation on agriculture. Examples are: rainfall analysis (*Palmer*, 1965), remote sensing (*Vogt et al.*, 2000), soil moisture analysis (*Narasimhan and Srinivasan*, 2005) and crop growth simulation (*Stafford-Smith et al.*, 1998).

For instance, the Palmer Drought Severity Index (PDSI) and Crop Moisture Index (CMI) have been extensively used for agricultural drought monitoring and forecasting. PDSI and CMI are based on a simple water balance model that calculates precipitation and evapotranspiration deficit (*Hytes*, 2003). The model assumes that parameters like land cover and soil properties are uniform over the entire climatic zone. However these assumptions are hardly met, as they vary in space and time. Currently, with the help of satellites, indices based on reflected and emitted radiation and on the energy balance, are used widely in combination with other geographical data for drought monitoring at various spatial scales. The Normalized Difference Vegetation Index and Evaporation Fraction which can be derived through satellite images, have been considered as being the most important indices for mapping of agricultural drought condition (*Vogt and Soma*, 2000). However, high costs, temporal and spatial limitations are the main limiting factors in applying these indicators. Also indices based on satellite images cannot be used in scenario analysis.

Crop growth simulation is an approach used widely in the assessment of environmental and climatic factors on agricultural systems. This approach can be applied to analyze drought events, because it incorporates meteorological and soil water information, and therefore takes into account a variety of factors that may affect agricultural production (*Kumar and Panu*, 1997).

In this thesis, a comprehensive agrohydrological model in combination with remote sensing and geographical data will be used to understand the interactions between soil, atmosphere, plant and water, which are key factors in recognizing agricultural droughts. In addition, these tools can help us to adapt water and crop managements to mitigate the impacts of agricultural drought. The irrigation system should be managed to achieve high *WP* with respect to the availability of water resources under drought conditions.

For the past several decades, physically based agro-hydrological models i.e. the Soil Water Atmosphere Plant (SWAP) model (*Feddes et al.*, 1978, *Van Dam et al.*, 1997, *Kroes and Van Dam*, 2003) have been developed to simulate the water balance components and plant growth development. These models can be used to simulate the impact of drought on agricultural crop production at various growth stages as well as to explore solutions to mitigate drought impacts. The models are strong in performing scenario analyses, and thus permit a better understanding of the impacts of possible changes in water management (Van Dam et al., 2003). The spatial variability of soils, crops and irrigation is however the main limitation for using crop simulation models on a regional scale.

Recently remote sensing techniques have been used successfully to extract data for regional hydrological modelling (*Schuurmans et al.*, 2003). With currently available remote sensing and geographical data, comprehensive eco-hydrological models can be used to analyze water balance components and crop growth at large spatial scales (*Van Dam and Malik*, 2003).

The research presented in this dissertation will provide a new foundation for geographical information system (GIS)-based approaches to assess, monitor and manage droughts through the development of an agricultural drought assessment system. The consideration of spatial variability of irrigation applications, land uses and soil types improves our ability to assess droughts at a much better spatial resolution. The increased spatial as well as temporal resolution of different RS-systems will provide the farming community, water managers and policy makers a much better tool to assess, forecast and manage agricultural drought on a much more precise scale.

1.4 Research Objectives

The general objective of this study is therefore: '*To develop an Comprehensive Agricultural Drought Assessment System (CADAS) based on water balance component and actual crop growth simulation using an agrohydrological model, in combination with remote sensing and a geographical information system*'.

The specific research objectives of this study are the following:

- Calibration and validation of the advanced field scale agrohydrological model SWAP using data from farmer's fields with current practices.

- Application of this field scale agrohydrological model to explore ways to increase water productivity of irrigated crops under limited water supply.

- Disaggregation of remotely sensed evapotranspiration data from low to high spatial resolution in order to extract more information from current satellites.

- Inverse modelling of irrigation scheduling using disaggregated remotely sensed evapotranspiration data in order to know how much water has been applied.
- Assimilation of satellite data into agrohydrological models to improve crop yield forecasts

1.5 Thesis outline

Chapter 2 gives a brief description of the study area, i.e. the Borkhar irrigation district, Esfahan, Iran. An overview is given of its physical environment, irrigation and cropping system. This chapter also highlights the important issues related to the water management in the Borkhar irrigation district.

In Chapter 3, the SWAP model will be calibrated and validated using the observations at farmer's fields in the Borkhar irrigation district during the agricultural year 2004-05. Inverse modelling for the estimation of soil hydraulic parameters and depth of irrigations will be briefly discussed. With the help of automated runs using the link between SWAP and the Parameter ESTimation model PEST (*Doherthy et al.*, 1995), water productivity *WP* curves will be presented for the main crops and for different irrigation practices. A set of *WP*-indicators based on the output of irrigated agriculture per unit water will be implemented for the analysis of the amount of water used, as well as for the evaluation of on-farm strategies performance under water scarce conditions. The maximum possible increase in *WP*-indicators will be derived graphically from *WP*-curves.

In recent years, a strong research interest has been developed in integrating physical based models with satellite remote sensing data to improve their prediction capabilities, especially at regional scales. However, due to limitations in spatial and temporal resolution of existing remotely sensed data, these data can not directly be used for routine estimation of evapotranspiration *ET* from individual fields. In Chapter 4, the Surface Energy Balance Algorithm (SEBAL) of *Bastiaanssen* (1998) will be applied to the MODIS and ASTER data for the Borkhar irrigation district. A new procedure is developed to disaggregate *ET* from 1000 m to field scale. The results of the proposed approach will be compared with two other disaggregation approaches, which are based on weighted ratios of high spatial resolution *ET-RS* over low spatial resolution *ET-RS*.

In Chapter 5, the possibility of deriving irrigation scheduling i.e. irrigation times and depths, by means of inverse modelling will be tested with numerical simulated *ET* data as well as with disaggregated remotely sensed *ET* data from MODIS images. Accurate quantification of irrigation scheduling is essential to simulate the water balance components and crop growth at regional scale. Specific attention in this chapter will be given to the well-posed nature of the inverse problem, the disaggregation of large scale satellite images, and the effect of observation errors.

Chapter 6 will be dealing with the implementation of the SWAP model in a distributed way. The study area will be divided into 250 m spatial resolution cells. Input data are defined for each cell using an overlay of spatial information maps such as weather, water supply, land cover and soil texture. In order to improve the accuracy of water balance components and simulated crop productions, remote sensing based data of relative evapotranspiration and leaf area index will be assimilated into the distributed model by means of a so called *"update"* method. Chapter 6 will address the question of whether assimilation of remotely sensed leaf area index and/or relative evapotranspiration data into the distributed SWAP model can predict total wheat production as an indicator of agricultural drought far in advance.

Finally, the results of this study will be summarized with conclusions and recommendations how to improve the regional agricultural drought assessment system as well as mitigate the drought impacts on the irrigated crops in the Borkhar irrigation district. A research outlook will be given with respect to distributed modelling at regional scale.

2. Description of the Borkhar irrigation district

10

2.1 Geographical description of the Borkhar district

The Borkhar district is located North of the ancient town of Esfahan, which has a long irrigation history (Fig. 2.1). The Borkhar district area spreads over 83300 ha, with about 24 % of this area being under cultivation (*APERI*, 2001).
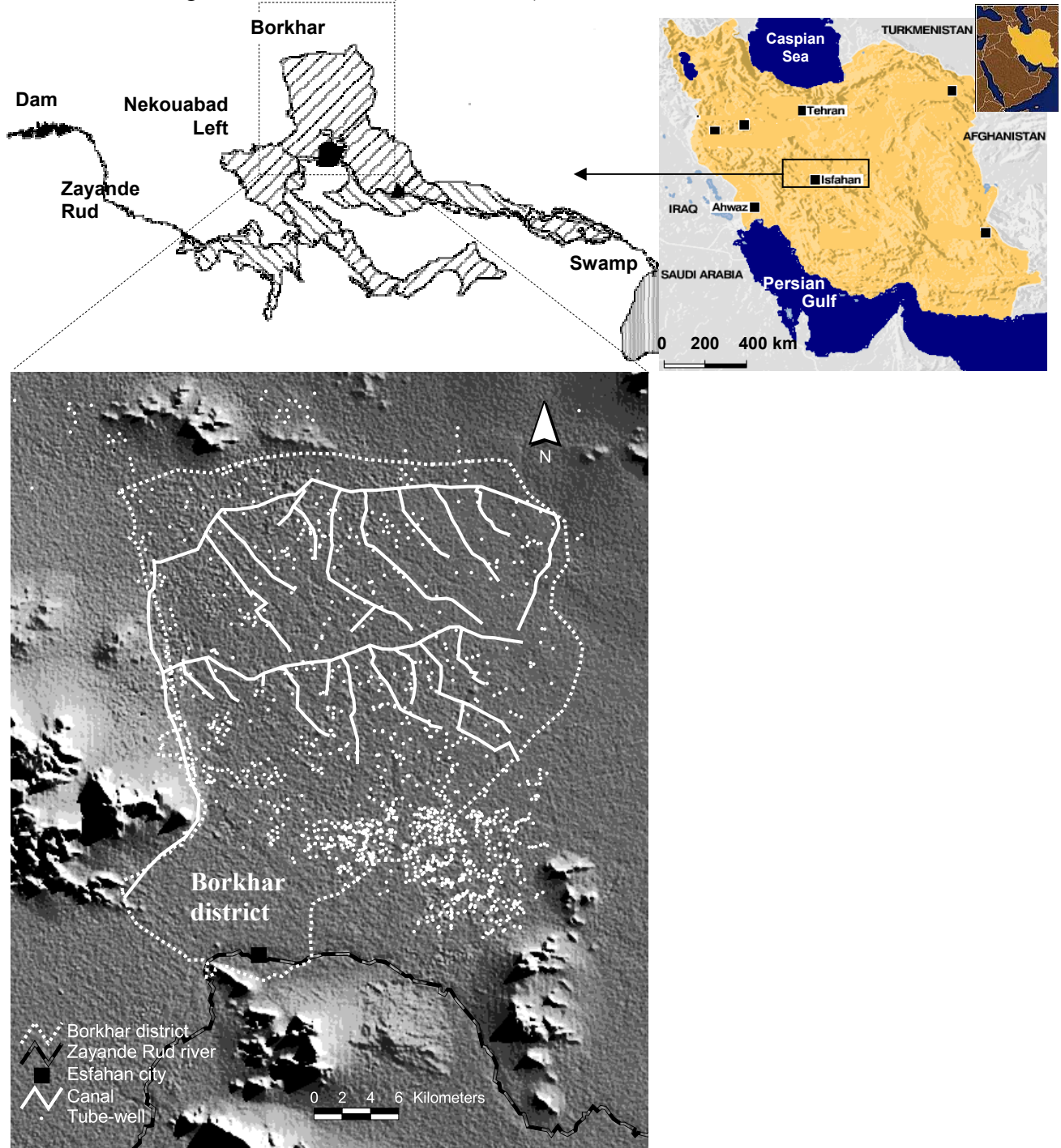
Figure 2.1 Geographical location of the Borkhar irrigation district, Esfahan, Iran.

The surface of the district is generally flat with a slope of 0-2 % in the West-East and North-South direction. The district elevations vary between 1531 and 1600 meter above Mean Sea Level. The majority of the area has thin soils overlying the stony alluvial fans, providing little basis for economic enterprise other than extensive grazing on the xerophytes

vegetation. The current population of Borkhar is about 1.8 million, with the main occupation being agriculture (*APERI*, 2001).

From hydrological point of view, the Borkhar district is part of the Zayande Rud basin. The Zayande Rud basin is a closed basin with no outlet to the sea and covers 41500 km^2. The main river in this basin is 350 km long. It originates from the Chadegan Storage Reservoir, with a capacity of 1500 million m^3. After running in a roughly West-East direction, the river passes the southern parts of the Borkhar irrigation district near the city of Esfahan, and terminates in the Gavkhuni Swamp. From January to March the river is fed largely by snowmelt and acts as main drainage canal in the Borkhar district. River water is also diverted to the main irrigation canal of the Borkhar area and meets a small part of the water demand. *The main source of irrigation is groundwater.* Since groundwater recharge has been insufficient to meet the water demand of the crops, during two last decades the groundwater level has decreased significantly. Hence, surface water is increasingly used for irrigation (*APERI*, 2001).

To keep up with the increasing demand in the basin, in recent years inter-basin transfers have been implemented. Three tunnels that can deliver 790 million m^3 yr^{-1} have been constructed to divert water from the Kuhrang River in the Chaharmahal-va-Bakhtiari province into the upper reaches of the Zayande Rud River In addition, treated waste water from the North Esfahan Refinery is used for irrigation in a cautious way. It is estimated that by 2010 about 63 million m^3 of treated wastewater will be applied to the irrigated areas of the Borkhar district (*Murray-Rust et al.*, 2000).

2.2 Climate

The basin has a predominantly arid to semi-arid desert climate. Four distinct seasons can be distinguished: winter, spring, summer and fall. Air temperatures are higher in summer, reaching an average of 40°C in July, and are lower in winter dropping to an average minimum temperature of 3°C in January.
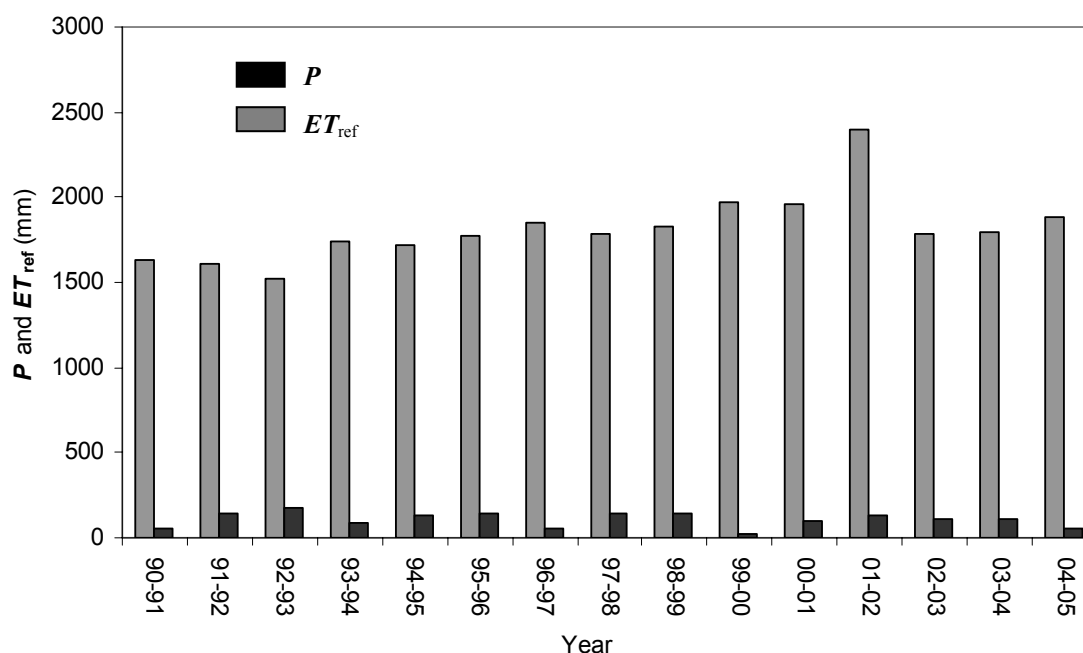
Figure 2.2 Inter-annual variation of reference evapotranspiration ET_{ref} in comparison with precipitation P in the Borkhar irrigation district.

The average annual rainfall **P** varies from 100 to 120 mm, which is only 5 to 6 % of the reference evapotranspiration ET_{ref} (Fig. 2.2). During the summer there is no effective rainfall, most of the rainfall is occurring in the winter months i.e. from December to April. Annual reference evaporation ET_{ref} is 1800 mm, and without reliable irrigation it is almost impossible to have any economic form of agriculture.

2.3 Irrigation water management

2.3.1 Canal water

The Borkhar Irrigation Network, is located north of Esfahan city and was built in 1997. The Borkhar irrigation network has about 20 canal commands varying in size from 500 to 5000 ha. It is served by two main canals: the Bel Main Branch in the northern and the Hajiabad Branch in the southern parts respectively (Fig. 2.3).
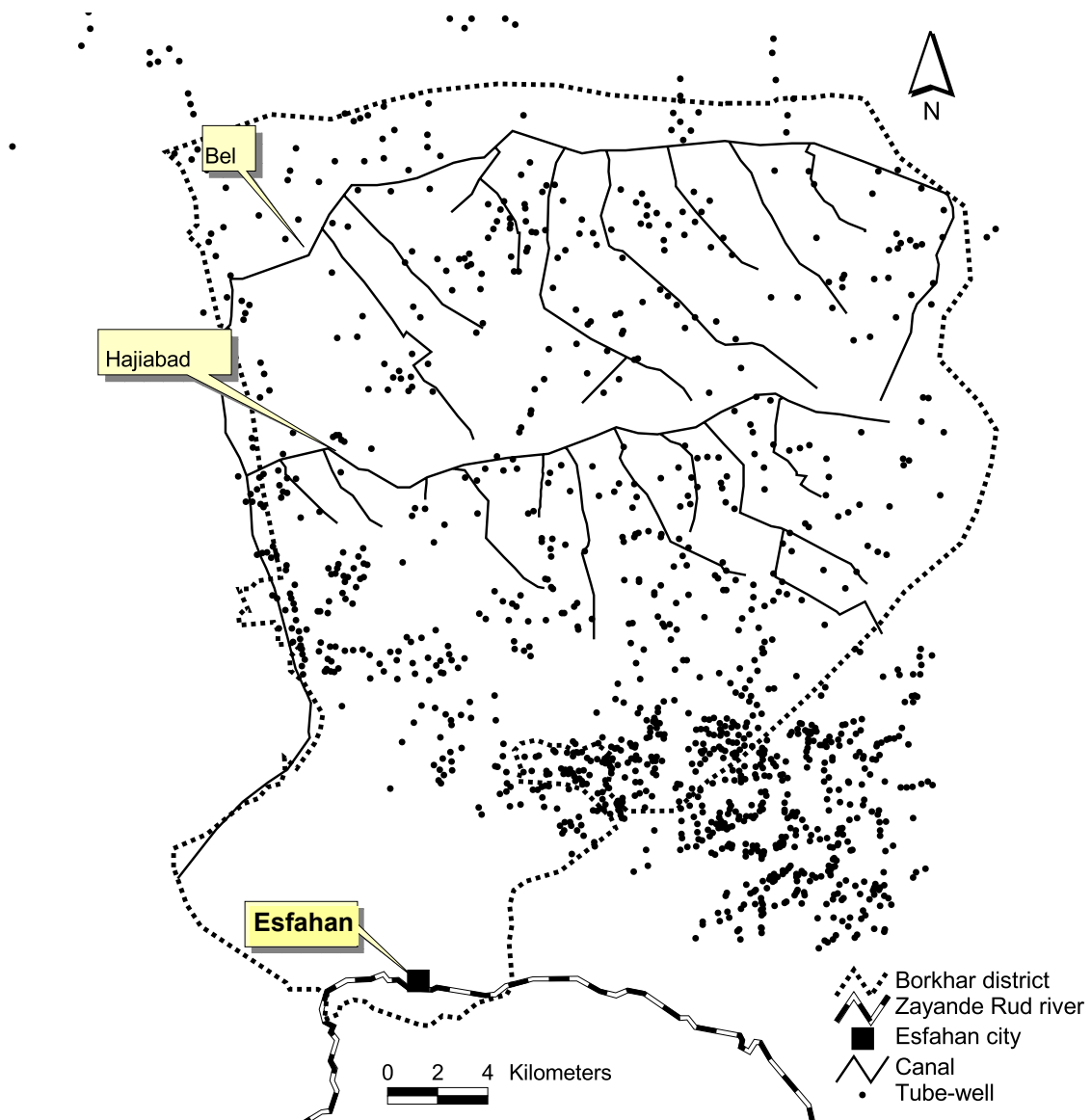
Figure 2.3 Location of the Borkhar Irrigation Network and tube-wells showing both the canal network and tube-wells.

These main canals have been designed for automatic upstream control, so that canal water levels are maintained at a constant level irrespective of actual demand. Only secondary and tertiary canals rely on simpler vertical sliding gates. The Borkhar irrigation network is essentially an extension of the Nekouabad Left Bank irrigation system, and it provides surface water to the areas where for several years has been substantial groundwater irrigation.

The water supply in this system originates from the Chadegan Storage Reservoir located at about 150 km distance in the north west of the Borkhar district. The reservoir water is released from 1 April to 1 October and the reservoir releases remain more or less constant in May, June, July and August. Total volumetric intake of the Borkhar irrigation network during this period generally exceeds 37.1 million m^3. Surface water supplies are delivered only when the annual water availability at the Chadegan reservoir is above normal. Hence, in less water scarce times farmers can use surface water and thereby protect their groundwater resources.

Because of limited water supply, about 18000 ha corresponding to 50% of its net irrigated area, receives canal water supply. The average canal water delivery of 0.56 mm d^{-1} is only 0.13 of the ET_{ref} of 4.1 mm d^{-1} (*Alizadeh and Vazifedoust*, 2000). The limited canal water supply is further reduced by the seepage losses from the main canals, distributaries and watercourses. The seepage loss from lined and unlined watercourses has been measured as 10 % and 30% respectively. Most of the canals and water courses in the Borkhar district are lined, while the field channels that distribute canal water among the fields are still unlined.

To prevent crop failure, irrigation systems in the area were designed to serve the biggest number of farmers possible, and to deliver the limited water supply over the largest area possible. The Mirhab (decentralized irrigation network management institution) is responsible for irrigation water management at district level. It has a very effective control over canal water up to the outlet, and the irrigation network is very well operated, managed and maintained. The water allocations between the outlets are based on: the degree of groundwater use in the outlet, the kind of water rights the outlets have, and the special conditions and socio-political networks that exist in these outlets.

The limited water supply at the outlets is rotated among groups of farmers in proportion to their water rights and land holding size. To ensure a uniform volumetric water distribution, water is allocated to the individual farmer for a specified period in that particular water course. During his turn, he decides on the amount of water to be applied at each field. Surface flooding is the most common method of irrigation application in the Borkhar irrigation district (*APERI*, 2001). The advantage of water distribution at this system is its simplicity in operation. However, types of soil, specific water requirement of crops and local drainage conditions are not considered.

In case of water scarcity conditions, water distribution at basin level is controlled by the water council of the Esfahan Water Authority (EWA). This council decides on the main lines of water allocation in the basin and reallocation of the surface water. At outlet level, farmers have also adopted several coping strategies to deal with water scarcity. They are, in first instance, aiming at maintaining their full water supply level, mostly by the increased use of groundwater. Only when this is not possible, farmers search for other solutions. The strategies applied include: selling land, water stealing, sharing water within the outlets, reducing the area under cropping, changing the cropping pattern, renting land elsewhere or moving to other activities outside the agricultural sector (*Hoogesteger*, 2005).

2.3.2 Groundwater

The Borkhar irrigation district is a well cultivated area with low annual precipitation and surface runoff. Therefore groundwater resources have a vital role in supplying agricultural, drinking, domestic and industrial water demands. The groundwater in the district occurs under unconfined and semi-confined aquifer conditions. The major sources of its recharge are rainfall, percolation from field irrigations and seepage losses from the canal network. The groundwater is extracted by underground tunnels called "*qanat*" (see Fig. 2.4) and shallow to relatively deep boreholes.

Qanat and hand dug wells are a traditional ways of tapping the groundwater. *Qanat*, which in Iran is known as "*kariz*", was first developed more than three thousand years ago by the inhabitants of the dry, mountainous region of western Iran for directing snowmelt through underground channels (*Wulff*, 1968).
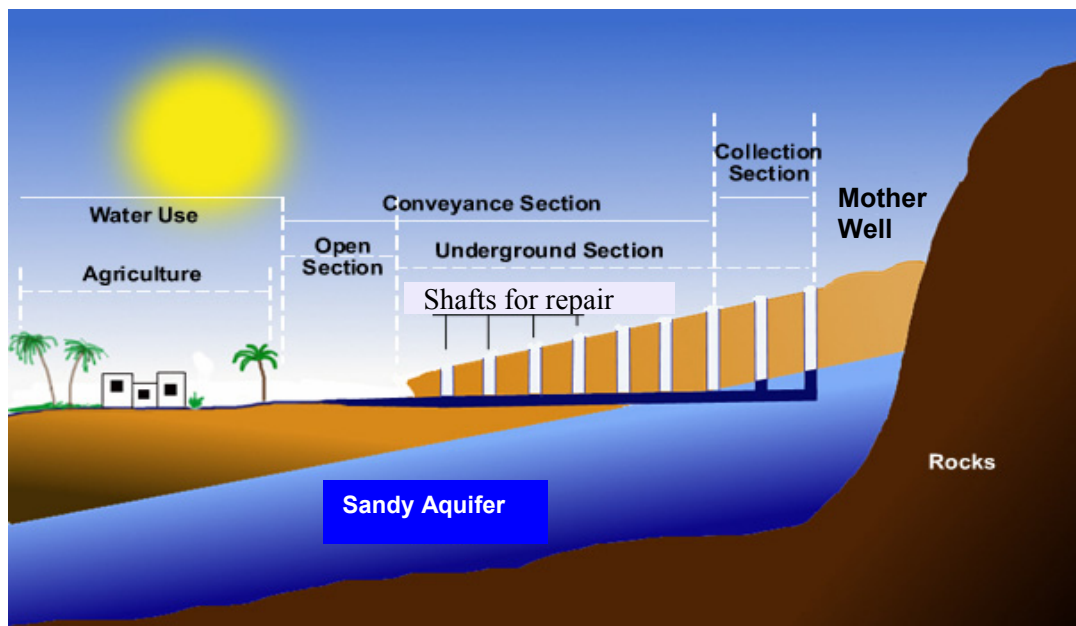
Figure 2.4 General scheme of a *qanat* for extracting groundwater in dry mountain basins of Iran.

In the early part of the first millennium B.C., Persians started constructing *qanat* for extracting groundwater in the dry mountain basins of present-day Iran. *Qanat* tunnels were hand-dug and just large enough to fit the person doing the digging. Along the length of a *qanat*, which can be several kilometers (up to 16 km), vertical shafts were sunk at intervals of 20 to 30 meters to remove excavated material and to provide ventilation and access for repairs. The vertical shafts usually range from 20 to 200 meters in depth. The main *qanat* tunnel slopes (1:1000 and 1:1500) gently down from pre-mountainous alluvial fans to an outlet at a village. From there, canals would distribute water to fields for irrigation. These amazing structures allowed Persian farmers to succeed despite long dry periods when there was no surface water available. Many strings of *qanat* are still in use stretching from China in

the East to Morocco in the West, and even to the Americas (*Kheirabadi*, 1991). There are significant advantages of a *qanat* water delivery system including:

- By putting the majority of the channel underground, water losses by seepage and evaporation is reduced;
- Since the system is fed entirely by gravity, the need for pumps is eliminated;
- It exploits groundwater as a renewable resource.

The rate of flow of water in a *qanat* is controlled by the level of the underground water table. Thus a *qanat* cannot cause significant drawdown in an aquifer because its flow varies directly with the subsurface water supply. When properly maintained, a *qanat* is a sustainable system that provides water indefinitely. The self limiting feature of a *qanat*, however, is also its biggest drawback when compared to deep tube-wells (*Motiee*, 2006).

In the past *qanat* was the most important way to extract water from deep aquifers. In 1973, the water delivery of 29 *qanat* in the Borkhar district was estimated at 22.2 million m^3 yr^{-1}, with a discharge varying between 0.005 and 0.013 m^3 s^{-1} (*APERI, Groundwater report of the Borkhar district*, 2001). However, after the Land Reform Act in 1981, groundwater use by tube-wells increased. Hence, during the last decade a large number of strings of *qanat* ran dry.

At present, in spite of the existing Borkhar irrigation network which is fed by surface water, many farmers rely on tube-wells in addition to the limited surface irrigation flows. The major portion of groundwater use originates from deep tube-wells being operated by individual farmers at their fields. In recent years many deep tube wells have been drilled to extract water from deep aquifers. The appropriate depth of shallow and deep tube-wells varies from 8 to 200 m, with discharges ranging from 0.001 to 0.095 m^3 s^{-1}. The total number of tube-wells in the entire Borkhar district has increased from 517 in the year 1973 to 1275 in the year 2000 (*APERI, Groundwater report of Borkhar district, 2001*). This increase in number of tube-wells is concentrated in areas of good quality groundwater (Fig. 2.3).

Because of over-extraction of the fresh water aquifer, the groundwater level has declined dramatically. Over the past years, saline water intrusion into shallow aquifers has therefore increased continuously. As a result, some of the abstraction wells have been abandoned and others have been deepened. *The decline of groundwater level and the decrease of groundwater quality in shallow aquifers are the two major factors limiting the extent of groundwater use in the region*. The groundwater depth below the surface varies from 89.6 m in the northeast to 8.2 m in the southern and eastern parts of the district. It follows the topography of the plain with slow movement from north to south direction. The average groundwater level above Mean Sea Surface Level has decreased from 1557 m in 1982 to 1540 m in 2000 and presents an annual groundwater decrease of 0.88 m yr^{-1} (Fig 2.5).

The groundwater quality in the central and eastern parts of the Borkhar irrigation district is rather poor i.e. 6.7 dS m^{-1}. In the northern and southern parts, it is about i.e. 1.1 dS m^{-1} which is good.
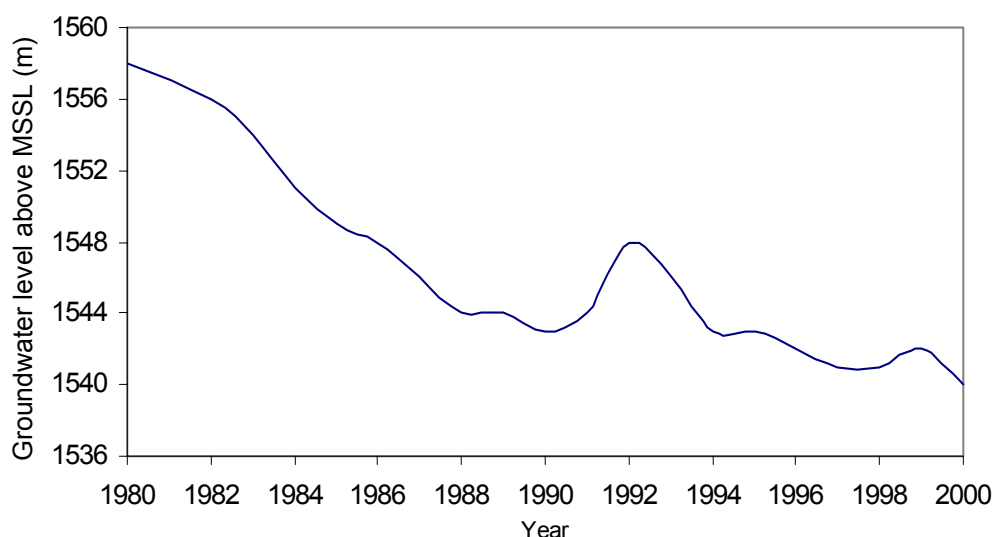
Figure 2.5 Average groundwater level above Mean Sea Surface Level (MSSL) over the period 1982 to 2000 in the Borkhar district (Source: Esfahan Water authority (EWA), 2001).

2.4 Cropping pattern and yields

Typically there is a two-season cropping pattern in the Borkhar district. Summer crops include fodder maize, sunflower, sugar beet and vegetables while winter crops are dominated by wheat and barley. In addition there are some annual and perennial crops, including alfalfa and orchards. Annual cropping intensity is about 85 %, with slightly higher values for winter than for summer crops. Depending on the weather conditions, the planting date of wheat and barley ranges from the beginning of October until the end of November. Maize and sunflower are planted in the period of June to the end of July. The planting date of sugar beet varies between April and May. The cropping pattern and their average yield for the main crops are shown in Fig. 2.6.
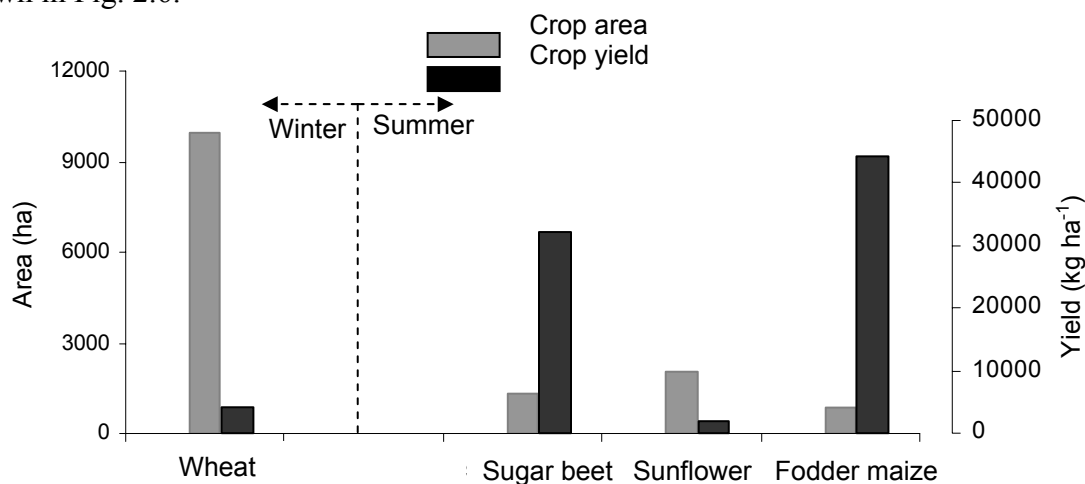
Figure 2.6 Average yield and cropping pattern for the main crops in the Borkhar irrigation district (Source: Organization of Jihad-e-Agriculture, Esfahan, Iran. [online]: http://www.esfahan.agri-jahad.ir/modiriat/tarh/amar%20nameh/index.htm, 01 September 2006).
.

Successful production of these crops without supplemental irrigation is hardly possible even during the monsoon season. From 1991 to 2003 the area under fodder maize has increased with more than 170 %. On the other hand, the area under sugar beet has decreased with more than 50 %. There is also a gradual fluctuation in area under wheat and sunflower during that period (Fig 2.7).
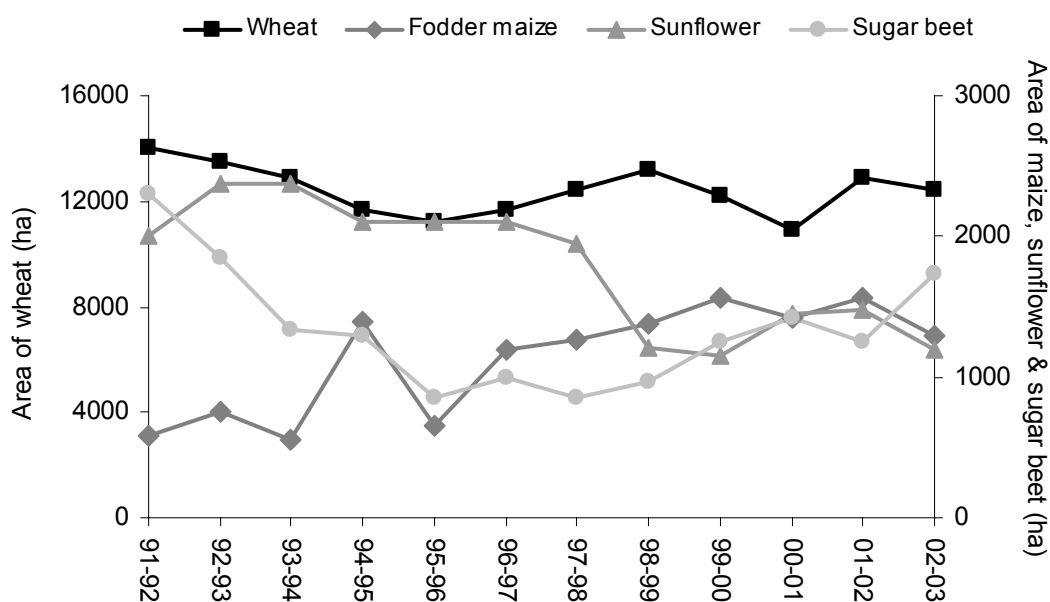
Figure 2.7 Areas of the main crops under cultivation in the Borkhar irrigation district over the from1991 to 2003. (Source: Organization of Jihad-e-Agriculture, Esfahan, Iran. [online]: http://www.esfahan.agri-jahad.ir/modiriat/tarh/amar%20nameh/index.htm, 01 September 2006)

Wheat and barely are the main crops during the winter season, which are followed by fodder maize and sunflower during the summer season. Intensive irrigation, being coupled with high yielding varieties, and increased use of fertilizer and pesticides over the years, has increased crop yields especially for fodder maize and sugar beet (Fig. 2.8). For instance, fodder maize yield has increased from 40 ton ha^{-1} in 1991 to 47 ton ha^{-1} in 2002. However, during drought years crop yields have decreased dramatically. For instance, the wheat crop yield decreased with more than 9 % in 1999, more than 15 % in 2000 and about 5 % in 2001.
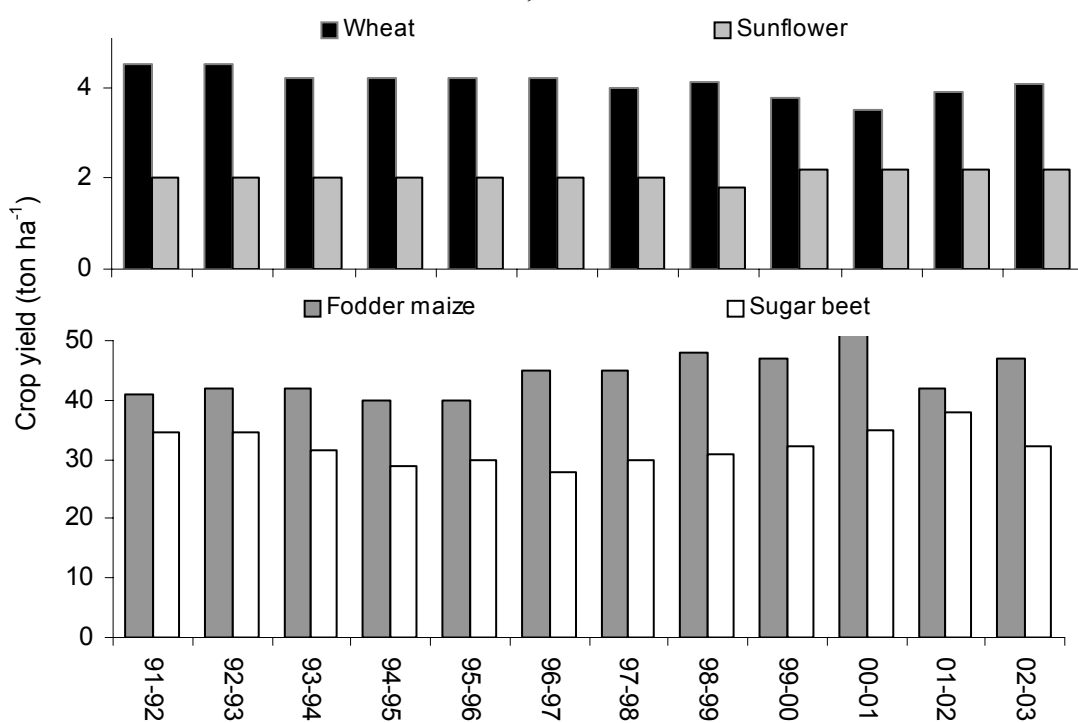
Figure 2.8 Average yield of the main crops in the Borkhar district over the years1991 to 2003. (Source: Organization of Jihad-e-Agriculture, Esfahan, Iran. [online]: http://www.esfahan.agri-jahad.ir/modiriat/tarh/amar%20nameh/index.htm, 01 September 2006).

18

2.5 Soil types

Dry weather conditions, geomorphology and other environmental factors induced the formation of different soil series. According to land evaluation and soil classification studies in 1973 (Soil and Water Research Institute (SWRI) of Iran), most of the soils in the district can be characterized as poorly drained, light brown to dark brown, single grained structure and clay loam to heavy clay loam. A high water holding capacity, low infiltration rate, low organic matter content and poor fertility status characterize the soils in the Borkhar irrigation district. The main soil series are the following (Fig 2.9):
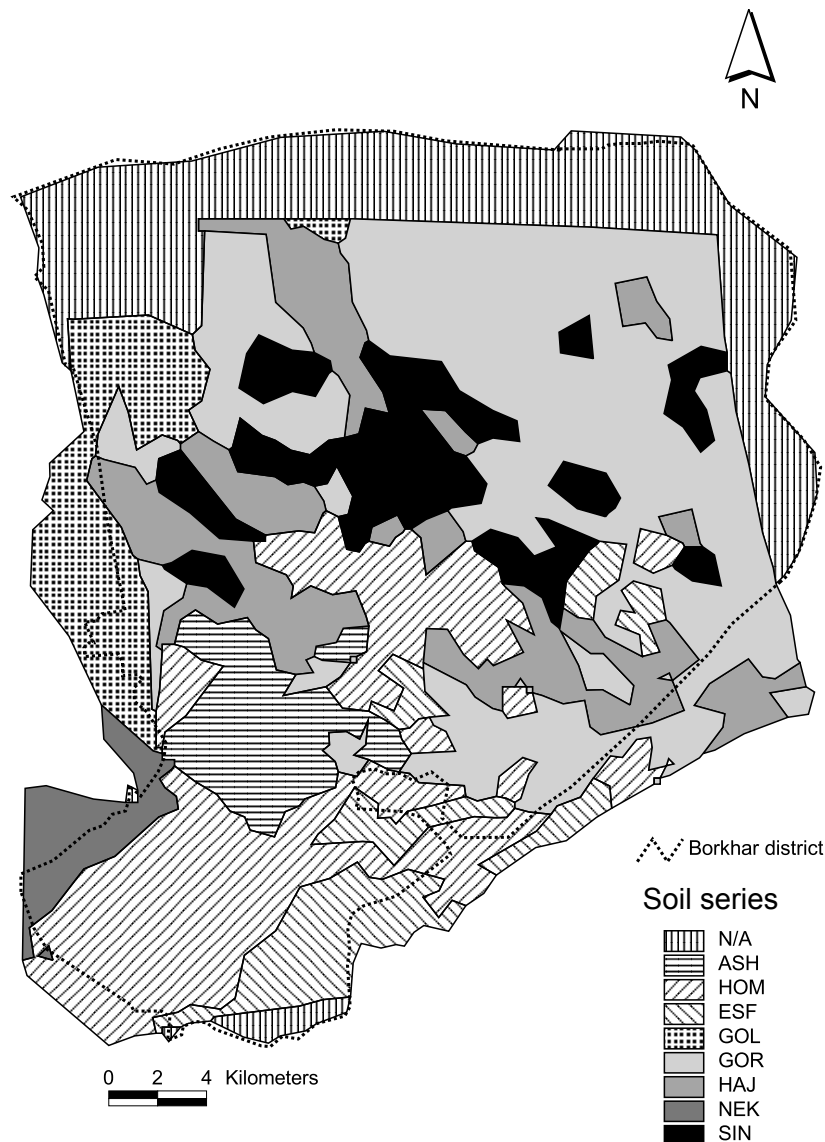
Figure 2.9 Soil series of the Borkhar irrigation district (Source: Soil and Water Research Institute of Iran, 1973) (ASH = Asheghabad, HOM = Homayonshahr, ESF = Esfahan, GOL = Golshahr, GOR = Gorgab, HAJ = Hajiabad, NEK = Nekoabad, SIN = Seen)

Golshahr (GOL) This soil series covers 17260 ha in the west north and south north of the Borkhar district. The parent materials of this soil are alluvial and colluvial fans. Soil texture in the profile layers varies between sandy clay loam and clay loam. In the

bottom layers, the soil colour varies from light brown to heavy brown. Soil permeability and natural drainage are rather good. From topographical point of view the area is completely flat with a small slope in west-east and north- south direction.

Homayonshahr (HOM) The parent material of this soil series is alluvial deposit. Soil texture differs from fine sandy clay loam to heavy clay loam. Soil colour varies between light brown and heavy brown. The drainage ability of this soil series is poor in the surface layers and increases in the deeper layers. Soil pH varies between 8.1 and 8.2 and organic matter percentage, i.e. about 0.5 %, is low. This soil series has been developed in the central parts of the district and its area is about 15966 ha. From topographical point of view, the area is martially flat with small slopes in west-east and north-south direction.

Seen (SIN) Soil texture differs from clay loam to clay in the profile. The pH varies between 7.6 and 8 and drainage ability is rather poor. The area of this soil series is about 7680 ha and covers the central parts of the district. From topographical point of view, the area is flat with small slopes in West–East and North-South direction.

Hajiabad (HAJ) Parent soil series has been developed under dry climatic conditions. Material of this soil series is alluvial material with a little gypsum. This soil series covers 10400 ha in the central parts of the district. Soil texture in the surface layers is mainly heavy clay and in the deeper layer clay loam. Soil pH varies between 7.9 and 8.1.

Gorgab (GOR) Soil texture varies between clay loam to heavy clay loam. Natural drainage is very poor. Total area of this soil series is about 25600 ha and covers the western and the central parts of the plain. The area is completely flat with a small slope in west-east direction.

Asheghabad (ASH) The initial materials of this soil series are of Calcirophic alluvial materials. Soil texture varies between clay loam and heavy clay loam, the drainage ability is poor. This soil series covers 4500 ha in the central parts of the district which are barren.

Esfahan (ES) This soil series covers 6400 ha lands in the southern parts of the district and north of Esfahan city. Soil texture is semi heavy and varies between clay loam and heavy clay loam. Drainage ability is rather good.

20

3. Increasing water productivity of irrigated crops under limited water supply at field scale

3.1 Defining water productivity of crops

In the period 2000-02 the Iranian Agricultural Engineering Research Institute (IAERI), together with the International Water Management Institute (IWMI), did several quantitative studies on water resources and the irrigated agricultural sector in the district. This studies basically the management of the major irrigation systems in the Zayande Rud basin (*Sally et al.*, 2001; *Salemi et al.*, 2000; *Droogers et al.*, 2000a, 2000b). In addition, satellite image interpretations were made for the assessment of irrigated area and land use (*Droogers et al.*, 2001; *Gieske et al.*, 2002a, 2002b). Although these studies give a good description of the hydrology, agriculture and water use changes of the district, *there is a general lack of field scale research on crop and water management strategies under water limited conditions.*

Under current water scarcity conditions, the limited available water should be used more efficiently (*Bessembinder et al.*, 2005). Taking into account that photosynthesis (and thus dry matter yield) and transpiration are related through the diffusion process of CO_2 and H_2O, the efficiency of crop water use can be defined as:

$$\text{Water use efficiency} = \frac{\text{Dry matter growth rate}}{\text{Transpiration rate}} = \frac{Y \text{ (kg ha}^{-1} \text{ d}^{-1})}{T \text{ (mm d}^{-1})} \tag{3.1}$$

In daily irrigation practices, 'water productivity' WP is a more relevant term for Eq. 3.1, where the meaning depends on the application. In the case that we integrate the rate of dry matter yield and transpiration over time i.e. the growing season, denoted as Y and T respectively. The efficiency of water used by the crop can then be expressed as water productivity WP_T:

$$WP_T = \frac{Y \text{ (kg ha}^{-1})}{T \text{ (mm)}} \rightarrow \frac{Y \text{ (kg ha}^{-1})}{T \text{ (m}^3 \text{ ha}^{-1})} \rightarrow \text{kg m}^{-3} \tag{3.2}$$

where 1 mm is equivalent with 10 m^3 ha^{-1}. When applying irrigation at field scale, it is generally difficult to distinguish plant transpiration T (mm) from soil evaporation E (mm). Hence, instead of WP_T, WP_{ET} may be used (*Molden et al.*, 1997; *Molden et al.*, 2001; *Droogers and Bastiaanssen*, 2002; *Kijne et al.*, 2003):

$$WP_{ET} = \frac{Y \text{ (kg ha}^{-1})}{ET \text{ (m}^3 \text{ ha}^{-1})} \rightarrow \text{kg m}^{-3} \tag{3.3}$$

where ET is the evapotranspiration of 'crop + soil'. Total dry matter yield Y may also be transformed into marketable yield i.e. Y_M.

If the amount of irrigation + precipitation water is considered as 'water use of the crop' then WP_{I+P} may be used:

$$WP_{I+P} = \frac{Y \text{ (kg ha}^{-1})}{[I + P] \text{ (m}^3 \text{ ha}^{-1})} \rightarrow \text{kg m}^{-3} \tag{3.4}$$

where *I* stands for amount of seasonal irrigation and *P* for the seasonal precipitation.

Under condition of very low precipitation as given in Fig. 2.2, WP_{I+P} may be converted to WP_I:

$$WP_I = \frac{Y \ (\text{kg ha}^{-1})}{I \ (\text{m}^3 \ \text{ha}^{-1})} \rightarrow \text{kg m}^{-3} \tag{3.5}$$

As the farmer is mainly interested in the economic yield of the crop, *WP* may be expressed in terms of money as:

$$WP_\$ = \frac{(\$ \ \text{kg}^{-1}) \ (\text{kg ha}^{-1})}{ET \ (\text{m}^3 \ \text{ha}^{-1})} \rightarrow \$ \ \text{m}^{-3} \tag{3.6}$$

where 1US $ is equivalent with 1$.

WP indicators express the benefit derived from the consumption of water and can be used for assessing the impact of on-farm strategies under water scarce conditions. They provide a proper vision of where and when water could be saved. *WP* indicators are also useful for looking at the potential increase in crop yield that may result from increased water availability (*Singh et al.*, 2006).

Quantitative information on *WP* indicators is therefore necessary to plan an efficient irrigation water management under water scarce conditions. In order to explore which farm strategies help us to achieve 'more crop per drop', we need to understand the interactions between soil, atmosphere, crop and water. Taking in account the spatial variability of the soil and the land use properties, as well as crop growth development, simulation of the water balance components will certainly increase our ability to improve water productivity under water shortage conditions.

In the past 30 years, physically based agrohydrological models such as the Soil Water Atmosphere Plant (SWAP) model (*Kroes and Van Dam*, 2003) have been developed to simulate crop growth and soil water processes. Simulation models are strong in scenario analyses and thus permit to explore viable ways of crop and water management which may help to mitigate the impact of drought. However, agrohydrological models use a large number of input parameters which may cause low performance and large uncertainty in simulation results such as actual evapotranspiration, deep percolation and dry matter yield (*Singh et al.*, 2006).

In this chapter, a methodology will be presented for evaluation of on-farm strategies under water limited conditions. The SWAP model will be calibrated and validated for the main crops in the Borkhar irrigation district using measurements from farmer's fields. Most of the input parameters collected from these fields will be used directly in the calibration procedures. The remaining unknown soil hydraulic parameters, irrigation depths and crop parameters will be determined indirectly by an inverse modelling technique (*Jhorar*, 2002; *Ritter et al*, 2003).

With the help of automated runs using the link between SWAP and the Parameter ESTimation model PEST (*Doherthy et al.*, 1995), *WP*–water consumption curves will be presented for the main crops and for different irrigation practices. On-farm strategies like

deficit irrigation scheduling and cropped area reduction will be evaluated using *WP* indicators. The maximum possible increases in *WP* indicators will be derived graphically from the *WP* curves.

3.2 Data collection at farmer's fields in the Borkhar irrigation district

Field measurements for four main crops, i.e. wheat during the winter season and fodder maize, sunflower and sugar beet during the summer season, were conducted in the Borkhar irrigation district. During the agricultural year 2004-05, detailed water, soil and crop parameters (Table 3.1) were collected from farmer's fields in the district.

In total 8 farmer's fields, denoted as W1 and W2 (wheat), M1 and M2 (Maize), Sa1 and Sa2 (sunflower), and Su1 and Su2 (sugar beet), were monitored intensively in the Borkhar irrigation district (Fig. 3.1).

W1, Su1 and M1 were located in the canal upstream of Hajiabad in the western part of the Borkhar irrigation district. In this area good water and crop management, fine soil texture (i.e. clay loam to silt clay loam) and access to both canal water and groundwater with good quality, are providing suitable growing conditions for wheat, maize and sugar beet.

The farmer's fields W2, M2, Sa2 and Sa1 were located along the main Bel canal in the north of the district. The cultivated area in this part of the district is depends on canal water amount. Traditional crop and water management as well as water shortage are the main limitations in providing sustainable growing conditions.

Field Su2 is located along the canal downstream of Hajiabad in the west of the district. The main source of irrigation water is groundwater which has a rather poor water quality. The soil texture is silt clay with a hardpan at the bottom of the root zone. Most of the soils in the selected fields have low organic carbon, and are rather sodic with a pH of about 8. The soil dry bulk density ranges from 1.35 to 1.46 g cm^{-3} in the heavy texture soils and from 1.48 to 1.7 g cm^{-3} in the lighter soil. The groundwater level is very deep and its salinity level is relatively low at all the selected farms (< 2 dS m^{-1}), except at field Su2.

Table 3.1 Overview of the data collected for calibration and validation of the SWAP model at the farmer's fields in the Borkhar irrigation district.

Data	Collection method	Frequency	Purpose
Meteorological data	Meteorology station	Daily	Input derivation
Soil properties			
Texture	International Pipette Method and USDA classification	Once	Input derivation
Bulk density	Core method	Once	Input derivation
Saturated hydraulic conductivity	Constant water head method	Once	Input derivation
Saturated percentage	Saturated paste method	Once	Input derivation
Organic Carbon	Wet digestion method (*Walkey and Black*, 1934)	Before Sowing	Input derivation
pH	In soil-water suspension of 1:2	Before Sowing	General
Soil moisture	Gravimetric Method	Weekly	Calibration and validation
Irrigation regime			
Discharge of irrigation source i.e. canal water or tube-well water	Current meter/ Co-ordinate/ Volumetric method	Once	Input derivation
Duration of irrigation	Field observation	Once	Input derivation
Irrigation depth	Irrigation depth was calculated by multiplying the discharge and duration of irrigation and then divided by field area	Once	Input derivation
Irrigation date	Field observation	After each irrigation	Input derivation
Irrigation quality	Conductivity meter	Once	Input derivation
Crop growth parameters			
Crop development stage i.e. emergence, panicle initiation, anthesis, maturity and harvest	Field observation	Once	Input derivation
Plant density and tillers	Field observation	4-5 times	Input derivation
Plant height	Field observation	4-5 times	Input derivation
Dry matter partitioning	Field observation and drying in oven	4-5 times	Calibration and validation
Leaf area	Field observation and leaf area meter	4-5 times	Calibration and validation
Rooting depth	Field observation	4-5 times	Input derivation
Crop yields	Field observation	Once	Calibration and validation
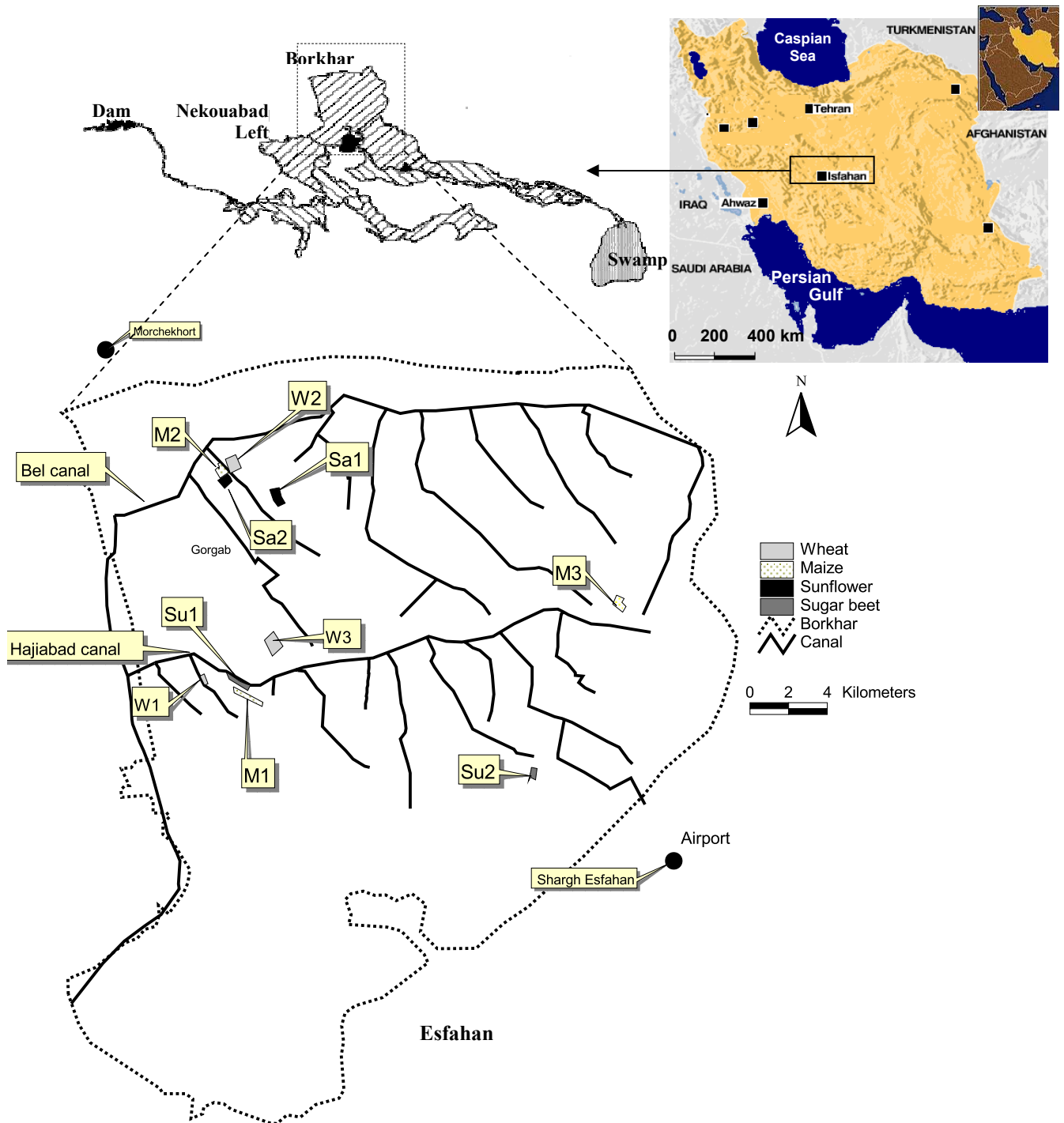
Figure 3.1 Location of the farmer's fields which were monitored in the Borkhar irrigation district during the agricultural year 2004-05.

3.3 Simulation model SWAP

Water balance and crop growth analysis were performed using the SWAP model (*Feddes et al.*, 1978; *Van Dam et al.*, 1997; *Kroes and van Dam*, 2003). SWAP is a comprehensive agrohydrological model for water, heat, and solute transport in the unsaturated-saturated zone. SWAP includes physically based modules to simulate irrigation practices and crop growth. Water movement simulation in SWAP is based on Richards' equation:

$$C_{\mathrm{w}}(h)\frac{\partial h}{\partial t} = \frac{\partial}{\partial z}\left[K(h)\left(\frac{\partial h}{\partial z}+1\right)\right] - S(z) \tag{3.7}$$

where C_{w} is the differential water capacity (cm^{-1}), h soil water pressure head (cm), K hydraulic conductivity (cm d^{-1}), S root water extraction (cm^3 cm^{-3} s^{-1}) and z soil depth (cm).

A finite difference scheme is used to solve Eq. (3.7) for the prevailing soil hydraulic functions and boundary conditions. The soil hydraulic functions are defined as relationships between hydraulic conductivity K, soil moisture θ and soil water pressure head h. In SWAP, analytical functions proposed by *Van Genuchten* (1980) and *Mualem* (1976) are used to define the soil moisture retention curve:

$$\theta(h) = \theta_{\mathrm{res}} + \frac{\theta_{\mathrm{sat}} - \theta_{\mathrm{res}}}{\left[1+\left|\alpha h\right|^n\right]^{\frac{n-1}{n}}} \tag{3.8}$$

where θ_{res} is residual water content (cm^3 cm^{-3}), θ_{sat} saturated water content (cm^3 cm^{-3}), and α (cm^{-1}) and n (-) empirical shape factors.

The hydraulic conductivity curve is described as:

$$K(\theta) = K_{\mathrm{sat}} S_{\mathrm{e}}^{\lambda}\left[1-\left(1-S_{\mathrm{e}}^{n/n-1}\right)^{\frac{n-1}{n}}\right]^2 \tag{3.9}$$

where K_{sat} is the saturated hydraulic conductivity (cm d^{-1}), $S_{\mathrm{e}} = (\theta - \theta_{\mathrm{res}}) / (\theta_{\mathrm{sat}} - \theta_{\mathrm{res}})$ relative saturation (-) and λ an empirical coefficient (-).

The upper boundary condition is determined by the fluxes of potential evapotranspiration, ET_{p} (mm d^{-1}), irrigation, I (mm d^{-1}), and precipitation, P (mm d^{-1}). ET_{p} is estimated by the Penman-Monteith equation, using daily weather data of solar radiation, air temperature, humidity and wind speed as well as crop characteristics such as minimum crop resistance, surface albedo and crop height (*Allen et al.*, 1998). Under field conditions where crops partly cover the soil, ET_{p} is partitioned into potential soil evaporation E_{p} and potential transpiration T_{p} using either the leaf area index or the soil cover.

As long as the soil is relatively wet, the actual soil evaporation flux E is governed by atmospheric demands and is set equal to E_{p}. Under dry conditions, E is controlled by maximum soil water flux, E_{max} in top soils. In SWAP, E_{max} is computed according to Darcy's law, using soil hydraulic functions of the top soil compartments. However due to effects of splashing rain, dry crust formation, root extension, and mechanical soil cultivation, in the top soil the soil

hydraulic functions may change and Darcy's law can overestimate the actual soil evaporation flux E. Therefore, in addition SWAP computes soil evaporation E using empirical functions, E_{emp}, of *Black et al.* (1969) and sets E as the minimum value of E_p, E_{max} and E_{emp}.

The potential transpiration flux T_p is computed as ET_p-E_p. Under non-optimal conditions i.e. either too dry, too wet or too saline, T_p will be reduced to the actual transpiration flux, T. For water stress, Feddes et al. (1978) proposed a transpiration reduction function as depicted in Fig. 3.2. The critical pressure head h_3 for too dry conditions depends on T_p. The values of the input variables h_1, h_2, h_{3h}, h_{3l}, and h_4 (cm) are assumed to be crop specific and can be found in the literature (e.g. *Taylor and Ashcroft* (1972, Table 14.3); *Doorenbos and Kassam*, 1979).
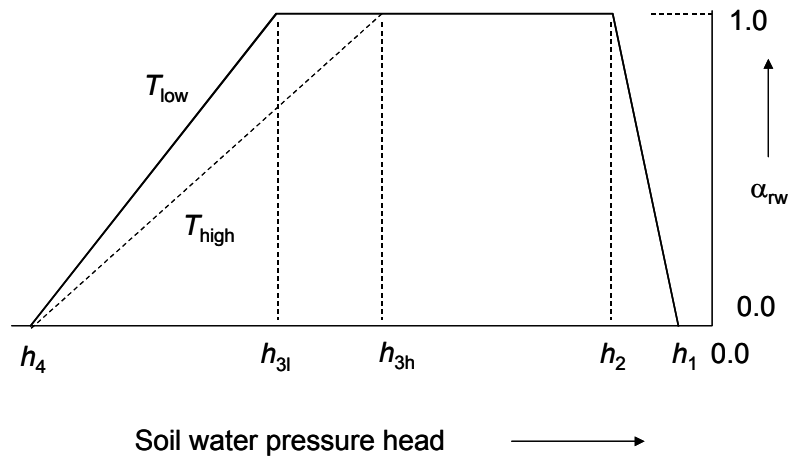
Figure 3.2 Reduction coefficient, α_{rw} (-), as a function of the soil water pressure head, h (cm) and the potential transpiration flux, T_p (mm d^{-1}) (after *Feddes et. al.*, 1978).

Crop growth can be simulated using the simple crop growth algorithm of Doorenbos and Kassam (1979) or by using a detailed crop growth simulation module. The latter has the advantage of simulating the actual and potential crop dry matter yield, Y and Y_p respectively. It is based on WOFOST 6.0 (*Supit et al.*, 1994). Dry matter growth rate Y_p (kg dry matter ha^{-1} d^{-1}) is simulated by computing the potential gross assimilation A_{pgross} (kg CO$_2$ ha^{-1} d^{-1}) of a crop under optimal conditions based on incoming radiation absorbed by the crop canopy and photosynthetic leaf characteristics:

$$A_{p\,gross} = A_{max}\left(1 - e^{\frac{\varepsilon_{PAR} PAR_{L,a}}{A_{max}}}\right)$$

(3.10)

where A_{max} presents the maximum assimilation rate (kg CO$_2$ ha^{-1} d^{-1}), ε_{PAR} initial slope or light use efficiency (kg CO$_2$ J^{-1} absorbed), and $PAR_{L,a}$ rate of absorbed radiation

(J m^{-2} leaf d^{-1}) at a depth L in the canopy. The instantaneous rates per leaf layer need to be integrated over the canopy leaf area index and over the day.

Taking into account water and/or salinity stress, $T\,T_p^{-1}$ is used to quantify actual gross assimilates (kg CO_2 ha^{-1} d^{-1}) being produced by the crop. Part of the produced assimilates are used to provide energy for maintenance and growth respiration. The remaining net assimilation rates integrated over crop height and time, i.e. crop growth season, are converted to crop dry matter yield (kg dry matter ha^{-1}) using a weighted average conversion factor C_e (kg kg^{-1}) for :

$$Y = C_e \sum_{t=1}^{N} \left(\frac{30}{44} T\,T_p^{-1}(t) A_{p\,gross}(t) - R_m(t) \right) \tag{3.11}$$

where the factor 30/44 stands for conversion of CO_2 to biomass, R_m the actual maintenance respiration rate (kg ha^{-1} d^{-1}) and N (d) is the total length of the growing season. The produced dry matter Y is partitioned among the roots, leaves, stems and storage organs, using conversion factors as function of the crop development stage (*Spitters et al.*, 1989). Net increase in leaf structural dry matter Y_L and specific leaf area S_{LA} (ha kg^{-1}) determines the dynamics of $LAI\,(= S_{LA}\,Y_L)$. On its turn, LAI determines the amount of light interception and indirectly affects the simulated dry matter of the plant organs.

The effect of nutrient deficiency, pests, weeds, and diseases on crop growth and its production have not been implemented in the present 3.0.3 version of SWAP. More details of the SWAP model can be found in the literature (*Kroes and Van Dam*, 2003).

3.4 Input data to the SWAP model

3.4.1 Upper boundary

The meteorological data (including minimum and maximum air temperature T_{min} and T_{max}, relative humidity RH, vapour pressure e_{air}, sunshine duration $\boldsymbol{n}$, wind speed U_2 and rainfall P) were collected at three synoptic meteorological stations in and around the Borkhar district: Shargh Isfahan (lat. 32° 40' N, Long. 51° 52'E) located at the South Western, Morchekhort (lat. 33° 05'N , long. 51° 29' E) located at the Northern and Meymeh (lat. 33° 26'N, long. 51° 10'E) located at the North Eastern parts of the Borkhar irrigation district. Fig. 3.3 shows the daily variation of solar radiation R_s, air temperature T_{air}, rainfall P and reference grass evapotranspiration ET_{ref} in the Borkhar irrigation district during the agricultural year 2004-05.

Since weather data were collected from non-agricultural weather stations, temperature and humidity data were adjusted with coefficients of 0.95 and 1.05 respectively (*Alizadeh and Vazifedoust*, 2000). Values of R_s were calculated from measured sunshine hours using the Angstrom formula (Angstorm, 1924). The value of R_s varied from 3.5 to 29.4 MJ m^{-2} d^{-1}. During summer time, the daily maximum air temperature T_{max} reached on individual days 36.1 ^{o}C.
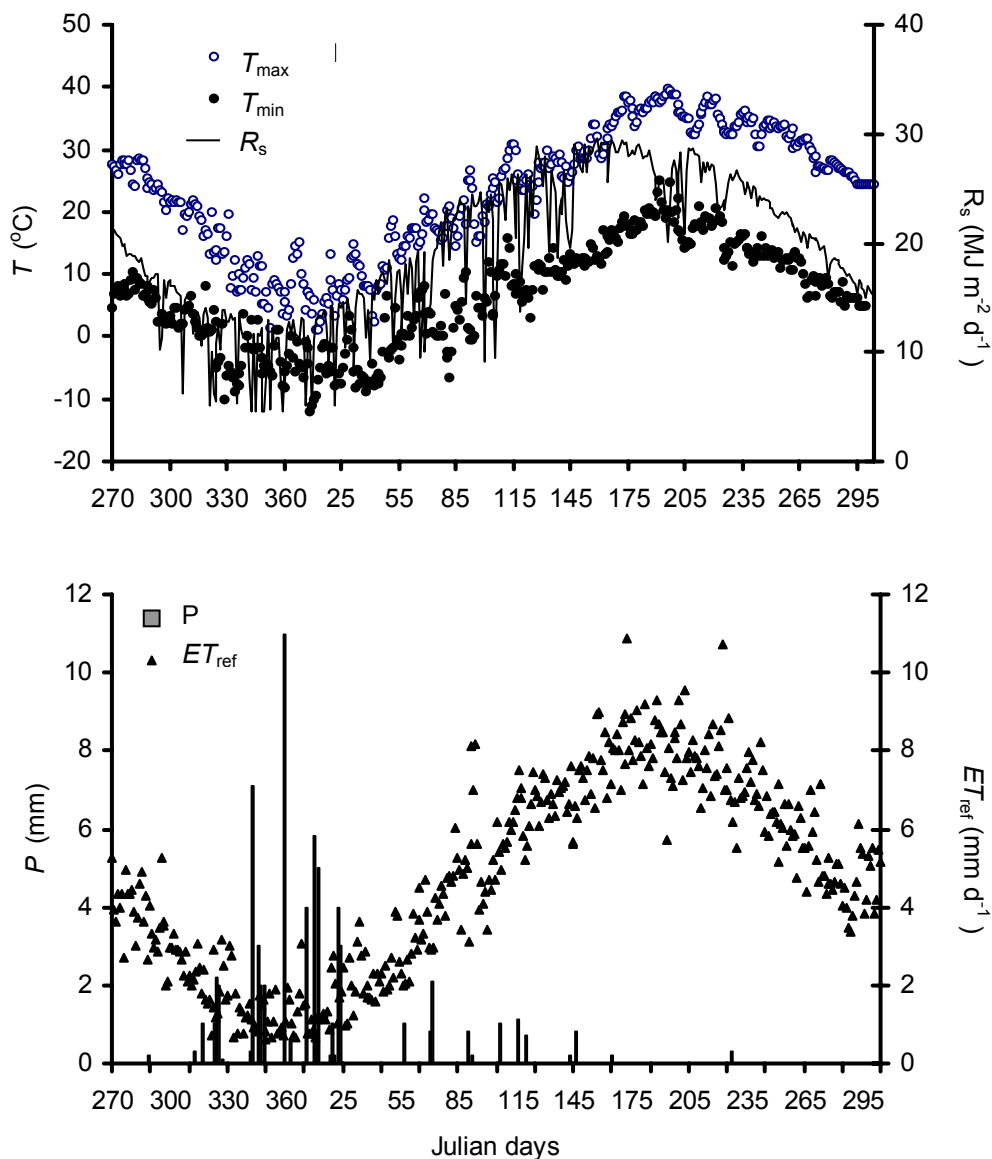
Figure 3.3 Variation of the maximum and minimum temperature, T_{max} and T_{min}, solar radiation R_s, rainfall P and reference grass evapotranspiration ET_{ref} in the Borkhar district during the agricultural year 2004-05.

3.4.2 Irrigation practices and soil hydraulic properties

Computed water balance components using simulation models are quite sensitive to the irrigation practices and the soil hydraulic parameters of the soil profile (*Jhorar*, 2002). During the measurements at monitored fields, the water quality and dates of irrigations were recorded. The irrigation depths were very variable in the Borkhar irrigation district and were difficult to measure at the farmer's fields. The irrigation depths were calculated once by multiplying the discharge and duration of irrigation and then divided by the area of the field (Table 3.1). However, due to the difficulty in measuring the volume of applied water, the estimated depth may not be the representative for the applied irrigation depth. Therefore, the irrigation depths were optimized automatically using an inverse modelling technique.

Of the parameters describing the soil hydraulic functions (Eqs. 3.8 and 3.9) θ_{sat} ($cm^3 cm^{-3}$) and K_{sat} ($cm\ d^{-1}$) have a clear physical meaning and were measured at the

monitored fields. The variables θ_{res} (cm^{3}cm^{-3}) and λ (-) show low sensitivities (*Van Dam and Malik*, 2003), and therefore were derived from pedotransfer functions (*Wösten*, 1998). Two soil hydraulic parameters remained uncertain: α (cm^{-1}) and *n*. These two parameters were optimized.

To derive the selected soil hydraulic parameters and irrigation depths inversely, a *non-linear parameter estimation program*, PEST (*Doherthy et al.*, 1995) was linked with SWAP. The PEST package is comprised of the PEST program, six utility programs for building and checking PEST input files, and also a SENSistivity Analysis (SENSAN) program for multiple running of the model using different parameter values for each run. The PEST program works in two different modes of "*parameter estimation*" and "*predictive analysis*". In the parameter estimation mode of PEST, the model is run with an initial guess of the parameters and compares the model results with observation data. PEST adjusted selected parameters using an optimization algorithm (Levenberg-Marquardt) and executes the model again. The procedure of adjusting selected parameters continued until either the difference between the model results and observation data or the number of iterations met a preset criteria. An overview of the parameters estimation procedure is shown in Fig. 3.4.
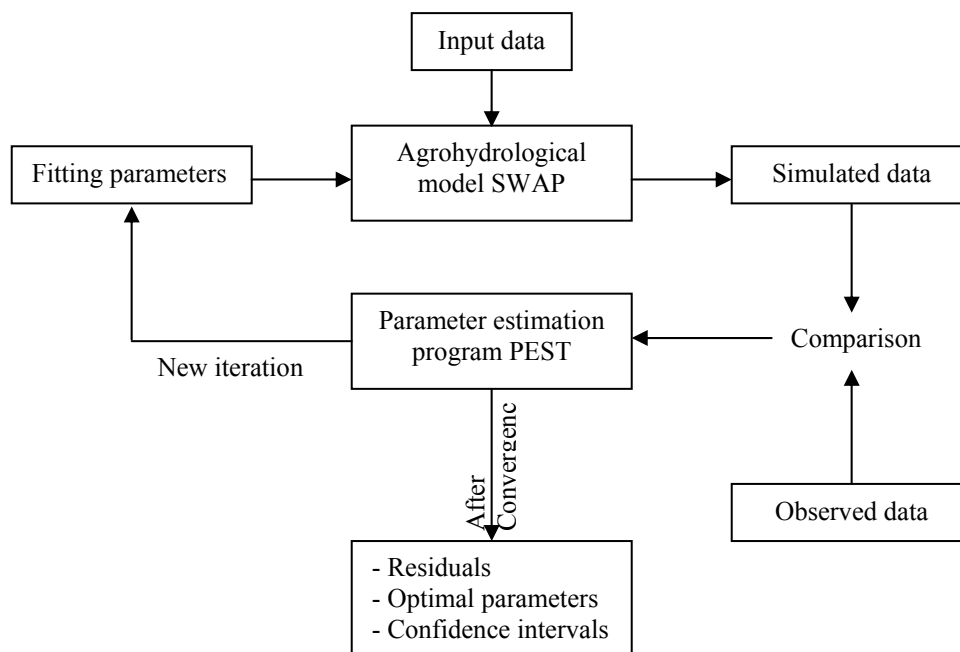
Figure 3.4 Communication between the agrohydrological model SWAP and the parameter estimation program PEST.

An objective function $O(\boldsymbol{b})$ was defined for quantifying the differences between model results and observations according to:

$$O(\boldsymbol{b}) = \sum_{i=1}^{N} (\theta_{\text{obs}}(t_i) - \theta_{\text{sim}}(\boldsymbol{b}, t_i))^2 \tag{3.12}$$

where $\theta_{\text{obs}}(t_i)$ is the observed soil moisture at time t_i, *N* number of measurements and $\theta_{\text{sim}}(\boldsymbol{b}, t_i)$ simulated values of θ using an array with parameter values $\boldsymbol{b}$. The inverse problem

was then to find an optimum combination of parameters that minimizes the objective function. The inverse problem can be well posed by a small number of fitting parameters. To reduce the number of parameters, irrigation depths were assumed to be constant in each irrigation event. This was a fair assumption for the Borkhar irrigation district due to the heavy traditional irrigations. Therefore, as the fields considered in this analysis possess two soil layers (Table 3.2), the total parameters to be optimized are 5.

Table 3.2 Soil texture (C=clay, Si=silt, L=loam) and dry bulk density at the monitored farmer's fields in the Borkhar irrigation district.

| Fields | Layer | Soil Texture | Soil physical properties | | | |
| | | | C | Si | ρ_d | OC |
	(cm)		%	%	kg m^{-3}	%
W1	0-90	C	46	36	1.4	1.20
	>90	CL	56	36	1.5	0.58
W2	0-60	SiC	40	43	1.6	0.74
	>60	C	48	35	1.7	0.07
M1	0-60	C	52	38	1.4	2.10
	>60	C	52	38	1.5	0.10
M2	0-30	SiCL	39	46	1.7	0.06
	>30	C	50	40	1.7	0.54
Sa1	0-30	C	41	34	1.6	0.29
	>30	CL	32	40	1.7	0.10
Sa2	0-30	SiCL	39	46	1.7	0.05
	>30	C	50	40	1.7	0.54
Su1	0-60	SiCL	44	41	1.5	0.86
	>60	CL	32	74	1.4	0.15
Su2	0-30	SiC	53	42	1.3	1.20
	>30	SiC	49	46	1.3	0.36

The soil moisture profiles measured at the monitored fields were used as observation data. The soil moisture data were measured gravimetrically at soil samples taken weekly from 5 different soil depths: 0-15, 15-30, 30-60, 60-90 and 90-120 cm. The observed soil moisture data were divided into two sets. The first part was used in the calibration procedures and the second part was used for validation of the optimized parameters. Fig. 3.5 shows the partitioning of observation data used in the calibration and validation process.
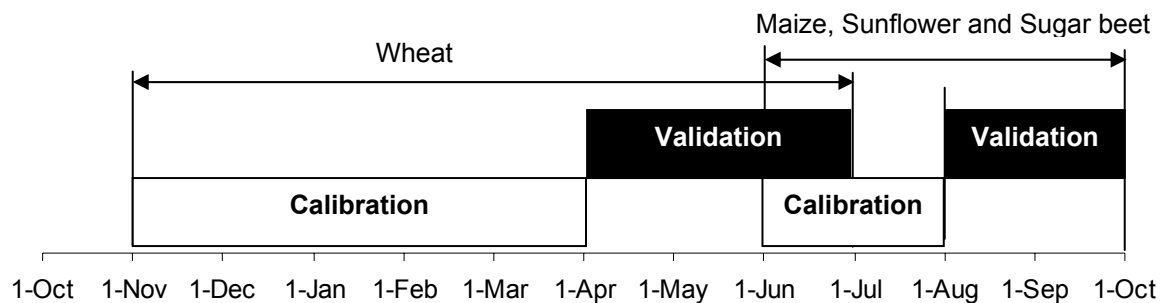
Figure 3.5 Partitioning of observation data for the calibration and validation of soil hydraulic properties and irrigation depth.

To evaluate the level of difference between the observed and simulated data with the optimized parameters, the Root Mean Square Error (*RMSE*) was computed as:

$$RMSE = \sqrt{\frac{\sum_{i=1}^{N}[\theta_{obs}(t_i) - \theta_{Sim}(t_i)]^2}{N}}$$

(3.13)

3.4.3 Crop parameters

The crop parameters in the detailed crop module of SWAP are classified as: crop height h_{crop}, root depth z_{root}, leaf surface area *LAI*, assimilation and conversion factors to biomass, dry matter partitioning to the organs, crop water use. Part of the crop parameters can be adjusted and determined on the basis of experimental data and/or literature (*Bessembinder et al.*, 2003). During the agricultural year 2004-05 detailed crop parameters such as the number of tillers per unit area, h_{crop}, *LAI*, dry matter and its partitioning to the organs, and z_{root} at different crop development stages, were measured at the monitored fields (Table 3.1). For the parameters that can not be fixed, a range of realistic values was determined, based on experimental data and literature.

Simulation of dry matter production in SWAP is relatively sensitive to S_{la}, ε, A_{max}, which are crop specific (*Bessembinder et al.*, 2003). These parameters were adjusted manually by running the model with various combinations of the values within the realistic ranges after calibration of irrigation depth and soil hydraulic properties using simple crop growth module. The input parameters used for the simulated crops wheat, fodder maize, sunflower and sugar beet are summarized in Table 3.3.

Table 3.3 Crop parameters of the detailed crop growth module used in the simulations.

Parameter	Winter Wheat	Fodder Maize	Sun flower	Sugar beet
Temperature sum from emergence to anthesis, TSUMEA, ($^{\circ}$C)	1300	870	1100	500
Temperature sum from anthesis to maturity, TSUMAM, ($^{\circ}$C)	750	950	1000	2250
Specific Leaf Area, S_{la}	0.0017	0.0046	0.0035	0.0023
Maximum relative increase in *LAI*, RGRLAI ($m^2 m^{-2} d^{-1}$)	0.008	0.029	0.029	0.029
Light extinction coefficient, K_{gr}	0.37	0.4	0.67	0.24
Light use efficiency, ε (kg ha^{-1}hr^{-1}/ J m^2 s^{-1})	0.4	0.6	0.5	0.5
Maximum CO_2 assimilation rate, A_{max} (kg ha^{-1} hr^{-1})	43.0	73	45	45

3.5 Calibration results of effective soil hydraulic parameters

The optimized values of α and n with other soil hydraulic parameters (θ_{res}, θ_{sat}, K_{sat} and λ) are given in Table 3.4. Repetition of the optimization process with different initial values of α and n resulted in the same values, which showed the uniqueness of the optimized parameters.

Table 3.4 Optimized soil hydraulic parameters at the monitored farmer's fields in the Borkhar irrigation district. Parameters α and n were optimized.

Fields	Layer (cm)	θ_{res} (cm^{3}cm^{-3})	θ_{sat} (cm^{3}cm^{-3})	K_{sat} (cm d^{-1})	α (cm^{-1})	λ (-)	n (-)
			Soil hydraulic properties				
W1	0-90	0.01	0.45	24.0	0.0167	-3.84	1.287
	>90	0.01	0.40	06.2	0.0036	-1.19	2.042
W2	0-60	0.05	0.40	30.0	0.0083	-2.73	1.162
	>60	0.05	0.40	07.0	0.0020	0.17	1.398
M1	0-60	0.05	0.43	24.0	0.0153	-3.83	1.140
	>60	0.05	0.38	06.6	0.0023	-1.19	1.512
M2	0-30	0.01	0.34	10.1	0.0070	-5.16	1.259
	>30	0.01	0.40	03.0	0.0182	-3.41	1.205
Sa1	0-30	0.05	0.36	30.0	0.0021	-2.73	1.580
	>30	0.05	0.40	07.0	0.0032	0.17	1.352
Sa2	0-30	0.01	0.32	13.8	0.0020	-5.16	1.318
	>30	0.01	0.31	30.5	0.0027	-3.41	1.122
Su1	0-60	0.05	0.45	24.3	0.0257	-3.83	1.229
	>60	0.05	0.40	07.5	0.0020	-1.19	1.365
Su2	0-30	0.05	0.57	22.1	0.0386	-5.03	1.207
	>30	0.05	0.52	30.6	0.0045	-2.37	1.533

The *RMSE* of soil moisture ranged from 0.02 to 0.052 cm^3 cm^{-3} showing that at the different fields the soil water flow was simulated quite well by SWAP (Table 3.5). The differences between the observed and simulated θ is partly due to spatial heterogeneity and observation errors, which are inevitable under field conditions (*Singh et al.*, 2006).

Table 3.5 Root mean square error (*RMSE)* and number of observations *N* of soil moisture content θ at the monitored farmer's fields in the Borkhar irrigation district for both the calibration and validation period.

Fields	Calibration θ (cm^3 cm^{-3})		Validation θ (cm^3 cm^{-3})	
	N	*RMSE*	*N*	*RMSE*
W1	20	0.048	20	0.052
W2	28	0.020	20	0.039
M1	24	0.028	16	0.038
M2	9	0.028	9	0.038
Sa1	12	0.040	8	0.049
Sa2	12	0.043	8	0.027
Su1	32	0.027	20	0.028
Su2	24	0.029	20	0.028

Typical observed and simulated soil moisture profiles of the sample fields W1 and M1 are shown in Fig. 3.6. During the calibration period, the *RMSE* at fields W1 and M1 were 0.048 and 0.028 cm^3 cm^{-3} respectively. The *RMSE* during the validation period were also small: 0.052 at field W1 and 0.038 cm^3 cm^{-3} at field M1.
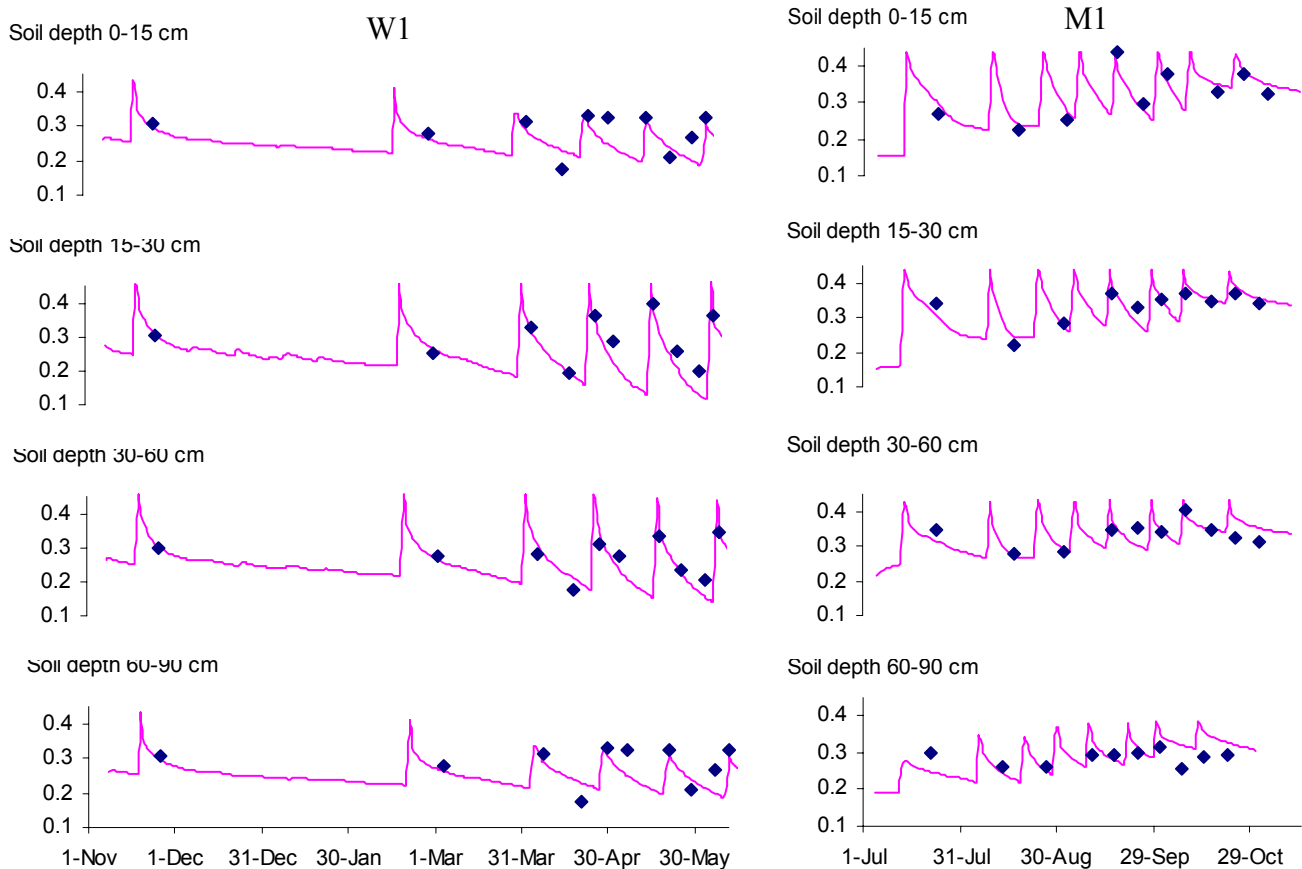
Figure 3.6 The observed and simulated soil moisture θ profiles at the fields W1 and M1 for the agricultural year 2004-05.

3.6 Computed soil water balance components using SWAP

The optimized soil hydraulic data (Table 3.4) and irrigation depths, in combination with other input data (Table 3.1 and Table 3.3) were used in SWAP to simulate the water balances components and the crop yields at different the farmer's fields. Accurate simulation of the water balance component and crop yields are necessary for the calculation of reliable *WP* indicators. Table 3.6 shows the computed water balance components at different farmer's fields in the Borkhar irrigation district.

Table 3.6 Computed water balance components (mm) by SWAP for the main agricultural crops at the farmer's fields in the Borkhar irrigation district

Water balance components	Fields							
	W1	W2	M1	M2	Sa1	Sa2	Su1	Su2
	Wheat		Fodder maize		Sunflower		Sugar beet	
P	33	33	0	0	0	0	0	0
I	1020	770	1280	900	800	700	990	1100
T_p	519	425	624	641	754	685	722	682
T	443	316	513	578	570	426	612	594
E_p	400	506	311	256	250	319	522	561
E	128	145	71	56	63	82	133	135
ET	572	462	584	634	632	508	745	729
Q_{bot}	-406	-140	-366	-46	-66	-22	-22	-187
ΔW [1]	75	201	330	220	102	170	223	184

(1) Computed for soil column of 1.2 m.

The rainfall contribution to crop evapotranspiration was mainly during the winter season, and very low (33 mm) in comparison to the irrigation supplies to the fields. The amount of irrigation I ranged from 770 to 1020 mm for the winter crops and 700 to 1280 mm for the summer crops. The high water supplies at W1, M1, Sa1 and Su1 are due to the access to both canal water and groundwater.

The optimized amounts of irrigations at farmer's fields are in agreement with average available water for irrigation at the Borkhar irrigation district. The total number of tube-wells in the agriculture area of the district is 478 (*APERI*, 2001). Average annual extraction from groundwater considering an average discharge capacity Q_{gw} of 100 m³ hr⁻¹ (*APERI*, 2001) and 20 hours working time for 10 months is 289 million m³. Annual releases water from the reservoir to the Borkhar district irrigation network varies from 0 to 50 million m³. Total irrigated area in both the winter and summer growing season is estimated at about 22250 ha (*Droogers et al.*, 2001). Assuming that 80% of the water is available for irrigation (*Droogers and Torabi*, 2002), total available water for irrigation varies from maximum 1000 to 1200 mm ha⁻¹.

ET_p simulated by the calibrated and validated SWAP was 925 mm for winter wheat during the period from Nov, 2004 to Jun, 2005. ET_p during growing period of maize and sunflower was 916 and 1004 mm respectively. The growing period of maize was from July to Oct, 2005. The growing period for sunflower was slightly shorter and ranged from July to Sep 15, 2005. ET_p for sugar beet during the period of June to Nov, 2005 was 1240 mm.

Under field conditions, simulated actual evapotranspiration ET for wheat ranged from 462 mm at field W2 to 572 mm at field W1 (Table 3.6). The lower ET at field W2 is due to lower amount of irrigation at this field. The simulated ET at sunflower farms ranged from 508 at Sa2 to 632 mm at Sa1. In spite of the higher irrigation application for maize at field M1, the simulated ET at this field was 8 % lower than simulated ET for maize at field M2. This indicates weak irrigation practices at field M1 which caused higher water stress at specific time in the growing season of maize. The water stress causes lower leaf area and finally results in lower T. In the same situation, simulated ET for sugar beet at field Su2 with

the higher amount of irrigation was almost similar to the **ET** value at field Su1. The simulated **ET** for sugar beet ranged from 729 mm at field Su2 to 745 mm at field Su1 (Table 3.6).

Due to heavy irrigation application, percolation Q_{bot} at fields W1, M1, Sa1 and Su2 was much higher than those at fields W2, M2, Sa2 and Su1, indicating the over irrigation of these fields. Low initial soil moisture at fields W2, M1, M2, Sa2, Su1 and Su2 caused high amount of stored moisture content in the soil profile *ΔW* at these fields.

3.7 Potential and water limited crop yield

Using the detailed crop growth module of SWAP and input parameters (Table 3.1, Table 3.3 and Table 3.4), crop dry matter yield, **Y**, and dry matter of storage organ, Y_{SO}, was simulated for the cultivated crops at the selected farmer's fields. Under water stress conditions, SWAP reduces the potential dry matter growth rate Y_p to the water limited growth rate *Y*. In addition to water stress under field conditions other factors such as nutrition deficiency, pests and diseases may affect potential dry matter yield Y_p. However SWAP does not consider other factors and assumes optimum nutrition conditions without any pest or diseases stress. Table 3.7 shows the simulated **Y**, Y_{SO} and marketable yield Y_M at different farmer's field during the agricultural year of 2004-05 at the Borkhar irrigation district.

Table 3.7 Simulated total dry matter yield **Y**, simulated dry matter of storage organ Y_{SO}, simulated marketable yields, Y_M, Root Mean Square Error (*RMSE*) and umber of observation *N* for the main crops in the Borkhar irrigation district during the agricultural year 2004-05.

Crop	Fields	**Y** ton ha^{-1}	**Accuracy of Y** ton ha^{-1}		Y_{SO} ton ha^{-1}	**Accuracy of Y_{SO}** ton ha^{-1}		Y_M ton ha^{-1}
			N	*RMSE*		*N*	*RMSE*	
Wheat	**W1**	15.3	5	1.11	6.5	3	0.70	5.6
	W2	10.4	5	1.90	4.1	3	0.95	3.5
Fodder Maize	**M1**	17.8	5	2.00	-	-	-	17.8
	M2	19.1	4	3.08	-	-	-	19.1
Sunflower	**Sa1**	9.7	4	2.09	5.6	2	0.96	1.9
	Sa2	6.5	3	1.51	4.0	3	1.23	1.4
Sugar beet	**Su1**	7.4	3	2.26	14.8	3	1.90	10.3
	Su2	6.4	6	2.72	15.0	3	1.38	10.4

The long term average of statistical data as reported by the Organization of Jihad-e-Agricultural in Esfahan, Iran (2006) indicates an actual yield of 4.1 ton ha^{-1} for wheat, 44.4 ton ha^{-1} for fresh fodder maize, 1.9 ton ha^{-1} for sunflower and 32 ton ha^{-1} for fresh sugar beet in the Borkhar irrigation district. In this study, simulated Y_{SO} for wheat varied from 4.1 to 6.4 ton ha^{-1}. Considering 85 % of Y_{SO} weight is grain (*Penning de Vries et al.*, 1983), the simulated Y_M for wheat ranged from 3.5 (field W2) to 5.6 (field W1) ton ha^{-1} with an average value of 4.5 ton ha^{-1} which is 10 % higher than the long term average of statistical data for the district.

The simulated Y for fodder maize ranged from 17.8 (field M1) to 19.1 (field M2) ton ha^{-1}. In spite of higher irrigation at field M1 (Table 3.6), actual Y for fodder maize at fields M1 and M2 are almost the same with an average value of 18.4 ton ha^{-1} which shows over irrigation at field M1. The simulated actual Y for fodder maize was almost 2 times higher than the long term averaged actual Y in the district, with considering a factor of 0.2 to convert fresh yield to dry matter yield (*Mokhtari*, 2006).

Simulated sunflower's Y_{SO} at the fields Sa1 and Sa2 were 5.6 and 4.0 ton ha^{-1} respectively. A harvest index (HI) factor of 0.33 (*Mokhtari*, 2006) defined as ratio of marketable yield to the Y_{SO}, was used to convert sunflower's Y_{SO} to seed yield. Calculated Y_M varied from 1.4 at field Sa2 to 1.9 ton ha^{-1} at field Sa1, which are in agreement with the long term reported data.

Taking into account that fresh storage organs of sugar beet contains 77 % water (*Penning de Vries et al., 1983*), fresh weight of simulated Y_{SO} was almost 3 times of the long term averaged data, which shows high variety in sugar beet yields in the district. Y_M of sugar beet, assuming 70 % of Y_{SO} is sugar (*Penning de Vries et al., 1983*), was 10.4 ton ha^{-1}.

To assess the accuracy of the crop yield simulation, the simulated aerial dry matter Y and water limited yield Y_{SO} was also compared with the observation data measured during the growing season (Table 3.7). The *RMSE* of Y ranged from 1.11 (field W1) to 3.08 (field M2) ton ha^{-1}. The *RMSE* of Y_{SO} ranged from 0.7 (field W1) to 1.9 (field Su1) showing that at the different fields both the Y and Y_{SO} were simulated quite well by SWAP. The differences between the observed and simulated Y / Y_{SO} are partly due to the spatial heterogeneity and observation errors.

3.8 Water productivity under current conditions

WP indicator values were calculated using simulated water balance components T, ET, I, the Y_M and market price of crop productions. A simple economic analysis was used based on three factors: price / kg crop, costs / kg crop, and fixed costs / ha. The price of water in the basin is very low (about $ 0.002 m^{-3}) and it is considered to be included in the fixed costs. Prices for crop were obtained from statistical data, but costs per kg and costs per hectare were estimated (Table 3.8).

Table 3.8 Prices ($ kg^{-1}) and costs ($ kg^{-1}) of the main crops in the Borkhar irrigation district for the calculation of net return and water productivity. (Source: Organization of Jihad-e-Agriculture, Esfahan, Iran. [online]: http://www.esfahan.agri-jahad.ir/modiriat/tarh/tanzimb/prise/prize85.htm, 01 September 2006).

Prices and costs	Wheat (grain) $ kg^{-1}	Fodder maize (dry fodder) $ kg^{-1}	Sunflower (grain) $ kg^{-1}	Sugar beet (sugar) $ kg^{-1}
Price	0.23	0.16	0.38	0.25
Fixed Costs	300	300	300	300
Variable Costs	0.02	0.02	0.02	0.005

Table 3.9 shows the *WP* values at different farmer's fields in the Borkhar irrigation district. Differences in *WP* for different crops during the respective seasons are due to the differences in chemical composition, harvest index and transpiration demands (*Singh et al., 2006*).

Table 3.9 Water productivity indicators WP_T, WP_{ET} and WP_I in units of kg m^{-3} as well as \$ m^{-3} in terms of $Y_M\ T^{-1}$, $Y_M\ ET^{-1}$ and $Y_M\ I^{-1}$ (see Eqs. 3.2 to 3.5) for the main crops at the farmer 's fields in the Borkhar irrigation district for the agriculture year 2004-05.

Water productivity indicators		Fields							
		W1	**W2**	**M1**	**M2**	**Sa1**	**Sa2**	**Su1**	**Su2**
		Wheat		**Fodder maize**		**Sunflower**		**Sugar beet**	
WP_T	kg m^{-3}	1.26	1.11	3.47	3.30	0.33	0.33	1.69	1.75
	\$ m^{-3}	0.22	0.16	0.50	0.48	0.07	0.05	0.37	0.39
WP_{ET}	kg m^{-3}	0.98	0.76	3.05	3.01	0.30	0.28	1.39	1.43
	\$ m^{-3}	0.17	0.11	0.44	0.43	0.07	0.05	0.31	0.32
WP_{Irr}	kg m^{-3}	0.53	0.44	1.39	2.12	0.24	0.20	1.04	0.95
	\$ m^{-3}	0.1	0.07	0.20	0.31	0.05	0.03	0.23	0.21

The average WP, expressed as $Y_M\ T^1$ (kg m^{-3}) was 1.18 for wheat, 3.38 for fodder maize, 0.33 for sunflower and 1.72 for sugar beet. The average WP, expressed as $\$\ T^1$ (\$ m^{-3}) was 0.19 for wheat, 0.5 for fodder maize, 0.06 for sunflower and 0.38 for sugar beet. *This indicates that fodder maize provides the highest economic benefit in the Borkhar irrigation district.* This may explain the fact that in the period 1991-2003 the area under fodder maize has increased from 580 to 1600 ha (Fig. 2.7).

High evaporative demand ET_p and flood irrigation methods at the Borkhar district reduce WP in term of $Y_M\ T^1$ to WP_{ET} in term of $Y_M\ ET^{1.}$ The average WP, expressed as $Y_M\ ET^1$ (kg m^{-3}) was 0.87 for wheat, 3.03 for fodder maize, 0.29 for sunflower and 1.41 for sugar beet. *Soil evaporation caused 11 to 27 % reduction in WP values. Zwart and Bastiaanssen* (2004) reported a global WP of 1.09 kg m^{-3} for wheat in term of $Y_M\ ET^1$ which is slightly higher than the estimated WP_{ET} for wheat at this study.

Furthermore, percolation of soil water Q_{bot} and stored moisture content in the soil profile ΔW may also reduce WP at field scale. The average WP, expressed as $Y_M\ I^1$ (kg m^{-3}) was 0.5 for wheat, 1.76 for fodder maize, 0.22 for sunflower and 1.0 for sugar beet which *show 24 to 42 % reduction in WP values compared with WP_{ET}.*

Under drought conditions and from a farmer's perspective Q_{bot} and ΔW are generally a loss. This is particularly true with uncertain rainfall and unreliable irrigation deliveries, which motivates farmers to under-irrigate. When farmer has uncertain and inadequate irrigation water to bridge the gap between rain and full ET for his holding, he will seriously under-irrigate to capture the maximum benefit from the available water. In addition, the groundwater level in the Borkhar irrigation district is very deep (> 100 m) and contribution of Q_{bot} to groundwater recharge may take a long time. The ΔW is depends on the amount of initial moisture content in the soil profile. When initial soil moisture content is high, the ΔW is low and in contrasts the Q_{bot} is high and vice versa. Because of land rotation in beginning of each growing season in the Borkhar irrigation district, the stored moisture content in the soil profile ΔW is useless and is therefore considered as a loss.

3.9 Increasing the water productivity of irrigated crops

Maximum *WP* can be achieved using optimal irrigation scheduling (*Singh*, 2005). However, from a practical point of view, optimal scheduling through surface irrigation is almost impossible in the Borkhar conditions. Instead, irrigation with constant depth and time interval is the most common method of surface irrigation in the Borkhar district (*APERI*, 2001).

To specify maximum possible *WP* and explore on-farm strategies which results in higher economic gains, the calibrated and validated SWAP model at fields W1, M1, Sa1 and Su1 was used. As on-farm strategies, *deficit irrigation scheduling, irrigation intervals and extend of cultivated area* were analyzed. All parameters in the model were held constant over all farms, except the time and depth of irrigation. The irrigation time was defined in the SWAP model as fixed intervals of 5, 10, 15 and 20 days. The irrigation depth was also defined as a fixed irrigation depth from 1 to 20 cm depth. To invoke SWAP for a variety of input depth and dates of irrigations automatically, SWAP was linked to the SENSAN program. *WP* indicators values were calculated using the simulated water balance components T, ET, I and the actual marketable yield Y_M. Figure 3.7 shows the relation between *WP* indicators (kg m^{-3}) in terms of $Y_M\,T^{-1}$, $Y_M\,ET^{-1}$ and $Y_M\,I^{-1}$.

The *WP* curves in terms of $Y_M\,I^{-1}$ were calculated for the agriculture year 2004-05 based on the different irrigation intervals of 5, 10, 15 and 20 days as well as the irrigation scheduling applied by the farmers at field W1 (wheat), field M1 (maize), field Sa1 (sunflower) and field Su1 (sugar beet). The crosses show *WP* values in terms of $Y_M\,I^{-1}$ (kg m^{-3}) under irrigation practices applied by the farmer. The symbols of E, Q_{bot} and ΔW are respectively referring to evaporation flux, percolation flux and moisture content stored in the soil profile. These three fluxes are considered as losses and are the main causes of reduction of the *WP* value from WP_T to WP_{ET} and WP_{ET} to WP_I.

The relation between $WP_{(E)T}$ and amount of water used for $(E)T$ demonstrates that *an increase in water consumption is accompanied by a proportionate increase in $WP_{(E)T}$.* However, the relationship between $WP_{(E)T}$ and $(E)T$ depends on several factors such as stability of harvest index HI, plant density per unit area, nutrient supply and fertilizers, and crop variety (*Keller and Seckler*, 2005). A substantial amount of the growth in crop yields over the past few decades has been due to increasing the 'harvest index' (HI) by plant. However, since about 1980 only minor increases in the harvest index have been achieved (*Sinclair and Gardner*, 1998). *Zwart and Bastiaanssen* (2004) showed that crop water productivity of wheat, rice and maize has changed only slightly in the past twenty-five years.

When, water supply is not enough to keep the actual T of a crop equal to T_p, the stomata in the leaves will close partially causing lower yield production. As shown in Fig. 3.7 $WP_{(E)T}$ *in terms of $Y_M\,(E)T^{-1}$ (kg m^{-3}) remains stable, irrespective of the irrigation scheduling.* This conclusion was also confirmed by other authors (*Tanner and Sinclair*, 1983; *Bessembinder et al.*, 2005). However, the WP_I does change with the irrigation timing and amount (*Hussain et al.*, 2003; *Bessembinder et al.*, 2005). As shown in Fig. 3.7 the WP_I *can be improved dramatically by applying deficit irrigation and changing the traditional irrigation intervals to shorter irrigation intervals.* For instance, in comparison with maximum possible WP_I using traditional irrigation practices, maximum possible WP_I for wheat (field W1) will increase up to 60 % using low irrigation intervals (10 days) and deficit irrigation scheduling (650 mm). In another example, applying more frequently irrigation events (5 days) will result in 20 and 26 % improvement in maximum possible WP_I at fields Sa1 and M1 respectively.
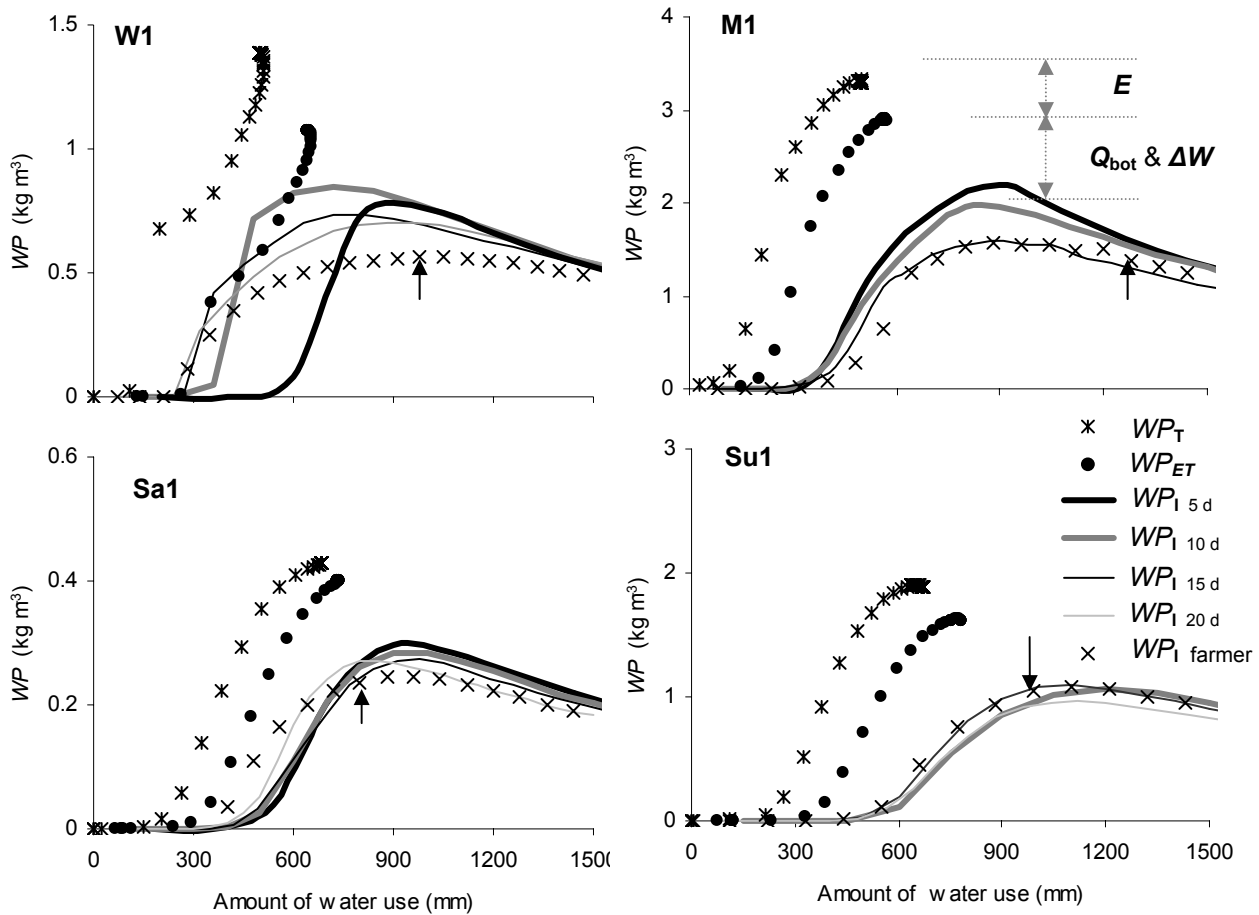
Figure 3.7 Relation between water productivity *WP* indicators (kg m^{-3}) in terms of $Y_M\,T^{-1}$, $Y_M\,ET^{-1}$ and $Y_M\,I^{-1}$, and amount of water use for transpiration *T*, evapotranspiration *ET* and irrigation *I* at field W1 (wheat), field M1 (maize), field Sa1 (sunflower) and field Su1 (sugar beet) and agricultural year 2004-05. Different irrigation frequencies of 5, 10, 15 and 20 days as well as current irrigation practices were considered in the simulations of crop growth and water balance components. The crosses show the *WP* values in terms of $Y_M\,I^{-1}$ (kg m^{-3}) under current irrigation practices as applied by the farmers. *E*, Q_{bot} and *ΔW* are symbols of evaporation, percolation fluxes and soil moisture stored in the soil profile respectively.

In spite of improvements in *WP*$_I$, *justification for shifting from traditional to modern irrigation practices is not straightforward*. A main reason is that maximum water productivity will often not coincide with farmers' interest, whose aim is a maximum land productivity or economic profitability. Maximizing of *WP*$_I$ requires a shift in irrigation science, irrigation water management and financial investment *to move away from 'maximum irrigation-maximum yield' strategies to 'less irrigation maximum WP' policies* which is often not a common interest between farmers and water managers (*Zwart and Bastiaanssen*, 2004).

Another on farm strategy which maximizes the *WP*$_I$ in water scarce conditions is *reduction of cultivated area*. Fig. 3.8 compares *WP*$_I$ values in term of $Y_M\,I^{-1}$ (kg m^{-3}) and amount of water used for irrigation for 100, 75, 50 and 33 % cultivated area in a unit land of 1 ha.
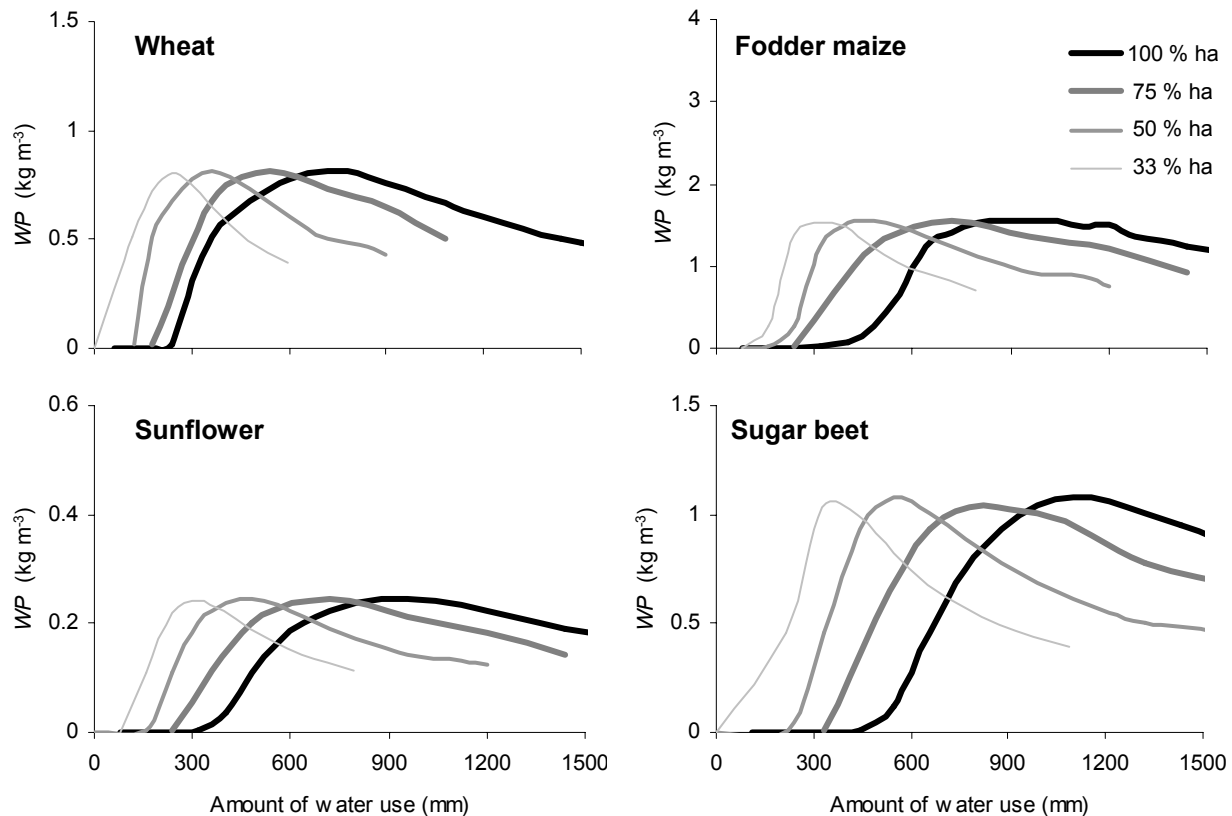
Figure 3.8 Relation between water productivity *WP* indicators (kg m⁻³) in terms of marketable yield per amount of water used for irrigation ($Y_M\ I^{-1}$) and cultivated area at field W1 (wheat), field M1 (maize), field Sa1 (sunflower) and field Su1 (sugar beet) for the agricultural year 2004-05 in the Borkhar irrigation district.

Using this figure, we can now answer the question which of the strategies '*deficit irrigation scheduling*' or '*reducing cultivated area*' will result in the highest *WP* or economic benefit. As shown in this figure, *improvement of WP_I depends on both the amount of available water and cultivated area. Under water scarcity conditions, reducing the cultivated area will result in higher water productivity in comparison with deficit irrigation scheduling strategy.*

3.10 Summary and conclusions

The Borkhar irrigation district is located in an arid to semi-arid region in Iran and regularly faces widespread drought. Given the current water scarcity, the limited available water should be used as efficient and productive as possible. To explore on-farm strategies which result in higher economic gains and water productivity *WP*, a physically based agrohydrological model, Soil Water Atmosphere Plant (SWAP), was calibrated and validated using measured data at 8 selected farmer's fields (wheat, fodder maize, sunflower and sugar beet) in the Borkhar irrigation district during the agricultural year 2004-05. Most of the input parameters collected from farmer's fields were used directly in the SWAP calibration procedures. The remaining soil physical parameters and irrigation depths were determined indirectly through inverse modelling and using weekly soil moisture observations. The calibrated model was used to determine the water balance components such as transpiration, soil evaporation and

43

percolation, and plant variables such as dry matter and marketable yields which are necessary in the calculation of *WP* indicators. The main conclusions of this study are:

- Good agreement between simulated and observed soil moisture (*RMSE* = 0.02 to 0.052 cm^3 cm^{-3}) indicates that the SWAP model for field scale agrohydrology can be used to quantify the water balance components. Good agreement between simulated and observed *Y* (*RMSE* = 1.11 to 3.08 ton ha^{-1}) and *Y*$_{SO}$ (*RMSE* = 0.7 to 1.38 ton ha^{-1}) shows that the SWAP model can also be used to quantify plant variables such as dry matter and crop yield.

- *WP* indicators express the benefit derived from the consumed water in the different hydrological process such as transpiration, evapotranspiration and percolation. The average *WP*$_T$, expressed as **$** *T*^{1} ($ m^{-3}) showed that fodder maize has the highest economic gains (Table 3.10).

Table 3.10 Water productivity indicators in terms of $Y_M T^{-1}$, $Y_M ET^{-1}$ and $Y_M I^{-1}$ for the main crops in the Borkhar irrigation district for the agricultural year 2004-05.

Water productivity indicators		Crops			
		Wheat	Fodder maize	Sunflower	Sugar beet
WP$_T$	kg m^{-3}	1.19	3.39	0.33	1.72
	$ m^{-3}	0.19	0.49	0.06	0.38
WP$_{ET}$	kg m^{-3}	0.87	3.03	0.29	1.41
	$ m^{-3}	0.14	0.44	0.06	0.32
WP$_I$	kg m^{-3}	0.49	1.76	0.22	1.00
	$ m^{-3}	0.09	0.26	0.04	0.22

- *Soil evaporation caused 11 to 27 % reduction in WP$_{ET}$ values*, expressed as $Y_M ET^1$ (kg m^{-3}), in comparison with *WP*$_T$. Furthermore, due to percolation $Q_{bot,}$ and the stored moisture content in the soil profile ΔW, the average *WP*$_I$ values, expressed as $Y_M I^1$ (kg m^{-3}), had *a 24 to 42 % reduction in comparison with WP$_{ET}$*.

- During a drought period, deficit *irrigation scheduling and reduction of the cultivated area as on farm strategies* can bring about higher economic gains. *WP*$_{(E)T}$ in term of $Y_M (E)T^{-1}$ (kg m^{-3}) remained more or less stable, irrespective of the irrigation scheduling, but *WP*$_I$ did change with the irrigation timing and amount. Improved practices in terms of irrigation timing and amount will multiply *WP*$_I$ by a factor of *1.5 for wheat and maize, 1.3 for sunflower and 1.1 for sugar beet.*

- Under water shortage conditions, *reduction of the cultivated area* even gives higher water productivity values in comparison to deficit irrigation.

- The substantial increase of WP$_I$ values and WP$_{(E)T}$ which can be attained indicates the need for improvement of irrigation management in the Borkhar irrigation district.

4. Disaggregation of remotely sensed evapotranspiration data: from low to high spatial resolution

4.1 Introduction

Evapotranspiration *ET* plays an important role in the hydrological cycle of arid and semi arid environments. Determination of the spatial distribution of *ET* over a range of space and time scales is a key factor for evaluation of water management.

Remotely sensed images of Earth's surface have the potential to provide detailed information about the spatial and temporal distribution of *ET*. During the last decades several algorithms were developed for estimation of actual *ET* using the energy exchanges between the atmosphere and the land surface from remotely sensed data (*Menenti and Choudhury*, 1993; *Bastiaanssen et al.*, 1998; *Su*, 2002; *Kustas et al.*, 2003). However, because of the spatial and/or temporal limitations of existing remotely sensed data, for routine estimation of *ET* in agriculture a large data set can not be used directly. For an accurate prediction of the water consumption of certain crop types during the growing season, we need to have images with fine temporal and spatial resolution that recognize individual fields.

The high temporal (daily or even twice daily) satellite data from the MODerate resolution Imaging Spectroradiometer (MODIS) have been successfully used for routine *ET* estimation (e.g. *Timmermans et al.*, 2004; *He et al.*, 2005). However, due to its low spatial resolution (1000 m), such images represent *ET* over areas larger than 100 ha, containing a mixture of different fields and crop types. The sizes of the agricultural fields in the Borkhar irrigation district are typically in the order of 1 to 50 ha (*APERI*, 2001). Hence, the 1000 m pixel resolution data of MODIS cannot be used to discriminate *ET* of individual fields. On the other hand, the 15 m resolution images of the Advanced Spaceborne Thermal mission and Reflection Radiometer (ASTER) are used for estimation of *ET* at field scale (e.g. *French et al.*, 2001, 2005). Because of the low temporal resolution of 15 days, these pixels are however also not suitable for routine *ET* estimation. Therefore to determine in a routine way *ET* at field scale, disaggregation of 1000 m MODIS data to the 15 m ASTER resolution is explored taking advantage of both the high temporal resolution of MODIS and the fine spatial resolution of ASTER data.

The problem of disaggregation has been addressed using weighted ratio maps, being derived from high and low spatial remotely sensed *ET* maps (*Chemin & Alexandridis*, 2004; *Hong et al.*, 2005). The weighted ratio maps are assumed to be constant between observation times in the growing season. However, due to the variation in planting dates and the continuous development of agricultural crops, this assumption may lead to inaccuracies.

Therefore, the main objective of this paper is to *evaluate different disaggregation methods to derive field scale ET values from 1000 m measured MODIS data*.

We will apply the Surface Energy Balance Algorithm (SEBAL) of *Bastiaanssen* (1998) to the MODIS and ASTER data being collected from the Borkhar irrigation district, Esfahan, Iran. The algorithm used is essentially from the year 2000 and does not fully match with the latest SEBAL versions. A new procedure based on a linear disaggregation approach will thereafter be described for disaggregating *ET* from 1000 m to field scale.

The results of the proposed approach will then be compared to two other disaggregation approaches being based on weighted ratios as derived from dividing *ET* maps of high and of low spatial resolution data. We focus on two days during respectively the winter growing season and the summer season. Both seasons show a large spatial variation of soil moisture and vegetation conditions.

To eliminate the effects of differences in geometry of the used images, the disaggregating procedures will be applied to simulated MODIS data being derived by linear aggregation of ASTER radiance data to the MODIS resolution. In this way, the accuracy of the disaggregated *ET* maps can be evaluated using *ET* directly from the original ASTER images. In addition, other effects such as radiometric accuracy, atmospheric disturbances, signal/ noise ratio and time of image acquisition, which are not related to scale change are eliminated.

4.2 Evapotranspiration

Traditionally, crop evapotranspiration flux under *optimum soil moisture conditions ET_p* (mm d^{-1}) is estimated using a grass reference ET_{ref} value that is multiplied by a crop coefficient K_c for the specific crop:

$$ET_p = K_c \ ET_{ref} \tag{4.1a}$$

Under *water stressed conditions*, the crop coefficient K_c is adjusted by multiplying it with a water stress coefficient, K_s (*Doorenbos and Pruitt*, 1977; *Allen et al.*, 1998):

$$ET = K_s \ ET_p = K_s \ K_c \ ET_{ref} \tag{4.1b}$$

Among the several formulations proposed for ET_{ref} (*Blaney and Criddle*, 1950; *Hargreaves and Samani*, 1982; 1985; *Doorenbos and Pruitt*, 1977), the Penman–Monteith equation is widely accepted as the best performing method (*Jensen et al.*, 1990; *Allen et al.*, 1994; *Allen et al.*, 1998). The Penman- Monteith Equation for a cropped soil surface is:

$$ET_p = \frac{86400 \times 10^3}{\lambda \ \rho_w} \frac{\Delta_v (R_s (1-\alpha_s) - R_L - G_0) + \rho_{air} c_{air} \left(\dfrac{e_{sat} - e_{air}}{r_{air}} \right)}{\Delta_v + \gamma_{air} \left(1 + \dfrac{r_s}{r_{air}} \right)} \tag{4.2}$$

where R_s represents the net incoming short wave radiation above the canopy (Wm^{-2}), R_L the net incoming long wave radiation above the canopy (Wm^{-2}), α_s the surface albedo (-), ρ_{air} is the mean air density at constant pressure (kg m^{-3}), c_{air} is the heat capacity of moist air per unit mass (J kg^{-1} K^{-1}), e_{sat} is the saturated vapor pressure (kPa), e_{air} is the actual vapor pressure (kPa), λ is the latent heat of vaporization (J kg^{-1}), ρ_w is the density of water (kg m^{-3}), Δ_v is the slope of the saturated vapour pressure temperature relationship (kPa K^{-1}), γ_{air} is the psychometric constant (kPa K^{-1}), r_{air} is the aerodynamic resistance for heat transport (s m^{-1}) , and r_s is the bulk surface resistance (s m^{-1}).

The r_{air} is generally calculated as a function of crop height h_{crop} (m) and wind speed u_z (m s^{-1}) (e.g. *Allen et al.*, 1998):

$$r_{air} = \frac{\ln\left(\dfrac{z_u - d}{z_{om}}\right) \times \ln\left(\dfrac{z_T - d}{z_{oh}}\right)}{k^2 u_z} = \frac{\ln\left(\dfrac{z_u - 0.66h_{crop}}{0.123h_{crop}}\right) \times \ln\left(\dfrac{z_T - 0.66h_{crop}}{0.0123h_{crop}}\right)}{0.168u_z} \qquad (4.3)$$

where, z_u and z_T are the measurement heights (m) for wind speed and air temperature (m), d is the zero-plane displacement height (m) and the variables z_{om} and z_{oh} represent the roughness lengths for momentum and heat transfer respectively, being estimated from h_{crop} (m). The symbol k is the von Karman's constant which is taken as 0.41 (-). Hence, by estimating h_{crop}, r_{air} can be computed for every crop and land use type.

Assuming a constant crop height of 0.12 m, a standardized height for wind speed, temperature and humidity at 2 m ($z_u = z_T = 2$ m), a fixed grass bulk resistance r_s= 70 s m^{-1} and surface albedo α_s= 0.23, the Penman- Monteith equation for a grass reference surface becomes (*Allen et al.*, 1998):

$$ET_{ref} = \frac{86400 \times 10^3}{\lambda \, \rho_w} \frac{\Delta_v(0.77R_s - R_L - G_0) + \rho_{air}c_{air}u_2\left(\dfrac{e_{sat} - e_{air}}{208}\right)}{\Delta_v + \gamma_{air}(1 + 0.34u_2)} \qquad (4.4)$$

Alternatively, several authors have shown that the Penman- Monteith equation (Eq. 4.2) with a variable r_s can be used to directly compute *ET* (*Rana et al.*, 1997; *D'Urso*, 2001; *Ortega-Farias et al.*, 2004; *Valde's et al.*, 2004). The surface resistance r_s in Eq. 4.2 represents the resistance to vapour flow through leaf stomata, within the canopy structure and within soil to the soil surface. Hence, r_s depends on incoming solar radiation R_s, vapour pressure deficit e_{sat}-e_{air}, soil water status θ, air temperature T_{air} and CO_2 concentration (*Jarvis*, 1976; *Stewart*, 1988). However, *Howell et al.* (1997) reported that other factors like crop species, h_{crop}, *LAI*, within canopy diffusion resistance may affect also the canopy resistances. These factors are usually combined in the minimum canopy resistance. Under potential conditions, i.e. when there is no restriction due to either biological control or soil water content, the surface resistance reaches a minimum value r_s that can be estimated using the expression (*Baldocchi et al.*, 1987):

$$r_s = \frac{r_{stomata}}{LAI_{eff}} \qquad (4.5)$$

where $r_{stomata}$ is the minimum stomata resistance of a single leaf. The $r_{stomata}$ varies usually between 100 to 250 s m^{-1} (*Howell et al.*, 1997). Several earlier studies recommended a fixed value of $r_{stomata}$ of 100 s m^{-1} for well-watered grass and alfalfa (*Allen et al.*, 1989; Jensen et al., 1990). *Steiner et al.* (1991) reported a $r_{stomata}$ of 163 s m^{-1} for full ground cover sorghum at Bushland. *Howell et al.* (1997) determined $r_{stomata}$ values of 135, 280, and 252 s m^{-1} for full groundcover wheat, sorghum, and maize.

LAI_{eff} is the fraction of leaf area index effectively taking part in the evapotranspiration process. A standardized estimation of $LAI_{eff} \approx 0.5\ LAI$ was suggested for dense grass and alfalfa reference crops by *Allen et al.* (1989; 1994; 1998) and *Jensen et al.* (1990).

4.2.1 Unstressed crop coefficient K_c

From Eq. 4.1a, the unstressed crop coefficient K_c can be expressed as:

$$K_c = \frac{ET_p}{ET_{ref}}$$

(4.6)

Hence, K_c depends on climatic conditions, soil type and phenological stage of crops. Experimental values of crop coefficients K_c have been proposed by *Doorenbos and Pruitt* (1997). Due to its simplicity, the tabulated coefficients provide a practical guide for scheduling irrigation, but due to their empirical nature considerable error in estimating crop water requirements may occur (*Jagtap and Jones*, 1989).

Remotely sensed data for spectral reflectance may provide an indirect estimate for K_c. The feasibility of estimating K_c from vegetation indices has been investigated in several investigations (*Neale et al.*, 1989; *Tasumi et al.*, 2005; *Calera et al.*, 2005). However, uncertainties in relating K_c to vegetation indices can arise from the variability of soil-vegetation interactions between wet and dry soils, since wet and dry soils generally have different reflectance (*Choudhury et al.*, 1994).

Alternatively, *D'Urso* (2001) introduced an analytical approach to estimate K_c at regional scale. He expressed the crop coefficient K_c as an explicit function of the canopy properties such as leaf area index *LAI*, albedo α_s, crop height h_{crop}, and of the meteorological data i.e. the ratio of Eq. 4.2 to Eq. 4.4. *D'Urso* (2001) concluded that the analytical approach appears more accurate when field observation of canopy parameters is available. The required crop parameters *LAI*, α_s and h_{crop} might be derived either directly from canopy reflectance or can be estimated by means of empirical relationships with vegetation indices, with the support of ground reference information simultaneous to different satellite passes (*D'Urso and Menenti*, 1995).

Therefore, *to map crop coefficients of irrigated areas, remotely sensed reflectance values can be used in combination with other detailed information about land*.

4.2.2 Water stress coefficient K_s

Estimation of K_s values and finally actual *ET* under water limiting conditions (Eq. 4.1b) requires information on the availability of water in the root zone. Estimation of soil water needs daily water balance computation which is not available at regional scale due to the variability of both irrigation applications and soil-crop properties.

An alternative means to estimate actual ET and water stress coefficient K_s is however the energy balance approach using existing remote sensed data.

4.3 SEBAL algorithm

SEBAL (*Bastiaanssen et al.*, 1998) is a one layer algorithm that computes actual *ET* at the time of the satellite overpass as a residual of the energy balance:

$$\lambda ET = R_n - H - G \tag{4.7}$$

where R_n is the net radiation flux (W m^{-2}), G the soil heat flux, H the sensible heat flux and, λET the the latent heat flux.

The main challenge when deriving the energy balance is to determine the partitioning of the available energy (R_n-G) into H and λET. The algorithm SEBAL comprises 25 computational steps that calculate actual ET rates as well as other surface exchanges between land and atmosphere. The computations are performed using both semi-empirical relations and simplifications of the energy balance formulation over extreme dry (assuming zero latent heat flux λET) and extreme wet (assuming zero sensible heat flux H) areas. The key input data to SEBAL consist of spectral radiances in the visible, near infrared and thermal infrared of the spectrum. SEBAL computes a complete radiation and energy balance along with resistances for momentum, heat and water vapor transport for every individual pixel. In addition to satellite image data, the SEBAL algorithm requires instantaneous as well as daily averaged weather data on wind speed u_z, relative humidity, solar radiation R_s and air temperature T_{air} near the Earth surface (Table 4.1). To express surface roughness, a simplified land use map is required.

Table 4.1 Weather data being used in the SEBAL algorithm from the Esfahan meteorological station, 5 km west south of the Borkhar irrigation district.

Date	Time (LST)	T_{air} (^{o}C)	RH (%)	U (m s^{-1})	R_s (W m^{-2})	ET_{ref} (mm d^{-1})
06 May 2005	7:15	16.8	12.8	4.6	703	6.07
13 May 2005	7:25	23.8	23	2.7	647	6.30
17 Aug 2005	7:25	26.6	15.8	1.9	590	5.37
20 Oct 2005	7:25	22.3	15.6	1.7	492	4.90

Satellite radiances were first converted to land surface characteristics such as broad-band surface albedo α_s, leaf area index LAI, vegetation index $NDVI$ and land surface temperature T_s. LAI was derived using a logarithmic function relating LAI with satellite observations of the Soil Adjusted Vegetation Index ($SAVI$) (*Choudhury et al.*, 1994). The broad-band surface albedo α_s was determined following the original formulation by *Menenti et al.* (1989) in two steps. First the planetary broad band reflectance was calculated from the narrow band reflectance of MODIS or ASTER images using the equations presented by *Liang et al.* (2000). A simple atmospheric correction was then applied using the path radiance and broad band shortwave atmospheric transmittance to convert the planetary surface albedo to the broadband surface albedo (*Chen et al.*, 1984). Surface temperature was calculated using a simple split-window technique by *Price* (1984) on MODIS channels 31 and 32 in combination with the broad band emissivity derived using the vegetation index. For ASTER images, 90 m spatial resolution surface temperature generated from ASTER's 5 thermal infrared channels was used.

Net radiation R_n was then computed as the algebraic sum of the shortwave and long wave radiation components, using incoming solar radiation, a first order estimation of air temperature to estimate down-welling long wave radiation, albedo, broadband emissivity and

surface radiometric temperature. The soil heat flux G was determined through semi-empirical relationships with R_n, surface albedo α_s, surface temperature, and vegetation index.

The sensible heat flux H is generally the most critical factor in the physically based remote sensing algorithms. This flux is a function of temperature gradient and aerodynamic resistance r_{air}. In SEBAL, H is computed using an iterative process of flux, aerodynamic resistance and temperature gradient estimation, assuming that the relation between vertical air temperature gradient and surface temperature is linear. At first, the surface roughness characteristics were determined using the vegetation indices. Then local scale friction velocity was computed from the logarithmic wind profile using wind speed measurements at observation height and calculated wind speed at blending height. The linear coefficients of the temperature gradient and the surface temperature relation were determined from inverting the sensible heat flux expression over dry non-evaporating land units and over wet surface types. Finally, an instantaneous *ET* was computed as the residual of the energy balance, which was subsequently scaled up to 24 hours and longer periods. More details of the applied SEBAL algorithm can be found in the literature (*Bastiaanssen et al.*, 1998; 2000; 2005).

In the Borkhar irrigation district study, the SEBAL algorithm has been applied to ASTER and MODIS images acquired on 6 May and 13 May 2005 during the winter growing season, and on 17 August and 20 October 2005 during the summer growing season. The characteristics of the satellite images, the level of products and their acquisition dates are listed in Table 4.2.

Table 4.2 The characteristics and acquisition dates of the ASTER and MODIS images.

Satellite	Sensor	Spatial resolution (m)	Temporal resolution (d)	Level of product	Selected bands	Acquisition dates in 2005
Terra	**MODIS**	250	1	1B[a]	1-2 aggregated to 1000 m,	13 May, 17 Aug
		500		1B[a]	3-7 aggregated to 1000 m,	
		1000		1B[a]	31,32	
Terra	**ASTER**	15	15	1B[a]	1-2 aggregated to 90 m,	6 May, 13 May, 17 Aug and 20 Oct
		30		1B[a]	4-9 aggregated to 90 m,	
		90		2 B03[b]	10-14	
		90		2 B04[c]	10-14	

a Calibrated and geo-located radiances at the sensor.
b Surface temperatures at 90 m resolution generated from ASTER's 5 thermal infrared channels.
c Surface emissivity at 90 m resolution generated from ASTER's 5 thermal infrared channels.

4.4 Disaggregation

4.4.1 Disaggregation using the linear mixing concept

Linear mixing assumes that each image pixel contains information about the proportion and the response of each component. The response of each pixel is considered as a linear combination of the responses of all components in the mixed target (*Shimabukuro et al.*, 1991; *Haertel et al.*, 2004; *Lobell et al.*, 2004). In this research, the linear mixing concept was implemented for disaggregating MODIS pixels and the response was expressed in terms of *ET* data instead of spectral data. *ET* of each MODIS pixel was considered as a linear combination of *ET* values of different components, weighted by the area fraction of each component within the pixel:

$$ET_{\text{MODIS}}(x, y, t) = \sum_{i=1}^{m} ET(x_i, y_i, t)\, A_{\text{f}}(x_i, y_i) + \varepsilon(x, y) \tag{4.8}$$

where $ET_{\text{MODIS}}(x, y, t)$ is *ET* derived from each MODIS pixel, $ET(x_i, y_i, t)$ is actual *ET* of the ith component within each MODIS pixel, $A_{\text{f}}(x_i, y_i)$ is the area fraction of the ith component within each MODIS pixel, $\varepsilon(x, y)$ is a residual representing the model error for each MODIS pixel, m is total number of components within each MODIS pixel, x and y are horizontal and vertical location of each MODIS pixel respectively, and t represents the time.

Alternatively, *ET* of each component can according to Eq. 4.1b be written as (Allen et al., 1998):

$$ET(x_i, y_i, t) = K_{\text{s}}(x_i, y_i, t)\, K_{\text{c}}(x_i, y_i, t)\, ET_{\text{ref}} \tag{4.9}$$

where $K_{\text{s}}(x_i, y_i, t)$ represents *the water stress coefficient* of the ith component within each MODIS pixel, $K_{\text{c}}(x_i, y_i, t)$ is the *unstressed crop coefficient* of the ith component within each MODIS pixel, and ET_{ref} is the reference grass *ET* computed from Eq. 4.4 using local weather data. Inserting Eq. 4.9 into Eq. 4.8, the *ET* from each MODIS pixel can be rewritten as:

$$ET_{\text{MODIS}}(x, y, t) = \sum_{i=1}^{m} K_{\text{s}}(x_i, y_i, t)\, K_{\text{c}}(x_i, y_i, t)\, ET_{\text{ref}}\, A_{\text{f}}(x_i, y_i) + \varepsilon(x, y) \tag{4.10}$$

ET derived from each MODIS pixel represents *ET* of an area of 100 ha, containing a mixture of different fields and crops. However, the agricultural area in the Borkhar irrigation district is surrounded by bare soils and the actual irrigated area within each MODIS pixel is always less than 100 ha. This implies that, *cultivated area within each MODIS pixel can be irrigated within a few days and hence, deficit irrigation within the each MODIS pixel is comparable.* On the other hand, sensitivity of crops to water stress within each MODIS pixel is almost the same because of the similarities in the crop genotypes during both winter and summer seasons. The main crop during the winter season is wheat and barley which has a moderate tolerance to water stress. In the summer season, the majority of lands are assigned to maize and sunflower, which have a higher sensitivity to water stress. Therefore, the water stress can be assumed to be constant within each MODIS pixel in the district. This assumption holds true as long as the components are irrigated simultaneously, which is a fair assumption for the conditions in the Borkhar irrigation district.

Assuming that the water stress coefficient in each MODIS pixel is constant for all the components, $K_s(x_i, y_i, t)$ become $K_s(x, y, t)$ and can be derived as:

$$K_s(x,y,t) = \frac{ET_{\text{MODIS}}(x,y,t) - \varepsilon(x,y)}{\sum\limits_{i=1}^{m} K_c(x_i,y_i,t)\, ET_{\text{ref}}\, A_f(x_i,y_i)} \qquad (4.11)$$

When both the water stress coefficient $K_s(x, y, t)$ and the unstressed crop coefficient K_c (x_i, y_i, t) are known, ET for each component can be calculated with Eq. 4.9. The resolution of the disaggregated ET map depends on the number of components within each MODIS pixel. The number of components to be discreted within each MODIS pixel depends on the crop types and their growing stages, which affect the variation in K_c values.

In this study, the K_c values were derived from 15 m spatial resolution ASTER data for both winter and summer crops on 13 May and 17 August using Eq. 4.6 (*D'Urso*, 2001) and tabulated weather data (Table 4.1). To calculate K_c values on these two days, both winter and summer crops were classified as early or late cultivated crops. The crop classification is not meant for K_c, but for h_{crop}. The h_{crop} maps were created using field data considering a certain h_{crop} for each crop type and early or as late cultivation. The map was applied to Eq. 4.3 to derive the aerodynamic resistance r_{air}. The surface resistance r_s was estimated using Eq. 4.5 and the r_{stomata} values of 135, 180, 180 and 100 s m^{-1} for wheat, maize, sunflower and sugar beet respectively. The values were derived through inversion of Eq. 4.2 to 4.6 and calibration against tabulated K_c values (*Doorenbos and Pruitt*, 1997).

In practice, K_c curves can be derived for the entire growing season for each ASTER pixel by having the distribution of K_c for one or two days. The temporal profile of K_c can also be derived for the entire growing season from 250 m spatial resolution MODIS data with high temporal resolution (daily or even twice daily).

To eliminate the effects of differences in geometrics and radiances spectral between the images, the disaggregating procedures are applied to the artificial MODIS data derived from aggregation of ASTER data to the MODIS resolution using the arithmetic average of ET flux:

$$ET_{\text{Sim.MODIS}}(x,y,t) = \frac{\sum\limits_{i=1}^{m} ET_{\text{ASTER}}(x_i,y_i,t)}{m} \qquad (4.12)$$

where $ET_{\text{Sim.MODIS}}(x, y, t)$ is the aggregated ET value of each simulated 1000 m pixel (kg m^2 s^{-1} or mm d^{-1}), $ET_{\text{ASTER}}(x_i, y_i, t)$ is the value of each pixel of the 11×11 set and m is the number of pixels of each set ($m = 11 \times 11 = 121$) with 90 m TIR ASTER pixels. A flow diagram of this linear disaggregation approach is given in Fig. 4.1.
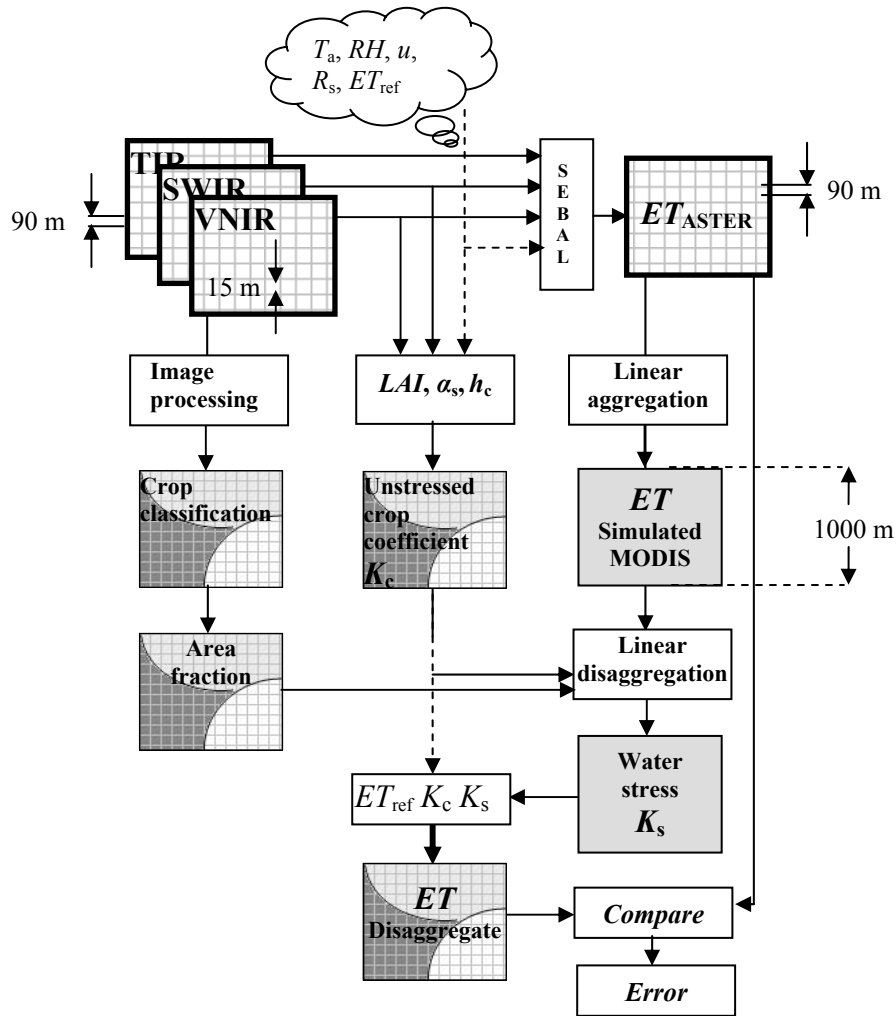
Figure 4.1 Flow diagram of the ***linear disaggregation procedure***. VNIR, SWIR and TIR are defined respectively as visible and near-infrared, short-wave infrared and thermal infrared bands of the electromagnetic spectrum. The symbols of *LAI*, h_{crop} and α_s are referring to leaf area index, crop height and surface albedo respectively.

To derive the *ET* maps, the SEBAL algorithm has been applied to the 90 m spatial resolution ASTER data. The *ET* maps were aggregated using Eq. 4.12 to the MODIS resolution. On the other hand, the 15 m spatial resolution ASTER data were applied to derive the crop properties such as *LAI*, α_s and h_{crop} as well as the K_c map using Eq. 4.6. Finally, a water stress map K_s was created using the simulated MODIS data and a K_c map using Eq. 4.11. To estimate the *ET* values of the components within the MODIS pixel, the K_s and K_c maps with ET_{ref} value were implemented in Eq. 4.9. The resulting disaggregated values were compared against the original 90 m ASTER-based $ET_{ASTER}(x_i, y_i, t)$ values.

4.4.2 Disaggregation using weighted ratio maps

The results of the developed linear disaggregation approach were compared with two other disaggregation approaches, being based on the weighted ratio of one high and one low spatial resolution *ET* maps. In the *first approach*, the *ET* map derived from the high spatial resolution ASTER and its aggregation to the MODIS resolution were used to characterize the

proportion ratios of pixels within one single large MODIS pixel as (*Chemin & Alexandridis,* 2004):

$$ET_{\text{Disaggregated}}(x_i, y_i, t) = \left(\frac{ET_{\text{ASTER}}(x_i, y_i, t-n)}{ET_{\text{Sim.MODIS}}(x, y, t-n)} \right) ET_{\text{Sim.MODIS}}(x, y, t) \qquad (4.13)$$

where $ET_{\text{Disaggregated}}(x_i, y_j, t)$ represents the disaggregated ET map (mm d^{-1}) on the t$^{\text{th}}$ day, $ET_{\text{Sim.MODIS}}(x, y, t-n)$ and $ET_{\text{ASTER}}(x_i, y_i, t-n)$ are ET maps derived from ASTER images and its aggregation to the 1000 m on the (t-n)$^{\text{th}}$ day. A flow diagram of the disaggregation procedure using this weighted ratio map is shown in Fig. 4.2.
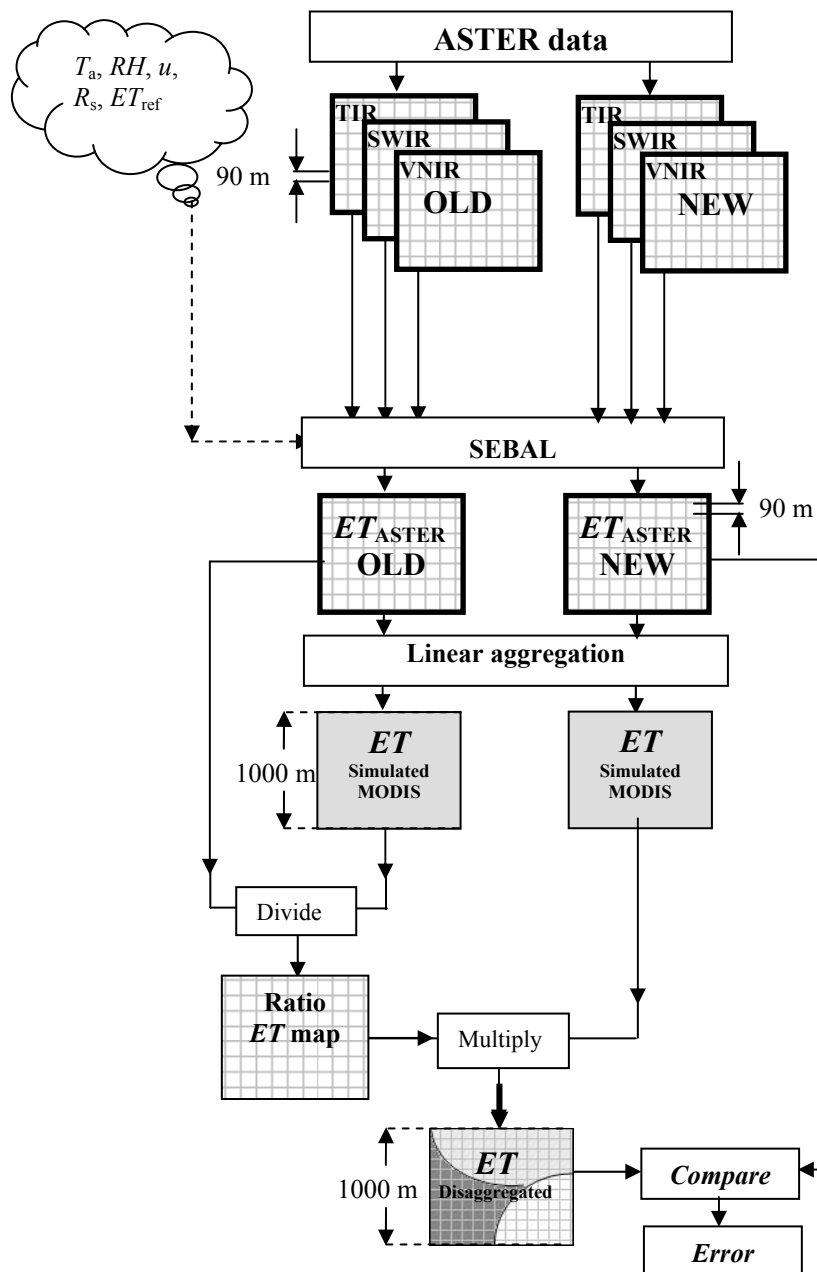
Figure 4.2 Flow diagram of the disaggregation procedure using the ***weighted ET ratio approach***. VNIR, SWIR and TIR are respectively referring to visible and near-infrared, short-wave infrared and thermal infrared bands of the electromagnetic spectrum.

56

In the *second approach*, the weighted ratio map was created by dividing the high spatial resolution *ET* map derived from ASTER and the global mean of its aggregation to the MODIS resolution (*Chemin & Alexandridis*, 2004). The weighed ratio map was multiplied with the global mean of the new simulated MODIS *ET* map:

$$ET_{\text{Disaggregated}}(x_i, y_i, t) = \left(\frac{ET_{\text{ASTER}}(x_i, y_i, t-n)}{ET_{\text{Sim.MODIS}}(x, y, t-n)} \right) \overline{ET_{\text{Sim.MODIS}}(x, y, t)} \qquad (4.14)$$

where $\overline{ET}_{Sim.MODIS}$ (mm d^{-1}) represents the global mean of simulated MODIS *ET* data.
The advantage of the second approach is that discontinuities in the disaggregated map are avoided.

4.4.3 Evaluation of the accuracy of disaggregation

To evaluate the accuracy of the derived disaggregated *ET* map, the *ET* map calculated from the ASTER images with 90 m spatial resolution was used as observed *ET* data. Then the global arithmetic average $\overline{ET}$, standard deviation σ and global root mean square error *RMSE* were computed to assess the level of agreement between the disaggregated *ET* map and the observed *ET* map:

$$\overline{ET} = \frac{\sum_{x=1}^{k} \sum_{y=1}^{p} \sum_{i=1}^{m} ET(x_i, y_i, t)}{k\,p\,m} \qquad (4.15)$$

$$\sigma = \frac{\sum_{x=1}^{k} \sum_{y=1}^{p} \sum_{i=1}^{m} (ET(x_i, y_i, t) - \overline{ET})^2}{k\,p\,m} \qquad (4.16)$$

$$RMSE = \sqrt{\frac{\sum_{x=1}^{k} \sum_{y=1}^{p} \sum_{i=1}^{m} (ET_{\text{Disaggregated}}(x_i, y_i, t) - ET_{\text{obs}}(x_i, y_i, t))^2}{k\,p\,m}} \qquad (4.17)$$

where $ET_{obs}(x_i, y_i, t)$ is *ET* (mm d^{-1}) derived from the original ASTER images as observation data on t^{th} day, k is the total number of pixels of the MODIS image in horizontal direction (-), p is the total number of pixels of the MODIS image in vertical direction (-), and m is the total number of ASTER pixels within each MODIS pixel (-). These statistical parameters were calculated for the agricultural area being present at the satellite image.

4.5 Results of crop classification

The crop classification map is required for deriving the area fraction A_f of components within MODIS pixels and creating the h_{crop} map. One ASTER image acquired on 13 May 2005 during the winter growing season, and two ASTER images acquired during the summer growing season on respectively 17 August and 20 October 2005, were used to assess the land cover as well as to classify both the winter and summer crops. Field research was conducted in the Borkhar irrigation district, which resulted in a data base of 120 ground truth points of

known land cover for winter crops and of 90 ground truth points for summer crops. The remote sensing land use classification was performed using a series of unsupervised and supervised classification steps. The results of the classification are presented in Fig. 4.3 for both winter and summer crops.
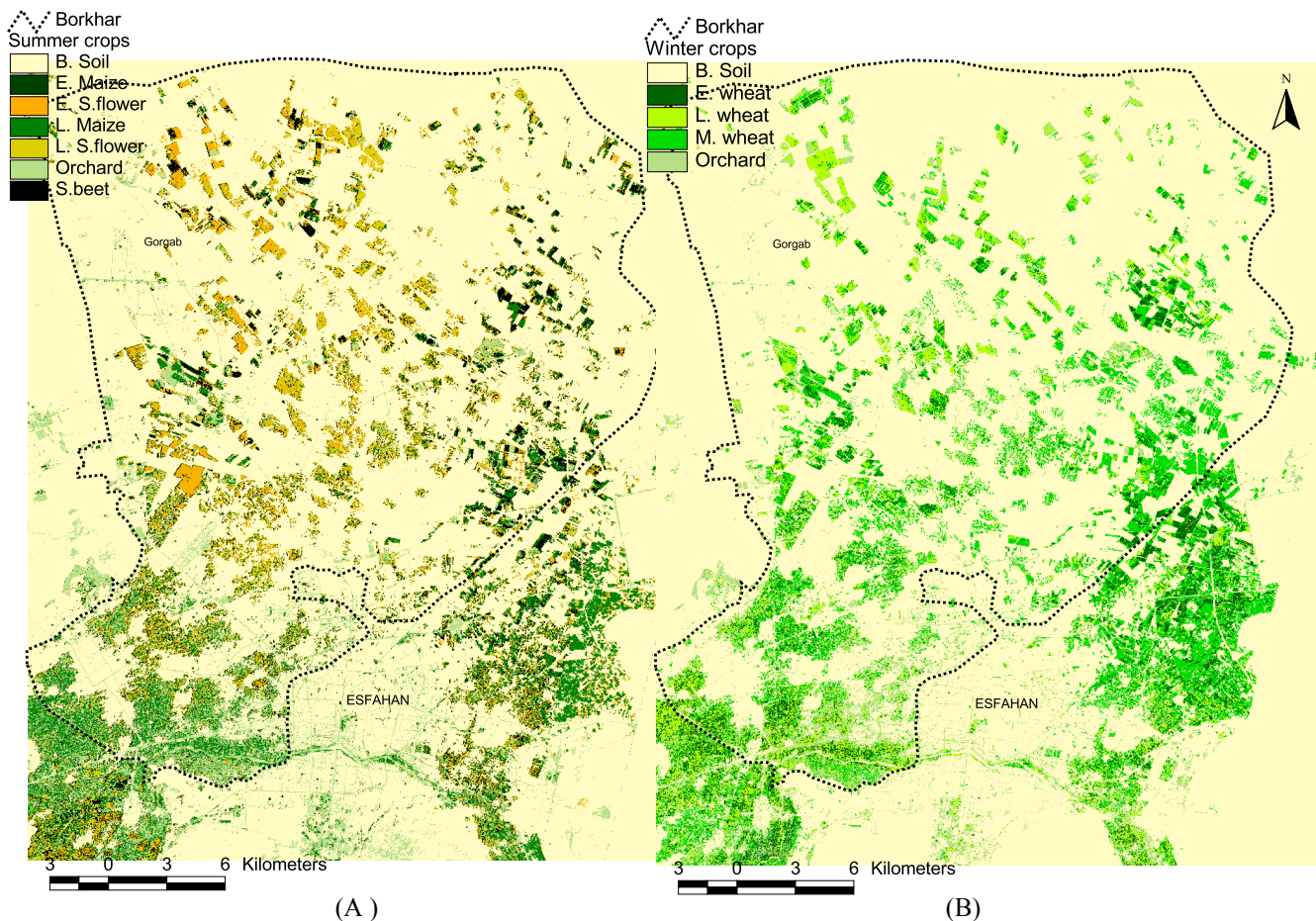
Figure 4.3 Land use classification in the Borkhar irrigation district based on satellite image (ASTER, spatial resolution $15m \times 15m$) during the agricultural year 2004-05: (A) the winter season (13 May, 2005) (B) the summer season (17 Aug and 20 Oct, 2005). (E. = early, L = late, M = middle).

The major crops grown during the winter season are wheat and barley. In this study, the barley farms were assigned to the wheat classes since the spectral signatures of wheat and barley fields are almost similar. During the summer growing season, the majority of cultivated areas were assigned to maize, sunflower, sugar beet, alfalfa and vegetables respectively. The spectral signatures for wheat as well as maize and sunflower were different due to the variability of sowing dates, crop variety and/or other management factors. To indicate these differences, the crops were classified as early, mid or late crops. The statistical data of the cultivated area are reported on district scale. To evaluate the accuracy of the crop classification, the Borkhar irrigation district was extracted from the image (Fig. 4.3). The results of the land cover classification for both the winter and summer growing season of the agricultural year 2004-05 are shown in Table 4.3.

Table 4.3 Results of the land cover classification for both the winter and summer growing season of the agricultural year 2004-05 in the Borkhar irrigation district, Esfahan.

Land cover type		Remote sensing		Statistical data	Differences = RS-Stat.
		ha	%	ha	(%)
Winter	**Wheat**	14064	16.8	14970	-6
	Orchard	4919	05.8	-	
	Bare soil	65400	77.5	-	
Summer	**Maize**	7084	08.5	5983	+15
	Sunflower	7400	08.8	5530	+25
	Sugar beet	564	0.72	1200	-41
	Orchard	4919	5.90	-	-
	Bare soil	63480	76.0	-	-

The total area under wheat has been classified as being 14064 ha which deviates only 6 % from the 14970 ha reported by the Esfahan Jihad-e-Agricultural Organization (2006). The total area under maize is 7084 ha which shows 15 % deviation from the statistical data. The total area of sunflower amounts to 7400 ha which is 25% higher than the reported data. The total area under sugar beet is 564 ha with 49% deviation from reality. A large fraction of the area i.e. 76% has been classified as bare soil which is almost constant during the summer and winter growing season. The accuracy of crop classification depends on the differences in spectral signature of the land cover classes, the heterogeneity of the land surface and the extent of field ground truth data. The accuracy of crop classification in summer time is lower due to the large variability of the crop types and limited ground truth samples.

4.6 Aggregation of evapotranspiration fluxes: from ASTER to MODIS resolution

To be able to compare the *ET* maps derived from the ASTER images with *ET* from the MODIS images, the *ET* maps derived from ASTER were aggregated from a base resolution of 90 m to 1000 m (which is equal to the MODIS resolution) using Eq. 4.12. Then the aggregated *ET* maps were used to geometrically correct the *ET* maps derived from the MODIS data. The coordinate system was converted from the Geographic Latitude/Longitude to the Universal Transverse Mercator coordinate system.

To evaluate the similarity between the *ET* values derived with MODIS and the aggregated ASTER, graphic representations of *ET* distribution pattern and frequency histograms were used (Fig. 4.4). The histograms are based on the agriculture area. As shown in Fig. 4.4A and 4.4B for 13 May, and 4.4D and 4.4E for 17 Aug, *both the overall ET maps as well as the ET histograms match well*.

Further, to gain a better insight of differences between aggregated *ET* and *ET* from the MODIS images, the maps of absolute *ET* differences and their histograms for the images of 13 May and 17 August are shown in Fig 4.4C and 4.4F. The differences between the MODIS outputs and aggregated ASTER outputs are higher in the area near the *Zayande Rud River* and the city area.
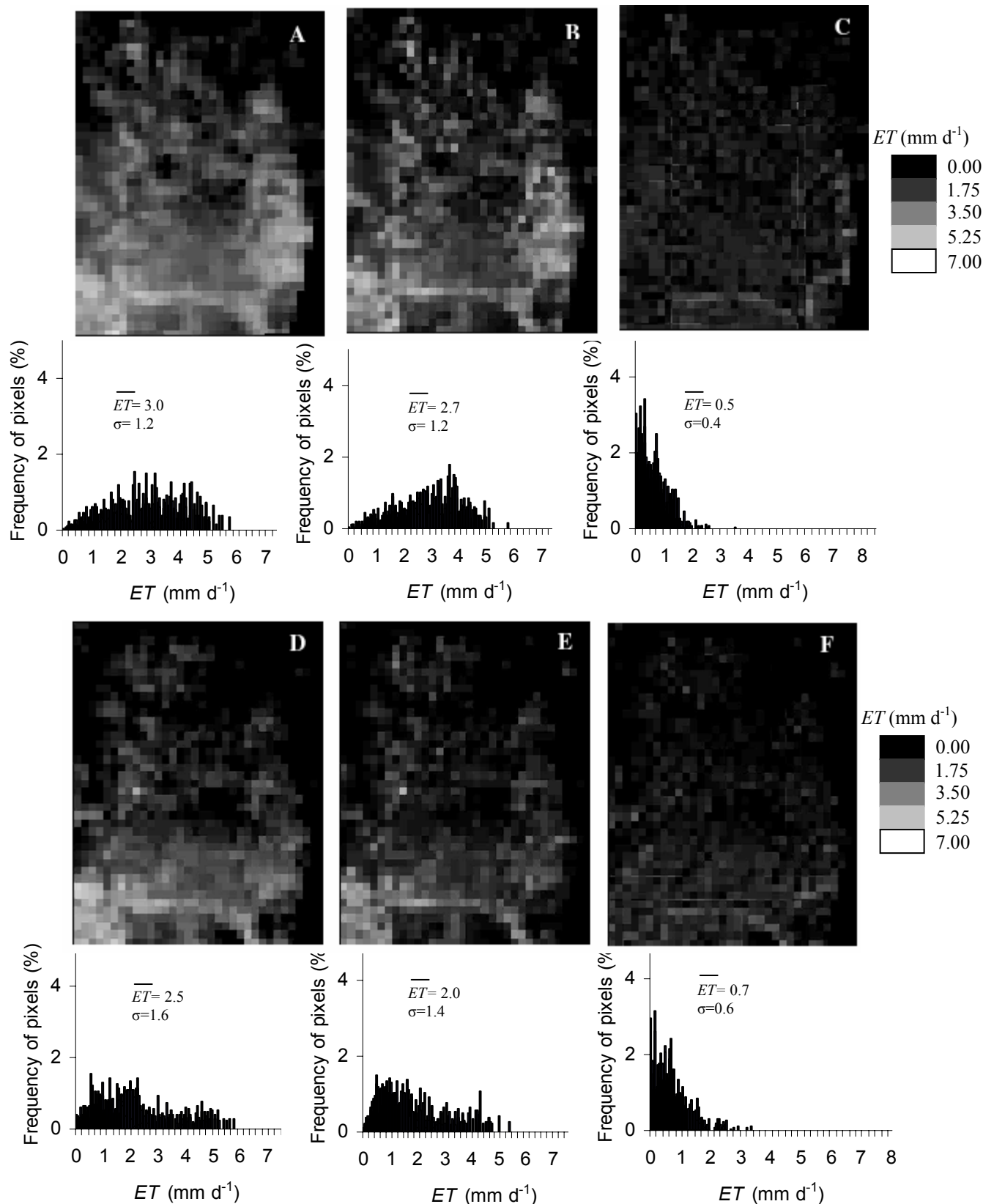
Figure 4.4 A) The *ET* map and its histogram derived from MODIS images; B) aggregated *ET* from ASTER image; C) map of absolute *ET* difference beswetten *ET* derived from MODIS and aggregated *ET* from ASTER (13 May 2005); D) the *ET* map derived from MODIS image; E) aggregated *ET* from ASTER image; F) map of absolute *ET* difference between *ET* derived from MODIS and aggregated *ET* from ASTER (17 August, 2005).

Table 4.4 lists the statistical measures and shows that *there is in general good agreement between the aggregated ET from ASTER and the ET from MODIS for both the winter and summer growing season.* However, $\overline{ET}$ values of MODIS images are respectively 9.5% and 19% higher than the $\overline{ET}$ values of the aggregated ASTER images on 13 May and 17 August. The global mean of the *ET* absolute differences i.e. $\overline{\overline{ET}}$ in both the winter ($\overline{ET}$ differences $= 0.5$ mm d^{-1}) and summer ($\overline{ET}$ differences $= 0.7$ mm d^{-1}) days are small.

Table 4.4 Statistical comparison of *ET* derived from MODIS images and aggregated *ET* derived from ASTER images, disaggregated *ET* maps derived from aggregated *ET* of ASTER images using three different disaggregation method with original *ET* maps on 13 May and 17 August, 2005.

Methods for *ET* (mm d^{-1}) estimation			13-May-05					17-Aug-05				
			$\overline{ET}$	σ	ET diff.	RMSE	r	$\overline{ET}$	σ	ET diff.	RMSE	r
Upscaling	Linear aggregation	**MODIS**	3.0	1.2				2.5	1.6			
		ASTER (aggregated to 1000m)	2.7	1.2	**0.5**	**0.7**	**0.77**	2.0	1.4	**0.7**	**0.8**	**0.74**
Downscaling	Linear disaggregation	**ASTER**	3.9	1.4				3.1	1.8			
		Disaggregated (aggregated ET to 1000m)	3.9	1.1	**0.9**	**1.1**	**0.65**	2.9	1.5	**0.9**	**1.1**	**0.76**
	Weighted ratios	**ASTER**	3.9	1.4				3.1	1.8			
		Disaggregated (*ET*ASTER & its aggregated)	4.0	1.7	**0.9**	**1.2**	**0.76**	3.2	2.1	**1.4**	**1.9**	**0.50**
		ASTER	3.9	1.4				3.1	1.8			
		Disaggregated (*ET*ASTER & mean of its aggregated)	4.0	1.9	**1.0**	**1.2**	**0.75**	3.2	2.0	**1.6**	**2.1**	**0.40**

To show how strongly pairs of variables are related to each other, scatter plots between the MODIS outputs and the aggregated ASTER outputs are presented in Fig. 4.5. *RMSE* and the correlation coefficient *r* values (Table 4.4) for both winter ($r = 0.77$, *RMSE*$=0.7$ mm d^{-1}) and summer ($r = 0.74$, *RMSE*$=0.8$ mm d^{-1}) days show also good agreement between the MODIS output and aggregated ASTER outputs.
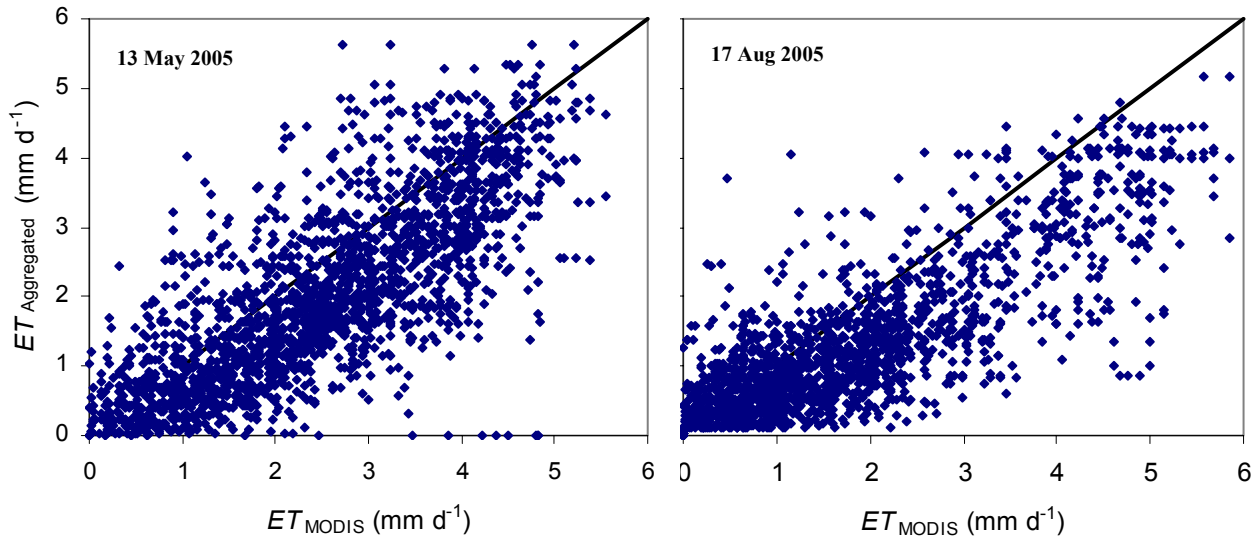
Figure 4.5 Scatter plots of *ET* derived from the MODIS, as well as from the ASTER data which have been aggregated to the MODIS resolution at two different dates.

Hence, it can be concluded that *ET from each MODIS pixel is a weighted arithmetic average of ET values of all components within the MODIS pixel.* Theoretically we may assume this to be true for fluxes like *ET*, and the retrieved results supports this assumption.

4.7 Results of the linear disaggregation approach

4.7.1 Distribution of unstressed crop coefficients K_c

In Fig. 4.6 the curves represent the derived distribution of individual unstressed K_c values for wheat on 13 May, and maize, sunflower and sugar beet on 17 August.
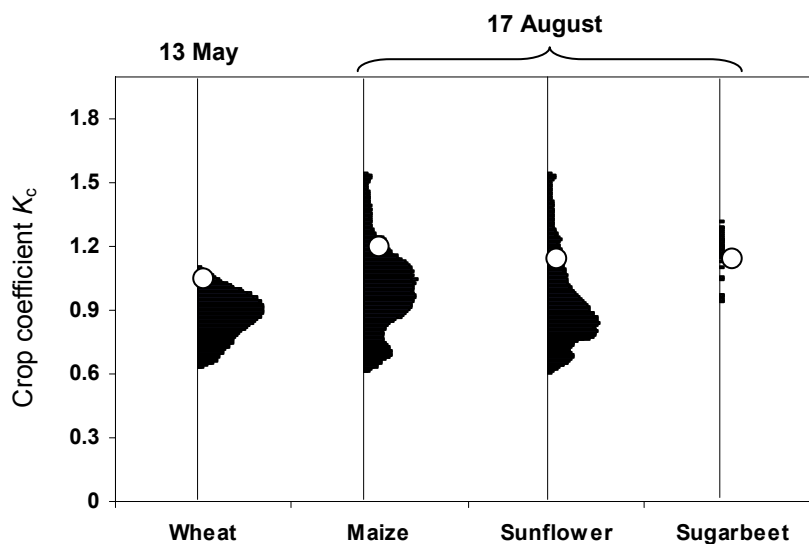
Figure 4.6 Unstressed crop coefficients K_c determined by Eq. 4.2 to 4.6 for the agricultural crops in the Borkhar irrigation district on 13 May and 17 August 2005. The white points show the tabulated K_c from literature (*Allen et al.*, 1998).

K_c-coefficients for wheat vary from 0.6 to 1.15 with an average of 0.95. 13 May is in the middle stage of the wheat growing season and at most fields the crop has reached its maximum height and *LAI*. Therefore the range of K_c variation for wheat is small. On the other hand, crop coefficients K_c derived on 17 August show a high variation for both maize and sunflower. The reason is that 17 August is in the development stage of the summer growing season which means that both crop height and *LAI* are highly variable due to the differences in planting dates.

As shown in Fig. 4.6 maize has the highest K_c value for both summer and winter crops and the largest cultivated area among the summer crops. The area under each histogram is proportional to the area of each crop.

As reliable reference measurements of K_c for different crop types and acquisition dates were not available, it was not possible to assess the absolute accuracy of the crop coefficients derived from remote sensing. Therefore, the average K_c values derived from remote sensing data were compared with K_c values reported in the literature, but adjusted for the climatic environment of the Borkhar region (*Allen et al.*, 1998). The satellite date suggest that results presented in Fig. 4.6 show that the K_c value of the curves taken from the literature compare well to the K_c value derived from remote sensing. There is a wide population of K_c values, also under the assumption of unstressed condition. This was also noted by *Tasumi et al.*, (2005) and implies that single K_c values should be treated with caution.

4.7.2 Linear *ET* disaggregation results

The linear disaggregating procedure shown in Fig. 4.1 was applied to the aggregated *ET* derived from the ASTER images of 13 May and 17 August 2005. This represents application of the linear disaggregation approach to the *ET*-data being derived from a MODIS image with 1000 m spatial resolution. The purpose is to test the $K_c \cdot K_s$ approach with special attention to the uniformity of K_s. Figs. 4.7 and 4.8 present the disaggregated and original *ET* maps, as well as their histograms for the images of 13 May and 17 August 2005, respectively. The overall *ET* maps as well as the *ET* histograms show that there is good agreement between the disaggregated *ET* and the observed *ET* map. On both dates, the $\overline{ET}$ value of the disaggregated *ET* map is almost identical to the $\overline{ET}$ value of the observed *ET*. The standard deviations σ of the disaggregated *ET* maps are slightly lower than the original *ET* maps.

The correlation coefficient r between MODIS outputs and the aggregated ASTER outputs are presented in Table 4.4. The disaggregated *ET* map on 13 May shows a moderate correlation of $r = 0.65$ with the original *ET* map. The correlation between the disaggregated *ET* map and the original *ET* map on 17 August is stronger ($r = 0.76$). Figure 4.9 provides a graphical impression of the correspondence between the disaggregated *ET* maps and the original *ET* maps.

To quantify the error, the maps of absolute *ET* differences between the disaggregated *ET* and the original *ET* maps are also shown in Figs 4.7 and 4.8. The highest differences are located at the borders of fields. The reason is that the disaggregated *ET* map was derived using the 15 m spatial resolution ASTER data, while the original *ET* map is based on the 90 m spatial resolution ASTER data. The low *ET* differences and *RMSE* on both the 13 May and 17 August indicate a good correspondence between the disaggregated and the original *ET* maps ($\overline{ET}_{differences} = 0.9$ mm d^{-1}, $RMSE = 1.1$ mm d^{-1}).
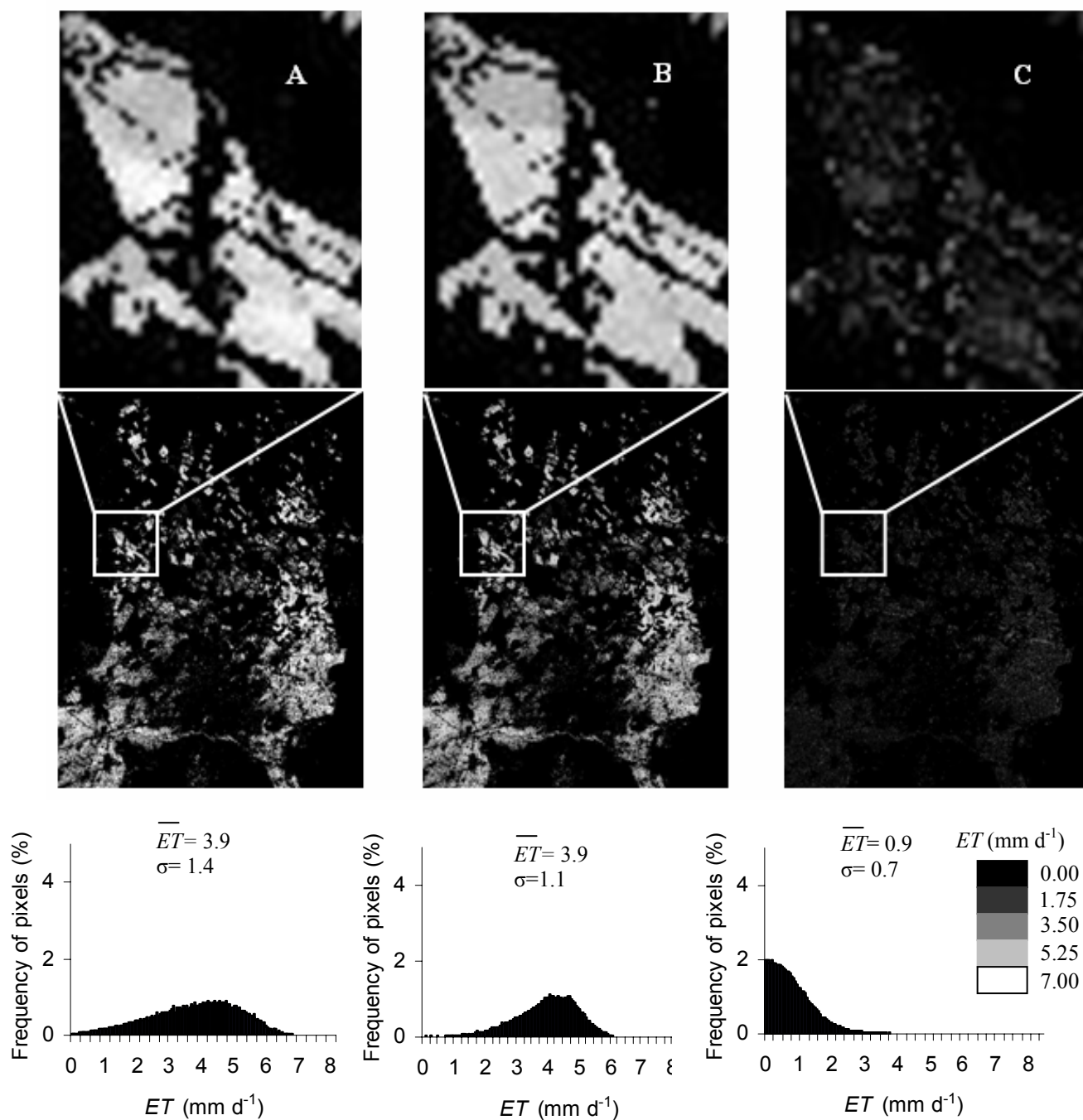
Figure 4.7 A)The *ET* map and its histogram derived from the ASTER image; B) Disaggregated *ET* using linear disaggregation; C) Map of absolute *ET* difference between *ET* derived from ASTER and disaggregated *ET* (13 May 2005)
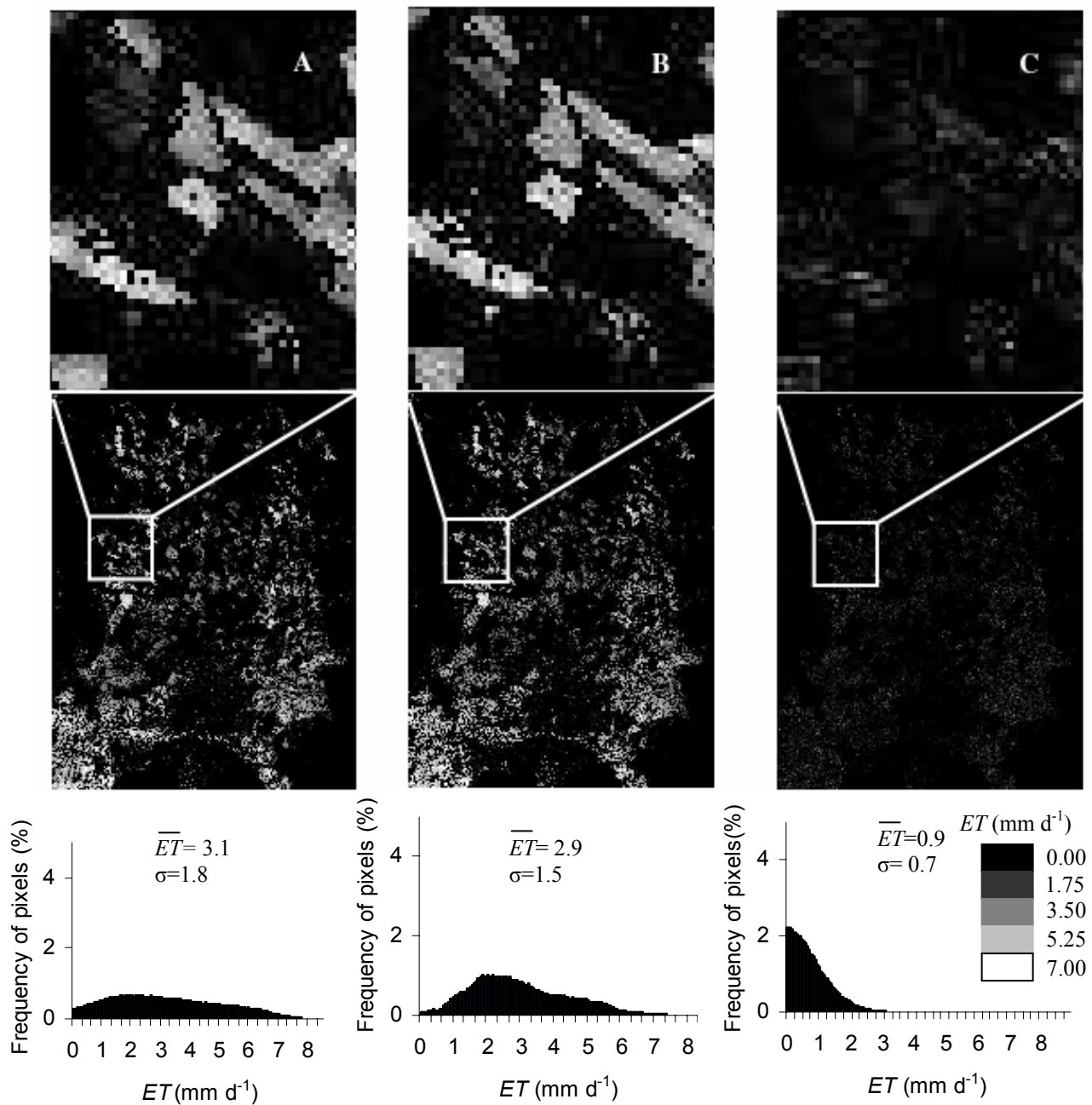
Figure 4.8 A)The *ET* map and its histogram derived from the ASTER image; B) Disaggregated *ET* using linear disaggregation; C) Map of absolute *ET* difference between *ET* derived from ASTER and disaggregated *ET* (17 Aug 2005)

4.8 Disaggregation using a weighted *ET*-ratio

4.8.1 Weighted *ET* ratio of *one old ASTER image and its aggregation*

The ratio of the *ET* map derived from the ASTER image of 6 May, 2005 and its aggregation to the 1000 m resolution was used as a weighted ratio map and was multiplied with the new aggregated *ET* derived from ASTER image of 13 May, i.e. according to the procedure described in Fig. 4.2. Both the histograms and the *ET* patterns showed good agreement between the disaggregated *ET* map of 13 May and the original *ET* map. Also the strong correlation coefficient *r* of 0.76 between disaggregated and original data confirms a good

agreement (Fig. 4.9). This is further supported by a low mean of absolute *ET* differences and *RMSE* as presented in Table 4.4 ($\overline{ET}_{\text{differences}}$ = 0.9 mm d^{-1}, RMSE=1.2 mm d^{-1}).
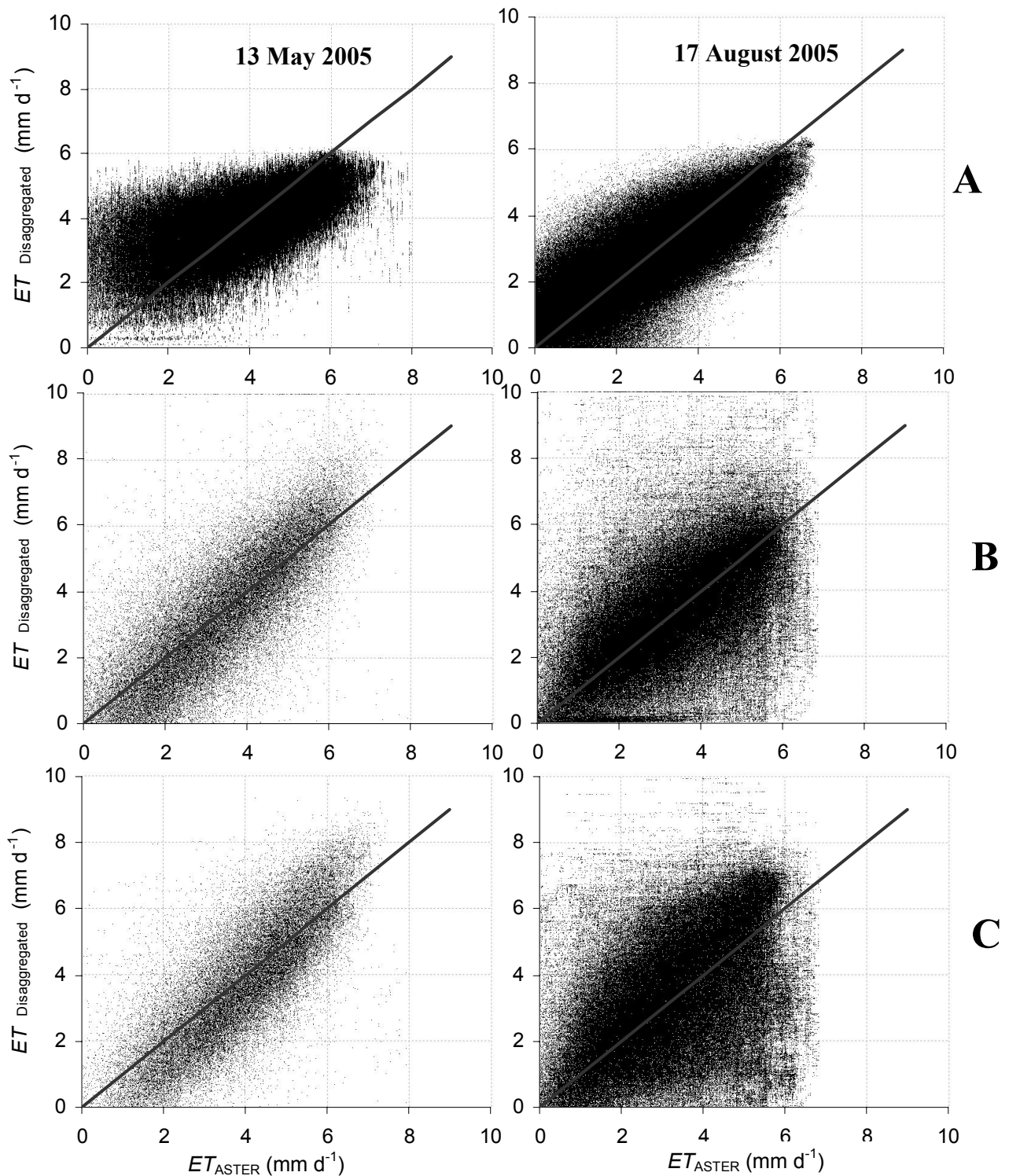
Figure 4.9 Scatter plot of *ET* derived from the ASTER image, and the disaggregated *ET* which has been derived using three different disaggregation methods at two different dates (13 May and 17 August 2005). A) Linear disaggregation B) Weighted ratio using one old *ET* map from ASTER data and its aggregation C) Weighted ratio using one old *ET* map from ASTER data and the global mean of its aggregation.

The same procedures were applied to the aggregated *ET* map derived from the ASTER image of 17 August. A weighted ratio map was created by dividing the *ET* map derived from the ASTER image of 20 October and its aggregation to the 1000 m resolution. The ratio map was multiplied to the aggregated *ET* derived from ASTER image of 17 August. Both the *RMSE* and mean of the *ET* differences computed for the disaggregated *ET* (17 August) are higher than expected ($\overline{ET}$ differences = 1.4 mm d^{-1}, *RMSE* = 1.9 mm d^{-1}). Also the correlation (r = 0.55) between disaggregated and original data is weak. The reason is that the weighted ratio map used in the disaggregation procedure was based on the *ET* maps derived from the ASTER image of 20 October. Since sunflower was harvested before this time, the derived ratios will differ from the active summer growing season.

4.8.2 Weighted *ET*-ratio of *one old ASTER and global mean of its aggregation*

The disaggregating procedures in the weighted ratio approach were again applied to the aggregated *ET* maps derived from the ASTER images of 13 May and 17 August. But, instead of dividing *ET* map and its aggregation, the weighted ratio map was created through dividing the *ET* map of the ASTER image and the global mean of its aggregation. Then the weighted ratio map was multiplied with the global mean of new simulated MODIS image (Eq. 4.14).

Strong correlation (r = 0.75), low absolute *ET* differences ($\overline{ET}$ differences = 1.0 mm d^{-1}) and low *RMSE* (*RMSE*=1.2 mm d^{-1}) between the disaggregated *ET* and the original *ET* map on 13 of May show a good correspondence. However, for August 17, the disaggregated *ET* (Fig. 4.9) shows a weak correlation (r = 0.44) with the original *ET* map due to the harvest of sunflower before 20 October.

4.9 Summary and conclusions

Remotely sensed images of the Earth's surface have the potential to provide detailed information about evapotranspiration *ET*. However, due to resolution limitations of existing remotely sensed data, these data can not be used directly for routine estimation of *ET* from individual fields. Therefore, disaggregation of *ET* maps derived from low spatial resolution data having a high temporal resolution is needed.

To derive daily *ET* fluxes the SEBAL algorithm was applied to the ASTER and MODIS images acquired on 6 May and 13 May 2005 during the winter growing season, and on 17 August and 20 October 2005 during the summer growing season in the Borkhar irrigation district, Iran. To eliminate the effects of differences in geometries of used images, *ET* derived from ASTER images was aggregated to the MODIS resolution. A new disaggregation technique based on linear disaggregation of *ET* components within each MODIS pixel was applied to the simulated MODIS images. Alterative disaggregation procedures based on a weighted ratio map of high and low spatial resolution *ET* i.e. weighted ratio using one ASTER and its aggregation, and weighted ratio using one ASTER and mean of its aggregation, were discussed. The main conclusions of this study are the following:

- ▪ The overall *ET* map derived from the aggregation of the ASTER data and *ET* maps derived MODIS data including their *ET* histograms matched well. $\overline{ET}$ values of MODIS images were respectively 9.5 % and 19 % higher than the $\overline{ET}$ values of aggregated ASTER images on 13 May and 17 August. Hence, it was concluded that SEBAL can be consistently applied to high as well as low resolution images. Further, *ET from each MODIS pixel showed a moderate to strong correlation with the*

weighted arithmetic average of ET values of all components within the MODIS pixel. Theoretically we assumed this to be true for fluxes like *ET*, and this assumption supported the linear disaggregation approach.

▪ The disaggregated *ET* maps derived by means of the linear disaggregation approach showed overall good agreement with the original *ET* maps. The disaggregated *ET* and observed *ET* map as well as their *ET* histograms matched quite well. The disaggregated *ET* maps derived using the *weighted ET ratio approach* on 13 May showed slightly higher correlation values than the results derived from the linear disaggregation approach. However, the disaggregated *ET* maps derived using *the weighted ET ratio approach* on 17 August showed significantly lower correlation.

▪ The advantages and disadvantages of the applied disaggregation approaches have been summarized in Table 4.5.

Table 4.5 Advantages and disadvantages of three different disaggregation methods: linear disaggregation; weighted *ET* ratio of one ET_{ASTER} map and its aggregation; weighted *ET* ratio of one ET_{ASTER} map and mean of its aggregation.

Disaggregation method	Advantages	Disadvantages
Linear disaggregation	-Low number of high spatial images -Good spatial coverage -Good temporal coverage	-Block structures -Complex -Uniform water stress enforced -K_c of non-irrigated crops need to be specified -Need for crop identification map
Weighted ratio of one ET_{ASTER} map and its aggregation to the MODIS resolution	-Good spatial coverage -Very simple	-High number of high spatial images -Block structures -Low temporal coverage
Weighted ratio of one ET_{ASTER} map and global *mean* of its aggregation to the MODIS resolution	-Good spatial coverage -Very simple	-High number of high spatial images -Low temporal coverage -Effects from non irrigated land use is included

▪ *The biggest advantage of linear disaggregation approach is that the number of high spatial resolution images needed in this method is low; it can even be applied by using only one land cover map.* However, the main assumption used in this method, i.e. the water stress being constant within each MODIS pixel, is restrictive as in reality the water stress varies according to the sensitivity of the crops and the amount of irrigation applied. In addition, block structures in the resulting image may be viewed as another disadvantage of this method.

▪ At disaggregation using both weighted ratio maps, the spatial resolution was ideal and its application was also very simple. The problem of block structure in the resulting image was solved by disaggregation using the weighted *ET* ratio map of one ASTER

image and the global mean of its aggregation. The disadvantage of disaggregation using the weighted *ET* ratio is that the temporal resolution was low. The assumption used in this method i.e. the weighted ratio is constant during growing season, was not realistic. *To increase the temporal resolution, we need to increase the number of high spatial resolution and high quality images during the growing season. In many regions this is currently not feasible.*

▪ It is finally recommended to compute spatially detailed results for a complete growing season and then compare the cumulative *ET* values.

5. Inverse modelling of irrigation scheduling using disaggregated remotely sensed evapotranspiration data

5.1 Introduction

Irrigation scheduling is defined as time and depth of applied irrigation. Irrigation flux I (mm d^{-1}) with precipitation and potential evapotranspiration fluxes i.e. ET_p and P (mm d^{-1}) determine the upper boundary condition in numerical simulation models. Water balance components computed by simulation models like SWAP are quite sensitive to the upper boundary conditions, which are specific to each location. ET_p is usually estimated from the reference grass evapotranspiration ET_{ref} using the Penman-Monteith equation, and an unstressed crop coefficient K_c (*Allen et al.*, 1998). Irrigation practices from one farm to another however do vary considerable. This may thus cause a high uncertainty when applying a distributed model like SWAP at regional scale. In the semi-arid regions, precipitation has a minor contribution to the water balance and is more evenly distributed than irrigation. Therefore, to simulate hydrological processes correctly, an accurate quantification of irrigation scheduling i.e. times and depth is essential.

During the past decades, inverse modelling has been used successfully for estimation of irrigation practices (*Ines et al.*, 2002a, 2005; *Droogers and Bastiaanssen*, 2002; *Olioso et al.*, 2005). In most of these studies, the possibilities of field measurements or high resolution RS-based data have been investigated for deriving irrigation practices. Much less work has been published on application of low to moderate spatial resolution remotely sensed data in inverse modelling.

In addition, the irrigation times in previous studies, were defined as a constant function of relative transpiration ($T\,T_p^{-1}$). In the Borkhar irrigation district, irrigations are based on a fixed rotation. Hence in practice, the irrigation times applied by farmer may not meet the identified times using such function.

Successful application of the inverse modelling technique depends on the availability of appropriate observation data in space and time. The observed data used in previous inverse modelling studies are mostly soil water content (*Singh et al*, 2006), and transpiration T and/or evaporation E (*Feddes et al.*, 1993; *Jhorar*, 2002; *Ins et al.*, 2002a, 2002b; *Droogers and Bastiaanssen*, 2002). In this study, we will use ET as observed data for the following reasons:

- ET data are most relevant to irrigation demands;
- Areal ET fluxes are available from remotely sensed data;
- As it is difficult to obtain transpiration separately from soil evaporation, observed ET data may be used as best data.

We need however to address the problem of spatial and/or temporal limitations of existing remotely sensed data. High spatial resolution data have been successfully used for ET estimation at field scale (*French et al.*, 2005). Because of their low frequency, the high risk of clouds and their high costs, these data are however not suitable for routine ET-estimation.

The high temporal (daily or even twice daily) satellite data from the MODerate resolution Imaging Spectroradiometer (MODIS) may be a practical alternative for routine ET-estimation (*Timmermans et al.*, 2004). These data combine a high temporal resolution with a wide spatial coverage at minimal costs (*MCST*, 2002). However, due to its low spatial resolution of 1000 m, MODIS images represent ET over areas larger than 100 ha, thus generally containing a mixture of different fields and crop types. Hence, the basic question

73

is: *Is it possible to derive irrigation practices from these low to moderate spatial resolution RS data?*

The objective of Chapter 5 therefore is: *To obtain spatial data of times and depths of irrigations for an irrigation system using an inverse modelling approach based on cumulative evapotranspiration data*. Specific attention will be given to:
- the well-posed nature of the inverse problem;
- the disaggregation of large scale satellite images;
- the effect of observation errors.

The possibility of deriving irrigation practices using inverse modelling will be tested by numerical SWAP simulated *ET* data, as well as by the use of disaggregated remotely sensed *ET* data from MODIS images. In the numerical experiment, forward simulations will be performed with the simulation model SWAP (Chapter 3) to generate *ET* between the Julian days 60 to 160 as if these were available from independent measurements. The effect of observation errors will also be considered in the numerical experiment.

In both cases, the parameters estimation program PEST (*Doherty et al.*, 1995) will be used to derive irrigation times and depth of irrigations.

5.2 Simulation of *ET* data using the SWAP model

To generate the *ET* data, forward SWAP simulations (see Chapter 3) were performed for a wheat crop at W1, W2 and W3 (see Fig. 3.1), assuming a deep groundwater levels by specifying free drainage as lower boundary condition. All simulations started from the sowing dates of wheat at W1 (8 November 2004), W2 and W3 (1 November 2004). Simulations were performed using the simple crop growth module and covered the growing season of the wheat crop for 218 days. Six post sown irrigations at W1, W2 and W3 were specified of which dates and depth are shown in Table 5.1.

Table 5.1 Time and depth of irrigations applied in forward simulations at the three farmer's fields W1, W2 and W3 being located in the Borkhar irrigation district during the agricultural year 2004-05.

Field	Irrigation depth (mm)	Irrigation times (days after planting)					
		Pre	1st	2nd	3rd	4th	5th
W1	170	1	12	104	147	171	193
W2	130	1	37	132	169	182	201
W3	120	1	35	131	165	174	196

As discussed in Chapter 3, due to the small size of the Borkhar irrigation district, an arithmetic average of weather data at three meteorological stations was implemented in the simulations.

Based on information of percentages sand, silt and clay, the soil profile in each field was reduced to two soil layers: topsoil and subsoil. The soil hydraulic properties were derived using pedotransfer functions (Hypress database for European soils by *Wösten et al.* in 1998)

based on information of soil texture, organic matter content and dry bulk density. The applied soil hydraulic parameters (θ_{res}, θ_{sat}, K_{sat}, α, n and λ) for these fields are given in Table 5.2.

Table 5.2 Soil layers, soil texture (C=clay, Si=silt, L=loam) and derived soil hydraulic parameters at three farmer's fields in the Borkhar irrigation district.

Field	Layer (cm)	Soil Texture	Soil hydraulic properties					
			θ_{res} (cm^{3}cm^{-3})	θ_{sat} (cm^{3}cm^{-3})	K_{sat} (cm d^{-1})	α (cm^{-1})	λ (-)	n (-)
W1	0-90	C	0.01	0.45	24.0	0.0286	-3.84	1.166
	>90	CL	0.01	0.42	06.2	0.0780	-1.19	1.102
W2	0-60	SiCL	0.01	0.48	30.0	0.0248	-2.73	1.164
	>60	SiL	0.01	0.42	07.0	0.0275	0.17	1.198
W3	0-60	SiC	0.01	0.38	34.0	0.0258	-2.76	1.151
	>60	C	0.01	0.49	15.0	0.0301	-0.05	1.130

The source of water (either canal or tube-well) and its quality, time and depth of irrigations were recorded during the measurements. Depth of irrigations in each irrigation event was assumed to be constant as the farmers apply traditionally large irrigations.

5.3 Simulation of *ET* using remotely sensed data

The 1999 version of SEBAL (Chapter 4) referred to as AHAS (*Parodi*, 2002) was applied to 1000 m spatial resolution MODIS data acquired for 18 different dates during the winter growing season of 2004-05. The characteristics of the satellite images, the level of products and their acquisition dates are listed in Table 5.3.

Table 5.3 The characteristics and acquisition time of ASTER and MODIS images ([a] Calibrated and geo-located radiances at the sensor).

Satellite	Sensor	Spatial resolution (m)	Temporal resolution (d)	Level of product	Selected bands	Acquisition dates in 2005
Terra	**MODIS**	250	1	1B[a]	1-2 aggregated to 1000 m	Mar: 15,21, 29 Apr: 04, 06, 09, 13, 22, 25, 27 May: 01, 06, 08, 13, 15, 22, 05, 09
		1000	1	1B[a]	31,32	Jun: 02, 05, 09
		250	1	2B[a]	1,2	Mar: 15,21, 29 Apr: 04, 06, 09, 13, 22, 25, May: 01, 06, 13, 22, 05, 09 Jun: 02, 09
Terra	**ASTER**	15	N/A	1B[a]	1-2	6 May, 13 May
		30		1B[a]	4-9	

As discussed in Chapter 4, MODIS data represent *ET* of a mixture of fields in pixels containing an area of 100 ha. Therefore, the remotely sensed evapotranspiration data from MODIS images were disaggregated to the field scale using linear disaggregation as has been described in Chapter 4:

$$ET(x_i, y_i, t) = K_s(x_i, y_i, t)\, K_c(x_i, y_i, t)\, ET_{\mathrm{ref}} \tag{5.1}$$

where *ET* (x_i, y_i, t) is *ET* of the ith component within each MODIS pixel using SEBAL, $K_s(x_i, y_i, t)$ represents *the water stress coefficient* of the ith component within each MODIS pixel, $K_c(x_i, y_i, t)$ the crop coefficient of the ith component within each MODIS pixel, and ET_{ref} the reference grass *ET* computed from the Penman–Monteith equation (see Chapter 4) using local weather data.

Assuming that the water stress coefficient in each MODIS pixel is constant for all the components, $K_s(x_i, y_i, t)$ can be derived as:

$$K_s(x, y, t) = \frac{ET_{\mathrm{MODIS}}(x, y, t)}{\displaystyle\sum_{i=1}^{m} K_c(x_i, y_i, t)\, ET_{\mathrm{ref}}\, A_{\mathrm{f}, i}} \tag{5.2}$$

where $ET_{\mathrm{MODIS}}(x, y, t)$ is *ET* derived from each MODIS pixel, $A_{\mathrm{f},i}$ is the area fraction of the ith component within each MODIS pixel, *m* total number of components within each MODIS pixel, *x* and *y* are horizontal and vertical location of each MODIS pixel respectively, and *t* represents the time.

The $K_c(x_i, y_i, t)$ values were derived from 250 m spatial resolution MODIS data acquired on 16 different dates during the winter growing season in 2005. $K_c(x_i, y_i, t)$ values were computed using the ratio of $ET_p(x_i, y_i, t)$ over ET_{ref} according to the approach proposed by *D'Urso et al.* (2001). To calculate K_c values on these dates, $ET_p(x_i, y_i, t)$ was calculated from the Penman–Monteith equation. The surface resistance r_s was estimated based on the minimum value of the stomata resistance ($r_{\mathrm{stomata}} = 135$ s m^{-1}) and the effective *LAI* values (Chapter 4).

Vegetation indices, such as the Soil Adjusted Vegetation Index (*SAVI*), are logarithmically related to the green leaf area index (*Choudhury et al.*, 1994). In this study, the coefficients of a logarithmic function relating field data of *LAI* with satellite observations of *SAVI,* were established on the basis of MODIS data. *LAI* maps were produced using the following derived relationship for MODIS:

$$LAI = -\frac{1}{0.27} \ln\left(\frac{0.618 - SAVI}{0.48}\right) \qquad (r^2 = 0.85) \tag{5.3}$$

The diffusion resistance to water vapour r_{air} was calculated as a function of crop height h_{crop} (m) and wind speed u_2 (m s^{-1}). The h_{crop} maps for winter wheat were produced using a polynomial relation derived from field data of *LAI* and crop height h_{crop}:

$$h_c = 0.125 - 0.0186 LAI + 0.0317 LAI^2 \qquad (r^2 = 0.94) \tag{5.4}$$

Since the cumulative **ET** data were needed in the inverse modelling procedures, the disaggregated *ET* data at 18 dates were extended to the whole growing season assuming *ET* ET_{ref}^{-1} being constant between observation dates.

5.4 Inverse modelling procedure of irrigation scheduling

The inverse approach was first applied to identify the depth and times of irrigation using simulated **ET** data at farmer's fields as observation. Thereafter, to show the practical application of inverse modelling, we derived the depth and irrigation dates using the disaggregated remotely sensed **ET** data.

The *non-linear parameter estimation program*, PEST (*Doherthy et al*., 1995) was linked with SWAP to derive the selected parameters inversely. An overview of the parameters estimation procedure was presented in Chapter 3 (Fig. 3.4). An objective function $O(\boldsymbol{b})$ was defined for quantifying the differences between model results and observations according to:

$$O(\boldsymbol{b}) = \sum_{i=1}^{N} \left[\left(\boldsymbol{ET}_{\text{obs}}(t_i) - \boldsymbol{ET}_{\text{sim}}(\boldsymbol{b}, t_i) \right)^2 \right] \tag{5.5}$$

where $\boldsymbol{ET}_{\text{obs}}(t_i)$ is the observed cumulative evapotranspiration at time t_i, $\boldsymbol{ET}_{\text{sim}}(\boldsymbol{b}, t_i)$ is the numerically calculated values of **ET** at time t_i corresponding to a trial vector of selected parameter values $\boldsymbol{b}$, where $\boldsymbol{b}$ is the *n*-dimensional vector containing the parameters that are optimized simultaneously. The inverse problem was then to find an optimum combination of irrigations times and depth that minimize the objective function.

The possibility of finding irrigation times and depth using only **ET** data in the objective function was explored using several data sets. In the numerical experiment, cumulative simulated **ET** data on a 5, 15 and 30 days basis in the period 60th (15 Mar) to 160th (09 Jun) Julian day were used in the inverse procedures. In practice, the main sources of regional *ET* data are remotely sensed satellite images. The typical accuracy of remotely sensed *ET* data as estimated by SEBAL varies from 85% for one single day and increases to 95 % on a seasonal basis (*Bastiaanssen et al*., 2005). Therefore, to emulate the real-world situation, taking into account the errors in SEBAL and the linear disaggregation procedure, 15 and 30 % random errors were included in the cumulative simulated **ET** data on the 5 day basis. In the practical part, the disaggregated remotely sensed **ET** data on the 5 day basis in the same period were implemented in the inverse procedures.

Initial values of 4 last post sown irrigation dates as specified during inverse optimization are respectively: 111, 141, 171 and 211 days after the planting date. The range of date variations was set as 60 to 218 days. To reduce the number of optimized parameters, the times of first post and pre-sown irrigations were considered as a known parameter. The initial value for irrigation depth was set as 10 mm and its variation range was limited between 1 and 200 mm. To investigate the uniqueness of the optimized parameter, optimization procedures were repeated with different initial values.

To evaluate the level of difference between the observed and simulated data with the optimized parameters, the Root Mean Square Error (*RMSE*) was computed as:

$$RMSE = \sqrt{\frac{\sum_{i=1}^{n}[\boldsymbol{ET}_{obs}(t_i) - \boldsymbol{ET}_{Sim}(t_i)]^2}{n}} \tag{5.6}$$

where $\boldsymbol{ET}_{obs}(t_i)$ is the observed $\boldsymbol{ET}$ at time t_i, N is number of observation and $\boldsymbol{ET}_{sim}(t_i)$ is the simulated value of cumulative $\boldsymbol{ET}$.

5.5 Disaggregation results of remotely sensed *ET* data

5.5.1 Distribution of unstressed crop coefficients K_c

Fig. 5.1 shows the distributions of unstressed K_c values (global mean and standard deviation) for wheat in the Borkhar irrigation district from the 70th (15 Mar) to 160th (09 Jun) Julian day. The K_c-coefficients were derived from MODIS images with a spatial resolution of 250 m using the Penman–Monteith equation (solid line). The global mean and standard deviation of K_s values was calculated using Eqs. 4.15 and 4.16 as discussed in Chapter 4.
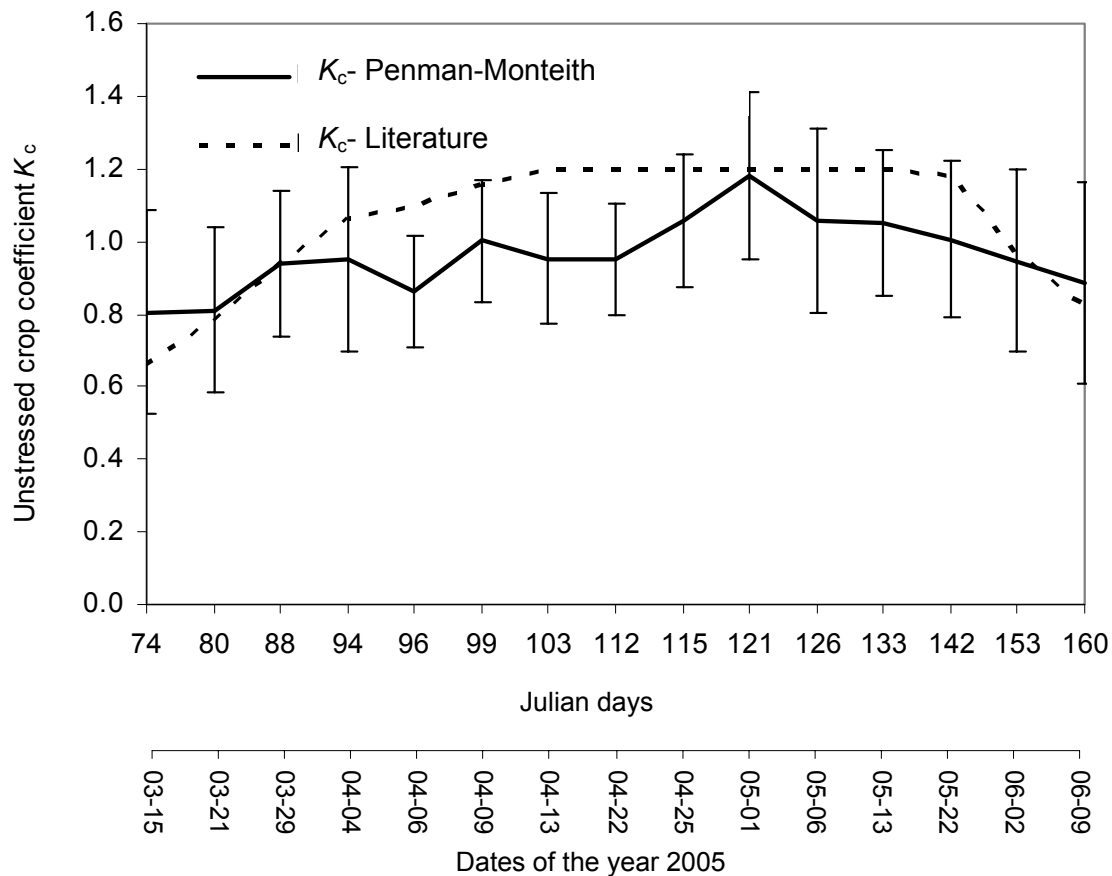
Figure 5.1 Distribution of unstressed crop coefficients K_c (global mean and standard deviation) over the Borkhar irrigation district from the 74th to 160th Julian day during the agricultural year 2004-05. The solid line shows K_c – values derived from 250 m spatial resolution MODIS images using the Penman–Monteith equation. The dotted line shows K_c – values derived from tabulated K_c values in the literature (*Allen et al.*, 1998).

As shown in Fig. 5.1 the K_c values increase slightly during period 74th to 88th day. This period corresponds to the development growth stage after a frost period in January and February. K_c values from the 88th day to 112th day which corresponds to the middle growing stage in April and May, shows some fluctuations. K_c values start decreasing from 133th day until the end of the wheat growing season in June (160th day).

The K_c values derived from remote sensing data were compared with K_c values derived from literature K_c curves being adjusted for the Borkhar region (*Allen et al.*, 1998). *The trend of the K_c value variation taken from the literature compares well with the K_c values derived from remote sensing as presented in Fig. 5.1.*

5.5.2 Distribution of water stress coefficients K_s

The global mean and standard deviation of water stress coefficients K_s (= ET / ET_p) at different dates during the wheat growing season from 74th (15 Mar) to 160th (09 Jun) Julian day are shown in Fig. 5.2. High K_s values indicate low water stress and vice versa.
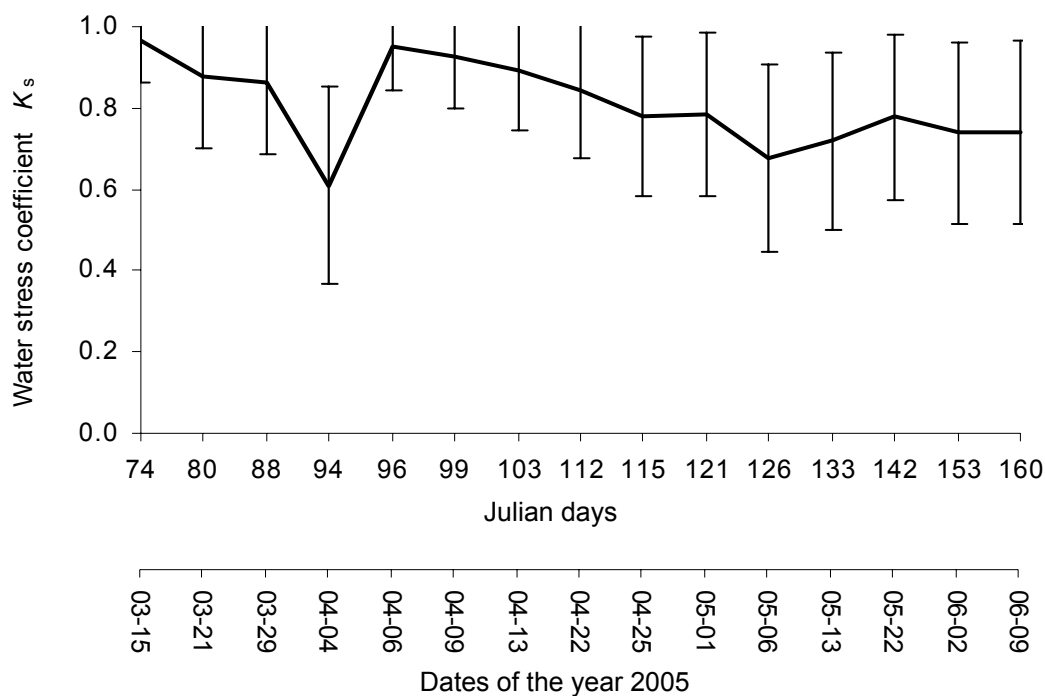
Figure 5.2 Distribution of the water stressed crop coefficient K_s (global mean and standard deviation) as derived from 1000 m spatial resolution evapotranspiration ET data by applying SEBAL to the MODIS images over the Borkhar irrigation district from the 74th to 160th Julian day during the agricultural year 2004-05.

The K_s values were derived from remotely sensed data using Eq. 5.2 assuming an equal water stress in the irrigated area of 1000 m spatial MODIS pixel. This assumption holds true as long as the components are irrigated simultaneously, which is a fair assumption for the

conditions in the Borkhar irrigation district. The global mean and standard deviation of derived K_s values was calculated using Eqs. 4.15 and 4.16 in Chapter 4.

As shown in Fig. 5.2 the K_s values from the 74th day (15 Mar) until the 103th day (13 Apr) indicate a low water stress except for the 94th day. High water stress during that day might be due to the high water demand on that day. During the period of the 115th (25 Apr) till 126th Julian day (6 May), the K_s values indicate rather high water stress. In this stage, the crop canopy has reached its maximum and has the highest water demand. From 126th (6 May) until the end of the growing season, the water stress decreases along with a reduction of the crop transpiration.

5.5.3 Comparison of disaggregated remotely sensed *ET* data with SWAP simulated *ET* values at individual farmer's fields

To evaluate the accuracy and reliability of disaggregated remotely sensed *ET* data, the latter data over the three farmer's fields W1, W2 and W3 were compared with SWAP simulated *ET* being considered as independent data. For comparison in this section only, the *ET* estimated by RS-SEBAL and SWAP is referred to as ET_{RS} and ET_{SWAP} respectively. The original *ET* from MODIS images is shown as $ET_{RS-MODIS}$ and disaggregated *ET* using linear disaggregation is referred to as ET_{RS-LD}.

Fig. 5.3 *shows a poor agreement between* $ET_{RS-MODIS}$ *and* ET_{SWAP} *on daily basis at the three farmer's fields, emphasizing the need for disaggregation of 1000 spatial resolution ET data to higher resolution.* The rather low *RMSE* between ET_{RS-LD} and ET_{SWAP} at field W1 (*RMSE* = 1.1) indicates a strong agreement between ET_{RS-LD} and ET_{SWAP} at this farmer's field.

While a high discrepancy between ET_{RS-LD} and ET_{SWAP} at W2 and W3 (*RMSE* = 1.5 and 1.4 mm d^{-1}) indicate rather weaker agreement between simulated and remotely sensed disaggregated *ET* data. The correlation between ET_{RS-LD} and ET_{SWAP} was respectively 0.50, 0.40 and 0.48 at W1, W2 and W3 which show a moderate correlation.

The cumulative ET_{RS-LD} over farmer's fields W1, W2 and W3 was respectively, 448, 413 and 317 mm from 74th to 160th Julian day during the agricultural year 2004-05. The cumulative ET_{RS-LD} in comparison with the cumulative ET_{SWAP} at W1 was 5 % lower, at W2 9 % higher and at W3 12 % lower.
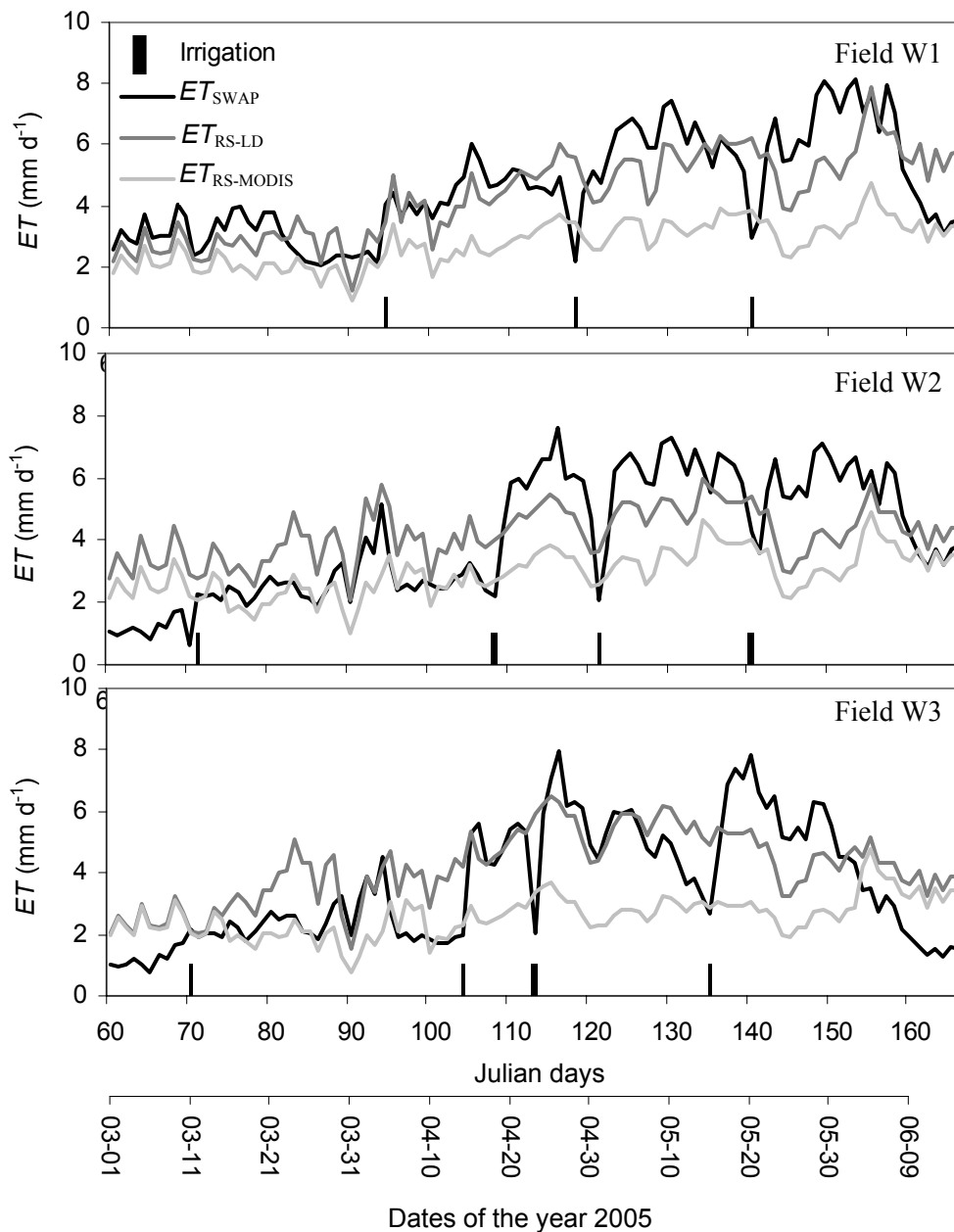
Figure 5.3 Comparison of evapotranspiration data *ET* at three farmer's fields W1, W2 and W3 in the Borkhar irrigation district during the agricultural year 2004-05 derived from:
- SWAP simulation model (ET_{SWAP})
- Original MODIS evapotranspiration data estimated by SEBAL algorithm ($ET_{RS-MODIS}$)
- Disaggregated remotely sensed evapotranspiration data using the linear disaggregation approach (ET_{RS-LD})

5.6 Results of inverse modelling of irrigation scheduling

In this section, *irrigation parameters like irrigation time and depth* are referred to as 'simulated' for the parameters identified by inverse modelling. Known irrigation parameters used in the forward simulations are referred to as 'reference'. Results of the inverse procedure are first presented for forward simulated and after that for disaggregated remotely sensed *ET* data.

5.6.1 Numerical experiment using *forward SWAP ET simulation*

Five different combinations of SWAP simulated *ET* data at the three farmer's fields W1, W2 and W3 were selected to study their influence on the accuracy of the inversely identified irrigation parameters (Table 5.4).

Table 5.4 SWAP simulated irrigation times and depth using different combinations of measurement data at three farmer's fields W1, W2 and W3 in the Borkhar irrigation district. Irrigation times are expressed as days after planting date. Irrigation depth is expressed as total amount of irrigation at six irrigation events using identical irrigation depths.

cases	Evapotranspiration data		Field	Identified irrigation times and depth							RMSE mm
				Depth		Times (days after planting)					
				mm	bias (%)	2nd	3rd	4th	5th	bias (d)	
1		5 days based cumulative *ET* data	W1	1020	0	104	147	171	192	1	0.01
			W2	768	-2	132	159	177	201	13	2.10
			W3	720	0	117	154	173	196	26	2.50
2	*ET*-Simulated data	5 days based cumulative *ET* data including 15 % random error	W1	1020	0	107	148	172	191	5	4.50
			W2	786	1	111	142	171	196	61	4.00
			W3	972	35	113	159	174	195	24	5.40
3		5 days based cumulative *ET* data including 30 % random error	W1	1026	1	101	148	173	190	2	14.8
			W2	672	-14	104	158	181	203	36	12.5
			W3	1164	62	95	154	171	195	49	11.4
4		15 days based cumulative *ET* data	W1	876	-14	83	134	166	192	38	3.90
			W2	1200	54	132	145	174	198	32	4.10
			W3	882	23	119	135	169	193	48	4.20
5		Monthly based cumulative *ET* data	W1	774	-24	104	144	175	192	3	0.36
			W2	672	-14	121	165	181	204	12	0.34
			W3	816	13	119	148	173	195	28	0.78
6	*ET*-Remotely sensed data	5 days based cumulative *ET* data	W1	588	-30	89	137	165	202	11	6.10
			W2	372	-18	121	152	179	203	28	7.40
			W3	840	4	133	159	180	211	18	5.10

The results of the simulated irrigation times and depth, and their bias for the 5 different cases being considered in testing the performance of inverse modelling are given in Table 5.4. For better insight, the simulated and reference irrigation times for all cases are also shown in Fig. 5.4. In all cases, the **ET**-based form of the objective function was used in the inverse procedures. The set of unknown parameters consisted of 4 last post sown irrigation times and

one fixed irrigation depth for all irrigation events. The bias for simulated irrigation times and depth was expressed as the difference between reference and simulated values in percentage and days respectively.
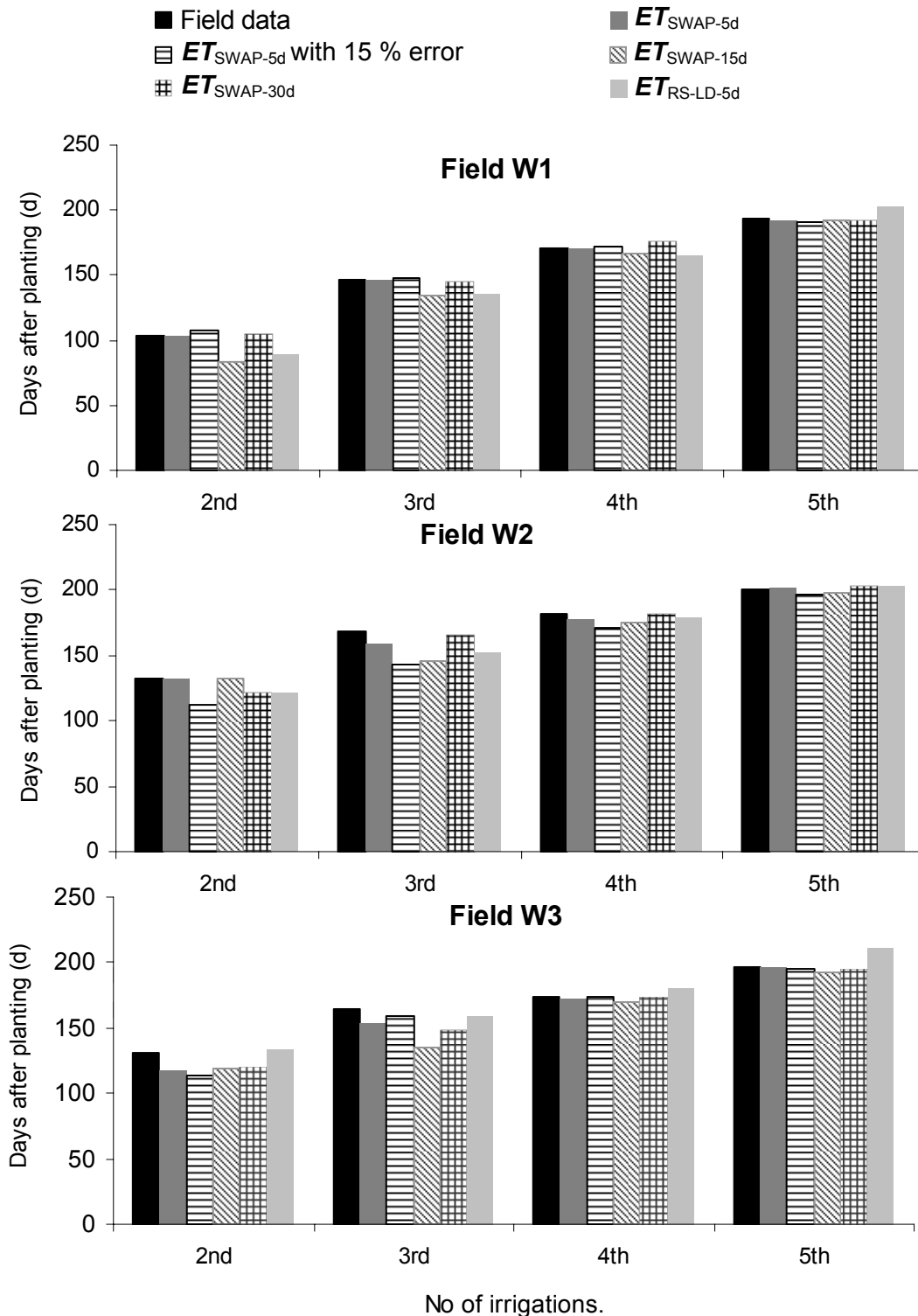

Figure 5.4 Comparison of simulated irrigation times using 5 different combinations of measurement data at three farmer's fields W1, W2 and W3 in the Borkhar irrigation district. Irrigation times are expressed as days after planting date.

In *Case 1* as observation in the inverse procedures, we used 5 days based cumulative ***ET*** data at three individual wheat fields W1, W2 and W3. As shown in both Fig. 5.4 and Table 5.4, the simulated irrigation times match quite well with the reference data except for the second and 3rd irrigation at W3, which indicates totally a 26-day-difference in comparison with the reference data. The simulated depths correspond well with the reference data for fields W1 and W3, but show a slight deviation at W 3 i.e. bias of -2 %. The repetition of inverse modelling procedures using different initial values for the times and depth of irrigations returned the same results. This shows that the *performance of inverse modelling is promising in identifying the irrigation time and depth of irrigation using 5 days based cumulative ET data.*

After adding 15 random errors to the observation data, an attempt was made in *Case 2* to identify the irrigation scheduling inversely. The errors were included in the observation data to emulate the real-world situation. In this case also the 5 days based cumulative ***ET*** data was used as observation. The *results indicated a good agreement (RMSE < 5.4 mm) between the simulated and reference **ET** data at three farmer's fields. Identified irrigation times were respectively 5, 61 and 24 days lower than reference data at W1, W2 and W3*. The identified depths of irrigation demonstrated good correspondence with the reference data at farmer's fields except for W3 with a 35 % higher value.

In *Case 3* the performance of the inverse modelling approach was tested using the 5 days based cumulative ***ET*** data including 30 % random errors. The results showed that *the performance of the inverse modelling approach in reproducing initial **ET** data and identifying the irrigation times and depth, decreases with increasing random error up to 30 %.*

In *Case 4* the possibility of identifying the irrigation practices was investigated using cumulative simulated ***ET*** data for longer periods i.e. 15 days. As shown in Fig. 5.4, high interval ***ET*** i.e. 15 days based have a larger effect on identified values than adding 15% error to the 5 day basis ***ET*** data. *High bias between the identified times and depth, and references data indicated a low performance for inverse modelling approach in case of using 15 days based cumulative **ET** data.*

In Case 5, the results of inverse modelling using monthly based cumulative ***ET*** data were investigated. In spite of rather weak results in identifying the irrigations times and depths in case 5, the simulated ***ET*** do match well with the reference ***ET*** data (*RMSE 0.8 mm*). This showed *the problem of non-uniqueness in identified parameters exists. The reason was that the parameters were insensitive to the observation data.*

Lower bias between identified times and depths of irrigation at the field W1 in comparison with biases at two other fields W2 and W3. This is due to the higher irrigation interval at the field W1.

High bias in identified depths at W2 using 15 based ***ET*** data or at W3 using 5 based ***ET*** data including 30 % error might be due to the fact that *the maximum identified depth, using the **ET**-based form of the objective function, is limited to the critical soil moisture content in the root zone.* As discussed in Chapter 3 (see Fig. 3.2) moisture in the soil profile lower than the critical soil moisture levels reduces the simulated ***ET***. These critical soil moisture are corresponding to the critical pressure heads i.e. h_3 and h_1. This means that irrigation depths which refill the soil moisture in the root zone between two critical soil moisture contents i.e.

θ (h_3) and θ (h_1) do not have effects on **ET**. Therefore, *in case of no water stress, inverse solution based on the **ET** form of the objective function only, shows high uncertainty in identifying the irrigation depth. Only if drought stress occurs, inverse modelling of irrigation amounts makes sense. Also over-irrigation (excessive leaching) can not be detected by inverse modelling.*

In spite of deviations shown in identified times and depth of irrigation in the numerical experiments, *the cumulative **ET** on seasonal basis at three farmer's field stands more or less constant irrespective of the irrigation times indicating low sensitivity of seasonal **ET** to irrigation times* (Fig. 5.5).
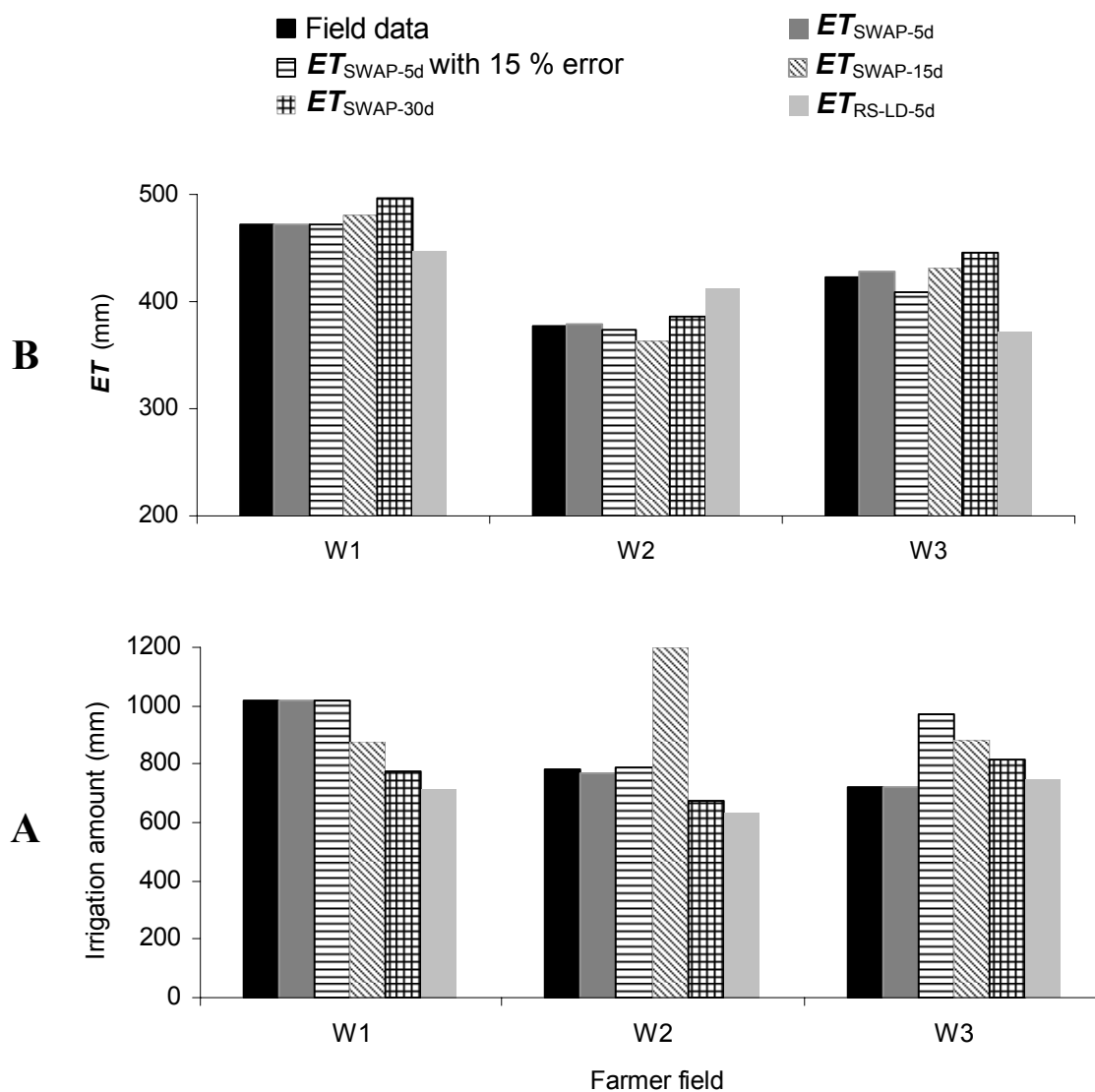

Figure 5.5 Simulated total irrigation depth (A) and cumulative **ET** on seasonal basis (B) using different combinations of measurements at three farmer's fields W1, W2 and W3 in the Borkhar irrigation district.

5.6.2 Experiment using remotely sensed *ET* data

The disaggregated remotely sensed evapotranspiration data at 18 different dates over three farmer's fields were first extended to the whole growing season. To simulate the irrigation depths and times, the cumulative *ET* data based on 5 days were used in the inverse procedure. The number of fitted parameters was set to 4 irrigation times and one fixed depth for the entire irrigation events. As shown in Table 5.4, *performance of inverse modelling in simulation of irrigation times is rather weak*, with a bias at the farmer's fields between 11 to 28 days. Table 5.4 indicates also a high discrepancy between identified irrigation depth and reference data especially at W1 and W2.

A possible explanation is the discrepancy between simulated and remotely sensed *ET* data over three farmer's fields (Fig. 5.3) and the *lack of a dry period* in the remotely sensed data set (Fig. 5.2). *Jhorar* (2002) have concluded already that such *a period is essential in a successful inverse modelling approach based on ET*.

5.7 Summary and conclusions

The ability of inverse modelling to reproduce exactly the initial irrigation times and depth was investigated using forward cumulative simulated *ET* data based on 5, 15 and 30 days and cumulative remotely sensed *ET* data based on 5 days. The simulated *ET* data were produced using the SWAP model at three farmer's fields. The remotely sensed *ET* data were produced by applying SEBAL to the 1000 m spatial resolution MODIS images at 18 different dates. The remotely sensed *ET* data were later disaggregated to field scale resolution using linear disaggregation. The main conclusions of this study are:

- Inverse modelling using accurate cumulative *ET* data in the objective function*, in case of high irrigation intervals and dry periods is a reliable approach in identifying irrigation times and depth.*

- When applying inverse modelling to determine the irrigation practices, *the 5 days based cumulative ET data performed better than 15 days or monthly based ET.* However, the differences between simulated and reference cumulative *ET* on seasonal basis data was small irrespective of deviations in irrigation times and type of *ET* intervals used in the inverse modelling procedures.

- In the inverse modelling the maximum number of optimized parameters depends on the type and accuracy of the observation and hydrological events. Because of the applied heavy flooding irrigation in the Borkhar irrigation district, assuming one fixed irrigation depth for all of post planting irrigations was fair assumption. However, in general we can not assume this.

- Maximum identified depth, using the ***ET***-based form of the objective function, is limited to the critical soil moisture corresponding to the critical pressure heads i.e. h_3 and h_1 in the root zone (see Fig. 3.2). *Irrigation amounts, which rewet the soil profile beyond field capacity and thus cause excessive percolation, can not be detected by the applied inverse modelling approach.*

- Successful application of the inverse methodology depended on the availability of reliable and rather accurate regional *ET* data, as well as on the interval of cumulative

ET data. The disaggregated remotely sensed *ET* showed a rather good correlation with SWAP simulated *ET* at three wheat fields. The performance of the remotely sensed *ET* data was however rather weak in identifying the irrigation times and depth in most of the irrigation events.

- *Because of using an optimization procedure in inverse modelling, identifying the irrigation scheduling at regional scale needs a large amount of computation time.*

.

6. Assimilation of satellite data into agrohydrological models to improve crop yield forecasts

6.1 Introduction

Wheat is the core commodity of the food and agriculture system, providing 40 percent of the energy and 45 percent of the total protein supply in Iran. Iran's domestic wheat consumption stands at about 14 million ton a year of which 2.5 to 7.5 million ton has being imported (*FAO*, 2005). The government intends to raise domestic wheat output to attain self-sufficiency in wheat production. However, due to the growing water scarcity caused by regular droughts and increasing water demands of industries, households and environment, the domestic wheat production may not be sustainable. Hence, a reliable drought assessment would be very beneficial for yield forecasting, proper operational decision making and food security.

To predict the crop yield, physically based agrohydrological models have been developed (*Bastiaanssen et al., 2007*). Further, to reduce the uncertainties in input parameters at regional scale, the agrohydrological models are currently applied in a distributed way (*Droogers et al.*, 2000c; *Singh*, 2005). The advantage of distributed models is that they represent the spatial distribution of various inputs and boundary conditions, and simulate outputs and internal state variables in a distributed fashion. However, because of the heterogeneity of soil-water-atmosphere-vegetation properties and rapid fluctuation of state variables, major problems of distributed modeling are over-parameterization and uncertainty.

Distributed models require an amount of spatial data that only remote sensing (RS) can provide. Therefore, inserting remotely sensed data into distributed agrohydrological models using data assimilation techniques is both appealing and necessary to reduce the uncertainty in outputs and internal state variables (*Schuurmans et al.*, 2003; *Jongschaap and Schouten*, 2005). Different strategies have been suggested to reach that goal.

RS-data can be used to evaluate model performance (*Kite and Droogers*, 2000), or to initialize, drive, update or re-calibrate models (*Droogers and Bastiaanssen*, 2002). When the error between model results and data is low, RS-based initialization of models would in principle be sufficient to provide the spatially distributed information. However, as all models simplify reality, an updating method by sequential assimilation of RS-based surface variables is a better option to keep the model on the track (*Boegh et al.*, 2004). For extensive review and discussion on different assimilation strategies, see *Fischer et al.* (1997) and *Moulin et al.* (1998).

The feasibility of using different RS-based data in hydrological modeling has been determined in several studies e.g. surface soil moisture (*Houser et al.*, 1998; *Hoeben and Troch*, 2000; *Van Loon and Troch*, 2002), latent heat flux (*Schuurmans et al.*, 2003), leaf area index *LAI* (*Bouman*, 1992, *Boegh et al.*, 2004, *Olioso et al.*, 2005), and *LAI* and canopy nitrogen (*Jongschaap*, 2006). In most of these studies, the possibilities of field measurements or high resolution RS-based data have been investigated. Much less work has however been published on the assimilation of low to moderate resolution RS data.

To improve the predictive performance of a distributed agrohydrological model we will *investigate the potential of using low to moderate resolution RS data*. For the Borkhar irrigation district in Iran for the year 2005 a series of 250 and 1000 m spatial resolution MODIS images are available. The time series of *LAI* data will be derived from moderate resolution MODIS data. Low spatial resolution of MODIS data will be converted into relative evapotranspiration $ET\ ET_p^{-1}$ estimates using the Surface Energy Balance Algorithm

for Land, SEBAL, (*Bastiaanssen et al.*, 1998) and applying the aggregation method developed by *Vazifedoust et al.* (2007a).

The main *objective* of this study is *to investigate whether data assimilation of remotely sensed LAI and/or ET ET_p^{-1} estimates from low to moderate resolution MODIS data can be used in combination with an agrohyrological model to predict total wheat production months in advance*.

To compute soil water balance components and to simulate crop growth at the Borkhar irrigation district for 2005, the physically-based Soil-Water-Atmosphere-Plant, SWAP (as described in Chapter 3) will be used in a distributed way on raster base. A sequential updating process will be performed using RS data. We will use a constant gain Kalman filter based on estimation of errors associated with RS observation and model outputs.

6.2 Application of the distributed agrohydrological model SWAP at regional scale

The implementation of the SWAP model at regional scale requires derivation of spatial and temporal distributed data. Therefore, the study area (see Chapter 2) was divided into 10655 homogeneous cells of 250 m spatial resolution. Only pixels containing the wheat crop (1589 pixels) were considered. To derive values for pixels of 250 m, parameters like soil types and land use at raster format were derived by remote sensing techniques and were preprocessed in a Geographic Information System (GIS). Temporal distributed data of water supply were produced using information from tube-wells and the surface irrigation network. *In order to link GIS data with SWAP, a coupling program was written by the first author in MATLAB*. This program took care for the transfer of in- and output data from one system to the other, and to run the model for each pixel. A schematic representation of the framework of the distributed SWAP model is shown in Fig. 6.1. A brief description of spatial input parameters as required for application of the distributed SWAP model at regional scale, is given in the sections 6.2.1 to 6.2.5. For details of methods and field data used in this study, see *Vazifedoust et al.* (2007b).

6.2.1 Weather

The meteorological data were collected at three synoptic meteorological stations (see Chapter 3). Because of the small size of the district, the arithmetic average of weather data at the three stations was implemented in the simulations.

6.2.2 Irrigation

Spatial information on the Borkhar Irrigation Network such as water rights and actual allocated water are available for the main and lateral canals. Information on ground water pumping such as number and average discharge of tube-wells, is also available. General irrigation information was used to derive an estimation of the irrigation amounts for each cell of the Borkhar irrigation district.
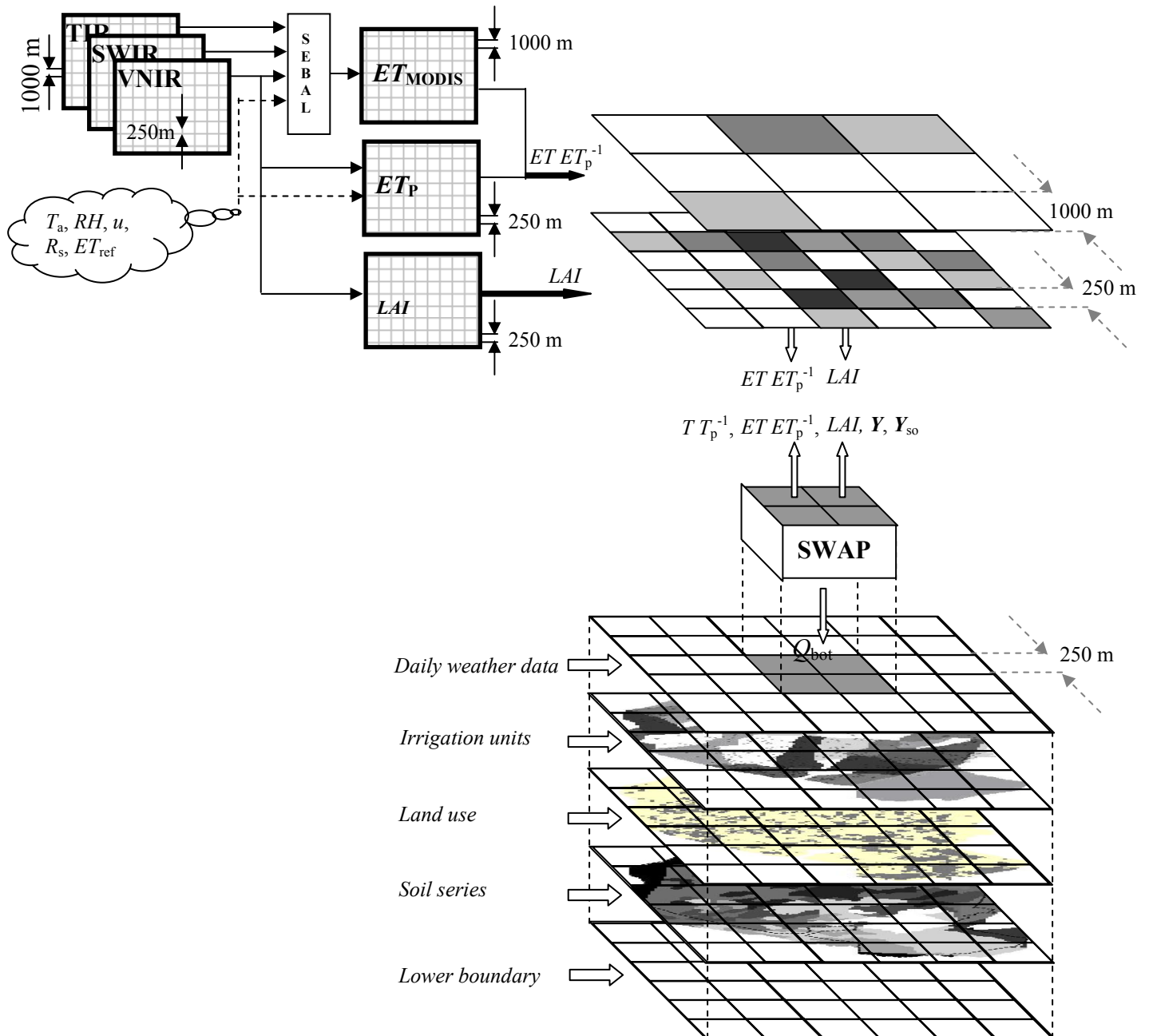
Figure 6.1 Schematic framework for application of the distributed SWAP model at regional scale. SWAP simulates total dry matter yield Y and dry matter of storage organ Y_{SO} using the regional data of the Borkhar irrigation district on a cellular basis. The simulations are continuously updated using remotely sensed data of leaf area index LAI and relative evapotranspiration $ET\,ET_p^{-1}$, whenever they are available. RS based LAI are derived from 250 m spatial resolution MODIS data and RS based $ET\,ET_p^{-1}$ data from 1000 m spatial resolution MODIS data using the SEBAL algorithm. V, NIR and TIR are respectively referring to visible, near-infrared and thermal infrared bands of the electromagnetic spectrum.

Canal water supply

The Borkhar Irrigation Network distributes the surface irrigation water among the farmers. Annual releases of water from the reservoir to the Borkhar Irrigation Network vary from 0 to

50 million m³ (*APERI*, 2001). The canal water distribution contains two main canal commands: Bell Main Branch and Hajiabad Main Branch. These two main canals are further divided into 9 and 11 lateral canals respectively. To ensure equal distribution of the limited amount of water, water supply in lateral canals is rotated over a group of gates and then allocated to the individual farmers for a specific period in a week.

Defining Q_{SL} as the seepage losses (m³ d⁻¹) in the distributaries and watercourses in a canal command, the monthly recorded Q_{cc} (m³ d⁻¹) for each lateral canal was converted to the canal water depth I_{cw} (mm d⁻¹) over the Cultivated Area under that Canal Command CA_{cc} (m²):

$$I_{cw,cc}(t) = \frac{1000\,(Q_{cc} - Q_{SL,cc} - Q_{SL,wc})}{CA_{cc}}(t) \tag{6.1}$$

In this study, 15 % of the entrance water into the canal was considered to be lost by seepage (*APARI*, 2001). Since information of the agricultural area attached with canal water rights was not available, CA_{cc} was derived from a 15 m spatial resolution ASTER image on 13 May 2005.

Groundwater pumping

Supply of groundwater through pumping I_{gw} (mm d⁻¹) from a region depends on the average discharge of the tube-wells D_{tw} (m³ hr⁻¹), total number of tube-wells N_{tw}, average working hours of the tube-wells per day H_{tw} and groundwater quality EC_{gw}:

$$I_{gw} = \frac{1000\,CF_{tw}\,N_{tw}\,D_{tw}\,H_{tw}}{CA_{cc}} \tag{6.2}$$

In Eq. 6.2, CF_{tw} is a reduction factor [-] that accounts for groundwater quality and restricts the groundwater pumping. In this study, the value of CF_{tw} was specified as 1.0, because in most of the area groundwater is of good quality ($EC_{gw} < 4$ dS m⁻¹). H_{tw} was specified at 20 hr d⁻¹.

Finally the actual irrigation depths I for each irrigation interval were computed for each CA_{cc} by adding I_{cw} and I_{gw}. The irrigation scheduling was set using an average irrigation calendar (Nov. 3rd & 30th, Mar. 5th, Apr 12th, May. 18th and Jun 5th). The spatial resulting distribution of total applied irrigation depth is shown in Fig. 6.2a. The results illustrate that because of the higher tube-well density with respect to the vegetated area, the Eastern, Northern and some parts of Western areas receive more water.

6.2.3 Cropping pattern

Land use types were obtained from 15 m spatial resolution ASTER images on 13 May 2005 and were then aggregated to 250 m spatial resolution (Fig. 6.2b). The major crops grown during the winter season were wheat, barley and orchards. In this study, the barley farms were assigned to the wheat classes since the spectral signatures of wheat and barley fields are almost similar. The planting date of wheat varies from the beginning of October until the end of November. For all simulations, a constant planting date was set as 4 November 2004.
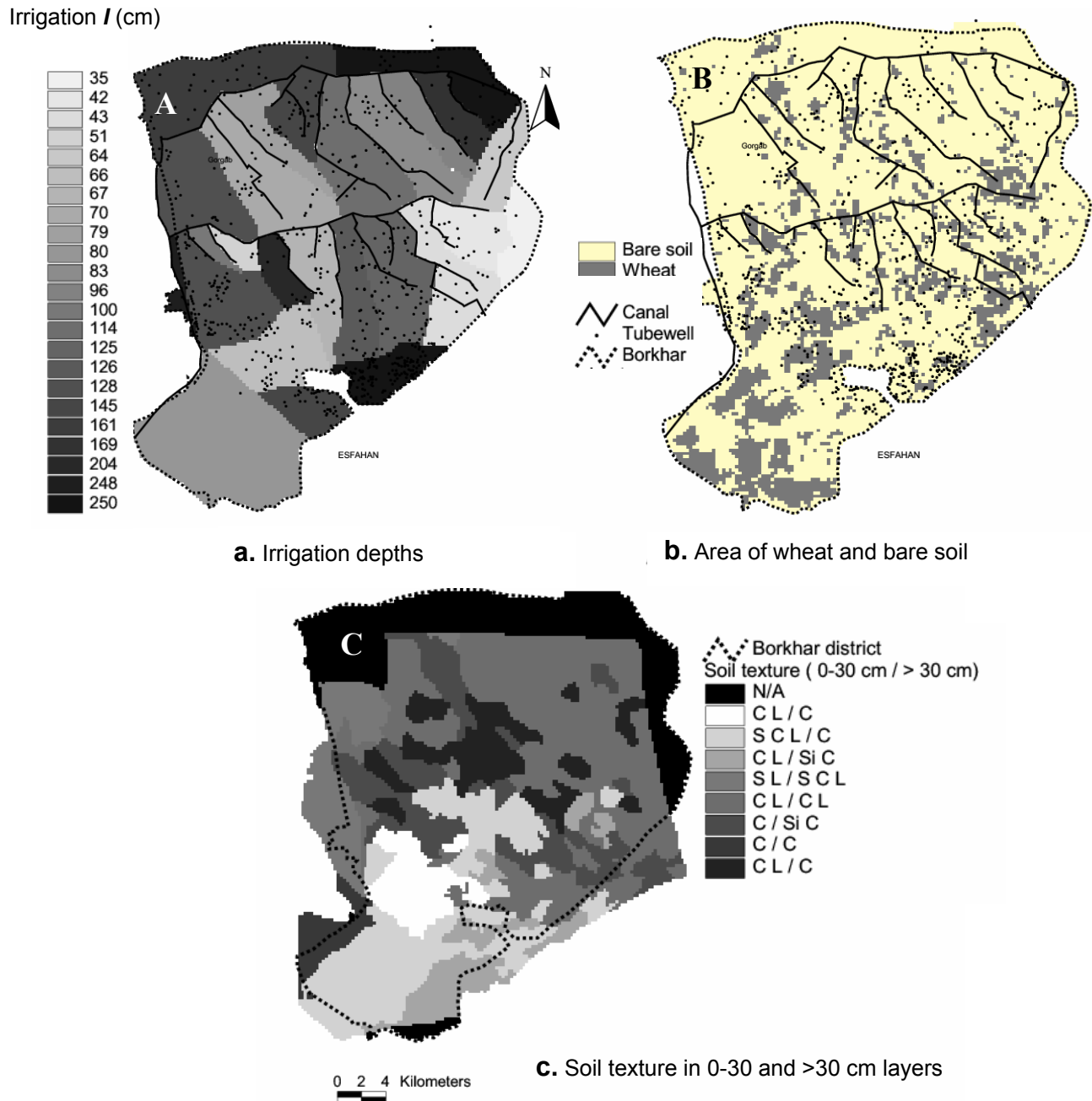
Figure 6.2 Spatial distributed information as input data for the distributed SWAP model on raster format with a grid size of 250 m:
A) Location of tube-wells, water canals and total amount of applied irrigation in each unit
B) Land use classification of the Borkhar irrigation district based on satellite image (ASTER, 13 May 2005)
C) Types of soil texture in the top (0-30 cm) and bottom layers (>30 cm). (C = clay, S = sandy, L loamy, Si= silt), (Source: Soil and Water Research Institute of Iran, 1973).
.

6.2.4 Soil texture

A soil texture map was prepared by digitizing the 9 soil series that were identified during a reconnaissance survey (*SWRI*, 1973) (Fig. 6.2c). Based on information of the fractions of sand, silt and clay, the soil profile of each series was reduced to two soil layers: topsoil (0-30 cm) and subsoil (30-300 cm). The prevailing soil texture varies from clay in the central part

of the district to sandy clay at the borders of the district. The soil hydraulic properties were derived using pedotransfer functions which were developed by *Wösten et al.* (1998) and are based on the Hypress database for European soils. Pedotransfer functions predict the hydraulic characteristics for a specific soil with more easily obtainable texture, organic matter content and bulk density.

6.2.5 Groundwater and its quality

According to the measurements at the observation wells spread over the Borkhar district, the groundwater depth below the surface varies from 89.6 m in the northeast to 8.2 in the southern and eastern parts of the district (*EWA*, 2001). Therefore, we assumed free drainage conditions for the entire district. The groundwater quality in the northern and the southern parts is good, in the central and east parts rather poor, but still remains below the salinity threshold value for wheat.

6.3 Remotely sensed data of relative evapotranspiration $ET\,ET_p^{-1}$ and leaf area index LAI

Relative transpiration is an indicator of crop water stress and can be defined as the ratio of actual and potential transpiration, $T\,T_p^{-1}$. Since separation of the transpiration flux from the remotely sensed ET flux is difficult, $T\,T_p^{-1}$ was set equal to the ratio of actual and potential evapotranspiration, $ET\,ET_p^{-1}$.

Figure 6.3 compares the variations of simulated $T\,T_p^{-1}$ and $ET\,ET_p^{-1}$ at wheat field W2 during the wheat growing season from 301th (6 Nov) Julian day in 2004 to 160th (9 Jun) Julian day in 2005. In the initial and development stages of the growing season, differences between the values of $T\,T_p^{-1}$ and $ET\,ET_p^{-1}$ are high because of the direct evaporation from soil in the crop canopy. Hence, $T\,T_p^{-1}$ values can be replaced with $ET\,ET_p^{-1}$ only when the soil is sufficiently covered by the crop. The experiments performed by *Feddes et al.*, (1971) for a potato crop showed that *for LAI >2, the $ET\,ET_p^{-1}$ values are very close to the $T\,T_p^{-1}$*. This confirms the reliability of using RS based $ET\,ET_p^{-1}$ data as $T\,T_p^{-1}$ data.
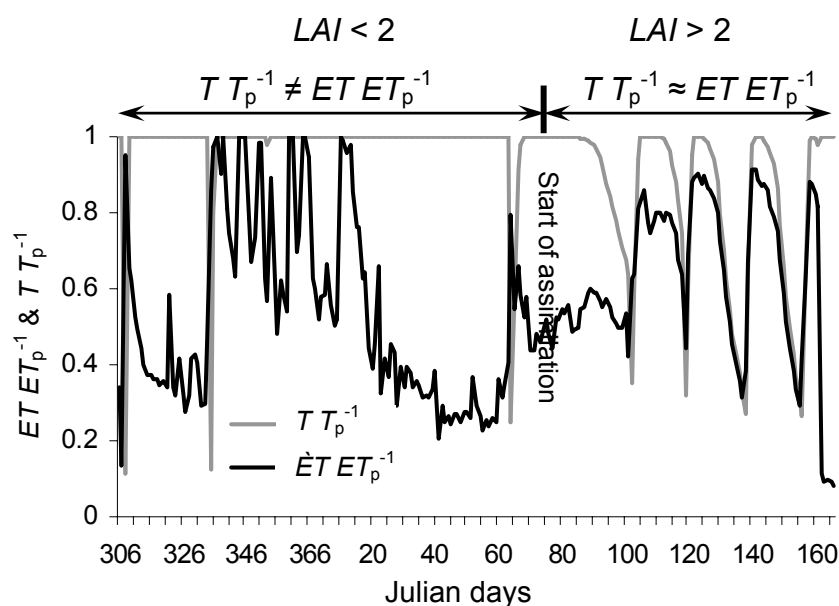

Figure 6.3 Comparison of simulated relative transpiration $T\,T_p^{-1}$ (gray line) with relative evapotranspiration $ET\,ET_p^{-1}$ (black line) during the agricultural year 2004-05.

To derive $ET\,ET_p^{-1}$, the 1999 version of SEBAL (referred to as AHAS, *Parodi*, 2002) was applied to 1000 m spatial resolution MODIS data acquired on 15 different dates in the winter growing season of 2005. However due to the coarse spatial resolution of MODIS data (pixels of 100 ha), the outputs represent *ET* of a mixture of fields. Therefore, $ET\,ET_p^{-1}$ was defined as ratio of *ET* from each MODIS pixel and the aggregated value $ET_p(x_i, y_i, t)$ of all components with different crop coefficients within each MODIS pixel (*Vazifedoust et al.*, 2007a):

$$T\,T_p^{-1}(x,y,t) \approx ET\,ET_p^{-1}\,(x,y,t) = \frac{ET_{\text{MODIS}}(x,y,t)}{\displaystyle\sum_{i=1}^{m} ET_p(x_i, y_i, t)\,A_{f,i}} \tag{6.3}$$

where $ET_{\text{MODIS}}(x, y, t)$ is the *ET* derived from each MODIS pixel, $ET_p(x_i, y_i, t)$ the potential evapotranspiration flux of the ith component within each MODIS pixel, $A_{f,i}$ the area fraction of the ith component within each MODIS pixel, m total number of components within each MODIS pixel, x is the horizontal and y is the vertical location of each MODIS pixel.

LAI maps were derived from 250 m spatial resolution MODIS data using a logarithmic function relating field data of *LAI* with satellite observations of *SAVI*. For details of the methods, characteristics of the satellite images, type of products and acquisition dates, see Chapter 5.

6.4 Direct assimilation of remotely sensed data into the distributed SWAP model

The assimilation of RS data into the distributed SWAP model was performed using the 'updating' method, where internal variables are continuously updated whenever an observed data is available. In this study, a simple sequential 'updating' algorithm was developed to assimilate the RS data into the distributed SWAP model:

$$X_{\text{upd}}(t) = X_{\text{sim}}(t) + K_g[X_{\text{obs}}(t) - X_{\text{sim}}(t)] \tag{6.4}$$

where X_{upd} and X_{sim} are simulated and the updated internal variables i.e. $ET\,ET_p^{-1}$ or *LAI* respectively at time t, X_{obs} are the measured data either from remote sensing or field data, and K_g is the optimum gain factor which depends on the relative magnitude of errors in observed and simulated values:

$$K_g = \frac{\sigma_{sim}^2}{\sigma_{sim}^2 + \sigma_{obs}^2} \tag{6.5}$$

where σ_{sim}^2 is the variance of the *model* error and σ_{sim}^2 is the variance of the *observation* error. To improve model prediction, an accurate estimation of K_g, associated with the errors into both simulation model and remotely sensed data, is essential (*Singh*, 2005). The Kalman filter can be used to calculate accurate values of K_g. However, the Standard Kalman filter has limited accuracy for non linear models such as SWAP. Instead, K_g might be estimated using an Ensemble Kalman filter (*Houtekamer and Mitchell*, 1998; *Aubert et al.*, 2003). Accurate estimation of K_g requires knowledge of the source of errors. In addition, it is very complex and requires time consuming computation. To simplify this computation, and to investigate

which value performs the best with respect to the observations, we did test different values of K_g.

In the present study, $T\,T_p^{-1}$ and/or *LAI* were chosen as internal variables and the sequential updating process was performed using RS based data of $ET\,ET_p^{-1}$ and/or *LAI*. The updated $T\,T_p^{-1}$ and *LAI* have a direct impact on simulated crop dry matter. For details of crop growth simulation and effect of $T\,T_p^{-1}$ and *LAI* on crop yield, we refer to Chapter 3.

Due to the more or less proportional relation between *LAI*, **Y** and dry matter of storage organ Y_{SO} (*Singh*, 2005), simulated Y and Y_{SO} were sequentially updated based on the ratio of updated and simulated *LAI*.

6.5 Comparison of simulated *LAI* and $T\,T_p^{-1}$ with remotely sensed data of *LAI* and $ET\,ET_p^{-1}$ without applying assimilation

Using Eq. 5.3 time series of *LAI* were derived from 250 m spatial resolution MODIS data and were smoothed by fitting an individual polynomial for time series of *LAI* in each pixel. Time series of $ET\,ET_p^{-1}$ were derived from 1000 m spatial resolution MODIS data for the period 74th (15 Mar) to 160th (9 Jun) Julian day and were set equal to $T\,T_p^{-1}$. For validation, the results are first compared with the SWAP simulated results of *LAI* and $T\,T_p^{-1}$ at regional scale, and later with the field data.

6.5.1 Regional scale

Generally, the maps derived from the low to moderate resolution RS-data are more heterogeneous than the results modeled by the distributed SWAP model. The within-field heterogeneity in the RS-derived data is caused by bare soil, crop types, non-uniform fertilizer application, buildings, trees and roads. Therefore, the RS-based *LAI* and $T\,T_p^{-1}$ may represent a mixture of various factors which are not accounted for in the distributed modeling.

Because of many similar soil types and vegetation types within the 1589 cells a discrete structure of modeled *LAI* and $T\,T_p^{-1}$ results. In contrast, the RS-based observations have a normalized distribution of *LAI* and $T\,T_p^{-1}$. Because of large differences in the spatial heterogeneity of modeled and RS-based results, a direct statistical comparison between the two spatial sets of information on a per-pixel basis is unsuitable. Instead, the global average of the distributed SWAP simulation and the RS-based results are compared with each other.

Fig. 6.4a illustrates a comparison between modeled and remotely sensed estimates of *LAI*. The average simulated and RS-based estimates of *LAI* for the agricultural area are statistically similar with respect to their mean values for the period of the 74th (15 Mar) to 121th (1 May) Julian day. This period corresponds to the crop development stage after a frozen soil period in January and March. The SWAP simulated average *LAI* for the period 121th to 160th Julian day is however significantly higher than those which are calculated directly from RS-data The high simulated *LAI* in this period is caused by setting a fixed harvesting date in the distributed SWAP model. Therefore, the simulated *LAI* starts decreasing a bit too late. On the other hand, *LAI-RS* represent *LAI* over areas larger than 6.2 ha and is influenced by reflectance of none vegetated areas. Therefore, the peak of *LAI-RS* value is less than SWAP simulated *LAI*.
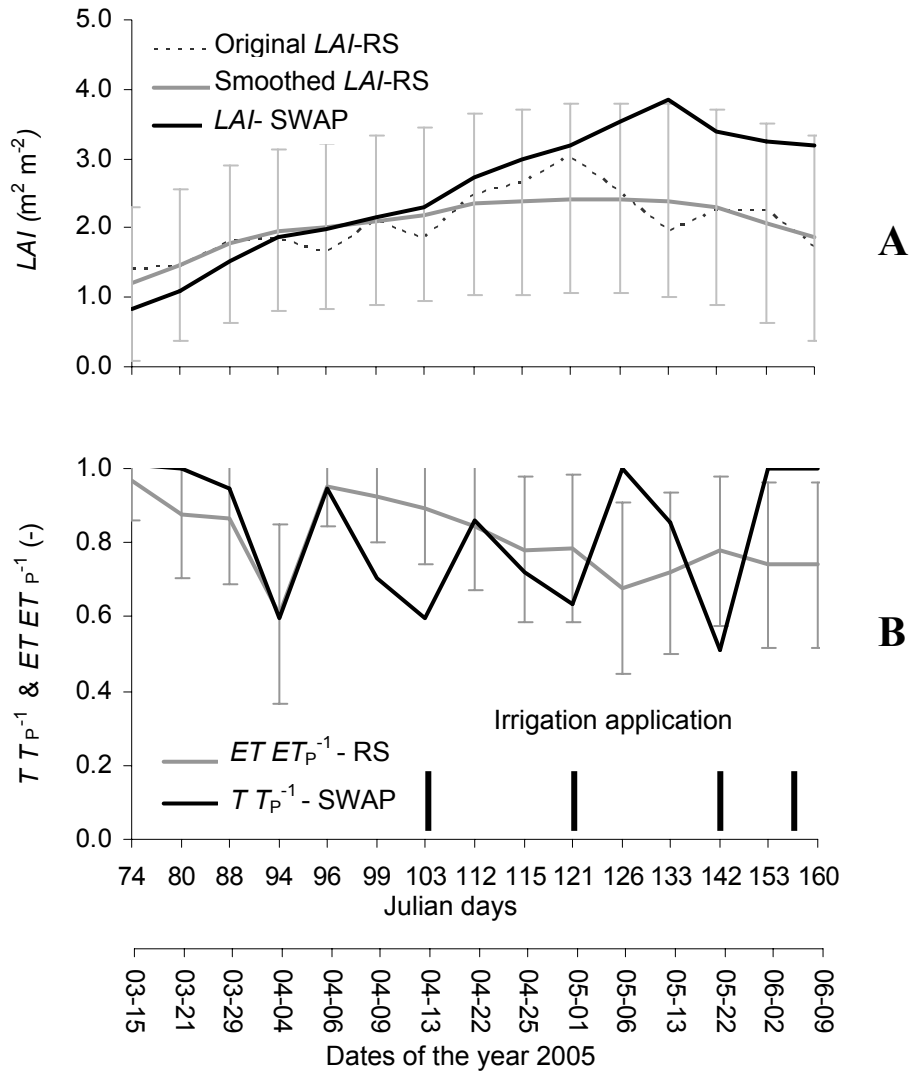
Figure 6.4 Regional scale results obtained during the wheat growing season from the 74th (15 Mar) to 160th (9 Jun) Julian day in 2005:

A) The global mean of simulated *LAI* by the distributed SWAP is compared with the global mean of original and smoothed RS-based *LAI* data being derived from 250 spatial resolution MODIS data.

B) The simulated $T T_p^{-1}$ by the distributed SWAP model is compared with $ET ET_p^{-1}$ derived from 1000 m spatial resolution MODIS data.

Fig. 6.4b compares for the same period the modeled $T T_p^{-1}$ with remotely sensed estimates of $ET ET_p^{-1}$ values. As shown in this figure, except for the 94th day the $T T_p^{-1}$ values from the 80th day (21 Mar) until the 103th day (13 Apr) indicate a low water stress. This period corresponds to the crop development stage after a frozen soil period. High water stress on the 94th day might be due to the high water demand (global mean of ET_p = 5.5 mm d^{-1}) at this day. During the period 115th (25 Apr) till 126th (5 May), the $T T_p^{-1}$ values indicate rather high water stress. This period corresponds to the middle growing stage. In this stage, the crop canopy has reached its maximum and has the highest water demand. From 133th (13 May) until the end of the growing season, the water stress decreases along with a reduction of T_p and *LAI*.

The fluctuation of simulated ET ET_p^{-1} over the agricultural area, however, is significantly higher than those which are calculated directly from RS-data (Fig. 6.4b). The

99

fluctuation of SWAP simulated T T_p^{-1} is caused by setting a fixed irrigation schedule for whole pixels. In reality, the fields are irrigated one after the other.

6.5.2 Field scale

Fig. 6.5a compares the simulated *LAI* with both field data and smoothed RS based *LAI* data at wheat fields W1 over the wheat growing season from 74th (15 Mar) to 160th (9 Jun) Julian day in 2005. The simulation of *LAI* was performed using the distributed SWAP model and implementation of regional data in the Borkhar irrigation district without further calibration. In the vegetative and final phases, the simulated *LAI* agree with the field data, but after reaching the peak *LAI*, the simulated *LAI* underestimates field data (*RMSE* = 1.03 m^2 m^{-2}) because of a low calculated irrigation depth (see Fig 6.2a). In Fig. 6.5a, the RS based *LAI* is also shown. The results of RS based *LAI* in all crop growth phases are in good agreement with the measurements (*RMSE* =0.7 m^2 m^{-2}). The peak *LAI* was predicted well and the rising limb of the *LAI* curve and its decrease is in general good agreement with the measurements.
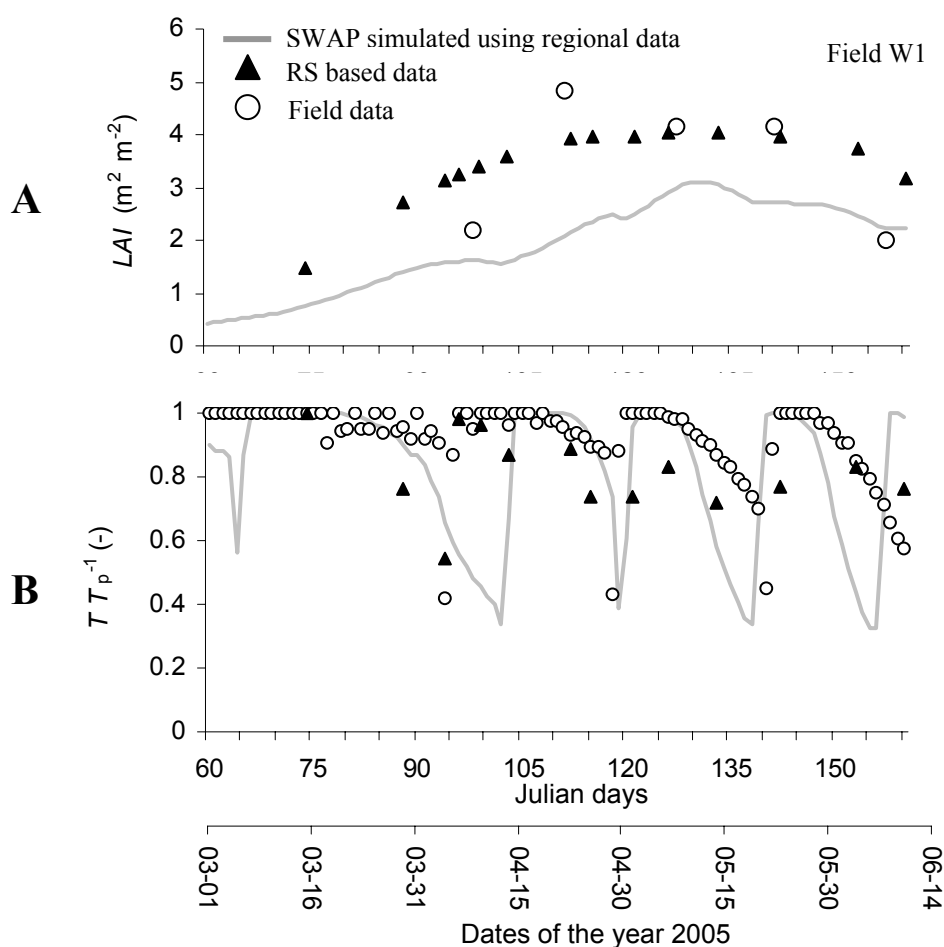
Figure 6.5 Comparison of SWAP simulated results with the both field data and RS based data at field W1 during the wheat growing season from the 74th (15 Mar) to 160th (9 Jun) Julian day in 2005:
A) The SWAP simulated leaf area index *LAI* by regional data (gray full lines) were compared with the field data (circles) as well as RS-based of *LAI* (triangles). The RS-based *LAI* data were derived from the 250 spatial resolution MODIS data. B) The SWAP simulated relative transpiration $T\ T_p^{-1}$ by regional data (gray full lines) were compared with the field data (circles) as well as RS-based data of $ET\ ET_p^{-1}$ (triangles). The RS-based $ET\ ET_p^{-1}$ data were derived from combination of the 250 and 1000 m spatial resolution MODIS data (Eq 6.3).

Fig. 6.5b compares the time series of RS based $ET\ ET_p^{-1}$ data with simulated $T\ T_p^{-1}$ using both the regional data and calibrated data over wheat fields W1 during the same period. The simulation results using calibrated data were considered as observed data of $T\ T_p^{-1}$. The simulated $T\ T_p^{-1}$ using regional data approaches the field data of W1 ($RMSE$ =0.27 cm cm^{-1}) but it shows a delay phase and underestimates the value of $T\ T_p^{-1}$ with respect to the field data. This is caused by setting a fixed planting date, fixed irrigation calendar and not accurate estimated irrigation depth for the cultivated area under each canal command.

The RS based $ET\ ET_p^{-1}$ over field W1 shows a good agreement with the SWAP simulated $T\ T_p^{-1}$ using calibrated data ($RMSE$ =0.12 cm cm^{-1}). However, in between the irrigation events the RS approach seems to not be able to monitor the water stress variations. This is due to the fact that RS based $ET\ ET_p^{-1}$ was derived from 1000 m spatial resolution MODIS data and represent an averaged $ET\ ET_p^{-1}$ value for an area of 100 ha.

The differences between the field data and the data determined by simulation or low to moderated *RS* data imply that these data alone are not accurate estimators for calculating crop yield. In principle, the output of simulation model contains certain errors due to a simplified representation of complex natural processes, and due to uncertainty in input parameters. On the other hand, the RS- based data include errors due to various factors such as atmospheric effects and influence of pixels by non vegetative area. *Therefore, assimilation of RS data into the SWAP simulation model with considering the associated errors in both, may improve the simulation output.* The effect of updating the modeled *LAI* and $T\ T_p^{-1}$, based on RS data is discussed in sections 6.6 and 6.7.

6.6 Assimilation results of RS based *LAI* and *ET ET*$_\text{p}^{-1}$ data into the SWAP model at field scale

To assimilate RS based data of *LAI* and *ET ET*$_\text{p}^{-1}$ data into the distributed SWAP*, the updating method* was implemented. Advantage of updating is that it requires only one run of the model and therefore, the computation time is limited. In addition, in case of a sudden reduction in *Y* due to water stress, pest or diseases attack, it might be incorporated through the updating process of RS based data of *LAI* and *ET ET*$_\text{p}^{-1}$. However, the magnitude of corrections during the sequential updating process depends on the values of the Kalman gain factor K_g.

Table 6.1 shows the *RMSE* value of updated *LAI and T T*$_\text{p}^{-1}$ based on different K_g values and the number of observations which was used in *RMSE* calculations. A K_g value of 0 implies that no assimilation was performed and a value of 1 implies that only the *LAI-RS* values were used in assimilation. The lower *RMSE* for *RS-* based data in comparison with the simulation-based data imply that *RS-* based data performed better. Therefore, higher weight was given to the RS-based data. In this study, K_g values of 0.8 respectively 0.6 were used in the assimilation process of *LAI* and *ET ET*$_\text{p}^{-1}$.

Table 6.1 Root mean square error *RMSE* of *updated leaf area index LAI and relative transpiration T T*$_\text{p}^{-1}$ based on remotely sensed data of *LAI* and *ET ET*$_\text{p}^{-1}$ using different optimum gain factors K_g at farmer's fields (W1, W2, W3) in the Borkhar irrigation district during the winter growing season of the agricultural year 2004-05. *N* is the number of observations which was used in the *RMSE* calculations.

Gain factor K_g	LAI				$T\ T_\text{p}^{-1}$			
	N	*RMSE* (m^2 m^{-2})			*N*	*RMSE* (-)		
		W1	*W2*	*W3*		*W1*	*W2*	*W3*
0	5	1.26	1.36	1.08	15	0.39	0.23	0.16
0.2	5	1.03	1.16	0.99	15	0.33	0.2	0.13
0.4	5	0.84	0.99	0.92	15	0.27	0.17	0.14
0.6	5	0.71	0.88	0.88	15	**0.21**	**0.16**	**0.17**
0.8	5	**0.69**	**0.85**	**0.86**	15	0.16	0.16	0.22
1	5	0.77	0.91	0.86	15	0.12	0.17	0.27

As an example for farmer field W1, Fig. 6.6 presents the SWAP simulation of *LAI*, *Y* and *Y*$_\text{SO}$ with and without the assimilation of remotely sensed data. The sequential updating process was performed using three sets of remotely sensed based data: *LAI*, *ET ET*$_\text{p}^{-1}$ and *LAI + ET ET*$_\text{p}^{-1}$. In order to investigate the ability of the data assimilation technique in prediction of yield, the updating process was stopped 30 days before the end of the growing season on 160th Julian day. As shown in Fig. 6.6, in case of using RS based *LAI* data, both the simulated *LAI* and *Y* are improved with respect to the observation values. *Assimilation of ET ET*$_p^{-1}$ *data only has hardly effect on simulated LAI and Y, and assimilation of both LAI + ET ET*$_p^{-1}$ *data results in the same graph as updating by LAI. This implies that the LAI has a dominant influence on the simulation process.* *LAI* determines the amount of intercepted radiation by the canopy and affects the simulated dry matter through an exponential function (see Eq. 3.10). *ET ET*$_\text{p}^{-1}$ affects the simulated dry matter through a linear function (see Eq. 3.11). In addition, the global mean of RS- based *ET ET*$_\text{p}^{-1}$ data (Fig. 6.4b) indicates a low

water stress ($K_s > 0.7$) in the period of the 74th (15 Mar) to 160th (9 Jun) Julian day in 2005. Hence, updating of *RS- based ET ET_p^{-1} data has a slight influence on the simulation process.*

As illustrated in Fig. 6.6, the simple sequential updating algorithm has introduced some modeling jumps into the simulation of *LAI* and **Y** during crop growth. If there are sufficient observations and the observation error is small, the introduced jumps will decrease.
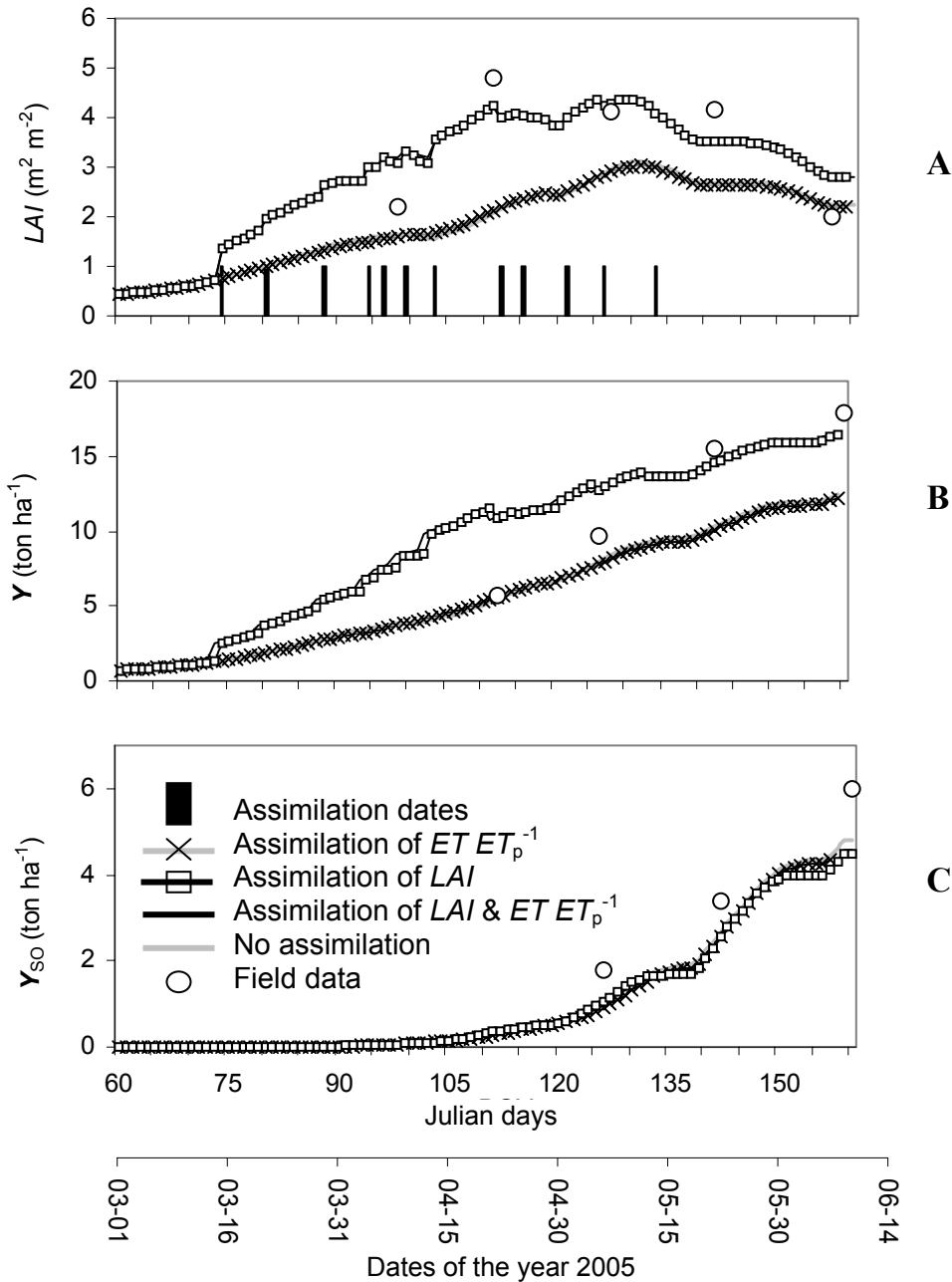
Figure 6.6 Comparison of SWAP simulated data with and without data assimilation, with the field data: A) Leaf area index *LAI*, B) Total dry matter yield **Y** (ton ha^{-1}), C) Dry matter of storage organ Y_{SO} (ton ha^{-1}). The field data were collected from a wheat farmer's field (W1) in the Borkhar irrigation district during the winter growing season of the agricultural year 2004-05. SWAP simulation with and without assimilation was performed using regional data of the Borkhar irrigation district. For assimilation RS based data of leaf area index *LAI* and / or relative evapotranspiration *ET* ET_p^{-1} were used.

103

Table 6.2 presents simulation results at harvest time of the wheat crop at the observed fields W$_1$, W$_2$ and W$_3$ with and without assimilation, and its statistical properties (mean and bias). The bias is equal to the difference between the simulated and the true value in percentage. The lower bias between the observed *Y* and simulated *Y* with *LAI* assimilation at the fields W2 and W3 confirms the results derived at field W1. However, assimilation of RS based *LAI* and/or *ET ET*$_p^{-1}$ data has only a slight effect on simulated *Y*$_{SO}$ at fields W1 and W3. The simulation of *Y*$_{SO}$ in SWAP is based on partitioning the produced total biomass among roots, leaves, stems and storage organs, using conversion factors as function of the crop development stage. The conversion factors for storage organs start shortly before the end of the growing season. *Hence, the assimilation of remotely sensed data can have less effect on the estimated dry matter of storage organ Y*$_{SO}$.

Table 6.2 SWAP simulated dry matter yield *Y* and dry matter of storage organ *Y*$_{SO}$ with and without assimilation (mean and bias) at three wheat farmer's fields W1, W2 and W3 in the Borkhar irrigation district in the agricultural year 2004-05. For the assimilations RS based data of leaf area index *LAI* and / or relative evapotranspiration *ET ET*$_p^{-1}$ were used. SWAP simulation with and without assimilation was performed using regional data of the Borkhar irrigation district.

Field	Method		*Y* (ton ha^{-1})		*Y*$_{SO}$ (ton ha^{-1})	
			Mean	Bias %	Mean	Bias %
W1	**Observation**		17.8		6.0	
	Without assimilation		12.4	**-30**	4.8	**-20**
	With assimilation	*ET ET*$_p^{-1}$	12.2	**-31**	4.7	**-22**
		LAI	16.5	**-7**	4.5	**-25**
		LAI & *ET ET*$_p^{-1}$	16.4	**-8**	4.6	**-23**
W2	**Observation**		14.2		5.9	
	Without assimilation		17.3	**22**	7.1	**20**
	With assimilation	*ET ET*$_p^{-1}$	16.1	**13**	6.8	**15**
		LAI	11.9	**-16**	5.8	**-2**
		LAI & *ET ET*$_p^{-1}$	11.7	**-18**	5.7	**-3**
W3	**Observation**		15.4		5.2	
	Without assimilation		13.9	**-10**	5.0	**-4**
	With assimilation	*ET ET*$_p^{-1}$	14.6	**-5**	5.3	**2**
		LAI	14.7	**-5**	4.8	**-8**
		LAI & *ET ET*$_p^{-1}$	14.9	**-3**	5.0	**-4**

6.7 Assessment of agricultural drought by assimilation of RS based data of *LAI* and *ET ET*$_p^{-1}$ into the distributed SWAP

Crop production is a very reliable indicator for assessing the agricultural drought. Fig. 6.7 illustrates the variation of wheat and barley production in the Borkhar irrigation district for the period 1991 to 2005. The low amount of production in the period of 1999 to 2001 is due to a devastating drought of which its cumulative effects affected Iran's agriculture and livestock production seriously (*UNDP*, 2003; *Foltz*, 2002). Farmers had reductions of 35-75 percent in wheat and barley grain and the government had to import a record seven million tons of wheat, partly because of reduced domestic production due to the drought.
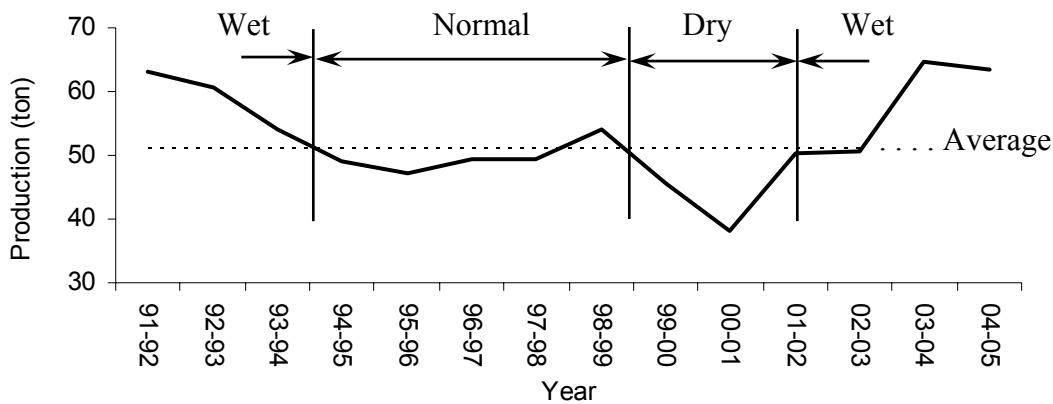
Figure 6.7 Statistical data of total productivity of wheat (ton) over the years 1991 to 2005 in the Borkhar irrigation district (Source: Organization of Jihad-e-Agriculture, Esfahan, Iran. [online]: http://www.esfahan.agri-jahad.ir/modiriat/tarh/amar%20nameh/index.htm, 01 September 2006).

To predict production for the agricultural year 2004-05, distributed simulation with and without assimilation was performed on a regional scale. For the assimilation, RS based data of *LAI* and *ET ET*$_p^{-1}$ were used. To have a prediction of production far in advance, the sequential updating process was stopped one respectively two months before the end of the wheat growing season. During the sequential updating process known weather data were used, while for the remaining part of the growing season different scenarios were considered based on weather data of a dry, a wet and a normal year. The *predicted production* for the agricultural year 2004-05 using the distributed simulation with assimilation of RS based *LAI* and *ET ET*$_p^{-1}$ is higher than the average value of the statistical data in Fig 6.7. This *implies a relatively wet year for the agricultural year 2004-05.*

Table 6.3 lists the statistical properties (mean and bias) of simulated *Y*, *Y*$_{SO}$ and the total amount of production (at harvest time of the wheat crop during the agricultural year 2004-05 one and two months in advance). The total amount of production was calculated by aggregation of simulated yield for all the wheat pixels within the district. Predictions of crop production through simulation without assimilation two or even one month in advance results in a high bias between the statistical data and predicted production (4 to 39 %).

105

Table 6.3 Prediction (mean and biases) of total dry matter yield *Y*, dry matter of storage organ Y_{SO} and total production of wheat using the distributed SWAP model with and without assimilation in the Borkhar irrigation district during the agricultural year 2004-05.
For assimilation, RS based data of leaf area index *LAI* and relative evapotranspiration $ET\,ET_p^{-1}$ were used. The predictions were performed for one respectively two months in advance. Weather data of a dry, normal and wet year were used for the unknown weather data of the remaining part of the year. Biases are based on deviation of predictions from statistical data of *Y* i.e. 4.5 ton ha^{-1} and total production of 63297 ton in the Borkhar irrigation district in percent.

Method			Dry matter Y (ton ha^{-1})	Grain Yield Y_{SO} (ton ha^{-1})	Total wheat production	
			Mean	Mean	Value (ton)	Bias %
Prediction one month in advance	Without assimilation	Dry	13.8	4.7	66145	4
		Normal	14.7	5.6	77871	23
		Wet	15.4	6.3	88147	39
	With assimilation	Dry	10.2	4.1	56835	-10
		Normal	10.9	4.7	65558	4
		Wet	10.5	4.9	68580	8
Prediction two months in advance	Without assimilation	Dry	13.3	5.4	75928	20
		Normal	15.9	5.7	79777	26
		Wet	15.4	6.2	87386	38
	With assimilation	Dry	13.2	5.2	73450	16
		Normal	15.0	5.6	77975	23
		Wet	14.9	6.1	84842	34

Small bias between the statistical data and short term prediction (±10 %) indicated that simulation with assimilation is very promising in prediction of crop production and in assessing the impacts of probable drought one month in advance. Longer forecasting i.e. two months in advance, benefited only slightly from data assimilation.

The *high bias (16 to 38 %) between the statistical data and long term predictions* using simulation with or without assimilation is *partly due to* the fact that the *effect of nutrient deficiency, pests, weeds, and diseases on crop growth* and its production have not been implemented in the present 3.0.3 version of SWAP. Extending the assimilation of RS based data into the simulation will incorporate the sudden reduction in *Y* due to water and nutrient stress, pest or diseases attacks.

The predictions of final crop production with or without assimilation is significantly affected by type of weather data i.e. a dry or wet year, which is used in one or two last months of the growing season in the simulations process. The forecasted final crop productions in comparison with the average weather data differ by -19 to 16 % for one month and -6 to 12 % for two months for dry and wet years, respectively. The variations slightly decreased after assimilation of RS based data into the simulations.

ig. 6.8 compares the histogram and spatial distribution of predicted Y one month in advance using the distributed SWAP simulation with assimilation. The histograms and pattern Y are presented for two different cases by using weather data of a wet and a dry year for the unknown weather data in last month of growing season. As shown in Fig 6.8, the area in the western and southern parts of the Borkhar irrigation district has higher Y. The high Y in the southern parts is due the vicinity of the Zayande Roud River and access to more water. The western parts are located in the beginning of two main water supply canals and receive more water.
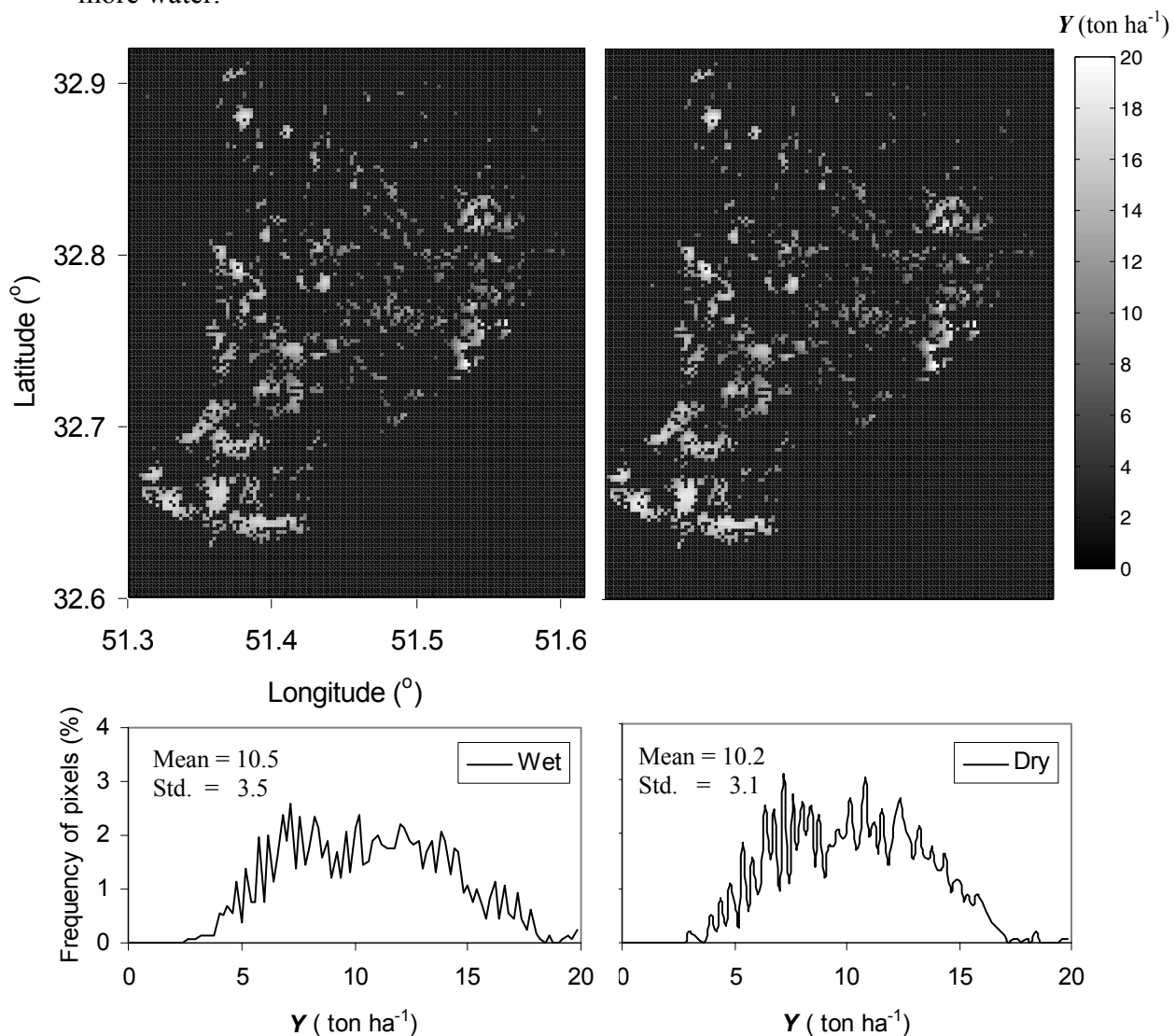
Figure 6.8 Histogram and spatial distribution of forecasted total dry matter yield Y of winter wheat one month in advance using assimilation of RS based data of LAI and $ET\ ET_p^{-1}$. The simulations were performed for the wheat growing season of the agricultural year 2004-05 in the Borkhar irrigation district. For the unknown weather data during the last month of growing season, the weather data of a dry and a wet year were used

6.8 Summary and conclusions

This Chapter demonstrated the potential of inferring valuable information from remotely sensed land surface data for improving the distributed simulation of wheat production and assessment of agricultural droughts impacts. The SWAP model was implemented in a distributed way using the spatial distributed information of soil types, land use, groundwater and water supply on a raster basis with a grid size of 250 m. The study area was divided into 10655 homogeneous cells with 250 m spatial resolution and simulations were performed for 1589 pixels with wheat crop. For data transfer to SWAP, a coupling program was written by the first author in MATLAB.

To predict production for the agricultural year 2004-05, distributed simulation with and without assimilation was performed at regional scale. For assimilation, three sets of remotely sensed based data (*LAI*, *ET ET*$_p^{-1}$ and *LAI + ET ET*$_p^{-1}$) derived from low to moderate spatial resolution MODIS data were used using a sequential updating process. The RS-based data of *LAI* and *ET ET*$_p^{-1}$ were derived from 250 and 1000 m spatial resolution MODIS data, respectively. To have a prediction of yield production far in advance, the sequential updating process was stopped one and two months before the end of the wheat growing season.

During the sequential updating process known weather data were used, while for the remaining part of growing season different scenarios were considered based on weather data of a dry, wet and normal year. The main conclusions, which can be drawn from this study are:

- The differences between the field data and the data determined by simulation or low to moderated *RS* data imply that these methods separately are not accurate estimators for calculating crop yield.

- The results of data assimilation at both the regional and field scale showed *significant improvement in accuracy of simulation in case of using both the* RS *based data of LAI and ET ET*$_p^{-1}$ *in the assimilation process*. The results showed also that *LAI data have a dominant influence in the assimilation process*.

- Predictions of wheat production for one month in advance using simulation with assimilation at regional scale was very promising with respect to the statistical data of the Borkhar irrigation district (bias = ±10 %). However, longer term predictions i.e. two month in advance resulted in higher bias between the simulated and statistical data.

- The forecasting of final crop production with or without assimilation were significantly affected by the type of weather data i.e. dry, normal or wet year, which are used in the last month or two last months of the growing season.

Summary and conclusions

Problem statement

Drought is an inevitable part of Earth's climate with no clear warning and without recognizable limits, causing billions of dollars in loss annually for the farming community (*Kagon*, 2000). Drought is often the result of many complex factors which act and interact within the environment without no distinct start or end. The impacts of drought vary by the sector affected such as agriculture, industry, households, making different definitions of drought. Droughts are commonly classified in four different forms: meteorological, agricultural/soil moisture, hydrological and socio-economical.

Agricultural drought in Iran is one of the natural disasters, which causes large economical and social damages. Iran is located in an arid to semi-arid region and is facing widespread droughts regularly. The agricultural sector is with 80-90 % by far the largest user of water in Iran and is often the first sector to be affected by drought. Unfortunately, water management in agriculture is also very poor and water productivity *WP* is far below potential. The growing water scarcity due to drought and the increasing water demands of industries, households and environment, are the major threats to sustainable agricultural development in Iran (*APERI*, 2001).

These threats emphasize the vulnerability of the agricultural sector to drought and the need for more research to understand and develop tools that would be helpful in planning to mitigate the impacts of drought. Reliable drought assessment would be beneficial for operational decision making on farms, for early warning, for identification of potential vulnerability of areas, for mitigation of drought impact and finally food security. The main objective of this study *is to develop an Comprehensive Agricultural Drought Assessment System (CADAS) based on the water balance and actual crop growth simulation using a comprehensive agrohydrological model, in combination with remote sensing and a geographical information system*'.

Study area

The Borkhar irrigation district was selected as study area, which is located North of the ancient town of Esfahan (Fig. 2.1). The altitude varies between 1540 and 1600 m above mean sea level. The district has a predominantly arid to semi-arid desert climate. Rainfall in the study area averages only 105 mm yr^{-1}, most of which is falling in the winter months from December to April. Annual reference evapotranspiration ET_{ref} using the Penman-Monteith method amounts to 1800 mm. In the area, profitable crop production without reliable irrigation is impossible.

The Borkhar irrigation district area spreads over 83,300 ha and about 24 % of this area is under cultivation. The designed irrigation canal command area is 36,000 ha large, of which 18,000 ha is fallow each year due to shortage of water resources. Cropping patterns consist during the winter season mostly of wheat and barley, and during the summer season of maize, sunflower, sugar beet and some vegetables. The prevailing soil texture varies from clay in the central part of the district to sandy clay at the borders of the district. The main water resource is groundwater. Since groundwater recharge is insufficient to meet the water demand of the crops, the groundwater level has been lowered significantly. The average decline is 0.9 m yr^{-1}. Hence, surface water is increasingly being used for irrigation. The surface water is diverted from the Zayande Rud river to the main irrigation canal in the Borkhar area (*APERI*, 2001).

Water productivity of irrigated crops under limited water supply at field scale

Given the current water scarcity, the limited available water should be used as efficient as possible. To explore on-farm strategies which result in higher economic gains and water productivity *WP*, a physically based agrohydrological model, Soil Water Atmosphere Plant (SWAP), was calibrated and validated in *Chapter 3* using measured data at 8 selected farmer's fields (wheat, fodder maize, sunflower and sugar beet) in the Borkhar irrigation district during the agricultural year 2004-05. Most of the input parameters collected from farmer's fields were used directly in the SWAP calibration procedures. The remaining soil hydraulic parameters and irrigation depths were determined indirectly through model calibration. A non-linear parameter estimation program PEST was linked with SWAP to perform automatic calibration, i.e. inverse modelling, of soil hydraulic parameters and irrigation depths, using the weekly soil moisture observations in the objective function.

Good agreement between the simulated and observed soil moisture (*RMSE* = 0.02 to 0.05 cm^3 cm^{-3}) was achieved during calibration. Simulated total dry matter yield *Y* (*RMSE* = 1.11 to 3.08 ton ha^{-1}) and yield of storage organ Y_{SO} (*RMSE* = 0.7 to 1.4 ton ha^{-1}) was also in good agreement with the observed data. This provided confidence to analyse the water productivity under current conditions at the selected farmer's fields in the Borkhar irrigation district using the SWAP simulated water balance components i.e. transpiration *T*, evapotranspiration *ET*, irrigation *I*, and the marketable yield Y_M of crop productions. The SWAP simulation model was also used to explore strategies for increasing water productivity *WP* under water scarcity conditions.

Firstly, the *WP* values of the main crops, wheat, fodder maize, sunflower and sugar beet were computed in different forms of WP_T, WP_{ET} and WP_I. (Table 3.9). This flexibility in defining water productivity provides useful indicators to evaluate irrigation water utilization, as well as to identify where and when water can be saved.

WP_T refers to Y_M T^1, and sets the lowest limit of water used by crop. The average WP_T (Table 1), expressed as Y_M T^1 (kg m^{-3}) indicated fodder maize as highest efficient crop in terms of physical crop production in the Borkhar irrigation district. The average WP_T, expressed as **$** T^1 ($ m^{-3}$) showed also that fodder maize has the highest economic gains.

Table 1 Water productivity indicators in terms of marketable yield Y_M, i.e. Y_M T^{-1}, Y_M ET^{-1} and Y_M I^{-1} for the main crops in the selected farmer's fields in the Borkhar irrigation district for the agricultural year 2004-2005.

Water productivity indicators		Crops			
		Wheat	Fodder maize	Sunflower	Sugar beet
WP_T	kg m^{-3}	1.2	3.4	0.3	1.7
	$ m^{-3}$	0.2	0.5	0.06	0.4
WP_{ET}	kg m^{-3}	0.9	3.0	0.3	1.4
	$ m^{-3}$	0.14	0.4	0.06	0.3
WP_I	kg m^{-3}	0.5	1.8	0.2	1.0
	$ m^{-3}$	0.1	0.3	0.04	0.2

Soil evaporation caused the average WP_{ET} to be significantly lower than the average WP_{T} i.e. about 27 % for wheat, 11 % for fodder maize, 12 % for sunflower and 18 % for sugar beet. Furthermore, due to percolation from root zone and stored moisture content in the root zone, the average WP_{I} values, expressed as $Y_{M} I^{1}$ (kg m^{-3}), had a 24 to 42 % reduction as compared with WP_{ET}.

Groundwater level in the Borkhar irrigation district is very deep i.e. > 100 m and contribution of percolation to groundwater recharge may take a long time. In addition, because of land rotation in the beginning of each growing season in the Borkhar irrigation district, the stored moisture content in the soil profile is also useless. Hence, under water scarcity conditions, the both percolation and stored moisture content with soil evaporation are generally considered as losses and are the main causes of reduction of the *WP* value from WP_{T} to WP_{ET} and WP_{ET} to WP_{I}. *The substantial differences between $WP_{(E)T}$ and WP_{I} indicates the need for improving on-farm irrigation management in the Borkhar irrigation district.*

Secondly, to specify maximum possible *WP* and explore on-farm strategies which results in higher economic gains, the calibrated SWAP model was invoked for a variety of irrigation depth and irrigation intervals automatically using a SENSistivity Analysis (SENSAN) program. The irrigation intervals were defined in the SWAP model as fixed intervals of 5, 10, 15 and 20 days. The irrigation depth was also defined as a fixed irrigation depth from 1 to 20 cm depth. The results were shown as *WP*–water consumption curves (Fig. 3.5). *WP* indicators values were calculated using the simulated water balance components T, ET, I and the actual marketable yield Y_{M} for the main crops and for different irrigation scheduling.

As on-farm strategies, *deficit irrigation scheduling, optimal irrigation intervals and extend of cultivated area* were analyzed. The results indicated that during the limited water supply period, on-farm strategies like *deficit irrigation scheduling* and *reduction of the cultivated area* can result in higher economic gains. Irrespective of the irrigation scheduling, $WP_{(E)T}$ in terms of $Y_{M} (E)T^{-1}$ (kg m^{-3}) remained more or less stable, but WP_{I} did change with the irrigation timing and amount. Improved irrigation practices in terms of irrigation timing and amount, increased WP_{I} by a factor of 1.5 for wheat and maize, 1.3 for sunflower and 1.1 for sugar beet. Under water shortage conditions, *reduction of the cultivated area* yielded higher water productivity values as compared to *deficit irrigation*.

This presents a large potential of the improvement of water productivity under limited water supply in the Borkhar irrigation district.

Disaggregation of remotely sensed evapotranspiration data

Although the agrohydrological models like SWAP offer the possibilities for simulation of water balance components as well as crop productions, they may become inaccurate due to over- or under parameterization, especially in distributed modelling at regional scale. In principle, the simulated model outputs contain errors due to a simplified representation in the model of the complex crop growth process and the uncertainty of input parameters i.e. irrigation scheduling, soil hydraulic parameters and planting dates. Hence, inserting accurate remotely sensed data into the agrohydrological models using data assimilation techniques i.e. updating, calibrating and forcing is necessary to reduce the uncertainty in application of these models at regional scale.

Remotely sensed images of the Earth's surface have the potential to provide detailed information about vegetation indices i.e. leaf area index *LAI,* and aerial flux i.e. evapotranspiration *ET*. Data of *LAI* might be derived from Visible and Near Infrared (VNIR) spectral bands of remote sensing data with moderate to high spatial resolution. However, due to resolution limitations of existing remotely sensed data i.e. thermal band, these data can not be used directly for routine *ET* estimation of individual fields. Thermal band is only regularly available beyond the size of a field. Therefore, current satellite images with high temporal but low spatial resolution should be disaggregated to higher spatial resolution.

To derive daily *ET* fluxes, the Surface Energy Balance ALgorithm (SEBAL) was applied to the Advanced Spaceborne Thermal mission and Reflection Radiometer (ASTER) and MODerate resolution Imaging Spectroradiometer (MODIS) images. The data were acquired during the winter growing season on 6 May and 13 May 2005, and during the summer growing season on 17 August and 20 October 2005 in the Borkhar irrigation district. To eliminate the effects of differences in geometries of used images, *ET* derived from ASTER images was aggregated to the 1000 m MODIS resolution and were then used as being simulated MODIS data.

A new disaggregation technique based on linear disaggregation of *ET* components within each MODIS pixel, was proposed and applied to the simulated MODIS data. In the linear disaggregation approach, *ET* of each MODIS pixel was considered to reflect a composite *ET* value, weighted by the area fraction of each component within the pixel (Eq. 4.8). *ET* of components was then calculated by multiplying the ET_{ref} with a water stress coefficient K_s and unstressed crop coefficient K_c ($ET = ET_{ref}. K_c. K_s$). We assumed that the water stress coefficient in each MODIS pixel is constant for all the vegetative components. The value of K_s was then defined as ratio of *ET* of each MODIS pixel to aggregation of ET_p of vegetative components within each MODIS pixel (Eq. 4.11). Unstressed crop coefficient K_c was also defined as ET_p/ET_{ref} and derived from using moderate and high resolution remote sensing data. A flow diagram of this linear disaggregation approach has been given in Fig. 4.1.

To support the assumption of linear disaggregation for flux densities such as *ET* within each MODIS pixel, the *ET* map derived from ASTER image was aggregated to 1000 m and after that it was compared to the 1000 m spatial resolution real MODIS data for the same day. $\overline{ET}$ values of the MODIS images were respectively *9.5 % and 19 % higher* than the $\overline{ET}$ values of aggregated ASTER images on 13 May and 17 August. Hence, *ET from each MODIS pixel showed a strong to moderate correlation with the weighted arithmetic average of ET values of all components within the MODIS pixel.*

To evaluate the accuracy of the proposed disaggregation approach, the disaggregated *ET* map, was compared to the original *ET* map calculated from the ASTER images with 90 m spatial resolution as original data. The disaggregated *ET* maps derived by means of the new linear disaggregation approach showed overall a good agreement with the original *ET* maps on the both winder and summer days.

The results of the linear disaggregation approach were further compared with two alternative disaggregation approaches, being based on the *weighted ratio* of one high and one low spatial resolution *ET* maps. In the *first weighted ratio approach*, the *ET* map derived from the high spatial resolution ASTER and its aggregation to the MODIS resolution was

used to characterize the proportion ratios of pixels within one single large MODIS pixel. In the second approach, the *ET* map derived from a high spatial resolution ASTER and global mean of its aggregation to the MODIS resolution was used.

The disaggregated *ET* maps derived using the *weighted ET ratio approaches* on 13 May showed slightly higher correlation values than the results derived from the linear disaggregation approach. However, the disaggregated *ET* maps derived using *weighted ET ratio approaches* on 17 August showed significantly lower correlation. This shows that the assumption of holding weighted ratio constant across the growing season is not realistic.

The advantages and disadvantages of the various disaggregation approaches have been summarized in Table 2. *The good advantage of the new linear disaggregation approach was that the number of high spatial resolution images needed in this method is low; it even can be applied by using one land cover map only.* However, the main assumption used in this method, i.e. the water stress being constant within each MODIS pixel, was restrictive. In reality the water stress varies according to the sensitivity of the crops and the amount of irrigation applied. For the purpose of regional scale drought assessment and impact on food security, MODIS scale data is, however, sufficient. To increase the accuracy of weighted *ET* ratio approach, we need to increase the number of high spatial resolution images during the growing season. *In many regions this is currently not feasible.*

Table 2 Advantages and disadvantages of three different disaggregation methods: linear disaggregation developed in this thesis; weighted *ET* ratio of one *ET*$_{ASTER}$ map and its aggregation; weighted *ET* ratio of one *ET*$_{ASTER}$ map and the global mean of its aggregation.

Disaggregation method	Advantages	Disadvantages
Linear disaggregation	-Low number of high spatial images -Good spatial coverage -Good temporal coverage	-Block structures -Complex -Uniform water stress enforced -K_c of non-irrigated crops need to be specified -Need for crop identified map
Weighted ratio of one *ET*$_{ASTER}$ map and its aggregation to the MODIS resolution	-Good spatial coverage -Very simple	-High number of high spatial images -Block structures -Low temporal coverage
Weighted ratio of one *ET*$_{ASTER}$ map and global *mean* of its aggregation to the MODIS resolution	-Good spatial coverage -Very simple	-High number of high spatial images -Low temporal coverage -Effects from non irrigated land use is included

Inverse modelling of irrigation scheduling using disaggregated remotely sensed evapotranspiration data

To evaluate the accuracy and reliability of linear disaggregation approach, the disaggregated remotely sensed *ET* data derived from real MODIS data over the three farmer's fields W1, W2 and W3 were compared with SWAP simulated *ET as* independent data. The remotely sensed *ET* data were derived by applying the SEBAL algorithm to 1000 m spatial resolution MODIS data acquired for *18 different dates* during the winter growing season of 2004-05.

The required unstressed crop coefficients in this approach were derived from 250 spatial resolution MODIS data acquired on 16 different dates during the winter growing season of 2004-05 using Eq. 4.6.

The results showed *a poor agreement between remotely sensed ET data from MODIS ($ET_{RS-MODIS}$) and simulated ET using SWAP data (ET_{SWAP}) on daily basis at three farmer fields. This result emphasizes the need for disaggregation of 1000 spatial resolution ET data to the higher resolution.* The rather low *RMSE* between disaggregated *ET* using linear disaggregation (ET_{RS-LD}) and ET_{SWAP} at fields W1, W2 and W3 indicated a strong to moderate agreement between ET_{RS-LD} and ET_{SWAP} at these farmer's fields.

Water balance components computed by numerical simulation models are quite sensitive to the upper boundary conditions and therefore to irrigation times and depth. In order to know how much water has been applied at three farmer's wheat fields W1, W2 and W3, the cumulative actual evapotranspiration data was used in the automatic calibration, i.e. inverse modelling of irrigation scheduling. The ability of inverse modelling to reproduce exactly the initial irrigation times and depth was first investigated using forward cumulative SWAP simulated **ET** data based on 5, 15 and 30 days. Thereafter, the cumulative disaggregated remotely sensed **ET** data based on 5 days was used in the inverse modelling process.

The results of inverse modelling using 5 days based cumulative *SWAP simulated ET* data indicated a quite good match between the simulated irrigation times and depth with the reference data at two individual wheat fields W1, W2 (Fig. 5.4). This shows that the *performance of inverse modelling is promising in identifying the irrigation time and depth of irrigation using 5 days based cumulative ET data.*

The possibility of identifying the irrigation practices was also investigated using cumulative *SWAP simulated **ET** data for longer periods i.e. 15 and 30 days. When *using 15 days based cumulative **ET** data, high bias between the identified times and depth, and references data indicated a low performance for inverse modelling.* The results of inverse modelling using monthly based cumulative simulated **ET** showed also a low performance in identifying the irrigation times and depth. However, in spite of rather weak results in identifying the irrigations times and depths, the simulated **ET** do match well with the reference **ET** data (*RMSE* 0.8 mm d^{-1}). *This showed the problem of non-uniqueness in identified parameters exists. The reason was that the parameters were insensitive to the observation data.*

Successful application of the inverse methodology depends on the availability of reliable and rather accurate regional *ET* data, as well as the interval of cumulative **ET** data. In most of the irrigation events, the performance of the inverse methodology using the remotely sensed **ET** data was rather weak. It might be due to *lack of a dry period* in the remotely sensed **ET** data.

The outcome was that using the **ET**-based form of the objective function, the maximum identified depth is limited to the critical pressure heads corresponding to field capacity in the root zone. *Irrigation amounts, which rewet the soil profile beyond field capacity and thus cause excessive percolation, can not be detected by the applied inverse modelling approach. Only if drought stress occurs, inverse modelling of irrigation amounts makes sense.*

116

Assimilation of satellite data into a distributed SWAP model

Due to the simplification of complex natural processes, and due to uncertainty in input parameters, the output of simulation models contains certain errors. On the other hand, the RS-based data include errors due to factor such as atmospheric effects and influence of pixels by non vegetative area. Hence, the SWAP simulation model or remote sensing data alone are not accurate tools for calculating water balance components and crop yield. *Assimilation of RS data into the SWAP simulation model with considering the associated errors in both, may improve the accuracy of simulation output.*

Assimilation of remotely sensed data into distributed SWAP by automatic calibration i.e. inverse modelling of irrigation scheduling needs a large amount of computation time, especially at regional scale. Therefore, in *Chapter 6* a simple assimilation technique i.e. updating was suggested.

Chapter 6 demonstrated the potential of inferring valuable information from remotely sensed land surface data for improving the distributed simulation of wheat production and assessment of agricultural droughts impacts. The SWAP model was implemented in a distributed way using the spatial distributed information of soil types, land use and water supply on a raster basis with a grid size of 250 m. Therefore, the Borkhar irrigation district was divided into 10655 homogeneous cells of 250 m spatial resolution. Only pixels containing the wheat crop (1589 pixels) were considered. To derive values for pixels of 250 m, parameters like soil types and land use at raster format were derived by remote sensing techniques and were pre-processed in a Geographic Information System (GIS). Temporal distributed data of water supply were produced using information from tube-wells and the surface irrigation network. *In order to link GIS data with SWAP, a coupling program was written in MATLAB.* This program took care for the transfer of in- and output data from one system to the other, and to run the model for each pixel. A schematic representation of the framework of the distributed SWAP model has been shown in Fig. 6.1.

To predict production for the agricultural year 2004-05, distributed simulation with and without assimilation was performed at regional scale. For assimilation, three sets of remotely sensed based data (*LAI* and/or relative evapotranspiration $ET\ ET_p^{-1}$) derived from low to moderate spatial resolution MODIS data, was used into the sequential updating process of the distributed SWAP model. Time series of *LAI* were derived from 250 m spatial resolution MODIS data and were smoothed by fitting an individual polynomial for time series of *LAI* in each pixel. Time series of $ET\ ET_p^{-1}$ were derived from 1000 m spatial resolution MODIS data.

To have a prediction of production far in advance, the sequential updating process was stopped one and two months before the end of the wheat growing season. During the sequential updating process known weather data were used, while for the remaining part of the growing season different scenarios were considered based on weather data of a dry, wet and normal year. We selected a value for the optimum gain factor K_g, that performed best with respect to the observations.

Using both the RS based data of LAI and ET ET_p^{-1}, the results of *data assimilation at the field scale showed significant improvement in the accuracy of simulation*. The results also showed that *in the assimilation process LAI data have a dominant influence*. Because of this dominant influence, we recommend to repeat the assimilation process using the *LAI data of most advanced satellite i.e. IRS-P6 (ResourceSAT1&2)* with higher spatial (56 m) and temporal resolution (3 days).

S*imulation with assimilation at the regional scale was also very promising for forecasting of crop production one month in advance* (bias = ±10 %). However, longer term predictions i.e. two months in advance, resulted in a higher bias between the simulated and statistical data.

The forecasting of final crop production with or without assimilation were significantly affected by the type of weather data i.e. dry, normal or wet year, which are used in the last one or two months of the growing season. The forecasted final crop productions in comparison with the average weather data differed by -19 to 16 % for one month and -6 to 12 % for two months for dry and wet years, respectively.

Since the Zayande Rud river is mainly fed by the snow melt from January to April, a comprehensive drought assessment system *on seasonal basis* can be developed by integration of the developed agricultural drought assessment system with the estimates of available surface water derived from snow pack and snow cover.

As a main conclusion, the developed model "*Comprehensive Agricultural Drought Assessment System* (CADAS)" can be sued as a reliable tool for assessment and mitigation of drought impact on agriculture sector, and for food security.

Samenvatting en conclusies

Probleemstelling

Droogte is onlosmakelijk verbonden met ons klimaat, treedt op zonder duidelijke waarschuwing en herkenbare grenzen, en kost de agrarische gemeenschap jaarlijks miljarden dollars (*Kagon*, 2000). Droogte is vaak het resultaat van veel complexe milieufactoren die voorkomen in nauwe wisselwerking zonder duidelijk begin of einde. De gevolgen van droogte hangen af van de getroffen sector zoals landbouw, industrie en huishoudens, wat leidt tot verschillende definities van droogte. Droogte wordt in het algemeen ingedeeld in vier verschillende vormen: meteorologische, landbouwkundige, hydrologische en sociaal-economische droogte.

Landbouwkundige droogte is in Iran één van de natuurlijke rampen die grote economische en sociale schade veroorzaakt. Iran is gelegen in een aride tot semi-aride regio en wordt regelmatig getroffen door wijdverbreide droogte. De landbouwkundige sector is met 80-90% verreweg de grootste gebruiker van water in Iran en is vaak de eerste sector die beïnvloed wordt door droogte. Tegelijkertijd is waterbeheer in de landbouw weinig efficiënt en waterproduktiviteit *WP* ver onder haar potentiële nivo. De groeiende waterschaarste door droogte en toenemende vraag van industrieën, huishoudens en milieu vormt een belangrijke bedreiging voor duurzame landbouwkundige ontwikkeling in Iran (*APERI*, 2001).

Deze bedreigingen laten de kwetsbaarheid zien van de landbouwkundige sector voor droogte en de onderzoeksnoodzaak voor meer proceskennis en voor ontwikkeling van hulpmiddelen om de invloed van droogte te temperen. Betrouwbare droogte inschatting zou zeer behulpzaam zijn voor besluitvorming op boerderijen, voor 'early warning', voor identificatie van kwetsbare gebieden, voor matiging van droogte-invloed en voor voedselzekerheid. De hoofddoelstelling van deze studie is daarom *het ontwikkelen van een betrouwbaar identificatiesysteem voor landbouwkundige droogte, gebaseerd op simulatie van de waterbalans en gewasgroei met een gedetailleerd agrohydrologisch model, in combinatie met remote sensing en een geografisch informatie systeem.*

Studiegebied

Het Borkhar irrigatiedistrict is geselecteerd als studiegebied en is gelegen ten noorden van de historische stad Esfahan (Fig. 2.1). The hoogte variëert tussen 1540 en 1600 m boven zeenivo. Het district heeft overwegend een arid tot semi-arid klimaat. De hoeveelheid neerslag in het studiegebied bedraagt gemiddeld slechts 105 mm j^{-1} en het overgrote deel hiervan valt in de wintermaanden van december tot april. De jaarlijkse referentieverdamping ET_{ref} volgens de Penman-Monteith methode bedraagt 1800 mm. Winstgevende gewas-productie is in het gebied onmogelijk zonder aanvullende irrigatie.

Het Borkhar irrigatiedistrict spreidt zich uit over 83.300 ha, waarvan 24% in gebruik is als landbouwgrond. Het ontworpen beheersgebied voor irrigatie bedraagt 36.000 ha. Hiervan ligt jaarlijks 18.000 ha braak door tekort aan water. Het gewaspatroon bestaat in het winterseizoen voornamelijk uit tarwe en gerst, en gedurende het zomerseizoen uit maïs, zonnebloem, suikerbiet en groenten. De bodemtextuur varieert van klei in het centrale deel van het district tot zandige klei aan de randen van het district. De belangrijkste waterbron is grondwater. Omdat de grondwateraanvulling geringer is dan de waterbehoefte van de gewassen, is de grondwaterstand sterk gedaald. De gemiddelde daling bedraagt 0.9 m j^{-1}. Het gevolg is dat voor irrigatie steeds meer oppervlaktewater wordt gebruikt. Het

oppervlaktewater wordt onttrokken aan de Zayande Roud rivier en verdeeld via het hoofdirrigatiekanaal van het Borkhar gebied (APERI, 2001).

Waterproduktiviteit van geïrrigeerde gewassen op veldschaal

Gegeven de huidige waterschaarste, dient het beschikbare water zo efficiënt mogelijk gebruikt te worden. Om strategieën voor hogere economische winst en waterproduktiviteit *WP* te analyseren op de boerderij, werd een fysische gebaseerd agrohydrologisch model, Soil Water Atmosphere Plant (SWAP), gecalibreerd en gevalideerd in *Hoofdstuk 3*. Hiervoor werd gebruik gemaakt van metingen op 8 geselecteerde landbouwvelden (tarwe, voedermaïs, zonnebloem en suikerbiet) in het Borkhar irrigatiedistrict gedurende het landbouwkundige jaar 2004-05. De meeste van de invoergegevens konden direct ontleend worden aan de metingen op de landbouwvelden. De overblijvende bodemfysische parameters en irrigatiediepten werden indirect bepaald via modelcalibratie. Het niet-lineaire parameter optimalisatie programma PEST werd gekoppeld aan SWAP om automatische calibratie mogelijk te maken van de bodemfysische parameters en irrigatiediepten. Bij de calibratie werden in de doelfunctie wekelijkse metingen van bodemvocht gebruikt.

Na calibratie werd een goede overeenstemming bereikt tussen gesimuleerde en gemeten bodemvocht (*RMSE* = 0.02 tot 0.05 cm^3 cm^{-3}). Ook de gesimuleerde totale droge stof opbrengst **Y** (*RMSE* = 1.11 tot 3.08 ton ha^{-1}) en oogstopbrengst Y_{SO} (*RMSE* = 0.7 tot 1.4 ton ha^{-1}) waren in goede overeenstemming met de metingen. Dit lag een goede basis voor de analyse van waterproduktiviteit voor de geselecteerde velden. SWAP simuleerde de waterbalanscomponenten, zoals transpiratie **T**, evapotranspiratie **ET** en irrigatie **I,** en tevens het oogstbaar product Y_M. Verder werd SWAP gebruikt om strategieën te analyseren die de waterproductiviteit bij watertekort verhogen.

Ten eerste werden de *WP*-waarden berekend voor de hoofdgewassen tarwe, voedermaïs, zonnebloem en suikerbiet. De *WP*-waarden werden uitgedrukt in verschillende eenheden: WP_T, WP_{ET} en WP_I (Tabel 3.9). Deze verschillende *WP*-waarden verschaffen bruikbare indicatoren om de efficiency van watergebruik te beoordelen, en om aan te geven waar en wanneer water gespaard kan worden.

Tabel 1 Indicatoren voor waterproductiviteit uitgedrukt in kg m^{-3} en \$ m^{-3} van economische opbrengsten Y_M, namelijk Y_M **T** $^{-1}$, Y_M **ET** $^{-1}$ en Y_M **I** $^{-1}$ voor de hoofdgewassen in de geselecteerde landbouwvelden in het Borkhar irrigatiedistrict voor het landbouwkundige jaar 2004-05.

Water productiviteits indicatoren		Gewassen			
		Tarwe	Voedermaïs	Zonnebloem	Suikerbiet
WP_T	kg m^{-3}	1.2	3.4	0.3	1.7
	\$ m^{-3}	0.2	0.5	0.06	0.4
WP_{ET}	kg m^{-3}	0.9	3.0	0.3	1.4
	\$ m^{-3}	0.14	0.4	0.06	0.3
WP_I	kg m^{-3}	0.5	1.8	0.2	1.0
	\$ m^{-3}	0.1	0.3	0.04	0.2

Het kental WP_T is gebaseerd op $Y_M\ T^{-1}$ en bepaalt de laagste hoeveelheid water die door het gewas gebruikt wordt. De gemiddelde WP_T (Tabel 1), uitgedrukt als $Y_M\ T^{-1}$ (kg m^{-3}) gaf aan dat in Borkhar irrigatiedistrict voedermaïs het meest efficiënte gewas is in termen van fysische gewasproduktie. De gemiddelde WP_T, uitgedrukt als $\$\ T^{-1}$ ($ m^{-3}) liet zien dat voedermaïs ook de hoogste economische opbrengst geeft.

Bodemverdamping is de oorzaak dat de gemiddelde WP_{ET} significant lager is dan de gemiddelde WP_T: circa 27% voor tarwe, 11% voor voedermaïs, 12% voor zonnebloem en 18% voor suikerbiet. Vervolgens, door percolatie uit de wortelzone en bergingsverandering in de wortelzone, waren de gemiddelde WP_I waarden, uitgedrukt als $Y_M\ I^{-1}$ (kg m^{-3}), 24 tot 42% lager in vergelijking tot WP_{ET}.

De grondwaterstanden in Borkhar irrigatiedistrict zijn erg diep (> 100 m), waardoor het lang duurt voor percolatiewater bijdraagt aan de grondwateraanvulling. Bovendien is, door de landrotatie aan het begin van ieder groeiseizoen in Borkhar irrigatiedistrict, de extra grondwaterberging in het bodemprofiel onbruikbaar. Daarom worden bij waterschaarste zowel de hoeveelheid percolatie als extra bodemvochtberging beschouwd als verlies en veroorzaken een reductie van WP_T tot WP_{ET} en van WP_{ET} tot WP_I. *Het grote verschil tussen $WP_{(E)T}$ en WP_I wijst op de noodzaak het waterbeheer op de boerderijen in Borkhar irrigatiedistrict te verbeteren.*

Ten tweede, om de maximale WP te bepalen en boerderijstrategieën te analyseren voor meer economische winst, werd het gecalibreerde model SWAP gedraaid met het SENSitivity Analysis (SENSAN) programma voor een groot aantal irrigatiediepten en -intervallen. De irrigatie-intervallen werden voor het SWAP model gedefinieerd als vaste intervallen van 5, 10, 15 en 20 dagen. De irrigatiediepte was ook gedefinieerd als een vaste irrigatiediepte, variërend van 1 tot 20 cm. De resultaten werden weergegeven als WP-waterconsumptie curven (Fig. 3.5). WP indicatoren werden berekend met behulp van de gesimuleerde waterbalanscomponenten T, ET en I en het oogstbare produkt Y_M voor de hoofdgewassen en voor verschillende irrigatie-schema's.

Wat betreft boerderijstrategieën werden *irrigatieschema's met waterstress, optimale irrigatie-intervallen en bebouwde oppervlakte* geanalyseerd. De resultaten lieten zien dat gedurende de periode met beperkte water giften, boerderij-strategieën als *irrigatieschema's met waterstress en geringere bebouwde oppervlakte* kunnen resulteren in hogere economische winst. Onafhankelijk van irrigatie-schema's, bleef $WP_{(E)T}$ uitgedrukt als Y_M $(E)T^{-1}$ (kg m^{-3}) min of meer constant, terwijl WP_I veranderde met het irrigatietijdstip en de irrigatiehoeveelheid. Verbeterde irrigatieschema's in termen van tijdstippen en hoeveelheden, lieten een WP_I toename zien met een factor 1.5 voor tarwe en maïs, 1.3 voor zonnebloem en 1.1 voor suikerbiet. Bij watertekorten resulteerde *reductie van het bebouwde oppervlakte* in hogere waterproduktiviteitscijfers vergeleken met de strategie *irrigatie met waterstress.*

Dit laat de grote mogelijkheden zien van verbetering van de waterproduktiviteit bij beperkte wateraanvoer in het Borkhar irrigatiedistrict.

Disaggregatie van satelliet-verdampingsmetingen

Ofschoon agrohydrologische modellen als SWAP allerlei mogelijkheden bieden voor simulatie van waterbalanscomponenten en gewasproductie, kunnen zij onnauwkeurig worden door over- en onderparameterisatie, vooral bij gedistribueerd modelleren op regionale schaal. In het algemeen bevatten model resultaten fouten door een vereenvoudigde weergave van

complexe gewasgroeiprocessen en door onzekerheid van de invoerparameters zoals irrigatiegiften, bodemfysische parameters en plant-tijdstippen. Daarom is assimilatie van nauwkeurige satellietgegevens in agrohydrologische modellen noodzakelijk om de onzekerheid bij toepassing van deze modellen op regionale schaal te verkleinen.

Satellietbeelden van het aardoppervlak bieden de mogelijkheid om gedetailleerde informatie te verschaffen over vegetatiekenmerken, zoals bladoppervlakte-index *LAI*, en over ruimtelijke fluxen, zoals evapotranspiratie *ET*. Gegevens van *LAI* kunnen worden ontleend aan het zichtbaar en nabij-infrarood spectrum van satellietbeelden met gemiddelde tot hoge ruimtelijke resolutie. Echter, in verband met beperkingen in de resolutie van bestaande satellietbeelden, kunnen deze beelden niet direct gebruikt worden voor routinematige berekening van *ET* voor individuele velden. De temperatuurbanden zijn in het algemeen alleen beschikbaar voor pixels groter dan een veld. Daarom dienen de huidige satellietbeelden met een hoge tijdsresolutie maar lage ruimtelijke resolutie gedisaggregeerd te worden naar een grotere ruimtelijke resolutie.

Om dagelijkse *ET* fluxen af te leiden, werd het Surface Energy Balance ALgorithm (SEBAL) toegepast op satellietbeelden van de Advanced Spaceborne Thermal mission and Reflection Radiometer (ASTER) en de MODerate resolution Imaging Spectroradiometer (MODIS). De gegeven werden verkregen in het Borkhar irrigatiedistrict tijdens het wintergroeiseizoen op 6 mei and 13 mei 2005, en gedurende het zomergroeiseizoen op 17 augustus and 20 oktober 2005. Om effecten van geometrieverschillen tussen gebruikte beelden te vermijden, werden de *ET* fluxen van ASTER beelden geaggregeerd tot de 1000 m resolutie van MODIS en vervolgens gebruikt als gesimuleerde MODIS metingen.

Een nieuwe disaggregatietechniek is ontwikkeld gebaseerd op lineaire disaggregatie van *ET* componenten binnen iedere MODIS pixel. Deze techniek is toegepast op de gesimuleerde MODIS data. In de lineaire disaggregatiemethode werd de *ET* van iedere MODIS pixel opgevat als een samengestelde *ET* flux, gewogen naar de oppervlaktefractie van iedere component binnen de pixel (Verg. 4.8). De *ET* flux van de componenten werd dan berekend door vermenigvuldiging van ET_{ref} met een waterstress-coëfficiënt en een gewascoëfficiënt K_c ($ET = ET_{ref}. K_c. K_s$). We namen aan dat de waterstress-coëfficiënt in iedere MODIS pixel constant is voor alle vegetatietypen. De waarde van K_s werd vervolgens gedefiniëerd als de verhouding van de *ET* van ieder MODIS pixel over de geaggregeerde waarde van ET_p van de vegetatietypen binnen iedere MODIS pixel (Verg. 4.11). De gewascoëfficiënt K_c werd ook gedefiniëerd als ET_p/ET_{ref} en afgeleid van satellietbeelden met gemiddelde tot hoge ruimtelijke resolutie. Een stroomdiagram van deze lineaire disaggregatiemethode is weergegeven in Fig. 4.1.

Om de aanname van lineaire aggregatie van fluxdichtheden zoals *ET* binnen MODIS-pixels te controleren, werd de op ASTER gebaseerde en tot 1000 m geaggregeerd *ET* kaart vergeleken met MODIS beelden met 1000 m ruimtelijke resolutie voor dezelfde dag. De $\overline{ET}$ waarden van MODIS beelden waren respectievelijk *9.5% en 19% hoger* dan $\overline{ET}$ waarden van geaggregeerde ASTER beelden op 13 mei en 17 augustus. *De ET van ieder MODIS pixel liet een gemiddelde tot sterke correlatie zien met de gewogen gemiddelde ET van alle componenten binnen de MODIS pixel.*

Om de nauwkeurigheid van de voorgestelde disaggregatiemethode te beoordelen, werd de gedisaggregeerde *ET* kaart vergeleken met de originele *ET* kaart zoals berekend voor de

ASTER beelden met 90 m ruimtelijke resolutie. De gedisaggregeerde *ET* kaarten afgeleid met de nieuwe lineaire disaggregatiemethode lieten op zowel winter- als zomerdagen een goede overeenstemming zien met de originele *ET* kaarten.

De resultaten van de lineaire disaggregatiemethode werden verder vergeleken met de twee alternatieve disaggregatiemethoden, die gebaseerd zijn op de gewogen verhouding van een *ET* kaart met hoge en één met een lage ruimtelijke resolutie. In de eerste alternatieve methode, werd de *ET* kaart, die was afgeleid van ASTER data en geaggregeerd tot MODIS resolutie, gebruikt om de gewichtsverhoudingen binnen MODIS pixels af te leiden. In de tweede methode, werd gebruik gemaakt van de *ET* kaart zoals afgeleid van ASTER data en het totale gemiddelde van het geaggregeerde beeld tot MODIS resolutie.

De gedisaggregeerde *ET* kaarten afgeleid met de alternatieve methoden lieten op 13 mei enigszins hogere correlaties zien dan de resultaten van de lineaire disaggregatiemethode. Echter, de gedisaggregeerde *ET* kaarten afgeleid met de alternatieve methoden gaven op 17 augustus een beduidend lagere correlatie. Dit laat zien dat de aanname in deze methoden van constante gewichtsverhoudingen gedurende het groeiseizoen niet realistisch is.

De voor- en nadelen van de verschillende disaggregatiemethoden zijn samengevat in Tabel 2. *Het grootste voordeel van de nieuwe lineaire disaggregatiemethode is dat het aantal benodigde satellietbeelden met hoge resolutie laag is; de methode kan zelfs worden toegepast met slechts één landgebruikskaart.* Echter, de belangrijkste aanname in deze methode, een constante waterstress binnen een MODIS pixel, is beperkend. In werkelijkheid varieert de waterstress afhankelijk van de gewasgevoeligheid en hoeveelheid irrigatiewater. Voor karakterisering van regionale droogte en het effect op voedselzekerheid, zijn gegevens op MODIS resolutie echter voldoende. Om de nauwkeurigheid van gewogen verhouding methoden te verhogen, dienen we het aantal satellietbeelden met hoge resolutie tijdens het groeiseizoen te vergroten. *In veel gebieden is dat momenteel niet mogelijk.*

Tabel 2 Voor- en nadelen van drie verschillende disaggregatiemethoden: lineaire disaggregatie zoals ontwikkeld in dit proefschrift; gewogen *ET* verhouding van één ET_{ASTER} kaart en zijn geaggregeerde; gewogen *ET* verhouding van één ET_{ASTER} kaart en het totale gemiddelde van zijn geaggregeerde.

Disaggregatiemethode	Voordelen	Nadelen

Lineaire disaggregatie	- Goede ruimtelijke dekking
	- Goede temporele dekking
	- Lage aantal satelliet-
	  beelden met hoge resolutie
		- Blokstructuren
		- Complex
		- Constante waterstress opgelegd
		- K_c van niet-geïrrigeerde
		  gewassen moet worden
		  opgegeven
		- Gewassenkaart noodzakelijk

Gewogen verhouding van één ET_{ASTER} kaart en zijn geaggregeerde tot MODIS resolutie	- Goede ruimtelijke dekking - Eenvoudig	- Blokstructuren - Geringe temporele dekking - Grote aantal satellietbeelden met hoge resolutie

Gewogen verhouding van één ET_{ASTER} kaart en het totale gemiddelde van zijn geaggregeerde tot MODIS resolutie	- Goede ruimtelijke dekking
	- Eenvoudig
		- Geringe temporele dekking
		- Grote aantal satellietbeelden met
		  hoge resolutie
		- Is beïnvloed door niet-
		  geïrrigeerde gronden

Inverse modellering van irrigatieplanning met gebruik van gedisaggregeerde satellietgegevens over verdamping

Om de nauwkeurigheid en betrouwbaarheid van de lineaire disaggregatiemethode te beoordelen, werden de gedisaggregeerde MODIS satellietgegevens van *ET* van de drie landbouwvelden W1, W2 en W3 vergeleken met door SWAP gesimuleerde *ET* waarden als onafhankelijke gegevens. De *ET* gegevens werden uit de satellietbeelden afgeleid door toepassing van het SEBAL algoritme op MODIS beelden met een ruimtelijke resolutie van 1000 m voor 18 dagen tijdens het wintergroeiseizoen van 2004-05. De benodigde gewascoëfficiënten werden in deze methode met Verg. 4.6 afgeleid van MODIS gegevens met een resolutie van 250 m en verkregen voor 16 verschillende datums tijdens het wintergroeiseizoen van 2004-05.

De resultaten lieten *op dagbasis voor de drie landbouwvelden een slechte overeenstemming zien tussen MODIS satellietgegevens van ET ($ET_{RS-MODIS}$) en door SWAP gesimuleerde ET (ET_{SWAP}). Deze resultaten benadrukken de noodzaak voor disaggregatie van ET gegevens met een resolutie van 1000 m naar een hogere ruimtelijke resolutie.* De relatieve lage *RMSE* tussen gedisaggregeerde *ET* met lineaire disaggregatie (ET_{RS-LD}) en ET_{SWAP} bij de velden W1, W2 and W3 duiden op een gematigde tot sterke overeenstemming tussen ET_{RS-LD} en ET_{SWAP} bij deze landbouwvelden.

Waterbalanscomponenten berekend met numerieke simulatiemodellen zijn gevoelig voor de bovenrandvoorwaarden en daarom voor irrigatiehoeveelheden en tijdstippen. Om te weten hoeveel water is gebruikt op de landbouwvelden W1, W2 and W3, werd de cumulatieve actuele evapotranspiratie gebruikt in een automatische calibratie, of te wel inverse modellering van irrigatieplanning. Eerst werd de capaciteit onderzocht van inverse modellering om exact de oorspronkelijke irrigatietijden en –hoeveelheden te reproduceren, gebruikmakend van door SWAP gesimuleerde ***ET*** gegevens voor tijdsintervallen van 5, 15 en 30 dagen. Vervolgens werden de cumulatieve, gedisaggregeerde *ET* satellietgegevens met tijdsintervallen van 5 dagen gebruikt in de inverse modelering-procedure.

De resultaten van inverse modelering gebruikmakend van door SWAP gesimuleerde cumulatieve ***ET*** met tijdsintervallen van 5 dagen, laten een goede overeenstemming zien tussen de gesimuleerde irrigatietijden en –hoeveelheden met de referentiegegevens voor de twee landbouwvelden W1 en W2 (Fig. 5.4). Dit laat zien *dat inverse modelering goede mogelijkheden biedt om irrigatietijden en –hoeveelheden vast te stellen, gebruikmakend van cumulatieve ET gegevens met tijdsintervallen van 5 dagen.*

De mogelijkheid om irrigatiepraktijken af te leiden werd ook onderzocht voor gesimuleerde cumulatieve ***ET*** gegevens met langere tijdsintervallen van 15 en 30 dagen. Bij tijdsintervallen van 15 dagen duiden grote verschillen tussen berekende irrigatietijden en – hoeveelheden op een slechte functioneren van inverse modelering. Ook de resultaten van inverse modelering met maandelijkse cumulatieve ***ET*** gegevens laten een slechte prestatie zien wat betreft vaststellen van irrigatietijden en –hoeveelheden. Echter, ondanks de zwakke resultaten met betrekking tot vaststellen van irrigatietijden en –hoeveelheden, corresponderen de gesimuleerde cumulatieve ***ET*** waarden goed met de referentiewaarden (*RMSE* = 0.8 mm d^{-1}). Dit duidt op niet-uniekheid van de optimalisatieparameters door een geringe gevoeligheid van deze parameters voor de meetgegevens.

Succesvolle toepassing van inverse modelering hangt af van de beschikbaarheid van betrouwbare en nauwkeurige regionale *ET* gegevens en het tijdsinterval van deze gegevens. Bij de meeste irrigaties functioneerde de inverse techniek met satelliet **ET** gegevens relatief slecht. Dat kan veroorzaakt zijn door het ontbreken van een droge periode in de satelliet **ET** gegevens.

Het resultaat is dat bij gebruik van een doelfunctie gebaseerd op **ET**, de maximaal vast te stellen irrigatiediepte beperkt is door de kritieke drukhoogte die overeenkomt met veldcapaciteit in de wortelzone. *Irrigatiehoeveelheden, die de wortelzone bevochtigen voorbij veldcapaciteit en dus veel percolatie veroorzaken, kunnen niet worden berekend door de toegepaste inverse modelering methode. Verder kan inverse modellering alleen worden toegepast als droogtestress voorkomt.*

Assimilatie van satellietgegevens in het gedistribueerde SWAP model

Door vereenvoudiging van complexe natuurlijke processen en door onzekerheid in invoerparameters bevat de uitvoer van simulatiemodellen fouten. Aan de andere kant bevatten ook gegevens gebaseerd op satellietbeelden fouten door factoren als atmosferische demping en niet-begroeide oppervlakken binnen pixels. Daarom zijn simulatiemodellen als SWAP of satellietgegevens op zichzelf geen nauwkeurige methoden om regionale waterbalanscomponenten en gewasopbrengsten te berekenen. *Assimilatie van satellietgegevens in het SWAP simulatiemodel, met inachtneming van de relatieve fouten van beide methoden, kan de nauwkeurigheid van de simulatieresultaten verhogen.*

Assimilatie van satellietgegevens in SWAP met automatische calibratie van bijvoorbeeld irrigatiegiften, eist voor regionale schaal een grote hoeveelheid rekentijd. Daarom werd in *Hoofdstuk 6* de eenvoudige assimilatiemethode van 'updating' voorgesteld.

Hoofdstuk 6 demonstreert de potentie van het gebruik van satellietbeelden van het aardoppervlak om gedistribueerde simulatie te verbeteren van tarweproductie en voor vaststelling van effecten van landbouwkundige droogte. Het SWAP model werd gedistribueerd toegepast, gebruikmakend van ruimtelijk verdeelde informatie van bodemtypen, landgebruik en watertoevoer op raster basis met een gridafstand van 250 m. Hiertoe werd het Borkhar irrigatiedistrict verdeeld in 10655 homogene pixels, waarbij alleen pixels met een tarwegewas (1589 in totaal) in de analyse werden meegenomen. Invoergegevens voor bodemtypen en landgebruik werden afgeleid met satellietgegevens en verwerkt in een Geografisch Informatie Systeem (GIS). Tijdsafhankelijke gedistribueerde gegevens van watertoevoer werden afgeleid van informatie over irrigatiepompen en het netwerk van irrigatiekanalen. *Om de GIS gegevens met SWAP te linken, werd een koppelprogramma geschreven in MATLAB.* Dit programma zorgde voor de overdracht van in- en uitvoergegevens van het ene systeem naar het andere en voor het runnen van het model voor iedere pixel. Een schematische weergave van de procedure voor toepassing van SWAP op regionaal nivo is opgenomen in Fig. 6.1.

Om de productie te voorspellen voor het landbouwkundige jaar 2004-05, werd gedistribueerde simulatie uitgevoerd op regionale schaal met en zonder assimilatie. Voor het achtereenvolgens updaten van het gedistribueerde SWAP model, werd gebruik gemaakt van drie verzamelingen satellietgegevens (bestaande uit bladoppervlakte-index LAI en/of relatieve verdamping $ET\ ET_p^{-1}$) afgeleid van de MODIS satelliet met lage tot gemiddelde ruimtelijke resolutie. Tijdseries van LAI werden afgeleid van MODIS gegevens met 250 m

ruimtelijke resolutie en vervolgens vereffend door het fitten van een polynoom voor iedere pixel. Tijdseries van $ET\,ET_p^{-1}$ werden afgeleid van MODIS gegevens met 1000 m ruimtelijke resolutie.

Om een voorspelling van de productie te maken, werd het assimilatieproces één of twee maanden voor het einde van het tarwegroeiseizoen gestopt. Tijdens het assimilatieproces werden bekende weergegevens gebruikt, terwijl voor het overblijvende deel van het groeiseizoen verschillende weerscenario's werden beschouwd gebaseerd op meteorologisch droge, natte en gemiddelde jaren. We selecteerden een 'gain factor' K_g voor het Kalman filter die het beste overeenkwam met de waarnemingen.

Gebruik van de satellietgegevens van LAI en ET ET_p^{-1} liet op veldschaal een duidelijke verbetering zien van de simulatieresultaten. De resultaten lieten ook zien dat *de assimilatie van LAI het grootste effect heeft.* Daarom raden we aan de assimilatiemethode te herhalen met LAI gegevens van de geavanceerde IRS-P6 satelliet, welke een hoge ruimtelijke (56 m) en temporele (3 d) resolutie heeft.

Simulatie met data-assimilatie op regionale schaal was ook veelbelovend voor het één maand vooraf voorspellen van gewasopbrengsten (afwijking circa 10%). Echter, voorspellingen op langere termijn (2 maanden en langer) lieten een grotere afwijking zien tussen gesimuleerde en statistische gegevens.

De voorspellingen van de uiteindelijke gewasopbrengsten met en zonder data-assimilatie, werden duidelijk beïnvloed door het type weergegevens (droog, nat of normaal jaar) in de laatste maand(en) van het groeiseizoen. De voorspelde gewasopbrengst verschilde in het natte en droge jaar, in vergelijking met de weergegevens van het gemiddelde jaar, met −19 tot 16% bij één maand vooraf en −6 tot 12% bij twee maanden vooraf.

Aangezien de Zayande Roud rivier voornamelijk gevoed wordt door afsmelten van sneeuw in de periode januari tot april, kan een gedetailleerd identificatiesysteem voor droogte worden ontwikkeld door integratie van het voorgestelde identificatiesysteem van landbouwkundige droogte met schattingen van beschikbaar oppervlaktewater uit de aanwezige hoeveelheid sneeuw.

Als belangrijkste conlusie kan het ontwikkelde 'Comprehensive Agricultural Drought Assessment System *(CADAS)*' werden gebruikt als een nauwkeurige methode voor identificatie en vermindering van droogte-invloeden op de landbouwkundige sector, en voor het creëren van meer voedselzekerheid.

توسعه سیستم ارزیابی خشکسالی کشاورزی

ترکیبی از مدل سازی اگروهیدرولوژیکی، داده های ماهواره ای و سیستم اطلاعات جغرافیایی

مجید وظیفه دوست

رساله دکتری

دانشکده منابع آب و تغییر اقلیم

گروه فیزیک خاک، اگروهیدرولوژی و مدیریت آبهای زیرزمینی

دانشگاه واگنینگن

هلند

آذر 1386

فصل اول -مقدمه

کشور ایران در منطقه اقلیمی خشک و نیمه خشک واقع شده و هر از چند گاه با خشکسالیهای فراگیر مواجه است که این پدیده طبیعی موجب وارد آمدن خسارت های سنگین اقتصادی و اجتماعی می شود. بخش کشاورزی با 80 تا 90 درصد مصرف آب کشور بیشترین آب مصرفی را به خود اختصاص می دهد و اغلب اولین بخشی است که تحت تاثیر خشکسالی واقع می گردد. در عین حال به دلیل مدیریت ضعیف منابع آب در بخش کشاورزی کارایی مصرف آب بسیار پایین تر از میزان پتانسیل آن می باشد. بحران در حال رشد کمبود آب به دلیل خشکسالی های مکرر و افزایش تقاضا برای آب از سوی بخشهای صنعت ، شهری و محیط زیست از سویی دیگر مهمترین عوامل تهدید در رسیدن به یک سیستم پایدار در کشاورزی و امنیت غذایی در ایران به شمار می روند. بنابراین توسعه یک سیستم ارزیابی خشکسالی کشاورزی می تواند به منظور ترسیم وضعیت خشکسالی، هشدار قبل از وقوع، تصمیم گیری های عملیاتی بموقع درسطح مزرعه و منطقه، تعیین مناطق آسیب پذیر و در نهایت کاهش اثرات ناشی از خشکسالی مورد استفاده قرار گیرد. در این مطالعه به دلیل در بر گرفتن تمامی عوامل جوی، آب ، خاک و گیاهی، میزان کل تولید و عملکرد محصول به عنوان شاخص خشکسالی کشاورزی مورد استفاده قرار می گیرد و به نظر نویسنده این کتاب، شاخص عملکرد و میزان تولید، مهمترین شاخص درترسیم و ارزیابی وضعیت خشکسالی کشاورزی در مناطق تحت آبیاری می باشد.

فصل دوم

در فصل دوم منطقه تحت مطالعه، برخوار اصفهان، مورد بررسی قرار می گیرد. در این فصل ضمن تشریح کامل منطقه، مشخصات اقلیمی، منابع آب و آبیاری، نوع پوشش گیاهی و خاکهای منطقه مورد بررسی قرار گرفت.

فصل سوم

بر همگان روشن است که در شرایط بحران و کمبود آب، باید بالاترین بهره ممکن از آبهای قابل دسترس موجود حاصل گردد. لذا در فصل سوم به منظور یافتن راهکارهای لازم در مقیاس مزرعه ای که منجر به افزایش کارایی مصرف آب و در نهایت سود بیشتر در شرایط کم آبی می گردد، یک مدل اگروهیدرولوژیکی که پایه فیزیکی دارد (SWAP) با استفاده از داده های مزرعه ای که از 8 مزرعه مختلف (گندم، ذرت ، آفتاب گردان و چقندر قند) در منطقه برخوار اصفهان در سال زراعی 1384–1383 جمع آوری گردیده بود، کالیبره گردید. با استفاده از مدل کالیبره شده ، راهکار های مختلف از قبیل کم آبیاری، بهینه کردن دوره های آبیاری و وسعت منطقه تحت کشت با استفاده از روابط بین شاخص های کارایی مصرف آب و میزان آب مصرفی مورد بررسی قرار گرفت. نتایج بدست آمده حاکی از امکان افزایش کارایی مصرف آب در شرایط کم آبی به میزان قابل توجهی بود.

اگرچه مدلهای اگروهیرولوژی امکان شبیه سازی و پیشبینی میزان عملکرد محصول را فراهم آورده اند، اما این مدل ها به دلیل عدم قطعیت در پارامتر های ورودی در این مدلها از قبیل زمان و میزان آب آبیاری، خصوصیات هیدرولیکی خاک و تاریخ کشت گیاهان دارای دقت زیادی در پیشبینی عملکرد محصول نیستند. مخصوصا زمانی که این مدل ها در مقیاس منطقه ای مورد استفاده قرار بگیرند که در این صورت بر میزان خطاها به میزان قابل توجهی افزوده می گردد. بنابراین به منظور کاهش اثرات عدم قطعیت در پارامتر های ورودی مورد لزوم در بکارگیری مدل SWAP و پیشبینی دقیق تر میزان تولید به عنوان شاخص خشکسالی کشاورزی در مقیاس ناحیه ای در فصل های چهارم، پنجم و ششم امکان استفاده از داده های ماهواره ای از قبیل شاخص سطح برگ و تبخیر و تعرق برای کاهش خطاها و بر طرف نمودن عدم قطعیت در محاسبات مربوط به متغیر های درونی مدل مورد مطالعه قرار گرفت.

فصل چهارم

داده های ماهواره ای شاخص سطح برگ (LAI) از باند های قابل روئیت و مادون قرمز از تصاویر ماهواره ای MODIS در 18 تاریخ مختلف و با دقت مکانی متوسط (250) بدست آمد. اما به دلیل محدودیت های موجود در دقت مکانی و زمانی داده های ماهوارهای این داده ها نمی توانند به صورت مستقیم برای تخمین تبخیر و تعرق مورد استفاده واقع شوند. بنابراین در فصل چهارم یک روش جدید به منظور افزایش دقت مکانی نقشه های تبخیر و تعرق که از تصاویر MODIS با دقت مکانی 1000 متر بدست آمده بودند، ارائه گردید. در این روش فرض گردید که تبخیر و تعرق محاسبه شده از هر پیکسل MODIS، یک ترکیب خطی از تبخیرو تعرق تمامی اجزا داخل آن پیکس MODIS می باشد. نتایج حاصله از روش پیشنهادی با نتایج بدست آمده از دو روش دیگر که بر اساس ثابت بودن نسبتهای

وزنی بین دو نقشه تبخیر و تعرق با دقت مکانی بالا و پایین بدست آمده بودند، مقایسه گردید. بزرگترین مزیت روش پیشنهادی برای افزایش دقت مکانی این بود که در این روش به تصاویر با دقت مکانی کم تری نیاز می باشد. این روش تنها با داشتن یک تصویر با دقت مکانی بالا نیز قابل استفاده است. به دلیل اینکه در اکثر مناطق دسترسی به تصاویر حرارتی با دقت مکانی بالا که در محاسبه تبخیر و تعرق استفاده می گردد، موجود نیست، روش پیشنهادی می تواند به عنوان روش جایگزین مورد استفاده قرار گیرد.

فصل پنجم

اجزا ی بیلان آب که توسط مدل SWAP محاسبه می شود بسیار حساس به شرایط مرزی در سطح خاک یعنی زمان و مکان آبیاری می باشد. بدین منظور در فصل پنجم امکان تخمین مقدار و زمان آب آبیاری بکار گرفته شده در منطقه، با استفاده از داده های تجمعی تبخیر و تعرق و با بکارگیری روش مدل سازی معکوس مورد بررسی قرار گرفت. امکان تخمین میزان و زمان آب آبیاری ابتدا با استفاده از داده های شبیه سازی شده تبخیر تعرق بدست آمده از مدل   SWAP   که بصورت دوره های تجمعی   5 ، 15 و 30 روزه بودند، مورد بررسی قرار گرفت. سپس از داده های تبخیر و تعرق واقعی بدست آمده از تصاویر ماهواره ای که بصورت دوره های تجمعی 5 روزه درآمده بودند، استفاده گردید. نتایج نشان داد که کارایی روش مدل سازی معکوس در تعیین زمان و مقدار آب آبیاری با استفاده از داده های شبیه سازی شده تبخیر و تعرق که به صورت دوره های تجمعی 5 روزه باشند، بسیار رضایت بخش می باشد. اما عمق های آبیاری که فراتر از ظرفیت مزرعه ای بودند و بنابراین به صورت نفوذ عمقی از منطقه ریشه ها خارج می شدند قابل پیشبینی با استفاده از این روش نبودند. علاوه بر این، کاربرد مدل سازی معکوس و به عبارتی دیگر روش کالیبره کردن با استفاده از داده های تبخیر و تعرق در مقیاس منطقه ای مستلزم صرف زمان بسیار زیادی بود که این باعث ایجاد محدودیت در استفاده از این روش می گردد.

فصل ششم

در فصل ششم داده های با ارزش شاخص سطح برگ و تبخیرو تعرق نسبی که از تصاویر ماهواره ای در 18 تاریخ مختلف درطول فصل رشد زمستانه بدست آمده بود، با استفاده از تکنیک ساده به روزکردن متوالی (updating) وارد مدل SWAP   گردید. بدین منظور پس از ایجاد تغییرات لازم در کد مدل SWAP، این مدل با استفاده از داده های مکانی نوع خاک، نوع پوشش گیاهی و میزان آب آبیاری بکارگرفته شده به فرمت مدل منطقه ای درآمد. بدین منظور منطقه تحت مطالعه به شبکه ای از سلول ها با ابعاد 250 متر در 250 متر تبدیل گردید. به منظور ایجاد ارتباط بین داده های مکانی نوع خاک، پوشش گیاهی و میزان آب آبیاری با مدل SWAP و وارد کردن داده های مورد نیاز از لایه های مختلف اطلاعاتی در هر سلول به مدل SWAP ، یک کد نرم افزاری در محیط برنامه نویسی MATLAB نوشته شد. این برنامه وظیفه خواندن داده ها ازلایه های مختلف اطلاعاتی، وارد کردن این اطلاعات به درون مدل SWAP و گرفتن خروجی های لازم از مدل   SWAP را بر عهده داشت.

به منظور پیشبینی مقدار کل تولید قبل از رسیدن به تاریخ برداشت ، عملیات به روز رسانی مدل با استفاده از داد ه های هواشناسی و ماهواره های شاخص سطح برگ و تبخیر و تعرق نسبی انجام و به ترتیب یک ماه و دو ماه قبل از رسیدن به تاریخ برداشت، متوقف گردید. در طول دوره به روز رسانی از داده های موجود هواشناسی استفاده گردید و در دوره باقیمانده رشد تا پایان فصل رشد از میانگین داده های درازمدت هواشناسی که از سالهای تر ، نرمال و خشک به عنوان سه گزینه مورد احتمال برداشت شده بودند، استفاده گردید. نتایج پیشبینی کوتاه مدت میزان تولید (یک ماه) که با استفاده از شبیه سازی محصول همراه با به روز رسانی متغیر های درونی LAI و تبخیر و تعرق نسبی انجام گردید، بسیار رضایت بخش بود (Bias = ±10%)..

References

Alizadeh, A., and M. Vazifedoust (2000), National water document for optimum water use in agriculture sector in Iran, report, Islamic Republic Of Iran Meteorological Organization, Tehran, Iran (*In Persian*).

Allen, R.G., L.S. Pereira, D. Raes, and M. Smith (1998), Crop evapotranspiration: guidelines for computing crop water requirements, *Irrig. and Drain., Paper 56, FAO, Rome, Italy.*

Allen, R.G., M. Smith, A. Perrier, and L.S. Pereira (1994), An update for the definition of reference evapotranspiration. *ICID Bull., 43(2),* 35-92.

Allen, R.G., M.E. Jensen, J.L. Wright, and R.D. Burman (1989), Operational estimates of reference evapotranspiration, *Agron. J., 81,* 650-662.

Angstrom, A., (1924), Solar and atmospheric radiation, *Q. J. R.. Meteorol. Soc. 50,* 122-125.

APERI (2001), General studies of agricultural development in Borkhar district, report, Agricultural Planning and Economic Research Institute, Tehran, Iran (*In Persian*).

Aubert, D., C. Loumagne, and L. Oudin (2003), Sequential assimilation of soil moisture and streamflow data in a conceptual rainfall-runoff model, *J. Hydrol., 280,* 145-161.

Baldocchi, D.D., B.B. Hicks, and P. Camara (1987), A canopy stomatal resistance model for gaseous deposition to vegetated surfaces, *Atmos. Environ. J., 21,* 91–101.

Bessembinder, J.J.E., P.A. Leffelaar, A.S. Dhindwal, and T. Ponsioen (2005), Which crop and which drop, and the scope for improvement of water productivity, *Agric. Water Manag., 73(2),* 113-130.

Bessembinder, J.J.E, A.S. Dhindwal, P.A. Leffelaar, T. Ponsioen, and S. Singh (2003), Analysis of crop growth, in *Water Productivity of Irrigated Crops in Sirsa District, India: Integration of remote sensing, crop and soil models and geographical information systems*, edited by Dam, J.C. van and R.S. Malik, pp. 59-82, Wageningen University, Wageningen.

Bastiaanssen, W.G.M., R.G. Allen, P. Droogers, G. D'Urso, and P. Steduto (2007), Twenty-five years modelling irrigated and drained soils: State of the art, *Agric. Water Manag., 93(3),* 111-125.

Bastiaanssen, W.G.M., E.J.M. Noordman, H. Pelgrum, G. Davis, B.P. Thoreson, and R.G. Allen (2005), SEBAl model with remotely sensed data to improve water-resources management under actual field conditions, *J. Irrig. and Drain. Engr., ASCE, 131,* 85-93.

Bastiaanssen, W.M.G. (2003), Crop and water productivity of the Pakistan wheat and rice systems, online available at: *Www.waterwatch.nl/download/projects/0053_Pakistan.pdf.*

Bastiaanssen, W.G.M. (2000), SEBAL-based sensible and latent heat fluxes in the irrigated Gediz Basin, Turkey. *J. Hydrol., 229,* 87-100.

Bastiaanssen, W.G.M., M. Menenti, R.A. Feddes, and A.A.M. Holtslag (1998), A remote sensing surface energy balance algorithm for land (SEBAL): 1. Formulation, *J. Hydrol., 212/213,* 198-212.

Black, T.A., W.R. Gardner, and G.W. Thurtell (1969), The prediction of evaporation, drainage, and soil water storage for a bare soil, *Soil Sci. Soc. Am. Proc., 33,* 655–660.

Blaney, H.F., and W.D. Criddle (1950), Determining water requirements in irrigated areas from climatological and irrigation data, *USDA Soil Conservation Service, SCS-TP96*, 44 pp.

Boegh, E., M. Thorsen, M.B. Butts, S. Hansen, J.S. Christiansen, P. Abrahamsen, C.B. Hasager, N.O. Jensen, P. van der Keur, J.C. Refsgaard, K. Schelde, H. Soegaard, and A. Thomsen (2004), Incorporating remote sensing data in physically based distributed agro-hydrological modelling, *J. Hydrol., 287,* 279–299.

Bouman, B.A.M. (1992), Linking physical remote sensing models with crop growth simulation models, applied for sugar beet, *Int. J. Remote Sens., 13,* 2565–2581.

Calera Belmonte, A.M. Jochum, A. Cuesta Garc´ıa, A. Montoro Rodr´ıguez and P.L. Fuster (2005), Irrigation management from space: Towards user-friendly products. *J. Irrig. and Drain. Sys*, *19,* 337-353.

Chemin, Y., and T. Alexandridis (2004), Improving spatial resolution of ET seasonal for irrigated rice in Zhanghe, China, *Asian J. Geoinformatics*, *5(1),* 3-11.

Chen, T.S., and G. Ohring (1984), On the relationship between clear sky planetary and surface albedo. *J. Atmos. Sci., 41,* 156-158.

Chimpanshi, A.C. (1995), Monitoring the effects of drought on wheat yields in Saskatchewan, PhD thesis, Saskatoon, University of Saskatchewan.

Choudhury, B.J., N.U. Ahmed, S.B. Idso, R. J. Reginato, and C.S.T. Daughtry (1994), Relations between evaporation coefficients and vegetation indices studied by model simulations. *Remote Sens. Environ., 50,* 1 –17.

Doherty, J., L. Brebber, and P. Whyte (1995), PEST: Model independent parameter estimation, Australian Centre for Tropical Freshwater Research, James Cooke University, Townsville, Australia, 140 pp.

Doorenbos, J., and A.H. Kassam (1979), Yield response to water, *Irrig. and Drain.,33, FAO, Rome, Italy.*

Doorenbos, J., and W.D. Pruitt (1977), Guidelines for predicting crop water requirements. *Irrig. and Drain., 24, FAO, Rome, Italy.*

Droogers, P., and W.G.M. Bastiaanssen (2002), Irrigation performance using hydrological and remote sensing modelling, *J. Irrig. and Drain. Engr., ASCE, 128,* 11-18.

Droogers, P., and M. Torabi (2002), Field scale scenarios for water and salinity management by simulation modelling, Report, *IAERI-IWMI,* Tehran, Iran.

Droogers, P., W.G.M. Bastiaanssen, A. Gieske, N. Toomanian, and M. Akbari (2001), Assessment of irrigation performance using NOAA satellite imagery, report, *IAERI-IWMI,* Tehran, Iran.

Droogers, P., M. Akbari, M. Torabi, and E. Pazira (2000a), Exploring field scale salinity using simulation modeling, example for Rudasht area, Esfahan Province, Iran, report, *IWMI-IAERI,* Tehran, Iran.

Droogers P., H.R. Salemi, and A. Mamanpoush (2000b), Exploring basin scale salinity problems using a simplified water accounting model: the example of Zayandeh Roud Basin, Iran, *IAERI-IWMI,* report, Tehran, Iran.

Droogers, P., W.G.M. Bastiaanssen, M. Beyazgül, Y. Kayam, G.W. Kite, and H. Murray-Rust (2000c), Distributed agro-hydrological modelling of an irrigation system in Western Turkey, *Agric. Water Manag., 43,* 183-202.

D'Urso, G. (2001), Simulation and management of on-demand irrigation systems: A combined agrohydrological and remote sensing approach, PhD thesis, Wageningen University, Wageningen, The Netherlands.

D'Urso, G., and M. Menenti (1995), Mapping crop coefficients in irrigated areas from Landsat TM images, paper presented at Proceeding of European Symposium on Satellite Remote Sensing II, Europto, Paris, SPIE Vol. 2585.

EWA (2001), Annual report on groundwater levels and observation tubewells in the Borkhar district, report, Esfahan Water authority, Esfahan, Iran (*In Persian*).

FAO (2005), Islamic Republic of Iran: a major wheat importer turning self-sufficient?, Food outlook No. 1, FAO, Rome, Italy, April 2005, online available at:
http://www.fao.org/docrep/007/j5051e/j5051e07.htm.

Feddes, R.A., M. Menenti, P. Kabat, and W.G.M. Bastiaanssen (1993), Is large-scale inverse modelling of unsaturated flow with areal evaporation and soil moisture as estimated from remote sensing feasible?, *J. Hydrol., 143,* 25–152.

Feddes, R.A., P.J. Kowalik, and H. Zaradny (1978), Simulation of field water use and crop yield. Simulation Monographs, Pudoc, Wageningen, The Netherlands, 189 pp.

Feddes, R.A. (1971), Water, heat and crop growth, PhD thesis, Wageningen, Agricultural University. The Netherlands.

Fischer, A., L. Kergoat, and G. Dedieu (1997), Coupling satellite data with vegetation functional models: review of different approaches and perspectives suggested by the assimilation strategy. *Remote Sens. Rev., 15,* 283–303.

Foltz, R.C. (2002), Iran's water crisis: cultural, political, and ethical dimensions, *J. Agric. and Environ. Ethics, 15,* 357-380.

French, A. N., F. Jacob, M. C. Anderson, W. P. Kustas, W. Timmermans, A. Gieske, Z. Su, H. Suf, M. F. McCabe, J. Prueger and N. Brunsell (2005), Surface energy fluxes with the Advanced Spaceborne Thermal Emission and Reflection radiometer (ASTER) at the Iowa 2002 SMACEX site (USA), *Remote Sens. Environ., 99,* 55-65.

French, A.N., T.J. Schmugge, and W.P. Kustas (2001), Estimating evapotranspiration with ASTER thermal infrared imagery, *Proc. of IGARSS*, Sydney, Australia.

Gieske, A., N. Toomanian, and M. Akbari (2002a), Irrigated area by NOAA-Landsat up-scaling techniques: Zayandeh Rud Basin, report, *IAERI-IWMI,* Tehran, Iran.

Gieske, A., A. Mamanpoush, M. Akbari, and M. Miranzadeh (2002b), Crop and land cover classification by LANDSAT 7 ETM (July 2000) for the Zayandeh Rud basin, *IAERI-IWMI,* Tehran, Iran.

Haertel, V., and Y.E. Shimabukuro (2004), Spectral Linear Mixing Model in Low Spatial Resolution Image Data, *Proc. of IGARSS*, Anchorage, USA.

Hargreaves, G.H., and Z. A. Samani (1985), Reference crop evapotranspiration from temperature. *Applied Engr. Agric., 1,* 96-99.

Hargreaves, G.H., and Z. A. Samani (1982), Estimating potential evapotranspiration. *J. Irrig. Drain. Engr., 108(3),* 225-230.

Hayes, M.J. (2003), Drought indices, National Drought Mitigation Centre, online available at: http://www.drought.unl.edu/whatis/indices.htm, accessed on 01 April 2004.

He, Y., Z. Su, L. Jia, Y. Zhang, G. Roerink, S. Wang, J. Wen, and Y. Hou (2005), Estimation of daily evapotranspiration in Northern China plain by using MODIS/TERRA images, *Proc. Int. Soc. for Optical Engr., SPIE 5976.*

Hoeben, R., and P.A. Troch (2000), Assimilation of active microwave observation data for soil moisture profile estimation, *Water Resour. Res., 36(10),* 2805–2819.

Hong, S.h., J.M.H. Hendrickx, and B. Borchers (2005), Effect of scaling transfer between evapotranspiration maps derived from LandSat7 and MODIS images, *Proc. Int. Soc. for Optical Engr., SPIE 5811.*

Hoogesteger, J.D. (2005), Making do with what we have: understanding drought management strategies and their effects in the Zayandeh Rud Basin, Iran, MSc. thesis, Wageningen University, Wageningen, The Netherlands.

Houser, P.R., W.J. Shuttleworth, J.S. Famiglietti, H.V. Gupta, K.H. Syed, and D.C. Goodrich (1998), Integration of soil moisture remote sensing and hydrological modelling using data assimilation, *Water Resour. Res., 34 (12),* 3405–3420.

Houtekamer, P., and H. L. Mitchell (1998), Data assimilation using an ensemble Kalman filter technique, *Mon. Wea. Rev., 126,* 796–811.

Howell, T.A., J. L. Steiner, A.D. Schneider, S. R. Evett, and J. A. Tolk (1997), Seasonal and maximum daily evapotranspiration of irrigated winter wheat, sorghum and corn- southern high plains, *Trans. ASAE, 40(3),* 623-634.

Hussain, I., R. Sakthivadivel, U. Amarasinghe, M. Mudassar, and D. Molden (2003), Land and water productivity of wheat in the western Indo-Gangetic plains of India and Pakistan: a comparative analysis, in *Research Report 65,* IWMI, Colombo.

Ines, A.V.M., and K. Honda (2005), On quantifying agricultural and water management practices from low spatial resolution RS data using genetic algorithms: A numerical study for mixed pixel environment, *Adv. in Water Resour., 28(8),*856-870.

Ines, A.V.M., and P. Droogers (2002a), Inverse modelling to quantify irrigation system characteristics and operational management. *Irrig. and Drain. Sys., 16,* 233-252.

Ines, A.V.M., and P. Droogers (2002b), Inverse modelling in estimating soil hydraulic functions: a Genetic Algorithm approach, *Hydrol. Earth Sys. Sci., 6,* 49-65.

IRNCID (2007), Water and irrigation in Iran, The 4th Asian regional conference and 10th international seminar on Participatory Irrigation Management (PIM), Iranian National Committee on Irrigation and Drainage, Tehran, Iran, online available at : http://www.irncid.org/pim2007/Irrigation.aspx, accessed on 25 May 2007.

Jagtap, W.S., and J.W. Jones (1989), Stability of crop coefficients under different climate and irrigation management practices, *Irrig. Sci., 10,* 231-244.

Jarvis, P.G. (1976), The interpretation of leaf water potential and stomatal conductance found in canopies in the field, *Phil. Trans. R. Soc.*, 273, 593-610, London.

Jensen, M.E., R.D. Burman, and R.G. Allen (ed) (1990), *Evapotranspiration and Irrigation Water Requirements.* ASCE Manuals and Reports on Engineering Practices No. 70, New York, NY, 360 p.

Jhorar, R.K. (2002), Estimation of effective soil hydraulic parameters for water management studies in semi-arid zones, PhD Thesis, Wageningen University and Research Centre, Wageningen, The Netherlands, 157 pp.

Jongschaap, R. E. E. (2006), Run-time calibration of simulation models by integrating remote sensing estimates of leaf area index and canopy nitrogen, *J. Agron., 24,* 328-336.

Jongschaap, R.E.E., and L.S.M. Schouten (2005), Predicting wheat production at regional scale by integration of remote sensing data with a simulation model, *Agron. Sustain. Dev., 25,* 481-489.

Kabat, P., R.W.A. Hutjes, and R.A. Feddes (1997), The scaling characteristics of soil parameters: From plot scale heterogeneity to subgrid parameterization, *J. Hydrol., 190 (3-4),* 363-396.

Kagon, F.N. (2000), Global drought detection and impact assessment form space, in *Drought: A Global Assessment*, Vol. 1, edited by D.A. Wilhite, pp 196-210, Routledge, London.

Keller, A., and D. Seckler (2005), Limits to the Productivity of Water in Crop Production, *California Water Plan Update, 4,* available online at*:* waterplan.water.ca.gov/docs/cwpu2005/vol4/, accessed on 01 May 2007.

Kheirabadi, M. (1991), *Iranian Cities: Formation and Development,* [ISBN 0-292-78517-8], University of Texas Press.

Kite, G.W., and P. Droogers (2000), Comparing evapotranspiration estimates from satellites, hydrological models and field data, *J. Hydrol., 229,* 3–18.

Kijne, J., R. Barker, and D. Molden, (Eds.) (2003), Water productivity in agriculture: limits and opportunities for improvement, c*omprehensive assessment of Water Management in Agriculture,* Series No. 1, CABI press, Wallingford, UK, 352 p.

Kroes, J.G. & J.C. Van Dam (eds) (2003), Reference manual SWAP version 3.03*,* Alterra Green World Research, Alterra report 773, ISSN 1566-7197. Wageningen University and Research Centre, Wageningen, The Netherlands, 211 p.

Kumar V., and Panu U. (1997), Predictive assessment of severity of agricultural droughts based on agro-climatic factors. *J. AWRA, 33,* 1255-1264.

Kustas W.P., J.M., Norman, M.C. Anderson, and A.N. French (2003), Estimating sub-pixel surface temperature and energy fluxes from the vegetation index-radiometric temperature relationship. *Remote Sens. Environ.*, *85,* 429-440.

Liang, S. (2000), Narrowband to broadband conversions of land surface albedo: I Algorithms, *Remote Sens. Environ.*, *76*, 213–238.

Lobell, D.B., and G.P. Asner (2004), Cropland Distributions from Temporal Unmixing of MODIS Data. *Remote Sens. Environ.*, *93(3),* 412-422.

MCST (2002), MODIS level 1B product user's guide, for level 1B version 4.0.9 (Terra) and version 4.1.1 (Aqua), MCST Document PUB-01-U-0202-REV B, MCST Internal Memo, M1039, 61 pp, Available online at www.**mcst.ssai.biz**/mcstweb/documents/M1054.pdf

Menenti, M., and B.J. Choudhury (1993), Parameterization of land surface evapotranspiration using a location- dependent potential evapotranspiration and surface temperature range, in Exchange processes at the land surface for a range of space and time scales, edited by H.J. Bolle et al., pp. 561-568, *IAHS Publ. No. 212.*

Menenti, M., T.N.M. Visser, J.A. Morabito, and A. Drovandi (1989), Appraisal of irrigation performance with satellite data and geo-referenced information, in *Irrigation Theory and Practice,* edited by J.R. Rydzewsky, and K. Ward, pp. 785-801, London.

Mokhtari, M.H. (2006), Agricultural drought impact assessment using remote sensing: a case study Borkhar district, Iran, MSc. thesis, ITC, Enschede, The Netherlands, 127 pp.

Molden, D., H. Murray-Rust, R. Sakthivadivel, and I. Makin (2001), A water productivity framework for understanding and action, presented at Workshop on Water productivity, Wadduwa, Sri Lanka, November 12 and 13.

Molden, D. (1997), Accounting for water use and productivity, SWIM Paper 1, International Irrigation Management Institute, Colombo, Sri Lanka.

Motiee, H. (2006), Assessment of the contributions of traditional qanats in sustainable water resources management, *Int. J. Water Resour. Dev., 22 (4),* 575-588.

Moulin, S., A. Bondeau, and R. Dele'colle (1998), Combining agricultural crop models and satellite observations from field to regional scales, *Int. J. Remote Sens., 19,* 1021-1036.

Mualem, Y. (1976), A new model for predicting the hydraulic conductivity of unsaturated porous media, *Water Resour. Res., 12,* 513-522.

Murray-Rust, H., H. Sally, H.R. Salemi, and A. Mamanpoush (2000), An overview of the hydrology of the Zayandeh Rud Basin, report, *IAERI-IWMI,* Tehran, Iran.

Narasimhan, B., and R. Srinivasan (2005), Development and evaluation of soil moisture deficit index (SMDI) and evapotranspiration deficit index (ETDI) for agricultural drought monitoring, *Agric. and Forest Meteorol., 133,* 69–88.

Neale, C.M.U., W.C. Bausch, and D.F. Heerman, 1989, Development of reflectance-based crop coefficients for corn, *Trans. ASAE, 32(6),* 1891–1899.

Olioso, A., Y. Inoue, S. Ortega-Faias, J. Demarty, J. P. Wigneron, I. Braud, F. Jacob, P. Lecharpentier, C. Ottele, J. C. Calvet, and N. Brisson (2005), Future directions for advanced evapotranspiration modelling: Assimilation of remote sensing data into crop simulation models and SVAT models, *Irrig. and Drain. Sys., 19,* 377–412.

Organization of Jihad-e-Agriculture (OJA) (2006), Cropping pattern, yields and total production of agricultural crops in Esfahan province, report, Organisation of Jihad-e-Agriculture, Esfahan, Iran, online available at: www.esfahan.agri-jahad.ir/modiriat/tarh/amar%20nameh/ index.htm, accessed on 01 September 2006.

Ortega-Farias, S. Olioso, A.R. Antonioletti, and N. Brisson (2004), Evaluation of the Penman–Monteith model for estimating soybean evapotranspiration, *Irrig. Sci., 23,* 1–9.

Palmer, W.C., (1965), Meteorological drought, research paper No. 45, U.S. Department of Commerce Weather Bureau, Washington, D.C.

Panu, U. S., and T. C. Sharma (2002), Challenges in drought research: some perspectives and future directions, *Hydrol. Sci. J., 47(S),* S19–S30.

Parodi, G.N. (2002), AHVRR hydrological analysis system: Algorithms and theory, version 1.3: AHAS algorithms and theory, ITC, Enschede, the Netherlands.

Penning de Vries, F.W.T., H.H. van Laar, and M.C.M. Chardon (1983), Bioenergetics of growth of seeds, fruits, and storage organs, in *Potential productivity of field crops under different environments*, pp. 37–59, Manila, International Rice Research Institute.

Peters, E. (2003), Propagation of drought through groundwater systems- illustrated in the Pang (UK) and Upper-Guadiana (ES) catchments, PhD. Thesis, Wageningen University, The Netherlands, 203 pp.

Price, J.C. (1984), Land surface temperature measurements from the split window channel of the NOAA 7 Advanced Very High Resolution radiometer, *J. Geophys. Res., 89,* 7231-7237.

Rana, G., N. Katerji, M. Mastrorilli, and M. Moujabber (1997), A model for predicting actual evapotranspiration under soil water stress in a Mediterranean region, *Theor. Appl. Clima., 56,* 45–55.

Reichle, R.H., J.P. Walker, R.D. Koster, and P.R. Houser (2003), Extended versus Ensemble Kalman Filtering for Land Data Assimilation, *J. Hydromet., 4,* 728–740.

Reichle, R., D.B. McLaughlin, and D. Entekhabi (2001), Variational data assimilation of microwave radiobrightness observations for land surface hydrology applications. *IEEE Trans. on Geosci. and Remote Sens., 39,* 1708–1718.

Ritter, A., F. Hupet, R. Munoz-Carpena, S. Lambot, and M. Vanclooster (2003), Using inverse methods for estimating soil hydraulic properties from field data as alternative to direct methods, *Agric. Water Manag., 59,* 77-96.

Salemi H.R., A. Mamanpoush, M. Miranzadeh, M. Akbari, M. Torabi, N. Toomanian, H. Murray-Rust, P. Droogers, H. Sally, and A. Gieske (2000), Water Management for Sustainable Irrigated Agriculture in the Zayandeh Rud Basin, Esfahan Province, report, *IWMI-IAERI,* Tehran, Iran.

Sally H., H. Murray-Rust, A. Mamanpoush, and M. Akbari (2001), Water supply and demand in four major irrigation systems in the Zayandeh Rud Basin, *IAERI-IWMI,* Tehran, Iran.

Schuurmans, J.M., P.A. Troch, and A.A. Veldhuizen (2003), Assimilation of remotely sensed latent heat flux in a distributed hydrological model, *Adv. in Water Resour., 26,* 151-159.

Shimabukuro, Y.E., and J. A. Smith (1991), The least-squares mixing models to generate fraction images derived from remote sensing multispectral data, *IEEE Trans. Geosci. Remote Sens., 29*, 16–20.

Sinclair, T.R., and F.P. Gardner (1998), *Environmental Limits to Plant Production*, Principles of Ecology in Plant Production, CAB International.

Singh, R., J.C. van Dam, and R.A. Feddes (2006), Water productivity analysis of irrigated crops in Sirsa district, India, *Agric. Water Manag., 82,* 253-278.

Singh, R. (2005), Water productivity analysis from field to regional scale: integration of crop and soil modelling, remote sensing and geographical information, PhD thesis, Wageningen University, Wageningen, The Netherlands.

Smith, A. (1953), *Blind White Fish in Persia*, George Allen and Unwin, London.

Soil and Water Research Institute (SWRI) (1973), Report of land evaluation and soil classification studies, Soil and Water Research Institute (SWRI), Tehran, Iran.

Spitters, C.J.T., H. van Keulen, and D.W.G. van Kraalingen (1989), A simple and universal crop growth simulator: SUCROS87, in *Simulation and systems management in crop protection* edited by R. Rabbinge, S.A. Ward, and H.H. van Laar, pp. 147-181, Pudoc, Wageningen, The Netherlands.

Stafford-Smith, D.M., and G.M. McKeon, (1998), Assessing the historical frequency of drought events on grazing properties in Australian rangelands, *J. Agric. Sys., 57,* 271-299.

Steiner, J.L., T.A. Howell, and A.D. Schneider (1991), Lysimetric evaluation of daily potential evapotranspiration models for grain sorghum, *Agron. J.*, *83,* 240-247.

Stewart, J.B. (1988), Modelling surface conductance of pine forest*, Agric. and Forest Meteorol., 43,* 19-37.

Su, Z. (2002), The Surface Energy Balance System (SEBS) for estimation of turbulent heat fluxes, *Hydrol. and Earth Sys. Sci., 6(1),* 85-99.

Supit, I., A.A. Hooyer, and C.A. Van Diepen (Eds.) (1994), System description of the WOFOST 6.0 crop simulation model implemented in CGMS. Vol. 1: Theory and algorithms, EUR publication 15956, Agricultural series, Luxembourg, 146 pp.

Tanner, C.B., and T.R. Sinclair (1983), Efficient water use in crop production: Research or re-search, in *Limitations to efficient water use in crop production,* edited by H.M. Taylor et al., pp. 1-27, ASA, Madison, WI.

Tasumi M., R.G. Allen R. Trezza, and J.L. Wright (2005), Satellite-based energy balance to assess within-population variance of crop coefficient curves, *J. Irrig. and Drain. Engr. ASCE 131(1),* 94-109.

Timmermans, W., A.S. Gieskea, W.P. Kustas, P. Wolskic, A. Arnethd, and G.N. Parodia (2004), Determination Of Water And Heat Fluxes With Modis Imagery-Maun, Botswana, Society Of Photo-Optical Instrumentation Engineers, *Proc. SPIE, 10th International Symposium On Remote Sensing For Agriculture, Ecosystems, And Hydrology,* 5232, 444-455.

Taylor, S. A., and G. M. Ashcroft (1972), *Physical Edaphology*, San Francisco: W.H. Freeman and Company.

United Nations Development Programme (UNDP) (2003), Iran's initial national communication to UN Framework Convention on Climate Change (UNFCCC), report, Climate Change Office, Tehran, Iran, available online at www.unfccc.int/resource/docs/natc/iranc1.pdf.

Valde´s, H., S. Ortega-Farias, M. Argote, B. Leyton, A. Olioso, and H. Pailla´n (2004), Estimation of evapotranspiration over a greenhouse tomato crop using the Penman–Monteith equation, *Acta Hort., (ISHS), 664,* 477–482.

Van Dam, J.C., and R.S. Malik, (Eds.) (2003), Water productivity of irrigated crops in Sirsa district, India: integration of remote sensing, crop and soil models and geographical information systems, WATPRO final report, including CD-ROM. ISBN 90-6464-864-6, pp. 59-82.

Van Dam, J.C., J. Huygen, J.G. Wesseling, R.A. Feddes, P. Kabat, P.E.V. Van Walsum, P. Groenendijk, and C.A. Van Diepen (1997), Theory of SWAP version 2.0: simulation of water flow, solute transport and plant growth in the Soil-Water-Atmosphere-Plant environment, report 71, Wageningen University, Wageningen, The Netherlands, 167 pp.

Van Genuchten, M.Th. (1980), A closed form equation for predicting the hydraulic conductivity of unsaturated soils, *Soil Sci. Soc. Am. J., 44,* 892-898.

Van Loon, E.E., and P.A. Troch (2002), Tikhonov regularization as a tool for assimilating soil moisture data in distributed hydrological models, *Hydrol. Proc., 16(2),* 531–556.

Vazifedoust, M., J.C. van Dam, R.A. Feddes, and W.G.M. Bastiaanssen (2007a), Disaggregation of remotely sensed evapotranspiration data: from low to high spatial resolution, *Remote sens. Environ. (Submitted).*

Vazifedoust, M., J.C. van Dam, and R.A. Feddes (2007b), Increasing water productivity of irrigated crops under limited water supply at field scale, *Agric. Water Manag. (in press).*

Vogt, J.V., and F. Soma (eds.) (2000), *Drought and Drought Mitigation in Europe*, 167-183, Kluwer Academic Publishers, printed in The Netherlands.

Walkley, A., and I. A. Black (1934), An examination of Degtjareff method for determining soil organic matter and a proposed modification of the chromic acid titration method, *Soil Sci. 37,* 29-37.

Wilhite, D.A., and M.D. Svoboda (2000), Drought early warning systems in the context of drought preparedness and mitigation, in *Early Warning Systems for Drought Preparedness and Drought Management*, edited by A. Wilhite, M.V.K. Sivakumar, and D.A. Wood, pp. 1–16, *Proc.* of an Expert Group Meeting, Lisbon, Portugal, September 5–7, 2000.

Wösten, J.H.M., A. Lilly, A. Nemes, and C. Le Bas (1998), Using existing soil data to derive hydraulic parameters for simulation models in environmental studies and in land use planning, report 156, DLO Winand Staring Centre, the Netherlands.

Wu, H., and D.A. Wilhite (2004), An operational agricultural drought risk assessment model for Nebraska, USA, *Natural Hazards, 33(1),*1-21.

Wulff, H.E. (1968), Qanats of Iran, *Scientific American, p. 94-105, online available at:* http://users.bart.nl/~leenders/txt/qanats.html, accessed on 01 May 2007.

Zwart, S.J., and W.G.M. Bastiaanssen (2004), Review of measured crop water productivity values for irrigated wheat, rice, cotton and maize, *Agric. Water Manag., 69(2),* 115-133.

List of frequently used symbols

The letters *a, b, m, n, p, q* are also used for any given constant. Some of the symbols used in a few consecutive equations falling outside the main line of argument are defined in the text only.

Symbol	Description	Dimension	Unit
A	Rate of photosynthetic assimilation of CO_2	$M\,L^{-2}\,T^{-1}$	$kg\,m^{-2}\,s^{-1}$
A_{max}	Maximum photosynthetic assimilation rate of CO_2	$M\,L^{-2}\,T^{-1}$	$kg\,ha^{-1}\,d^{-1}$
b	Vector containing parameters to be optimized	variable	variable
C_w	Differential water capacity ($d\theta\,/dh$)	L^{-1}	m^{-1}
e_{air}	Actual vapour pressure	$M\,L^{-1}\,T^{-2}$	Pa
e_{sat}	Saturation vapour pressure	$M\,L^{-1}\,T^{-2}$	Pa
E	Actual soil evaporation (volume flux)	$L\,T^{-1}$	$m\,s^{-1}$
$\boldsymbol{E}$	Actual soil evaporation flux integrated over time	L	m
E_{emp}	Soil evaporation flux according to an empirical function	$L\,T^{-1}$	$m\,s^{-1}$
E_p	Potential soil evaporation flux	$L\,T^{-1}$	$m\,s^{-1}$
$\boldsymbol{E_p}$	Potential soil evaporation flux integrated over time	L	m
ET	Actual evapotranspiration flux	$L\,T^{-1}$	$m\,s^{-1}$
$\boldsymbol{ET}$	Actual evapotranspiration flux integrated over time	L	m
ET_p	Potential evapotranspiration flux	$L\,T^{-1}$	$m\,s^{-1}$
$\boldsymbol{ET_p}$	Potential evapotranspiration flux integrated over time	L	m
ET_{ASTER}	Actual evapotranspiration flux from each ASTER pixel	$L\,T^{-1}$	$m\,s^{-1}$
$ET_{Disaggregated}$	Disaggregated actual evapotranspiration flux	$L\,T^{-1}$	$m\,s^{-1}$
$ET_{Observation}$	Observed evapotranspiration flux	$L\,T^{-1}$	$m\,s^{-1}$
ET_{MODIS}	Actual evapotranspiration flux from each MODIS pixel	$L\,T^{-1}$	$m\,s^{-1}$
ET_{ref}	Grass reference evapotranspiration flux	$L\,T^{-1}$	$m\,s^{-1}$
G	Heat flux into the soil	$M\,T^{-3}$	$W\,m^{-2}$
h	Soil water pressure head	L	m
h_1	Pressure head below which roots start to extract water from the soil	L	m
h_2	Pressure head below which roots start to extract water optimally from the soil	L	m

Symbol	Description	Dimension	Unit
h_{3h}	Pressure head below which roots cannot extract optimally any more, at a high potential transpiration rate	L	m
h_{3l}	Pressure head below which roots cannot extract water optimally any more, at a low potential transpiration rate	L	m
h_4	Pressure head below which no water uptake by roots is possible ('wilting point')	L	m
h_{crop}	Crop height	L	m
H	Sensible heat flux into the air	$M\,T^{-3}$	$W\,m^{-2}$
I	Irrigation flux in to the soil	$L\,T^{-1}$	$m\,s^{-1}$
$\boldsymbol{I}$	Irrigation flux integrated over time	L	m
$\boldsymbol{I_{cw}}$	Canal water irrigation integrated over time	L	m
$\boldsymbol{I_{gw}}$	Groundwater irrigation integrated over time	L	m
K_{sat}	Saturated hydraulic conductivity	$L\,T^{-1}$	$m\,s^{-1}$
K	Hydraulic conductivity	$L\,T^{-1}$	$m\,s^{-1}$
K_c	Unstressed crop coefficient defined by Eq. 4.1*a*	-	-
K_s	Water stress coefficient defined by Eq. 4.1*b*	-	-
LAI	Leaf area index	-	-
n	Empirical shape factor in the Van-Genuchten model	-	-
P	Precipitation flux	$L\,T^{-1}$	$m\,s^{-1}$
$\boldsymbol{P}$	Precipitation flux integrated over time	L	m
P_i	Precipitation flux interception rate	$L\,T^{-1}$	$m\,s^{-1}$
Q_{bot}	Bottom flux (positive upwards)	$L\,T^{-1}$	$m\,s^{-1}$
$\boldsymbol{Q_{bot}}$	Bottom flux integrated over time (positive upwards)	L	m
r_{air}	Diffusion resistance to water vapour of the air layer surrounding the leaves	$L^{-1}\,T$	$s\,m^{-1}$
r_s	Diffusion resistance to water vapour of both crop and soil surface	$L^{-1}\,T$	$s\,m^{-1}$
$r_{stomata}$	Minimum stomatal resistance of a single leaf	$L^{-1}\,T$	$s\,m^{-1}$
R_n	Net radiation flux	$M\,T^{-3}$	$W\,m^{-2}$
R_s	Net incoming short wave radiation flux above the canopy	$M\,T^{-3}$	$W\,m^{-2}$

Symbol	Description	Dimension	Unit
R_L	Net incoming long wave radiation flux above the canopy	$M\,T^{-3}$	$W\,m^{-2}$
S	Root water extraction rate	$L^3 L^{-3} T^{-1}$	$m^3\,m^{-3}\,s^{-1}$
T	Actual transpiration flux	$L\,T^{-1}$	$m\,s^{-1}$
$\mathbf{T}$	Actual transpiration flux integrated over time	L	m
T_p	Potential transpiration rate	$L\,T^{-1}$	$m\,s^{-1}$
$\mathbf{T_p}$	Potential transpiration integrated over time	L	m
T_{air}	Air temperature	-	^{o}C
T_{max}	Maximum air temperature	-	^{o}C
T_{min}	Minimum air temperature	-	^{o}C
u_z	Wind speed at elevation z	$L\,T^{-1}$	$m\,s^{-1}$
WP_T	Water productivity in terms of marketable yield per amount of water used for transpiration	$M\,L^{-3}$	$kg\,m^{-3}$
WP_{ET}	Water productivity in terms of marketable yield per amount of water used for evapotranspiration	$M\,L^{-3}$	$kg\,m^{-3}$
WP_I	Water productivity in terms of marketable yield per amount of water used for irrigation	$M\,L^{-3}$	$kg\,m^{-3}$
$\Delta \mathbf{W}$	Change in soil water storage in the root zone integrated over time	L	m
Y	Dry matter growth rate	$M\,L^{-2}\,T^{-1}$	$kg\,m^{-2}d^{-1}$
$\mathbf{Y}$	Total dry matter yield of crop integrated over time	$M\,L^{-2}$	$kg\,m^{-2}$
$\mathbf{Y}_p$	Potential total dry matter yield of crop integrated over time	$M\,L^{-2}$	$kg\,m^{-2}$
$\mathbf{Y}_{SO}$	Dry matter yield of storage organ integrated over time	$M\,L^{-2}$	$kg\,m^{-2}$
$\mathbf{Y}_M$	Marketable yield of crop integrated over time	$M\,L^{-2}$	$kg\,m^{-2}$
z	Vertical coordinate (positive upwards)	L	m
z_{oh}	Roughness lengths for heat transfer	L	m
z_{om}	Roughness lengths for momentum	L	m
z_{root}	Rooting depth	L	m
z_T	Measurement height for air temperature	L	m
z_u	Measurement height for wind speed	L	m
t	Time	T	s

Symbol	Description	Dimension	Unit
ρ_{air}	Density of air	$M\,L^{-3}$	$kg\,m^{-3}$
ρ_w	Density of water	$M\,L^{-3}$	$kg\,m^{-3}$
$\varDelta_v$	Slope of the saturation vapour pressure curve	$M\,L^{-1}\,T^{-2}\,\Theta^{-1}$	$Pa\,K^{-1}$
γ_{air}	Psychrometric constant	$M\,L^{-1}\,T^{-2}\,\Theta^{-1}$	$Pa\,K^{-1}$
α	Empirical parameter in the Van-Genuchten model	L^{-1}	m^{-1}
α_s	Surface albedo	-	-
ε	Light use efficiency of crop	$L^{-2}\,T^{2}$	$kg\,J^{-1}$
λ	Latent heat of vaporization of water per unit mass	$L^{2}\,T^{-2}$	$J\,kg^{-1}$
θ	Volumetric soil water content	-	$m^{3}\,m^{-3}$
θ_{obs}	Observed volumetric soil water content	-	$m^{3}\,m^{-3}$
θ_{res}	Residual volumetric water content	-	$m^{3}\,m^{-3}$
θ_{sat}	Saturated volumetric water content	-	$m^{3}\,m^{-3}$
θ_{sim}	Simulated soil water content	-	$m^{3}\,m^{-3}$

List of abbreviations

Abbreviation	Description
APERI	Agricultural Planning and Economic Research Institute
APAR	Actual Photo synthetically Active Radiation absorbed by a plant
ASTER	Advanced Spaceborne Thermal Emission and Reflection Radiometer
EWA	Esfahan Water Authority
F	Denotes the farmer's field
GIS	Geographical Information System
IAERI	Iranian Agricultural Engineering Research Institute
IMSRT	Iranian Ministry of Science, Research and Technology
ISWRI	Iranian Soil and Water Research Institute in Esfahan
IWMI	International Water Management Institute
M	Denotes the field where maize is grown
MODIS	Moderate Resolution Imaging Spectroradiometer
MSSL	Mean Sea Surface Level
PAR	Photo synthetically Active Radiation
PEST	Parameter ESTimation
RS	Remote Sensing
Sa	Denotes the field where sunflower is grown
Su	Denotes the field where sugar beet is grown
SEBAL	Surface Energy Balance Algorithm for Land
SWAP	Soil-Water-Atmosphere-Plant
SIWARE	SImulation of WAter management in Arid REgions
TSUMEA	Temperature SUM from emergence to Anthesis
TSUMAM	Temperature SUM from Anthesis to Maturity
W	Denotes the field where wheat is grown
WOFOST	WOrld FOod STudies

Netherlands Research School for the
Socio-Economic and Natural Sciences of the Environment

CERTIFICATE

The Netherlands Research School for the
Socio-Economic and Natural Sciences of the Environment
(SENSE), declares that

Majid Vazifedoust

Born on: *22 June 1975* at: *Kashmar, Iran*

has successfully fulfilled all requirements of the
Educational Programme of SENSE.

Place: *Wageningen* Date: *28 November 2007*

the Chairman of the
SENSE board

Prof. dr. R. Leemans

the SENSE Director
of Education

Dr. C. Kroeze

The SENSE Research School declares that Mr. Majid Vazifedoust has successfully fulfilled all requirements of the Educational PhD Programme of SENSE with a work load of 37 ECTS, including the following activities:

SENSE PhD courses:

°   Environmental Research in Context
°   Research Context Activity:
°   Physical Modelling
°   The Art of Modelling

Other PhD and MSc courses:

°   Advanced Use of Remote Sensing in Water Resources Management, Irrigation and Drainage
°   Introduction Geo-information Science
°   Remote Sensing
°   Soil Physics and Agrohydrology
°   The Art of Writing
°   PhD Scientific Writing

Presentations:

°   Poster presentation: 3rd International Symposium on Integrated Water Recourses Management, 26 – 28 September 2006, Bochum, Germany
°   Oral Presentation: European Geosciences Union, General Assembly, 15 – 20 April 2007, Vienna, Austria
°   Poster Presentation: International Workshop of Catchment-scale Hydrological Modelling & Data Assimilation (CAHMDA-III), 9 – 11 January 2008, Melbourne Australia
°   Oral Presentation: 4th GIS86 Conference and ISPRS Workshop on Geo-information and Decision Support Systems, 6 – 7 January 2008, Tehran, Iran

Dr. A. van Dommelen
Deputy director SENSE

Curriculum Vitae

Majid Vazifedoust was born on 22th June 1975 in Kashmar, Iran. After finishing the primary school at his birth place, he continued his secondary education in Physics and Mathematics in the historical city of Neyshabour. In 1994 he was accepted at the Ferdowsi University of Mashhad, Mashhad, Iran. There he obtained his B.Sc degree in the field of Irrigation in 1998. In the same year, he joined the Ferdowsi University of Mashhad where he accomplished his M.Sc degree in 2001 in the field of Irrigation and Drainage.

In 2001, he was appointed as a researcher in the National Salinity Research Center in Yazd. In 2002, he was awarded a full-time PhD scholarship by the Iranian Ministry of Science, Research, and Technology.

In October 2003, he joined the Soil Physics, Ecohydrology & Groundwater Management (SEG) Group of Wageningen University and Research Centre (WUR), the Netherlands. He initiated his research by focusing on elements of a real time agricultural drought assessment system. He attended several postgraduate courses. On 28 November 2007, he obtained his PhD degree at Wageningen University on a thesis in titled: Development of an agricultural drought assessment system: Integration of agrohydrological modeling, remote sensing and geographical information.

After his PhD, he will start his new job as assistance professor at the Water Engineering group of Guilan University, Rasht, Iran.

Vazifedoust can be contacted via: majid.vazifedoust@yahoo.com.

Publications

Journal Articles:

M. Vazifedoust, J.C.van Dam, R.A. Feddes, 2007. Increasing water productivity of irrigated crops under limited water supply. *Agricultural water management* (In press).

M. Vazifedoust, J.C.van Dam, R.A. Feddes, W.G.M Bastiaanssen, 2007. Disaggregation of remotely sensed evapotranspiration data: from low to high spatial resolution. *Remote sensing of Environment* (under review).

M. Vazifedoust, J.C.van Dam, R.A. Feddes, W.G.M Bastiaanssen, 2007. Inverse modeling of irrigation scheduling using disaggregated remotely sensed evapotranspiration data. *Irrigation and Drainage Systems* (submitted).

M. Vazifedoust, J.C.van Dam, W.G.M Bastiaanssen, R.A. Feddes, 2007. Numerical forecasting of drought impact on wheat yield by combining an agrohydrology model, remote sensing and data assimilation. *International Journal of Remote Sensing* (submitted)

Conferences/ Professional Society Proceedings:

M. Vazifedoust, J.C.van Dam, R.A. Feddes, W.G.M Bastiaanssen, 2007. Disaggregation of remotely sensed evapotranspiration data: from low to high spatial resolution. *European Geosciences Union, general Assembly 2007*. Vienna, Austria, 15-20April 2007 (Oral presentation).

M. Vazifedoust, J.C.van Dam, R.A. Feddes, W.G.M Bastiaanssen, 2006. Agricultural drought monitoring from space using remote sensing data. 3rd *International Symposium on Integrated Water Resources Management*, Bochum, 26 - 28 September 2006 - Ruhr-University, Bochum, Germany.